António José Vilela Pontes

SHRINKAGE AND EJECTION FORCES IN INJECTION MOULDED PRODUCTS

Tese submetida à Universidade do Minho para obtenção do grau de Doutor em Ciência e Engenharia de Polímeros

UNIVERSIDADE DO MINHO

2002

ABSTRACT

The development and manufacture of injection moulds for high quality technical parts is a complex task implying an integrated knowledge of the injection moulding process and the material changes undergone during processing. In the case of the design of moulds with deep cores (e.g. for piping accessories), the prediction of the mould dimensions in order to obtain parts with the correct size and shape after moulding, and the prediction of the forces required for the ejection of the mouldings, are two important task.

In this work the shrinkage and the ejection force are studied in injection moulding samples. Two types of mouldings are produced: a edge gated rectangular plate and a spider gated cylindrical tube. To produce the spider gated tube an instrumented mould was designed and manufactured. The mould has the means to measure the pressure and temperature histories, and the force evolution during the ejection process. The monitoring of the variables is done in real processing conditions and time. For the tube mouldings only, the force evolution during the ejection was measured.

Two materials were used for the mouldings: a polycarbonate and an isotatic polypropylene, as paradigms of amorphous and semi-crystalline materials.

The strain gauge technique was used to monitor the shrinkage variation during moulding cycle and proved to be very useful to address the effect of constraint in the shrinkage and to measure the onset of shrinkage.

The recorded pressure and temperature during the processing are analysed and compared with simulations performed using a commercial software C-Mold v. 99.7, and a open code UNISA developed at the Università di Salerno. The experimental data are qualitatively in agreement with those predicted by the softwares. However some discrepancies can be observed when the effect of pressure on viscosity and mould deformation are not considered.

The as-moulded shrinkage is analysed and compared with simulations performed using the C-Mold v. 99.7 and a thermo-mechanical model originally developed at the Università di Salerno and modified within this research to suit specific aspects of the geometries being studied. This thermo-mechanical model gives a satisfactory description of the shrinkage and shows the relevance of using the degree of crystallinity as criterion of solidification.

The ejection force is well described by a thermo-mechanical model accounting for crystallinity effects and the shrinkage evolution developed in this work

ACKNOWLEDGEMENTS

This work would not be possible without the valuable support and help provided by several individuals, institutions and industrial companies. I want to express my gratitude to and refer those whose contribution were of major importance.

Professor António Sérgio Pouzada, research and scientific supervisor, for the continuous support and availability even in difficult periods of his duties as Dean of *Escola de Engenharia* of *Univerisidade do Minho*. I hope to be and continue meritorious of his friendly encouragement.

Professor Giuseppe Titomanlio, co-supervisor of this research work, for his scientific guidance, valuable suggestions and availability, and help on the logistics at Salerno.

The *Departamento de Engenharia de Polímeros* (DEP) of the *Universidade do Minho* (UM) for the facilities and equipment provided and for supporting this research program.

The *Instituto de Materiais* (IMAT) and the *Centro de Engenharia de Polímeros* (CEP) for supporting this research program.

The *Dipartimento di Ingegneria Chimica* e *Alimemtare of the Università Degli Studi Salerno*, where part of this work was performed, for the facilities and equipment provided and the kind hospitality.

The *Centimfe, Marinha Grande,* where part of this work was performed, for the facilities and equipment provided and the kind hospitality.

The *Fundação Calouste Gulbenkian* and *Instituto de Cooperação Científica e Tecnológica Internacional* (ICCTI) by the financial support during the working periods at the *Università Degli Studi di Salerno.*

The IC-PME programme that provided most of the financial support to the activities within the project through the project *Mouldforce (grant P015)*, from April 1998 to June 2001.

Finally, the conclusion of this thesis would not be possible without the valuable help of several individuals and industrial companies. To them my sincere acknowledgements:

Dr. António Brito (from the *Departamento de Engenharia de Polímeros* of *Universidade do Minho*) for his valuable suggestions during this work.

Dr. Nuno Neves (from the *Departamento de Engenharia de Polímeros* of *Universidade do Minho*) for his valuables suggestions and encouragements.

Dr. Roberto Pantani (from the *Dipartimento di Ingegneria Chimica e Alimemtare* of the *Università Degli Studi Salerno*) for the scientific and technical guidance on the strain gauge technique and shrinkage characterisation in iPP plates mouldings. I will never forget the friendship and kind hospitality provided by Roberto during my work in Salerno.

Dr. Vito Speranza (from the *Dipartimento di Ingegneria Chimica e Alimemtare* of the *Università Degli Studi Salerno*) for the technical guidance on the UNISA software, friendship and kind hospitality during my work in Salerno.

Mr Agostinho Febra (from SOMOLTEC, Lda) for the valuable suggestions in the mould design and manufacturing.

Eng. Jorge Oliveira (from Moliporex, Lda) for the valuable suggestions in the mould and instrumentation design.

Eng. António Selada (from Centimfe) for the valuable suggestions in the mould design and manufacturing.

The students who help in this work: Paulo Oliveira, for the injection and shrinkage characterisation of the PC plates mouldings; Billy Araújo for the injection and ejection force assessment of the tubular mouldings.

My colleagues at DEP for their direct or indirect contribution for this work, and their continuous help and friendship.

TABLE OF CONTENTS

CONTENTS

CONTENTS V

LIST OF FIGURES XIII

LIST OF FIGURES

2- STATE OF THE ART

3- PREDICTION OF SHRINKAGE AND EJECTION FORCE

4- INSTRUMENTED INJECTION MOULD

5- EXPERIMENTAL METHODS AND SIMULATION TECHNIQUES

6- RESULTS AND DISCUSSION

A1- RECTANGULAR PLATE MOULDING

A2- TUBE MOULDING

LIST OF TABLES

5- EXPERIMENTAL METHODS AND SIMULATION TECHNIQUES

6- RESULTS AND DISCUSSION

A1- RECTANGULAR PLATE MOULDING

A2- TUBE MOULDING

LIST OF SIMBOLS

A1 - Constant in Cross-WLF (eq. 5.4)

A2 - Constant in Cross-WLF (eq. 5.4)

A_c - Contact area

B - Half thickness of the rectangular impression.

b1m - Constant in Tait equation (eq. 5.6)

b1s - Constant in Tait equation (eq. 5.7)

b2m - Constant in Tait equation (eq. 5.6)

b2s - Constant in Tait equation (eq. 5.7)

b3m - Constant in Tait equation (eq. 5.6)

b3s - Constant in Tait equation (eq. 5.7)

b4m - Constant in Tait equation (eq. 5.6)

b4s - Constant in Tait equation (eq. 5.7)

b5 - Constant in Tait equation (eq. 5.8)

b6 - Constant in Tait equation (eq. 5.8)

b7 - Constant in Tait equation (eq. 5.7)

b8 - Constant in Tait equation (eq. 5.7)

b9 - Constant in Tait equation (eq. 5.7)

C - Universal constant in Tait equation (eq. 5.5)

C_M - Mould compliance

D - Constant in equation 5.17

D - Diameter

D1 - Constant in Cross-WLF (eq. 5.4)

D2 - Constant in Cross-WLF (eq. 5.4)

D3 - Constant in Cross-WLF (eq. 5.4)

D_{imp} - Dimension in the impression in the *i* direction

D_{part} - Dimension in the part in the *i* direction.

E - Elastic modulus

Fe - Ejection force

$F_{i,w}$ - Elastic response of the mould wall in the *i* direction

$F_{i,fr}$ - Friction force in the *i* direction

H - Thickness of the tubular impression

K_0 - Crystallisation kinetic constant

k_i - Gauge factor

n - Avrami index

n - Constant in Cross-WLF (eq. 5.3)

p - Pressure

p_0 - Reference pressure

p_c - Contact pressure acting on the core surface

p_{gf} - Pressure distribution inside the impression at the instant of the gate solidification

Ph - Holding pressure

R_0 - Internal radius

R_1 - External radius

R_m - Average radius

Sh_i - Shrinkage in i direction

S_{ii} - Stress component in the *i* direction

ta - Time after holding stage

t_c - Local contact time between polymer and mould

t_e - Ejection time

th - Holding time

t_i^* - Shrinkage onset in the *i* direction

t_{s0} - Start of solidification

t_{sz} - Solidification onset of a layer z.

T - Temperature

T_0 - Reference temperature

T_s - Solidification temperature

T_{inj} - Injection temperature

T_{max} - Temperature of Maximum crystallization rate

T_{mold} - Mould temperature

Tw - Mould wall temperature

v - Material specific volume

v_s - Specific volume at the moment of solidification

x_s - Solidified section

z_R - Mass fraction of EPR

z_s - Solidified layer thickness

z_T - Mass fraction of talc

α - Angle

α - Coefficient of thermal expansion

μ - Coefficient of friction

ρ - Density

β - Material compressibility

ΔR - Strain gauge resistance variation

ε_{ii}^{obs} - Observable strain in the *i* direction

ε_{ii}^{T} - Thermal strain in the *i* direction

η - Material viscosity

γ - Shear rate

τ - Shear stress

σ - Stress

χ_e - Equilibrium crystallinity degree

ν - Poisson's ratio

1- INTRODUCTION

The widespread application of thermoplastics in almost every area of the modern industry results in an increasing need for injection moulds that must satisfy the stringent specification of high quality parts.

Portugal is a leading manufacturer of tools for the injection moulding industry. The export of moulds produced by the mouldmaking industry is about 90% of its production and grew 4.5% in 1999 [1]. The major sector for Portuguese moulds is the automotive industry, which is very demanding in terms of quality and delivery times.

Injection moulds for technical applications are usually quite complex pieces of equipment to which high dimensional accuracy is associated. Furthermore the design process of these moulds and their manufacture must be made more efficiently and quickly, without compromising the product quality. To guarantee the quality of technical parts made by injection moulding a precise characterisation and monitoring of the injection process is required.

The introduction of Computer Aided Engineering (CAE) in the design with plastics has been very important to pursue those objectives and to help the mould designer on decisions such as the gate position, the runner dimensions and balancing, the architecture of the cooling channels, or the air vent location.

One of the factors that determine the mould performance and moulding quality is the material shrinkage during the injection cycle. The shrinkage is a geometric change (that can be a

reduction or an expansion) in the size of the part. The driving force of the shrinkage is the volumetric change of the material as it cools from the molten state to a solid. Despite the apparent simplicity of this statement the relationship between the volumetric shrinkage and the linear shrinkage of the component is affected by mechanical properties and mould constraints and is of very complex description.

The shrinkage data enables the mould designer to consider the variation in the product size with respect to the impression dimensions, in order to obtain parts with the final dimensions within the specified tolerances. Therefore the prediction of shrinkage is of great importance for mould design proposes and for the setting of the processing variables.

In the case of some specific shapes (boxes, cylinders) the shrinkage is partially constrained by the mould geometry. The plastic moulding shrinks on the core of the mould. Thus, upon ejection, it will be necessary to overcome the frictional forces arising from the shrinkage. This aspect has significant implications in the mechanical design of the injection moulds especially when deep cavities are involved. In the design of such moulds, the accurate prediction of the ejection force may contribute for a more precise and economically efficient decision of the ejection system. In fact, if the designer knows the force likely to be required during the moulding ejection, he will be able to make a proper decision for a less complex and cheaper ejection system: mechanical, pneumatic, or hydraulic. The capability of predicting the ejection force may also help to optimising the mould design and to guaranteeing the structural integrity of the mouldings

The research work embodied in this thesis is intended to provide a deeper knowledge on the shrinkage behaviour and its relation with the force required for the part ejection in real moulding conditions and, if possible its prediction.

Experimental data obtained from a fully instrumented mould producing a tubular moulding are compared with predictions from existing simulation programs - C-Mold and UNISA (pressure and temperature) - and from a prediction algorithm (ejection force) based on a thermo-mechanical model., developed in the context of this work. Semi-crystalline (iPP) and amorphous (PC) materials were used to expand the amplitude of the research, enabling a first insight on the influence of the type of material on the physical process.

The structure of this thesis is as follows: Firstly, in an introductory chapter, the thermo-mechanical environment that occurs during the injection moulding process and the evolution of its modelling during the last years are described. This is followed by the literature review on the

shrinkage predictions approach and the influence of processing variables on its behaviour. This chapter 2 concludes with a discussion on the new trends of the mould design activity, a particular attention being given to the ejection system and to the influence of processing variables on the ejection force and its prediction.

The chapter 3 reviews the theoretical principles associated to the shrinkage and the ejection forces in injection moulding. The main equations to predict the shrinkage in injection moulded plates are described according to the thermo-mechanical model developed by Titomanlio and Jansen. Upon using the same thermo-mechanical approach, a model is developed to calculate the shrinkage and the ejection forces in tubular injection mouldings that will be compared with experimental results in chapter 6.

Then, in chapter 4, the design of the instrumented mould for assessment of the force during the ejection process of tubular mouldings in real processing conditions is described. This novel instrumented tool also makes possible the experimental assessment of the pressure in the impression and the surface temperature of the moulding during its processing.

Next, in chapter 5, the experimental methods and simulation techniques used in this work are described.

In chapter 6 the recorded pressure and temperature profiles during processing are analysed and compared with simulations using the C-Mold v. 99.7 and the “open” program UNISA. The effects of the pressure on the viscosity, and the mould deformation on the predicted pressure evolution are examined. The shrinkage evolution was measured using a recent technique making use of resistance strain gauges, and the shrinkage after ejection was calculated at room temperature. The results are analysed and compared with simulations using the C-Mold v. 99.7 and a thermo-mechanical model originally developed at the Università di Salerno and modified to suit specific aspects of this research, as obtained in chapter 3. The ejection force assessed with the instrumented mould is analysed and compared with predictions using the thermo-mechanical model developed in this work.

Finally, in chapter 7, the principal conclusions obtained in the work are drawn, and some recommendations for further work are proposed in chapter 8.

2- STATE OF THE ART

2.1- Injection moulding

2.1.1-The process

Injection moulding is a leading process for plastics that allows, in a single operation, the production of very complex moulded products at high production rates and with enormous scope for automation. The basic equipment for the process consists of an injection moulding machine and a mould. In several cases auxiliary equipments is involved in the process in order to increase the quality and efficiency of the production. These equipments are the thermo-regulators for the mould temperature control, material dryers, material handling systems and robots for moulding handling [2].

The injection moulding process is a processing technique in which highly complex physical processes take place. In the figure 2.1 it is depicted the injection moulding cycle showing the main phases where by the material passes until a product is obtained: injection, holding, plasticating, cooling and ejection.

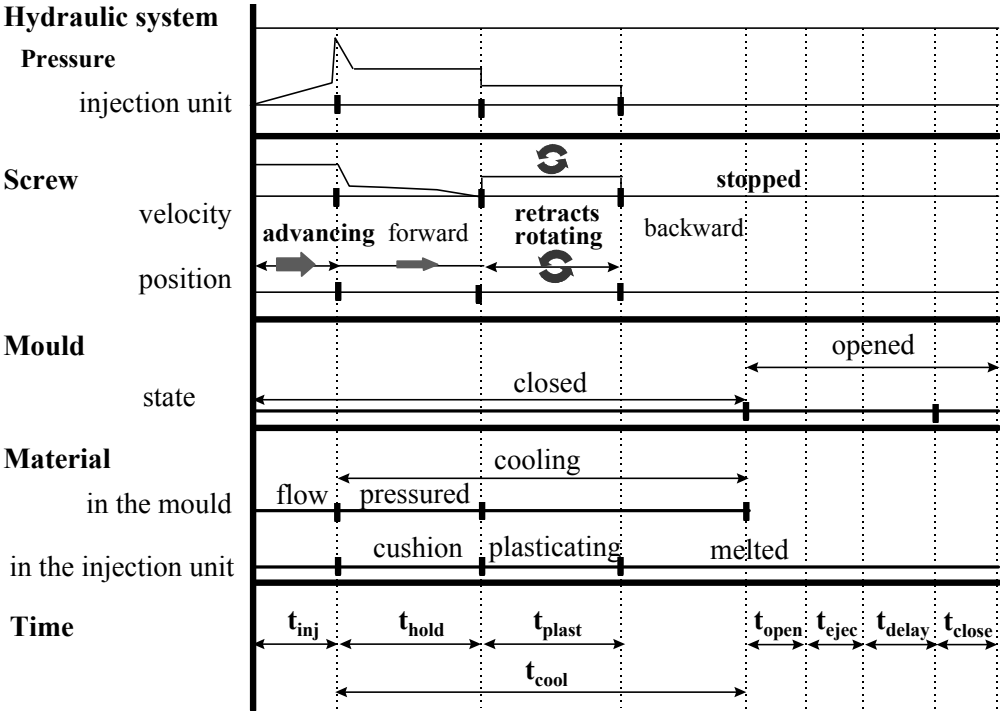

Figure 2.1- Injection moulding cycle (t_{inj} - injection time, t_{hold} - holding time, t_{plast} - plasticating time, t_{cool} - cooling time, $t_{open/close}$ - mould opening/closing time, t_{ejec} - ejection time, t_{delay} - delay time). [3]

The material, usually in granule form, enters in the barrel through the hopper. The granules are then melted inside the barrel which is externally heated by the electric heaters. The reciprocating screw is used to transport and pressurising, and plays a fundamental role in the plasticisation of the material. Plasticisation results not only from the electrical heating but also from the heat generation caused by friction between the screw and the material granules. During plasticisation the screw moves backward against the adjustable hydraulic pressure, until the amount of material (shot volume) required for the next cycle is plasticised.

Once the injection signal is given, the reciprocating screw moves forward and presses the melt through the machine nozzle and runner/gate system into the impression of the mould (injection phase). The melt is prevented to flow back into the barrel by a non-return valve at the tip of the screw.

Once the mould has been volumetrically filled, the holding phase starts. During this phase more melt is forced to flow into the impression for as long as possible, in order to compensate the densification of the material resulting from thermal contraction and phase changes in the material.

Simultaneously with the holding phase the cooling process is initiated in the polymer corresponding to the cooling phase. During this phase, the average temperature through thickness of the material falls down to the mould temperature, essentially by conduction.

Normally the mouldings are removed when the mould opens (ejection phase) at a temperature higher than the mould due to economic reasons. The mould closes again and the process is repeated for producing a new moulding.

The injection moulding process is described extensively in the literature as, for example in [2,4-6]. Recently other moulding techniques evolved from the conventional injection moulding to process specific classes of polymers and/or to produce products with special design features and properties. Some examples of these non-conventional moulding techniques are [7]: the injection-compression moulding, the gas-assisted injection moulding, the structural foam moulding, reactive moulding, the co-injection moulding or the injection moulding with controlled microstructure.

2.1.2- The thermo-mechanical environment

During the injection moulding cycle the material is submitted to a complex thermo-mechanical environment. The flow of the polymer melt into a cold mould impression is a typical example of an unsteady, non-isothermal, three-dimensional flow of a compressible, viscoelastic fluids.

During this process each particle in the material is subjected to a different mechanical and thermal history. When the melt flows through the gate into the impression, a frozen layer of solidified material is formed due to the cold mould walls (figure 2.2).

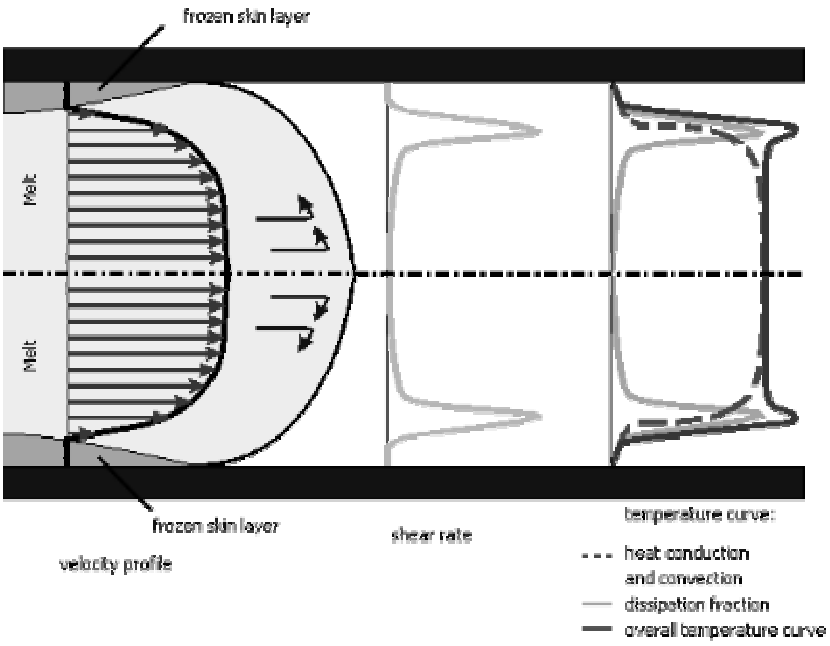

Figure 2.2- Velocity, shear rate and temperature profiles through thickness (adapted from [8])

As schematised in the figure 2.2, the shear rate is maximum near the interface between the frozen skin layer and the melt, and null at the centre. The figure also shows typical profiles of the temperature resulting from the contributions of temperature profiles resulting from the heat generated by conduction and convection, and by viscous dissipation. The cooling rate is high near the mould wall where the orientation caused by the stresses induced by the flow is not able to relax. The interior will cool down more slowly due to the insulation effect of the already solidified polymer. The resulting high thermal gradient and the constrained shrinkage introduce residual stresses in the mouldings [e.g. 9].

All these variables that are shown in the figure 2.2, together with the pressure evolution inside the mould impression, define the thermo-mechanical environment that constrain the overall morphology development and affecting the final mechanical properties in the product [e.g. 3, 10,11]

If the thermo-mechanical history variables (pressure, temperature, flow and cooling rate), can be monitored directly or indirectly in the impression, the moulded product properties can be accurately and consistently predicted.

In recent research, the pressure at the impression has been considered the most important parameter to establish a correlation with the dimensions and weight of the moulded part [12], and it is considered a finger print of the process [8]. The figure 2.3 shows a typical pressure evolution inside the mould impression and its main features.

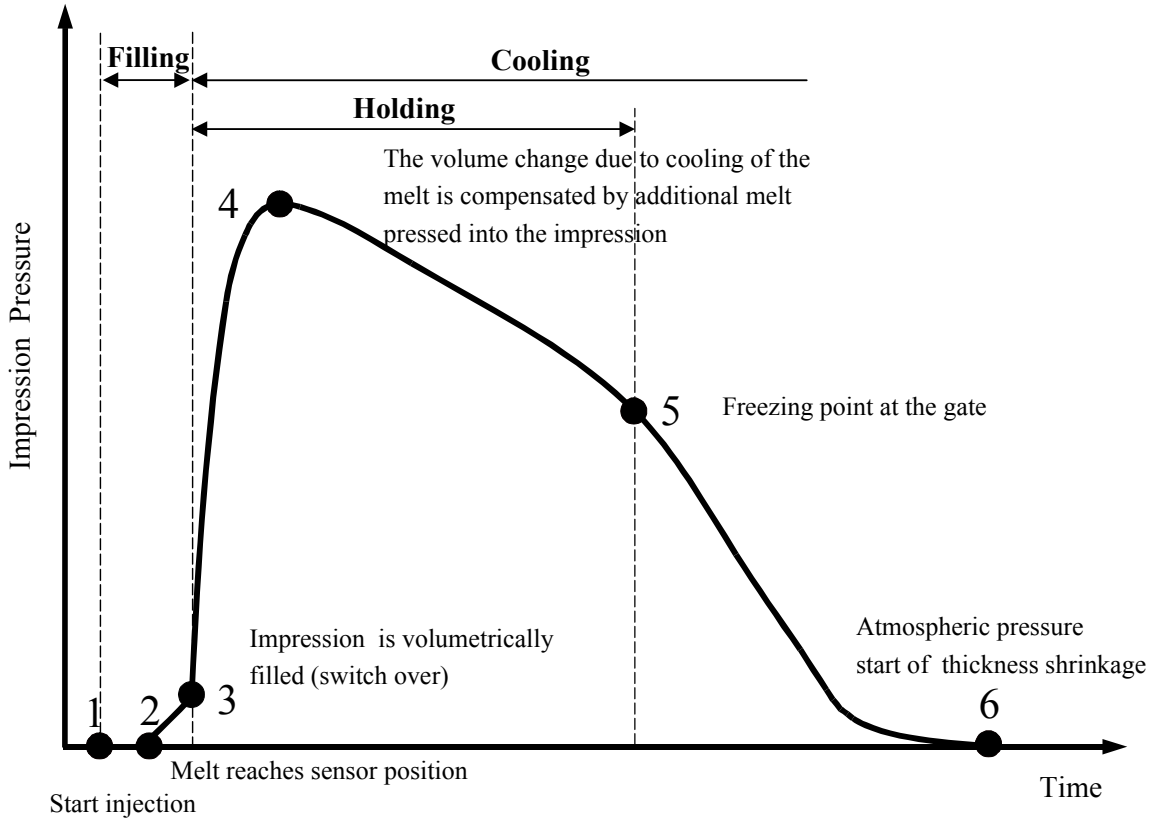

Figure 2.3- Typical pressure evolution inside the mould impression (adapted from 2)

Any changes in the injection moulding process due to temperature, flow rate, holding pressure and time cause changes in this profile. The figure 2.4 shows the effect of changes of these variables in the pressure evolution profile inside the impression as a net result of the simple variation of a moulding variable.

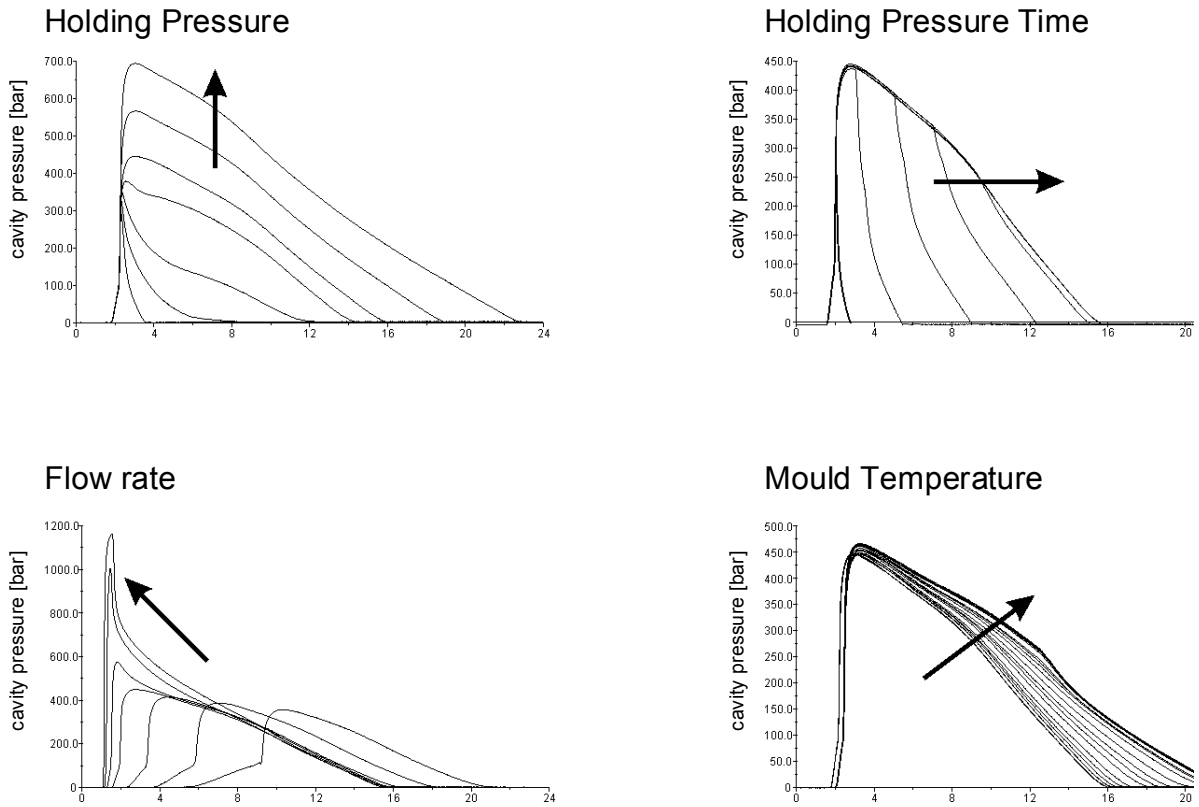

Figure 2.4- The influence of some injection moulding variables in the pressure evolution profile inside the impression (adapted from 8)

Normally, the thermo-mechanical environment associated with a specific moulding, can be estimated by the simulation of the mould filling. In the next section the main evolution that was occur during the development of the numerical simulations for the injection moulding process will be treated.

2.1.3- Modelling of the injection moulding process

In many technical products it is mandatory that they meet close specifications in terms of their properties and the final dimensions. As a consequence, the main aim of the numerical simulations of the injection moulding process, that combines the mathematical and numerical methods, is not only to analyse the processing stage, but also to predict the properties, starting from the material properties and the processing conditions.

To obtain the mathematical models its necessary to combine:

- physical laws (conservation of mass, momentum and energy);
- material response models (constitutive equations for viscosity and/or viscoelaticity, pvT behaviour)
- information about the process (geometry and processing variables).

The objective of the numerical methods like finite elements, finite differences, boundary elements, and control volume, is to solve the equations of the mathematical models. Details on the most used numerical methods are reviewed by Tucker [13]

After the work of Harry and Parrot [14] in 1970, a large number of studies where done for the simulation of the injection moulding process. They have varying degrees of complexity in terms of the mathematical formulation of the flow equations, the constitutive equations, the related material properties, the microstructure characteristics (morphology and orientation distribution), and the way how the results are presented.

The injection moulding process is broadly divided into three phases: filling, holding (or packing) and cooling.

Mould filling

The numerical simulation of the injection moulding was initially restricted to the mould filling phase. The pioneering studies on the numerical methods to simulate the mould filling are attributed to Kamal and Kenig [15,16] and Williams and Lord [17,18] who used the finite difference method to predict the temperature, velocity and pressure fields in simple geometries. In their studies the flow was considered uni-dimensional and purely viscous, and the lubrication theory was applied. In a subsequent paper [19] Lord introduced in the constitutive equation, the effect of pressure on the viscosity in order to improve the accuracy of the pressure predictions.

The initial studies on the bi-dimensional analyses of the filling phase are attributed to Broyer *et al.* [20], who proposed a bi-dimensional analysis of the flow problem of Newtonian and non-Newtonian fluids. In this analysis the flow-analysis network (FAN) method was used. A Hele-Shaw isothermal and fully developed flow is considered. The lubrication theory is applied.

Later, Ryan *et al.* [21] studied the effect of the gate dimensions on the pressure distribution inside the impression and on the flow front advance. A bi-dimensional viscous flow in a rectangular impression is considered. The extension of this type of analysis to the non-isothermal case of a non-Newtonian fluid was done by Kuo *et al.* [22].

Hieber and Shen [23] gave an important improvement to the injection moulding simulation when they introduce a hybrid numerical scheme (finite element/finite difference) to model the filling phase as a generalised Hele-Shaw flow for an inelastic, non-Newtonian fluid under non-isothermal conditions. The utility to used the Hele-Shaw model stems from replacing the full three-dimensional melt flow problem by an equivalent two-dimensional flow problem in the plane of the impression.

Later, Wang *et al.* [24] based on the reference [23] developed a computational system, for simulating the mould filling flow in three dimensional thin parts, that includes pre-processors for geometry definition and mesh generation to graphic post-processors. This computer system was the base for the development of the commercial software C-Mold.

The first attempt to incorporate the effects of viscoelasticity into the modelling of the mould filling process was made by Isayev and Hieber [25]. The prediction of residual stresses, orientation and birefringence was made based on uni-dimensional non-isothermal flow of a viscoelastic melt described by the Leonov model [26]. Later, Papathanasiou and Kamal [27,28] used a viscoelastic model for the analysis of the filling of a complex shape impression. The ram velocity was used for calculate the position of the flow front. The agreement between predictions and experiments was satisfactory.

Kamal *et al.* [29] dealt with the simulation of the fountain flow phenomenon at the advancing melt in order to better understand the relationship between the fluid element deformation, the flow-induced stresses, and the microstructure development at the surface of the mouldings. The simulation was done using a marker-and-cell (MAC) computational scheme, incorporated a viscoelastic rheological equation and took the non-isothermal crystallisation kinetics into consideration. The modelling of the fountain flow was also analysed in detail by Mavridis *et al.* [30,31]. It was qualitatively demonstrated that the fountain flow is responsible for the orientation pattern of the surface layer of injection moulded parts. It was also found, in qualitative terms, that no difference exists between a Newtonian fluid and the shear thinning fluids in the front flow region.

In order to predict the final properties of the mouldings like mechanical, optical geometrical or surface attributes, it is necessary to simulate the filling, holding and cooling phases of the injection moulding process.

Holding phase

The initial attempts to model the holding phase under non-isothermal conditions were developed by Kuo and Kamal [32]. The analysis includes the inertia effect of impinging flows and regards compressibility of polymer melts as the dominant feature in the compression flow. Simultaneously Titomanlio *et al.* [33,34] extended the Williams and Lord [17,18] mould filling analysis to the holding phase. In the energy equation, the crystallisation effect was considered using a equivalent specific heat that considers the heat generated by the crystallisation.

In these analyses of the holding phase, the effect of viscoelasticity was ignored. Nguyen and Kamal [35] derived governing equations to model the holding phase in a two-dimensional impression for a viscoelastic fluid. The Galerkian finite element method was used to solve the set of governing equations.

The unified model for injection moulding

A good review of the modelling attempts for the post-filling stage of injection moulding of thermoplastics, in early studies, was made by Huilier [36]. In his work it mentions the need to work towards unified equations of a compressible type for the entire moulding cycle. Chiang *et al*. [37,38] developed a unified theoretical model to simulate the filling and post-filling stages of the injection moulding process based on early works of Wang *et al.* [24] and Hieber [39]. A generalised Hele-Shaw flow of a compressible viscous polymeric melt under non-isothermal conditions is assumed in the analysis. The numerical solution is based on a hybrid finite element/finite difference method to solve for the pressure, flow and temperature fields, and a control volume method for the melt front calculation.

Recent trends in injection moulding simulation

The recent developments of moulding simulation are on the 3D modelling of the injection moulding process, the incorporation of the crystallisation kinetics, the predictions of the microstructure development, and the simulation of non-conventional techniques.

The three-dimensional (3D) simulation is an important improvement to accurately predict some aspects occurring during the mould filling that can not be possible using the Hele-Shaw approximation. A 3D model for example will permit the modelling of the fluid behaviour at the flow front, near to and at the solid walls.

In 1998 Hétu *et al.* [40] presented a 3D finite element model capable of predicting the time dependent velocity and pressure fields as well as the position of the flow fronts. The governing Stokes equations were used. These equations and the Carreau constitutive model were solved using a Galerkian formulation. Later, Ilinca and Hétu [41] presented a fully 3D program to solve the holding and cooling stages, providing a unified numerical approach for the entire process simulation of the injection moulding.

Other example of simulation programm based on 3D calculations, is the Rem3D, presented by Coupez and co-workers [42,43] that makes possible the injection moulding simulation without geometrical or kinematic approximations and, for instance provides a 3D solution of the fountain flow.

Verifying the simulations

The 3D modelling of the injection moulding process requires new experimental techniques to validate/verify the simulations. The visualisation of the filling process inside the mould using the glass-inserted mould technology, seems to be very effective principally to visualise the melt flow front [44,45].

The glass-insert mould technology was applied by Brito and Cunha [44,46,47], to develop a special mould with the purpose to visualise the melt flow across the thickness direction of the impression. This tool seems to be very important for the development of the simulations programs and to validate the predictions.

2.2- Shrinkage

The dimensions of an injection moulded product are dependent on the change of dimensions with respect to those of the impression. This change results from the influence of material properties, processing variables, mould and part design. The plastic product shows an as-moulded shrinkage defined as the reduction in the size of a moulded part in relation to the impression. The shrinkage varies in the space and it is usually quoted at room temperature just after the part has been ejected from the mould:

$$Sh_i = \frac{D_{imp} - D_{part}}{D_{imp}} \tag{2.1}$$

where D_{imp} is the dimension in the impression in the i direction and D_{part} is the corresponding part dimension.

Due to the importance in obtaining reliable final dimensions of the moulded product, extensive research was started in 1967, mainly by Williams and Pacoast [48], to analyse the effect of processing variables, mould and part design on the as-moulded shrinkage in different thermoplastics.

2.2.1- Variables affecting shrinkage

Systematic studies to analyse the effect of processing variables on the as-moulded shrinkage were more recently conducted e.g. by Pierick *et al.* [49], Bain *et al.* [50], Mamat *et al.* [51], Jansen *et al.* [52] and Chang *et al.* [53]. All these studies concluded that the holding pressure and the injection temperature are the most important process variables affecting shrinkage. A higher holding pressure reduces the part shrinkage in all directions. Increasing the injection temperature is usually seen as reducing the shrinkage because of the better pressure transmission [e.g. 52]. However, if the melt temperature is further increased, the gate takes longer to freeze off and if the gate freeze-off time exceeds the holding time the shrinkage increases. The mould temperature influence does not show a general trend for all materials. Increasing the mould temperature was reported by some authors to increase the shrinkage [49,51,54] while others concluded differently [50].

Mamat *et al* [51] in their study with PP and 40% calcium carbonate filled PP used marks made on the mould cavity to measure the shrinkage at various points in the flow path. It was verified that the local pressure is directly correlated with the local shrinkage variation along the flow path. This observation was also reported by Leo and Cuvelliez [55]. These authors also analysed the effect of the gate thickness on the shrinkage. The results highlight the importance of the gate design on the dimensional accuracy of the part. The mould elastic deformation was also measured using strain gauges. It was verified that the mould deformation can play a significant role in the pressure field, even for a seemingly stiff mould construction.

2.2.2- Shrinkage anisotropy

The shrinkage is important to the mould designers but usually the information available is restricted to a single and meaningless value. The shrinkage of injection moulded products change along the flow path and can show different values when measured in the flow or the across flow directions.

Jansen [56] and Mamat *et al.* [51] verified, for PP, that in most cases the shrinkage in the across flow direction is slightly larger than the shrinkage in the flow direction, and that the relative difference depends on the processing variables. Chang *et al.* [53], who use three unreinforced thermoplastics, observed that the extent of the anisotropy shrinkage in the flow direction and the across flow direction for HDPE is different from PS and ABS. More shrinkage occurs in the across flow direction. The reverse was found true for PS and ABS. The observations indicate a important role of the crystallinity in the development of the shrinkage field.

For short fibre reinforced polymers, large differences between shrinkage in the flow and the across flow directions was detected. Jansen *et al.* [57] (in PC) and Shay *et al.* [58] (in PC and PA) reported values typically close to 0.2% on the shrinkage in the flow direction. In the across flow direction the values were close to the unfilled polymer. This observation was also reported by other authors for the case of PP [59].

2.2.3- In-mould shrinkage

In the studies on the shrinkage mentioned before, the shrinkage was measured after moulding and at room temperature. Pantani *et al.* [60] were the first to use the strain gauge technique to measure the local in-plane shrinkage development from the moment it starts inside the mould to soon after ejection. The experimental results obtained by this technique were compared with the as-moulded shrinkage performed with other techniques and were with good agreement.

In the studies of Titomanlio and Jansen [61], and Bushko and Stockes [62] the possibility of the shrinkage to occur inside the mould, in some processing conditions, was also mentioned.

Jansen *et al.* [63] studied the effect of the holding pressure and time on the shrinkage behaviour of PS rectangular plates. It was found that if a constraint prevents the in-mould shrinkage from taking place before complete solidification, the as-moulded shrinkage may decrease with respect to the unconstrained case. The effect of constraint was found to be more effective when the holding pressure and time are small.

2.2.4- Prediction of the shrinkage

2.2.4.1- Statistical modelling approach

To predict the shrinkage, studies [e.g. 50,51,53,64] have been done based on the *statistical modelling approach*. According to this approach the effect of moulding processing variables and design factors were analysed and the experimental results fitted to mathematical models and implemented in computational programs.

As described by Austin in his paper [65] and also in corporate technical literature [66] the commercial code Moldflow is one example of a software that uses the statistical analysis method to construct a multi-linear model that considers volumetric, crystallisation, mould constraint and orientation components. The material shrinkage data to be used in the fitting model is generated from a simple straight strip moulded under different moulding conditions and with different thicknesses.

The approach used at Moldflow takes into account the real conditions of the injection moulding process, but it is based on a costly process of experimental data generation. As it was mentioned by Stizt [67], another shortcoming in that approach lies in the material data required for the model (such as crystallisation, relaxation, orientation constants and pvT diagram values) that should be measured experimentally by standard methods.

2.2.4.2- Thermodynamic modelling approach

Another approach to predict shrinkage consists on following the volumetric shrinkage from the pvT (pressure-volume-temperature) diagrams. This *thermodynamic modelling approach* is based on the shrinkage of the polymers dependence on a succession of thermodynamic states during the process. The figure 2.5 shows the correlation between specific volume and temperature at different pressures for typical amorphous and semi-crystalline polymers. The figure shows the difference between the two types of material which shows up at the transition from the molten state to the solid phase.

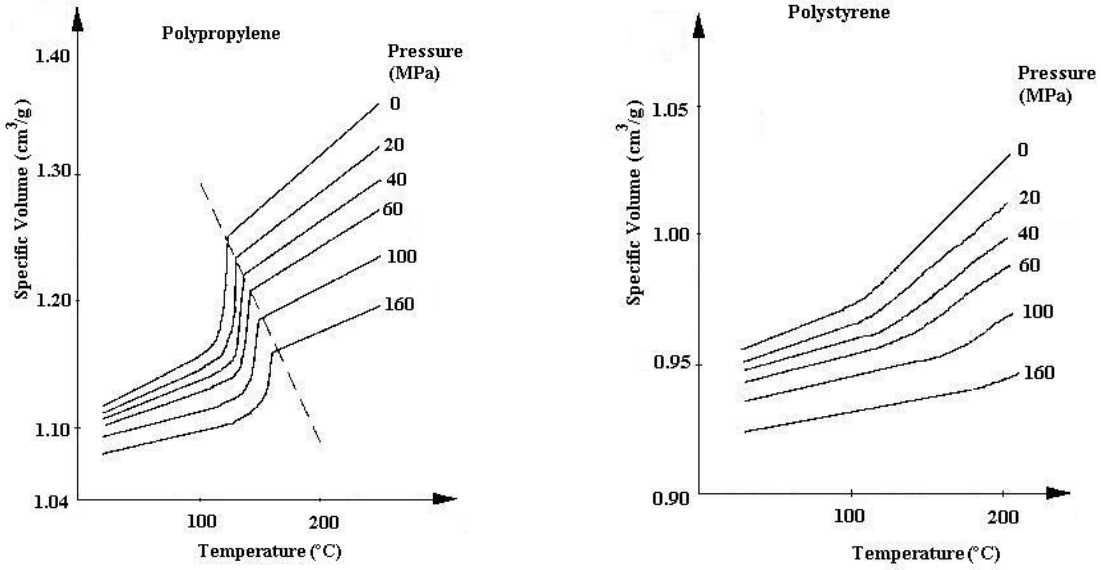

a) semi-crystalline b) amorphous polymer

Figure 2.5- pvT diagrams [68]

For semi-cristalline materials, the specific volume curves display a sharp step associated to the crystallisation. Below the crystallisation temperature the variation in the specific volume is due to the thermal contraction and to the crystallisation evolution.

According to Isayev and Hariharan [69], the volumetric shrinkage may be predicted by using models that describe the pvT behaviour of the material (as the Tait equation) in combination with the temperature and pressure histories. The works of Menges *et al.* [70] and Yang *et al.* [71] are other examples of studies that used the pvT diagrams to predict the shrinkage.

This approach is limited to the prediction of the isotropic shrinkage. In fact, the thickness shrinkage can be much larger than in the in-plane direction. Furthermore the shrinkage in the flow and the across flow directions may differ due to filler or crystallisation effects [*e. g.* 51-53,57-59]. As it is shown in this thesis and was published elsewhere [72] another cause to the shrinkage anisotropy is the presence of constraints in the mould.

Another limitation of the *thermodynamic modelling approach* to predict the shrinkage is the pvT diagrams normally being obtained from tests in equilibrium conditions that do not describe exactly the material behaviour in effective processing conditions. The pvT behaviour is affected by the cooling-rate (in amorphous and crystalline materials) [73-76] and by the shear-induced crystallisation [74].

In the figures 2.6 the specific volume variation is shown with different cooling rates for a semi-crystalline and for a amorphous polymer [73,75]. The data show that the transition from the molten state to the solid phase is delayed with the increase of the cooling rate for semi-crystalline polymers and vice-versa for amorphous polymers.

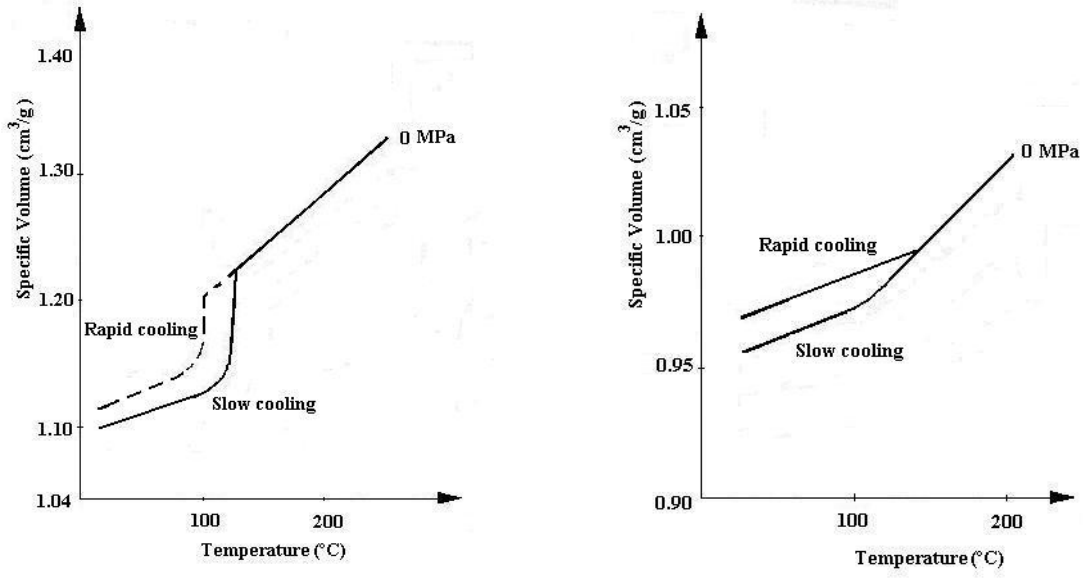

a) semi-crystalline b) amorphous polymer

Figure 2.6- Schematic curves showing the cooling rate dependence of the specific volume

2.2.4.3- Thermo-mechanical modelling approach

The material is usually free to shrink in thickness direction while the in-plane shrinkage is restricted by the already solidified layers and by the mould (geometrical constraints and friction effects). As suggested by Menges *et al.* [70], to predict the linear shrinkage it is necessary to combine a thermodynamic analysis with a thermo-mechanical one.

To allow for a more realistic anisotropic shrinkage prediction a *thermo-mechanical modelling approach* was developed. In this theory the solidification of a molten layer of thermoplastic between cool parallel plates is used to model the mechanism of part shrinkage and the build up of stresses in the injection moulded process as in figure 2.7 [77]. As the melt cools down, each layer would like to shrink according to its temperature and pressure history, following the material pvT behaviour.

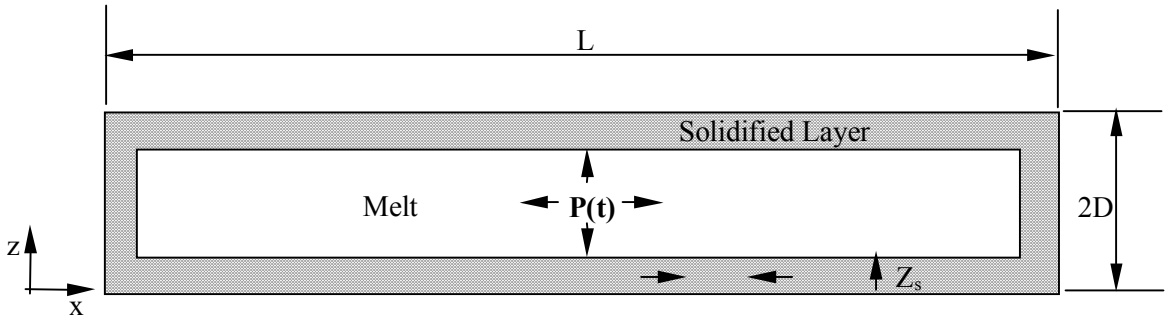

Figure 2.7- Schematic view of the thermo-mechanical mechanism [77]

Jansen and Titomanlio [61,78] proposed a thermo-elastic model taking into account a non-constant pressure effect, but neglecting the viscoelastic effects.

Bushko and Stokes [62, 79-81] proposed a more complete viscoelastic theory for the prediction of the shrinkage and residual stresses. The flow effects are neglected and a simple thermo-viscoelastic material model was assumed. Baijens *et al*. [82,83] also used a viscoelastic model to predict the residual stresses, but they assumed that no shrinkage occurs during solidification.

As it was described by Chiang *et al.* [84] and implemented in the commercial software C-Mold [85] the linear shrinkage is predicted, assuming that no shrinkage takes place inside the mould. This software uses the data obtained with integrated analyses of the flow, holding and cooling phases, using a algorithm based on the finite element method to perform the equilibrium stress analysis.

In the Titomanlio and Jansen [61] and in the Bushko and Stokes [62] models, the possibility of the shrinkage to occur inside the mould is considered. The models are developed considering that the local shrinkage evolution is regulated by the mechanical equilibrium between internal stresses and external forces acting on the solid layers.

Pantani *et al*. [86] examined experimentally the effect of holding pressure and holding time on the shrinkage evolution of rectangular plates moulded in PS, using the strain gauge technique. The results showed that the thermo-mechanical model proposed by Titomanlio and Jansen satisfactorily predicts the onset of the shrinkage inside the mould and the shrinkage evolution.

Other studies of experimental validation of shrinkage predictions are available in the literature [*e. g.* 58,87-91]. In spite of the substantial progress made on the predictions of the final dimensions of injection-moulded parts, the precise estimation of the moulding dimensions in changing processing conditions is still a challenge.

The *thermo-mechanical modelling approach* and the reported Jansen and Titomanlio model [61,78] will be followed to predict the shrinkage in the studies reported in this thesis.

2.3- Tool design: an overview

Today the big challenges for the mould-making industry [92, 93] are the capability to:

- Produce better and cheaper tools
- Faster delivery of tools
- Produce tools for small batch size in an economical way
- Produce tools for increasingly complex plastic parts

These challenges require new approaches to the design and manufacture of injection moulds.

2.3.1- The new trends

To cope with those challenges the mouldmaking industry has been introducing new manufacturing techniques, such as the High Speed Machining (HSM), Rapid Prototyping (RP)

and the Electro-Discharge Machining (EDM). At the same time new computer techniques have been introduced, such as Computer Aided Design (CAD), Computer Aided Machining (CAM), Computer Aided Engineering (CAE) and Computer Numerical Control (CNC).

The introduction and implementation of those techniques implies capital intensive investments. In 1998 the Portuguese mouldmaking industry invested about 11% of its total volume sales [1].

In order to spread the cost involved on the mould design and manufacture it is necessary to produce very large batches of parts. However the changing market conditions brings new constraints such as the request for a greater variety of parts and shorter production series, that imply cheaper moulds.

In the cycle of the development of a new product, the design process of the mould is an essential task. Too long the development time of the mould will delay the product launch, which may cause the loss of a market opportunity. Therefore for a injection moulder it is essential to obtain a good mould right at the first time [94].

The involvement of the injection moulder on the early stages of a new product design process can increase the manufacturing feasibility and also input ideas to develop a better quality mould.

2.3.2- Computer aided mould design

The general character of the mould design for injection moulding of polymers, is still an experience based activity. However, in the last decades efforts have been made to make mould design a engineering activity based on found theoretical bases and relying on experience proved principles.

In the diagram shown in figure 2.8, Pouzada and co-workers [95] propose an overview of the main stages of the whole process of developing a plastic part where the design of the mould plays an important role. The concurrent nature of this design process is helped by the systematic used of computer aided tools (CAD/CAE/CAM) and rapid prototyping/rapid tooling techniques.

The CAD/CAE software can be used to achieve a decisive improvement in mould design, to optimise the process and, above all, to improve and speed up the design of injection moulds [96]. Those softwares are very important to predict defects which may occur during the injection moulding process, such as those deriving from the unfilled mould or the excessive pressure. The

prediction of the localisation of the weld lines or air traps, and helping the mould-maker in designing a good gate system and impression shape are other advantages when the CAD/CAE softwares are used in the mould design. However, to derive automatically the dimensions and shape of the impression it is necessary to compensate the impression geometry for shrinkage. The implementation of this feature is very weak even for the best CAD/CAE/CAM systems due the difficulty to predict the shrinkage, as was mentioned in the section 2.2.

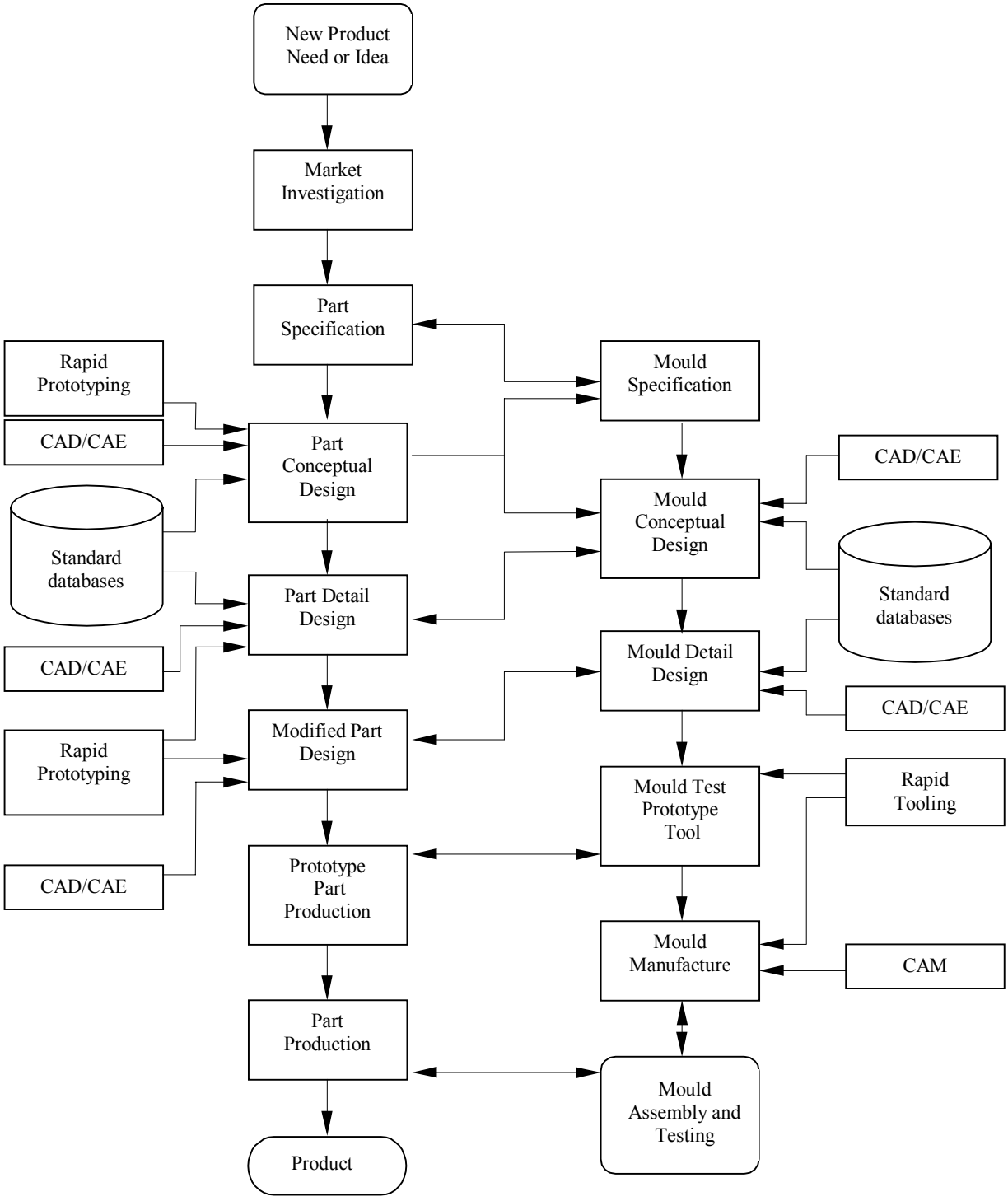

Figure 2.8- Concurrent engineering in the design of injection plastic parts and moulds [95]

2.3.3- Ejection system design

Once the mould cavity and gating system are designed, the mouldmaker still has to define the cooling system, guide system and ejection system. The ejection system may require a more precise design when, for example, the parts have long ejection paths, or high ejection forces resulting from the excessive rigidity or shrinkage of some thermoplastics.

The ejector pins must work safely and precisely, and must be applied principally on ribs and side panels. These design details, that are introduced to increase the rigidity of the part, make the ejection difficult.

The ejection system may cause deformations, marks, or even breakage of the part. To avoid these damaging or catastrophic effects it is necessary to optimise the number, location and dimensions of the ejector pins and air vents [97].

Normally the ejector pins cause a vestige in the part. In some products this is not acceptable and thus it will be necessary to pay especial attention to the design of the ejector system. When lower viscosity materials are used, attention must be paid to the adjustment and tolerancing of the ejection pins, to prevent flashing.

The ejection system is traditionally designed based on experience, and ejector pins are majority used. Some good practice to design the layout of the ejector pins may be found in literature [98,99].

Only a few research studies can be found in the literature on the design of the ejection systems that make use of ejector pins. The most interesting studies were done by Wang, H. *et al.* [100,101] and Wang, Z. *et al.* [97] were different layouts of the ejector pins were considered to examine the effect of the number, location and size of the pins on the ejection.

Considering the aspects associated to the ejection system during the mould design stage will contribute to an earlier start of the automatic production of a large run of products. One of the aspects that frequently must be sorted out is the estimation of the ejection forces as it will be dealt with in the next section.

2.3.3.1- Variables affecting the ejection force

During injection moulding the material solidifies until the product has achieved sufficient rigidity to be ejected from the mould. The solidification of the polymer causes it to shrink inside the mould and internal stresses to build up [*e. g.* 102,103]. In the case of some specific shapes (boxes, cylinders) the shrinkage is partially restricted by the mould. The plastic moulding shrinks against the core, inserts or pins, and thus, upon ejection, it will be necessary to overcome the frictional forces resulting from the shrinkage. This aspect has significant implications in the mechanical design of the injection moulds especially when deep cavities are involved.

In the design of such moulds, the accurate prediction of the ejection force may contribute to a more precise and economically efficient decision of the ejection system. In fact, if the designer knows the ejection force likely to occur during the moulding ejection, he will be able to make a proper decision for a less complex and cheaper ejection system: mechanical, pneumatic, or hydraulic [98,99].

Normally the ejection system must overcome the following resistance forces [104-107]:

- the frictional and adhesive forces generated in the mould-part interface;
- the vacuum force generated by the atmospheric pressure not acting between the mould and the part during ejection;
- the friction forces between the components of the ejection system, depending mainly on the tribological features of the system.

The frictional forces in the mould-part interface are normally the more intense to be overcome by the ejection system. Kaminski [104,105] indicates many causes to the rising of forces during the ejection. In general, the ejection force is regarded as the result of the interaction between part geometry, mould geometry and material, moulding material and processing conditions.

Malloy *et al.* [107,108] studied the influence of some processing conditions on the ejection force of a edge gated box shaped moulding. They verified experimentally that the ejection force increases with the cooling time and with the roughness of the mould wall. These studies showed that the coefficient of friction between the part and the mould core does have a significant influence on the ejection process.

Wang H. *et al.* [106] analysed the effect of injection temperature and the cooling time in the ejection force of small boxes (122×50×27 mm) of PS and HDPE. These results show a behaviour different from other works [104,107]. At a given injection temperature the ejection force decreases and then increases with the increasing cooling time. These results suggested the existence of an optimal cooling time when the ejection force is lower. As the melt temperature increases, the optimal cooling time tends to shift towards a longer time. The mechanisms proposed by Wang *et al* [106] relate the ejection force with warpage (that decreases with the cooling time) and with the dependence of material stiffness on temperature (that increases when temperature decreases).

The influence of the geometry of cylindrical injection moulded tubes (thickness, diameter, length and draft angle of the moulding) on the ejection force was investigated by Shen *et al.* [109]. In their work, the ejection force was measured using a tensile testing machine. After the mould opening the core was removed from the mould with the moulding still in place, and installed on a tensile testing machine. The ejection force was measured by pulling the core out of the moulding. In spite of the method to measure the ejection force being likely to lead to some errors in the measurements and instabilities on the process, the results suggest that the ejection force increases with the increment of the moulding thickness and diameter, and decreases with the increasing of the draft angle.

Sasaki *et al*. [110] studied the effect of the core roughness and injection pressure on the ejection force, to clarify the factors that causes it to increase. The experimental data shows that the general trend of the reduction of the ejection force with the roughness is inverted at low surface roughness level.

Pontes *et al.* [111] also reported for the case of PP the existence of an optimal surface roughness when the ejection force is lower. In their study a special mould that produces a lateral gated tube was used. However, the complex flow that is developed in the moulding, disk flow, make difficult the interpretation of the effect of the processing variables on the ejection force.

The effect of several types of coating were also investigated by Sasaki *et al.* [110] indicating that, in general, the coating films applied in the core wall reduce the ejection force even with low surface roughness levels.

2.3.3.2- Prediction of the ejection force

To operate successfully the ejection system must provide a balance ejection without damaging the moulding or the ejector components. For it, it is essential the estimation of the ejection forces.

One approach to predict the ejection force in simple geometries [104,107,112], such as sleeves, consists of calculating the ejection force by multiplying the contact pressure p_c acting on the core surface, the contact area, A_c, and friction coefficient (μ) at ejection time between the plastic-steel.

$$Fe = \mu.p_c.A_c \tag{2.2}$$

This methodology is embodied in the technical literature for mould design, e.g. Menges and Mohren [98].

An important factor in ejection is the static coefficient of friction between the plastic and metal surfaces in contact. Menges and Bangert [113] were the first that developed a suitable mould to measure the coefficient of static friction in identical conditions that occurs during the ejection. In their study it was demonstrated that the static coefficient of friction is greatly influenced by the surface roughness, contact temperature and some processing variables like cooling time, melt temperature and holding pressure.

Recently Wang, H. *et al.* [101], proposed an numerical approach to predict the ejection forces and to optimise the layout of ejector pins, based on thermal stress calculations [114]. Special attention was given to the proper modelling of the thermal condition during the injection moulding, namely to verify if the assumption of a constant mould temperature and "perfect contact condition" was valid.

2.4- Objectives of the work

In spite of the work done to make the mould design activity more structured and based on theoretical principles, aspects such as the definition of the impression dimensions and the ejection system design, which depend on a rigorous prediction of shrinkage still require further study. Thus, the main objectives of this work that aims at contributing to a more precise mould design activity are:

- To design an instrumented mould for the assessment of the processing variables associated to the ejection process and to monitor the ejection mechanism;
- To study the process of shrinkage in amorphous and in semi-crystalline thermoplastics (polycarbonate and isotatic polypropylene will be used as paradigms) in mouldings with a free shrinking geometry (rectangular plates) and a constrained shrinking geometry (cylindrical tubes);
- To monitor the shrinkage history in real moulding conditions;
- To model the shrinkage of mouldings in constrained shrinking conditions, namely over cylindrical cores;
- To develop a model for the prediction of the ejection force in deep core mouldings;
- To validate the shrinkage and ejection force models with experimental data obtained from the instrumented mould.

3- PREDICTION OF SHRINKAGE AND EJECTION FORCE

This chapter starts with a focused review of the theoretical principles associated to the shrinkage and the ejection forces in injection moulding. The main equations to predict the shrinkage in injection moulded plates are described according to the thermo-mechanical model developed by Titomanlio and Jansen [61,78].

Upon using the same thermo-mechanical approach, a model is developed for the shrinkage and the ejection forces in tubular injection mouldings.

The shrinkage of a injection moulded part was defined as

$$Sh_i = \frac{D_{imp} - D_{part}}{D_{imp}} \tag{2.1}$$

where D_{imp} is the dimension in the impression in i direction and D_{part} is the corresponding part dimension. According to this definition the shrinkage is positive when the part undergoes a negative strain, i.e. the following relationship applies

$$\mathrm{Sh_i} = -\varepsilon_{ii}^{obs}$$

where ε_{ii}^{obs} is the measured strain in the i direction

3.1- Thermo-mechanical model to predict the shrinkage of flat plates [1]

Consider a rectangular impression of a injection mould with the thickness 2B much smaller than the width, W, and the length, L. Let *z* denote the thickness co-ordinate, ranging from zero, at the surface, to B at the mid-plane, and let *x* and *y* be two mutually perpendicular directions in the plane of the impression (figure 3.1).

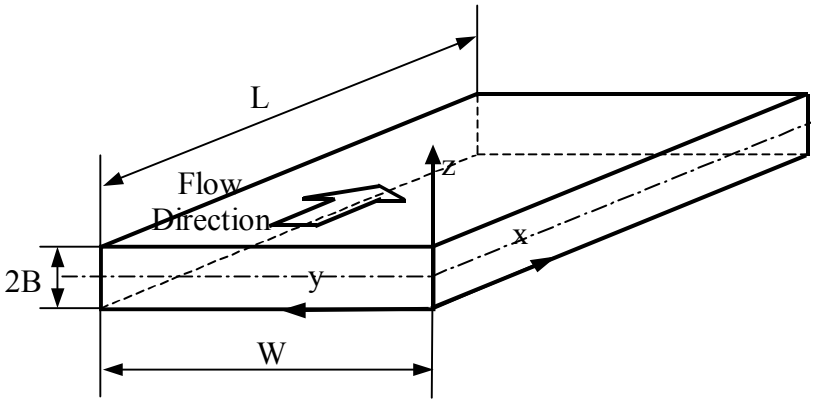

Figure 3.1- Perspective view of the impression and reference axis

It is considered that when the impression is completely filled (end of the injection phase), the holding phase begins. By simplicity it is also considered that the temperature distribution in the polymer is uniform across the flow direction (*y* direction) and the polymer solidifies in layers from the outer surfaces to the centre, at each moment and under a varying pressure.

The solidifying plate consists of two solid layers, with polymer melt between them. Considering the symmetry in relation to the centre, and a constant temperature in the across flow direction, the distance of the solid-melt interface to the wall will be constant at a fixed distance from the gate, as indicated by $z_s(x,t)$ (figure 3.2).

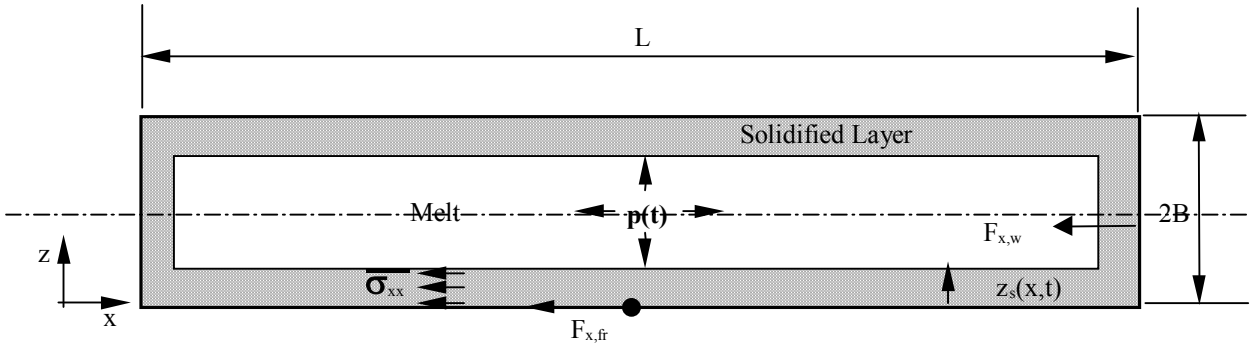

Figure 3.2- Schematic view of a cross-section of the solidifying plate

[1] This section reviews the model developed by Titomanlio and Jansen [61,78] for the prediction of the shrinkage.

The solid layers shrink uniformly in the flow and across flow directions, and are considered perfectly elastic. This assumption follows the consideration that the polymer cools so fast while passing its solidification temperature, T_s, that the relaxation processes can be neglected [83].

Considering σ_{zz}=-p(x,t) (the melt pressure is the only stress in the thickness direction), the Hooke's law can be written as:

$$\sigma_{xx} = \frac{\mathrm{E}}{1-\nu^2}\left[\varepsilon_{xx} + \nu\varepsilon_{yy}\right] - \frac{\nu}{1-\nu}\mathrm{p}$$

$$\sigma_{yy} = \frac{\mathrm{E}}{1-\nu^2}\left[\varepsilon_{yy} + \nu\varepsilon_{xx}\right] - \frac{\nu}{1-\nu}\mathrm{p} \qquad (3.1)$$

$$\sigma_{zz} = -\mathrm{p}$$

where

$$\varepsilon_{ii} = \varepsilon_{ii}^{obs} - \varepsilon_{ii}^{T} \qquad (3.2)$$

$\varepsilon_{ii}^{obs}(x,z,t) \Rightarrow$ observable strain ($\Delta L/L$)

$\varepsilon_{ii}^{T}(x,z,t) \Rightarrow$ thermal strain, given by

$$\varepsilon_{ii}^{T}(x,z,t) = \int_{T_s}^{T} \alpha.dT \cong \alpha\left(T - T_s\right)$$

with

$$\alpha = \frac{1}{3.\mathrm{v}(x,\mathrm{z},\mathrm{t})}\left(\frac{\partial \mathrm{v}}{\partial T}\right) \text{ (linear thermal expansion)}$$

The specific volume, v, is a function of pressure, temperature and crystallisation (if present).

Upon replacing these terms of the instantaneous strain in the equation 3.1 it is obtained for σ_{xx}

$$\sigma_{xx} = \frac{\mathrm{E}}{1-\nu^2}\left[\varepsilon_{xx}^{\mathrm{obs}} - \varepsilon_{xx}^{T} + \nu(\varepsilon_{yy}^{\mathrm{obs}} - \varepsilon_{yy}^{T})\right] - \frac{\nu}{1-\nu}\mathrm{p}$$

or, after reorganisation, and making $\varepsilon^{p}(x,t)$ the hydrostatic strain given by

$$\varepsilon^{P}(x,t) = -\int_{0}^{p} \beta.dp \cong -\beta.p$$

with

$$\beta = -\frac{1}{3\mathrm{v(x,z,t)}}\left(\frac{\partial \mathrm{v}}{\partial p}\right) \cong \frac{1-2\nu}{\mathrm{E}} \text{ (linear compressibility of the material),}$$

$$\sigma_{xx} = \frac{\mathrm{E}}{1-\nu^2}\left[\varepsilon_{xx}^{\mathrm{obs}} - \varepsilon_{xx}^{T} - \varepsilon^{p} + \nu(\varepsilon_{yy}^{\mathrm{obs}} - \varepsilon_{yy}^{T} - \varepsilon^{p})\right] - \mathrm{p} \tag{3.3}$$

More briefly this equation can be written as

$$\sigma_{xx} = S_{xx} - \mathrm{p} \tag{3.4}$$

where the function $S_{xx}(x,z,t)$ is

$$S_{xx} = \frac{\mathrm{E}}{1-\nu^2}\left[\varepsilon_{xx}^{obs} - \varepsilon_{xx}^{T} - \varepsilon^{p} + \nu(\varepsilon_{yy}^{obs} - \varepsilon_{yy}^{T} - \varepsilon^{p})\right] \tag{3.5}$$

As soon as the shrinkage starts in the flow direction, the average stress at the solidified layer must satisfy the force balance at the interface between the solid material and the mould, as shown in figure 3.2

$$\int_0^B \sigma_{xx}(x,z,t)dz = \int_{z=0}^{z_s(t)} S_{xx}(x,z,t).dz - (\mathrm{B} - z_s(t)).p(x,t) - z_s(t).p(x,t) = F_{x,w}(t) + F_{x.fr}(t)$$

or

$$\int_{z=0}^{z_s(t)} S_{xx}(x,z,t).dz = F_x(t) \tag{3.6}$$

with

$$F_x(t) = F_{w,x}(t) + F_{fr,x}(t) + \mathrm{B}.p(x,t)$$

The B.p(x,t) term actually consists of two parts, the first being the stretching force exerted by the melt, (B-z_s).p(x,t), and the second following from the definition of S_{xx} in equation 3.4. In these expression:

$F_{x,w}(t)$ - is the elastic response of the mould wall

$F_{x,fr}(t) = \mu\int_x^L p(x,t)dx$ - friction force in the flow direction

$F_{y,fr}(t) = \mu.p(x,t).\frac{W}{2}$ - friction force in the across flow direction

μ - coefficient of friction (considered as constant)

The force balance is evaluated at each time interval dt. For it, the Leibnitz's theorem is used to differentiate the equation 3.6 with respect to *t*

$$\frac{d}{dt}\int_{z=0}^{z_s(t)} S_{xx}(x,z,t).dz = \int_{z=0}^{z_s(t)} \dot{S}_{xx}(x,z,t).dz + S_{xx}(x,z_s,t).\dot{z}_s = \dot{F}_x(t)$$

From hereon, the dot denotes the derivative with respect to time, defined as:

$$\dot{f}(x,t) = \frac{\partial f(x,t)}{\partial t}$$

The function $S_{xx}(x,z_s,t)$ is the stress without the pressure contribution (equation 3.4). At the solid-melt interface it is zero. $\dot{S}_{xx}(x,z,t)$ results from differentiating S_{xx} in equation 3.5.

$$\dot{S}_{xx} = \frac{E}{1-\nu^2}\left(\dot{\varepsilon}_{xx}^{obs} + \nu\dot{\varepsilon}_{yy}^{obs}\right) - \frac{E}{1-\nu}\left(\dot{\varepsilon}_{xx}^{T} + \dot{\varepsilon}^{p}\right) \tag{3.7}$$

or

$$\dot{S}_{xx} = \frac{E}{1-\nu^2}\left(\dot{\varepsilon}_{xx}^{obs} + \nu\dot{\varepsilon}_{yy}^{obs}\right) - \frac{E}{1-\nu}\left(\frac{1}{3.v}\dot{v}\right) \tag{3.8}$$

where

$$\dot{\varepsilon}_{xx}^{T} + \dot{\varepsilon}^{p} = \dot{\varepsilon}_{yy}^{T} + \dot{\varepsilon}^{p} = \alpha.\dot{T} - \beta.\dot{p} = \frac{1}{3.v}\dot{v}$$

Equations similar to equations 3.6 and 3.8 can be derived for the *y* direction by interchanging the subscripts *x* and *y*.

Since $\dot{\varepsilon}_{xx}(t)$ is not a function of the thickness co-ordinate (as a consequence of the assumption of uniform deformation of the solid layer), it can be obtained after differentiating the equation 3.6:

$$\int_{z=0}^{z_s(t)} \dot{S}_{xx}(x,z,t).dz = \dot{F}_x(t)$$

Upon replacing with equation 3.8 it results

$$\int_{z=0}^{z_s(t)}\left[\frac{\mathrm{E}}{1-\nu^2}\left(\dot{\varepsilon}_{xx}^{obs}+\nu\dot{\varepsilon}_{yy}^{obs}\right)-\frac{\mathrm{E}}{1-\nu}\left(\frac{1}{3.\mathrm{v}}\dot{\mathrm{v}}\right)\right].dz=\dot{F}_x(t)$$

or, after integration,

$$\frac{\overline{\mathrm{E}}}{1-\nu^2}\left(\dot{\varepsilon}_{xx}^{obs}+\nu\dot{\varepsilon}_{yy}^{obs}\right)-\frac{1}{1-\nu}\left(\overline{\mathrm{E}\frac{1}{3.\mathrm{v}}\dot{\mathrm{v}}}\right)=\frac{\dot{F}_x(t)}{z_s(t)} \tag{3.9}$$

The bar over the variables stands for averaging over the solidified layer thickness, $z_s(t)$. The average function is defined as

$$\overline{f}(x,t)=\frac{1}{z_s(t)}\int_{z=0}^{z_s(t)}f(x,z,t).dz$$

Now, $\dot{\varepsilon}_{xx}$ (t) can be obtained from equation 3.9 as

$$\dot{\varepsilon}_{xx}^{obs}=\frac{(1+\nu)}{\overline{\mathrm{E}}}\left(\overline{\mathrm{E}\frac{1}{3.\mathrm{v}}\dot{\mathrm{v}}}\right)+\frac{\dot{F}_x(t).(1-\nu^2)}{z_s(t).\overline{\mathrm{E}}}-\nu\dot{\varepsilon}_{yy}^{obs} \tag{3.10}$$

Equations similar to equations 3.9 and 3.10 can also be written for the *y* direction by interchanging the subscripts *x* and *y*. Substituting in to equation 3.10 the similar equation for $\dot{\varepsilon}_{yy}^{obs}$ it results

$$\dot{\varepsilon}_{xx}^{obs}=\frac{1}{\overline{\mathrm{E}}}\left(\overline{\mathrm{E}\frac{1}{3.\mathrm{v}}\dot{\mathrm{v}}}\right)+\frac{\dot{F}_x(t)-\nu\dot{F}_y(t)}{\mathrm{z_s}(t).\overline{\mathrm{E}}} \tag{3.11}$$

At the solidified fraction the general equation for the in-plane strain variation, is obtained by integrating the equation 3.11 from the solidification onset of a layer z, t_{sz}, to the instant $t > t_{sz}$

$$\varepsilon_{xx}^{obs}(x,y,z,t)\Big|_{t_{sz}}^{t}=\int_{t_{sz}}^{t}\left(\frac{1}{\overline{\mathrm{E}}}\left(\overline{\mathrm{E}\frac{1}{3.\mathrm{v}}\dot{\mathrm{v}}}\right)+\frac{\dot{F}_x(t)-\nu.\dot{F}_y(t)}{\mathrm{z_s}(t).\overline{\mathrm{E}}}\right).dt \tag{3.12}$$

The stress component $S_{xx}(x,y,z,t)$ is obtained by integration over time of the stress rate defined in equation 3.8.

$$S_{xx}=\int_{t_{sz}}^{t}\left\{\frac{\mathrm{E}}{1-\nu^2}\left(\dot{\varepsilon}_{xx}^{obs}+\nu\dot{\varepsilon}_{yy}^{obs}\right)-\frac{\mathrm{E}}{1-\nu}\left(\frac{1}{3.\mathrm{v}}\dot{\mathrm{v}}\right)\right\}.dt \tag{3.13}$$

The strain variation $\varepsilon_{xx}^{obs}\Big|_{t_{s0}}^{t}$ is constant through the thickness in the interval $[t_{s0},t]$ and gives the local strain variation in the flow direction at the solid layer. At the start of solidification, $t_{s0,}$ the

reference dimensions coincide with the impression dimensions of the mould. Thus, the local shrinkage, $Sh_x(x,y,t)$, with respect to the mould dimensions coincides with $\varepsilon_{xx}^{obs}\Big|_{t_{s0}}^{t}$.

In the case of the solidified layer the shrinkage of the part in the *x* and *y* directions is calculated through the integration of the local shrinkage of the part

$$\mathrm{Sh}_x(y,t) = \left(\frac{1}{\mathrm{L}} \int_0^{\mathrm{L}} \mathrm{Sh}_x(x,y,t).dx \right) \tag{3.15a}$$

$$\mathrm{Sh}_y(x,t) = \left(\frac{1}{\mathrm{W}} \int_0^{\mathrm{W}} \mathrm{Sh}_y(x,y,t).dy \right) \tag{3.15b}$$

It is useful that several special cases are analysed as a result of the model. The superscript in the shrinkage refers to the special cases that will be analysed. The shrinkage function will be calculated under the assumption that the modulus of the polymer is taken as constant.

3.1.1– Thickness shrinkage

The part is allowed to shrink in the thickness direction as soon as the pressure in the impression vanishes The amount of material in the mould remains constant. Therefore, the onset of the thickness shrinkage, t_z^*, is defined by the condition:

$$p(t_z^*)=0$$

The strain in the thickness direction for the solid layers is obtained from the Hooke's law considering that $\sigma_{zz} = -\mathrm{p}$, whereas for the molten part it results from the effect of the volume shrinkage:

for the solid part
$$\varepsilon_{zz,solid}^{obs} = \frac{1+\nu}{1-\nu} \int_{t_z^*}^{t} \left(\frac{1}{3.\mathrm{v}} \dot{\mathrm{v}} \right) dt - \frac{\nu}{1-\nu} \left(\dot{\varepsilon}_{xx}^{obs} + \dot{\varepsilon}_{yy}^{obs} \right) \Big|_{t_z^*}^{t} \tag{3.16a}$$

for the molten part
$$\varepsilon_{zz,molten}^{obs} = \int_{t_z^*}^{t} \left(\frac{1}{3.\mathrm{v}} \dot{\mathrm{v}} \right) dt \tag{3.16b}$$

The thickness shrinkage $\mathrm{Sh}_z(x,t)$ is obtained by integrating $\varepsilon_{zz}^{obs}(x,y,z,t)$ from the surface of the plate to its mid-plane; and considering the contribution of the elastic deformation of the mould.

$$\mathrm{Sh}_z(x,t) = -\frac{1}{\mathrm{B}}\left(\int_0^{z_s} \varepsilon_{zz,solid}^{obs}.dz + \int_{z_s}^{B} \varepsilon_{zz,molten}^{obs}.dz\right) - C_M.p_{gf} \tag{3.17}$$

The term $C_M.p_{gf}$, gives the contribution to the relative thickness variation of the as-moulded product due to the mould deformation. p_{gf} is the pressure distribution inside the impression at the instant of the gate solidification. C_M is a constant that is related to the rigidity of the mould, which has dimensions of a compliance (usually of the order of 1 GPa^{-1}) and is given by:

$$\mathrm{C_M} = \frac{\mathrm{k}_M}{2.\mathrm{B.E}} \tag{3.18}$$

where

k_M = 428 mm for the mould that produces the edge gated plates (as from [90]);

E - elastic modulus of the mould material (typically 210 GPa, for steel);

B - half thickness of the impression.

The value of C_M to be added in the thickness shrinkage predictions of the plates is of 1 GPa^{-1} for a 2 mm thick moulding and of 0.5 GPa^{-1} for a 4 mm thick moulding.

3.1.2– Flow direction shrinkage

In this case it is assumed that no shrinkage takes place in the thickness and in the across flow directions until ejection, shrinkage occurring in the flow direction before ejection. The onset of the longitudinal shrinkage, t_x^*, follows from the force balance (equation 3.6). Before the shrinkage onset the sum of $F_{x,fr}(t)$ and $B.p(x,t)$ is larger than the integral over $S_{xx,}$ and the difference is transmitted to the mould wall ($F_{x,w}(t)$ <0). At the longitudinal shrinkage onset, $F_{x,w}$ vanishes.

During the longitudinal shrinkage ($t>t_x^*$), the equation 3.12 is used to describe the shrinkage evolution.

$$\varepsilon_{xx}^{obs}(x,t)\Big|_{t_x^*}^{t} = \int_{t_x^*}^{t}\left(\overline{\frac{1}{3.\mathrm{v}}\dot{\mathrm{v}}} + \frac{\dot{F}_x(t) - \nu.\dot{F}_y(t)}{\mathrm{z_s}(t).\overline{\mathrm{E}}}\right).dt \tag{3.19}$$

3.1.3– Constrained shrinkage

This case considers the situation where, during injection moulding, the part is completely constrained during its solidification either due to the friction between polymer and moulding surface or to geometrical effects. At the instant of ejection all external forces acting in the three spatial directions are suddenly released making the part free to shrink.

In this case the part can not shrink over the thickness and in the plane directions while it is in the mould. Thus there is no shrinkage inside the mould, this implying that

$$\varepsilon_{xx}^{obs} = \varepsilon_{yy}^{obs} = \varepsilon_{zz}^{obs} = 0$$

The equation 3.19 can be applied here, provided that the time t_x^* is substituted by the ejection time, t_e. The integral of external forces at ejection time, t_e, can be calculated using the equation 3.11 from the start of solidification, $t_{s0,}$ until the ejection time, t_e. Therefore, the in-plane shrinkage after ejection ($t>t_e$) is given by:

$$\varepsilon_{xx}^{obs}(x,t) = \int_{t_e}^{t}\overline{\left(\frac{1}{3.\mathrm{v}}\dot{\mathrm{v}}\right)}.dt + \frac{F_x(t_e) - \nu.F_y(t_e)}{\mathrm{z_s}(t_e).\overline{\mathrm{E}}} = \int_{t_e}^{t}\overline{\left(\frac{1}{3.\mathrm{v}}\dot{\mathrm{v}}\right)}.dt + \int_{t_{s0}}^{t_e}\overline{\left(\frac{1}{3.\mathrm{v}}\dot{\mathrm{v}}\right)}.dt$$

or, after integration

$$\varepsilon_{xx}^{obs}(x,t) = \frac{1}{3}\overline{\ln\left(\frac{\mathrm{v}(x,z,t)}{\mathrm{v_s}(x,z)}\right)} \tag{3.20}$$

The function $v_s(x,z)$ is the specific volume at the moment of solidification.

The thickness shrinkage can be obtained using the equation 3.20 in equations 3.16a and 3.17:

$$\mathrm{Sh}_z^{\mathrm{sh0}}(x,t) = -\frac{1+\nu}{1-\nu}\frac{1}{3}\overline{\ln\left(\frac{\mathrm{v}(x,z,t)}{\mathrm{v}(x,z,t_z^*)}\right)} + \frac{2\nu}{1-\nu}\frac{1}{3}\overline{\ln\left(\frac{\mathrm{v}(x,z,t)}{\mathrm{v_s}(x,z)}\right)} - C_M.p_{gf} \tag{3.21}$$

If a residual pressure is present the specific volume at the onset of thickness shrinkage, $v(x,z,t_z^*)$, is changed to specific volume just before ejection, $v(x,z,t_e)$. Therefore, the thickness shrinkage equation contains a term that takes into account the material expansion due to residual pressure.

3.2- The case of cylindrical tubes

Using the same reasoning followed by Titomanlio and Jansen (as reviewed in the previous section) to develop the thermo-mechanical model for the shrinkage and internal stresses in injection moulded rectangular flat plates, a model will be next developed to predict the shrinkage and the ejection forces in tubular parts moulded over a cylindrical core.

3.2.1- Stress field before ejection

Consider a thin tube of thickness H, that is cooled from the inside and the outside. Let *r* be the radial co-ordinate, ranging from R_0 at the internal surface to R_1 at the external surface, θ the angular co-ordinate and *x* the longitudinal co-ordinate of the tube (figure 3.3).

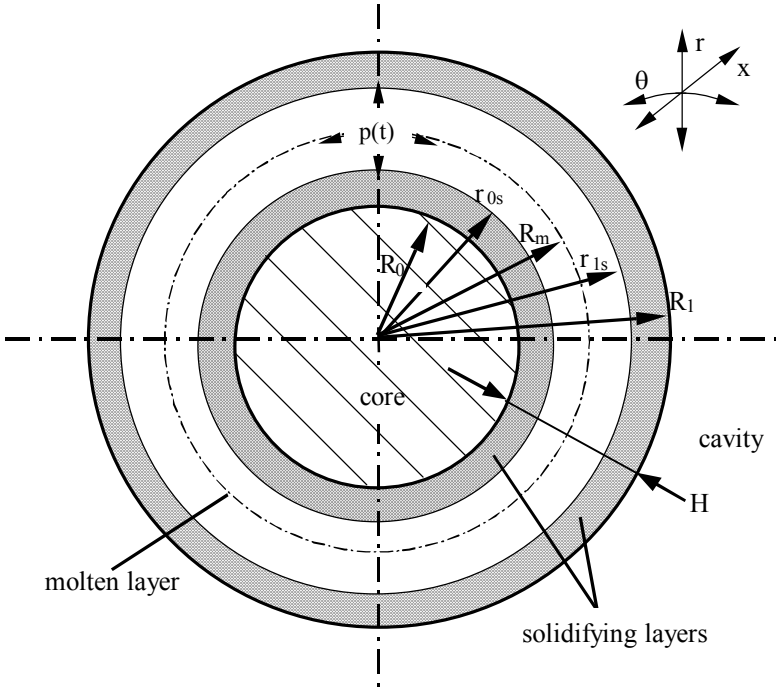

Figure 3.3- Schematic cross-section of the solidifying tube.

As it was considered for the solidifying plate, the solidifying tube consists of two solid layers, with molten polymer between them. It is assumed that there is symmetry in relation to the R_m (average radius) and a constant temperature profile in the tangential direction (across flow). The positions of the solid-melt interfaces are indicated as $r_{0s}(r,t)$ and $r_{1s}(r,t)$, at each instant before complete solidification.

Assumptions

Further to the assumption of solidification symmetry with respect to the average radius, the following assumptions will be considered:

1. Continuity of stress and strain at the solid-melt interface;
2. The tangential stress, $\sigma_{\theta\theta}$, at any radial position is constant as resulting from the symmetry;
3. The radial stress, σ_{rr}, is independent from the radial co-ordinate, *r*;
4. The shear components can be neglected in the solidified layer ($\tau_{\theta x}=\tau_{xr}=\tau_{\theta r}=0$ and $\gamma_{\theta x}=\gamma_{xr}=\gamma_{\theta r}=0$).
5. The deformation of the solidified layer is uniform (the deformation in the θ and x directions do not depend on r)
6. No out of plane deformation occurs during solidification.
7. The solid polymer is elastic, whereas the melt is considered unable to withstand relevant tensile stresses [83,115].
8. The frozen-in flow-induced stresses can be neglected (flow-induced stresses are typically one order of magnitude lower than the thermal-pressure induced stresses [82]).
9. Temperature, pressure, position of solid-melt interface and crystallisation status are known at each instant.

The stresses σ_{ii} and strains ε_{ii} (i= *x*, *θ*, *r)* can be obtained in cylindrical co-ordinates, in the same way as it was done for the plates (section 3.1) by substituting the subscripts *x*, *y* and *z* by *x*, *θ* and *r*, respectively [*e.g.* 116 or 117].

Accordingly the stress components for the solid layer can be written as

$$\sigma_{xx} = \frac{E}{1-\nu^2}\left[\varepsilon_{xx} + \nu\varepsilon_{\theta\theta}\right] - \frac{\nu}{1-\nu}p(x,t)$$

$$\sigma_{\theta\theta} = \frac{E}{1-\nu^2}\left[\varepsilon_{\theta\theta} + \nu\varepsilon_{xx}\right] - \frac{\nu}{1-\nu}p(x,t) \qquad (3.22)$$

$$\sigma_{rr} = -p(x,t)$$

or, more briefly

$$\sigma_{xx} = S_{xx}(x,r,t) - \mathrm{p(x,\ t)}$$

$$\sigma_{\theta\theta} = S_{\theta\theta}(x,r,t) - p(\mathrm{x,\ t}) \tag{3.23}$$

$$\sigma_{rr} = -p(\mathrm{x,\ t})$$

where

$$S_{xx} = \frac{\mathrm{E}}{1-\nu^2}\left(\varepsilon_{xx}^{obs} + \nu\varepsilon_{\theta\theta}^{obs}\right) - \frac{\mathrm{E}}{1-\nu}\left(\varepsilon_{xx}^{T} + \varepsilon^{p}\right)$$

$$S_{\theta\theta} = \frac{\mathrm{E}}{1-\nu^2}\left(\varepsilon_{\theta\theta}^{obs} + \nu\varepsilon_{xx}^{obs}\right) - \frac{\mathrm{E}}{1-\nu}\left(\varepsilon_{\theta\theta}^{T} + \varepsilon^{p}\right) \tag{3.24}$$

$$S_{rr} = 0$$

The strain field is described in terms of a observable strain, a thermal dependent strain and a pressure dependent strain:

$$\varepsilon_{ii} = \varepsilon_{ii}^{obs} - \varepsilon_{ii}^{T} - \varepsilon^{p} \tag{3.25}$$

All the components of the strain are dependent on the co-ordinate x and on time, t.

The strains are related to the displacements in the radial direction, *u,* and in the longitudinal direction, *w*, in the following way:

$$\varepsilon_{rr}^{obs}(x,r,t) = \frac{du}{dr}$$

$$\varepsilon_{\theta\theta}^{obs}(x,r,t) = \frac{u}{r}$$

$$\varepsilon_{xx}^{obs}(x,r,t) = \frac{dw}{dr}$$

The thermal strain is given by

$$\varepsilon_{ii}^{T}(x,r,t) = \int_{T_s}^{T} \alpha.dT \cong \alpha\left(T - T_s\right)$$

with

$$\alpha = \frac{1}{3.\mathrm{v}(x, \mathrm{z}, \mathrm{t})}\left(\frac{\partial \mathrm{v}}{\partial T}\right) \text{ (linear thermal expansion)}$$

The specific volume is a function of pressure, temperature and crystallisation (if present).

Finally the hydrostatic strain that is dependent on pressure is given by

$$\varepsilon^{P}(x,t) = -\int_{0}^{p} \beta.dp \cong -\beta.p$$

where the linear compressibility of the material is.

$$\beta = -\frac{1}{3\mathrm{v}(\mathrm{x},\mathrm{z},\mathrm{t})}\left(\frac{\partial \mathrm{v}}{\partial p}\right) \cong \frac{1-2\nu}{\mathrm{E}}$$

The stress distribution is evaluated after each time interval dt. After differentiation of equation 3.24 with respect to time it results:

$$\dot{S}_{\theta\theta} = \frac{\mathrm{E}}{1-\nu^{2}}\left(\dot{\varepsilon}_{\theta\theta}^{obs} + \nu\dot{\varepsilon}_{xx}^{obs}\right) - \frac{\mathrm{E}}{1-\nu}\left(\frac{1}{3.\mathrm{v}}\dot{\mathrm{v}}\right) \tag{3.26}$$

The dot denotes derivation with respect to time, and

$$\dot{\varepsilon}_{xx}^{T} + \dot{\varepsilon}^{p} = \dot{\varepsilon}_{\theta\theta}^{T} + \dot{\varepsilon}^{p} = \alpha.\dot{T} - \beta.\dot{p} = \frac{1}{3.\mathrm{v}}\dot{\mathrm{v}}$$

During the solidification process inside the mould, the moulding will be considered as constrained in the flow direction (zero shrinkage in the mould). However, it is allowed to shrink in the thickness direction as soon as the pressure measured in the cavity side vanishes.

The strain in the thickness direction, as derived from the Hooke's law, and considering $\sigma_{rr} = -p(\mathrm{x},\mathrm{t})$ is given by

$$\varepsilon_{rr}^{obs} = \frac{1+\nu}{1-\nu}\left(\frac{\partial \mathrm{v}}{3.\mathrm{v}}\right) - \frac{\nu}{1-\nu}\left(\varepsilon_{\theta\theta}^{obs} + \varepsilon_{xx}^{obs}\right) \tag{3.27}$$

The through thickness shrinkage must evaluated as from its onset at $t=t_r^*$.

t_r^* is determined from the condition:

$$p(t_r^*) = 0$$

The through thickness shrinkage until ejection is determined by considering the strains in both solid (equation 3.27) and molten layers

(solid) $$\varepsilon_{rr,solid}^{obs} = \frac{1+\nu}{1-\nu}\int_{t_r^*}^{t_e}\frac{1}{3\mathrm{v}}\dot{\mathrm{v}}dt - \frac{\nu}{1-\nu}\left(\varepsilon_{\theta\theta}^{obs} + \varepsilon_{xx}^{obs}\right)\Bigg|_{t_r^*}^{t_e}$$

(molten) $$\varepsilon_{rr,molten}^{obs} = \int_{t_r^*}^{t_e}\frac{1}{3\mathrm{v}}\dot{\mathrm{v}}.dt$$

At the start of thickness shrinkage, t_r^*, the reference dimensions coincide with the mould dimensions. Considering symmetry in relation to the average radius (R_m) the thickness shrinkage $Sh_r(x,t)$ is obtained by integrating $\varepsilon_{rr}^{obs}(x,r,t)$ from the internal surface, R_0, of the tube to its average radius, R_m:

$$\mathrm{Sh_r}(x,t)\Big|_{t_r^*}^{t_e} = -\frac{1}{\mathrm{R_m - R_0}}\left(\int_{R_0}^{r_{0s}}\varepsilon_{rr\ solid}^{obs}.dr + \int_{r_{0s}}^{R_m}\varepsilon_{rr\ melt}^{obs}.dr\right)\Bigg|_{t_r^*}^{t_e} \tag{3.28}$$

The shrinkage in the thickness direction causes strain changes in the tangential direction (figure 3.4).

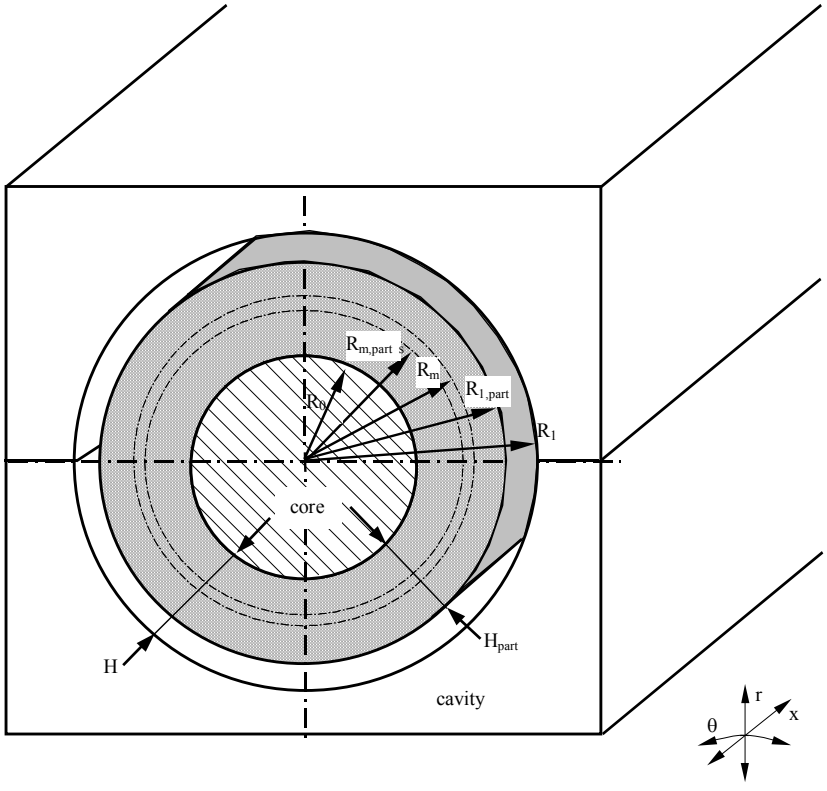

Figure 3.4- Schematic cross-section of part shrinking inside the mould

After t_r^* the cross section dimensions of the shrinking part will be dependent on time, as follows:

External radius $R_{1,part}(t) < R_1$

Average radius $R_{m,part}(t) = \frac{R_{1,part}(t) + R_0}{2} < R_m$

Internal radius R_0=constant

and

Part thickness $H_{part}(t) = R_{1,part}(t) - R_0 < R_1 - R_0 = H$

where

H is the thickness of the impression

Thus the tangential strain at each moment is

$$\varepsilon_{\theta\theta}^{obs} = -\frac{\pi.R_m - \pi.R_{m,part}}{\pi.R_m} = -\frac{R_1 + R_0 - R_{1,part} - R_0}{R_1 + R_0} = -\frac{R_1 - R_{1,part}}{2.R_m} \qquad 3.29$$

and the thickness shrinkage

$$\varepsilon_{rr}^{obs} = -Sh_r = -\frac{H - H_{part}}{H} = -\frac{R_1 - R_0 - R_{1,part} + R_0}{H} = -\frac{R_1 - R_{1,part}}{H} \qquad 3.30$$

Substituting the equation 3.30 in equation 3.29, the relation between the shrinkage in the thickness direction and the strain changes in the tangential direction at each moment are related by:

$$\varepsilon_{\theta\theta}^{obs}(x,t) = \frac{\mathrm{H}}{2.R_m}\varepsilon_{rr}^{obs}(x,t)$$

Consequently, from the shrinkage onset, t_r^*, until ejection

$$\varepsilon_{\theta\theta}^{obs}(x,t)\Big|_{t_r^*}^{t_e} = -\mathrm{Sh}_r(x,t)\Big|_{t_r^*}^{t_e}\frac{\mathrm{H}}{2.R_m} \qquad (3.31)$$

Considering that until ejection, $\dot{\varepsilon}_{xx}^{obs} = 0$, by integrating equation 3.26, over time from the moment of the solidification of the first layer, it results for the stress distribution before ejection:

$$S_{\theta\theta}(x,r,t) = -\int_{t_{s0}}^{t} \frac{E}{1-\nu}\frac{1}{3.v}\dot{v}.dt + \int_{t_t^*}^{t} \frac{E}{1-\nu^2}\varepsilon_{\theta\theta}^{obs}.dt \qquad (3.32a)$$

It must be noted that $\dot{\varepsilon}_{\theta\theta}^{obs} = 0$ as from the moment of solidification of the first layer,t_{s0}, until the start of thickness shrinkage, t_r^*.

An equation similar to equation 3.32a can be written for the *x* direction by interchanging the subscripts θ and *x*, and multiplying the observable strain $\varepsilon_{\theta\theta}^{obs}$ by the Poisson's ratio.

$$S_{xx}(x,r,t) = -\int_{t_{s0}}^{t} \frac{E}{1-\nu}\frac{1}{3.v}\dot{v}.dt + \int_{t_r^*}^{t} \frac{\nu.E}{1-\nu^2}\varepsilon_{\theta\theta}^{obs}.dt \qquad (3.32b)$$

3.2.2- Ejection force

Consider an element of the tube represented in figure 3.5. It is to remark that there is a slight variation in the diameter resulting from the draft angle, α, that mouldings of this type obligatory must have.

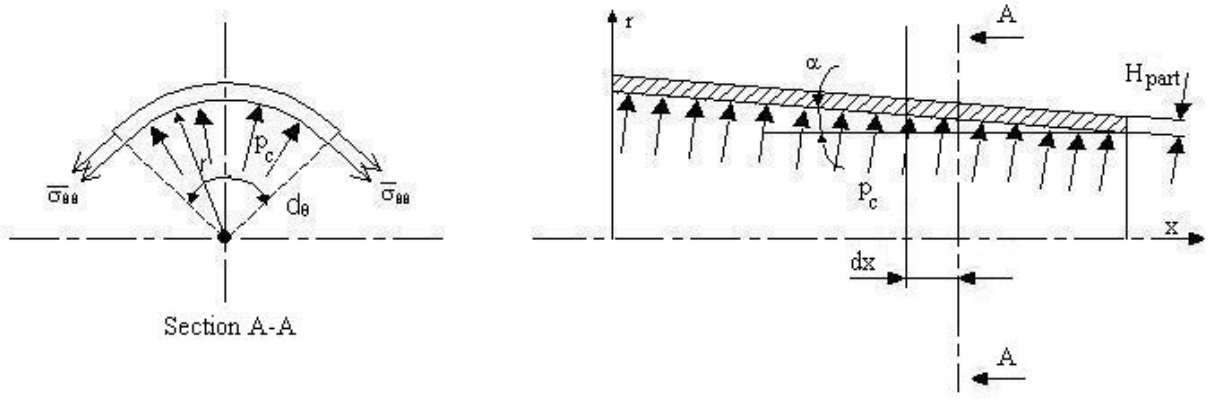

Figure 3.5- Diagram of force balance before ejection

At the instant of ejection there is a pressure field, p_c, acting in the internal surface of the tube.

Making the force balance in the radial direction, it results for a radial element of amplitude dθ and length dx, at the co-ordinate x:

$$\frac{p_c(x)}{\cos(\alpha)}.d\theta.r(x).dx - 2.\overline{\sigma_{\theta\theta}}(x,t_e).H_{part}.dx.\sin(\frac{d\theta}{2}) = 0$$

As $sin(\frac{d\theta}{2}) \approx \frac{d\theta}{2}$ it results

$$p_c(x) = \frac{\overline{\sigma_{\theta\theta}}(x,t_e).H_{part}.\cos(\alpha)}{r(x)} \tag{3.33}$$

When the tube is ejected from the mould core, as shown schematically in the figure 3.6, the ejection force, Fe, must overcome the friction force, μN (where μ is the coefficient friction which is considered here as a constant), generated by the contact pressure acting internally in the tube.

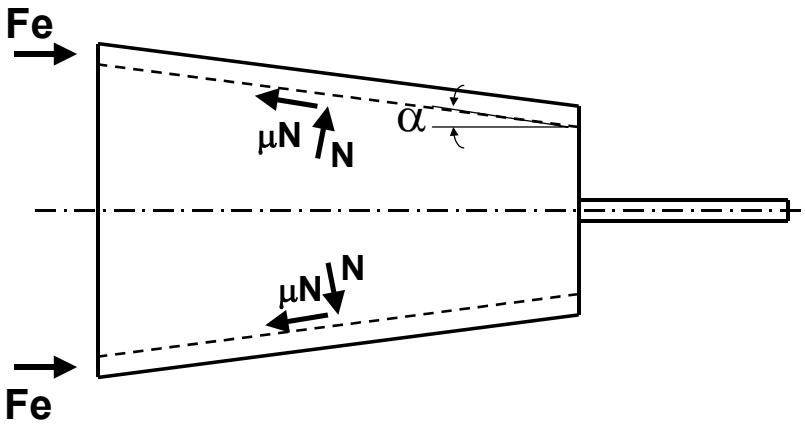

Figure 3.6- Free body diagram of the tube at ejection

The normal force, N, can be obtained by integrating the contact pressure over the total contact area between the tube and the core. Thus, considering that the draft angle is small, the ejection force can be calculated as

$$F_e = \mu \int p_c.dA \tag{3.34}$$

where dA is the elementary area of integration given by

$$dA = \frac{2.\pi.r(x).dx}{\cos(\alpha)} \tag{3.35}$$

Substituting into equation 3.34 the corresponding value of the elementary area (equation 3.35) where the contact pressure is applied and its corresponding function (equation 3.33), it results

$$F_e = 2.\pi.\mu.H_{part}.\int_o^L \overline{\sigma_{\theta\theta}}(x,t_e).dx \tag{3.36}$$

The average tangential stress before ejection, $\overline{\sigma_{\theta\theta}}(x,t_e)$, is obtained substituting in equation 3.32a the equation 3.31 and averaging it over the thickness. In this analysis it is considered that the modulus of the polymer is constant and equal to the modulus at the average ejection temperature, $E(\overline{T_e})$, and the melt pressure at ejection, $p(x,t_e)$, is zero. Thus

$$\overline{\sigma_{\theta\theta}}(x,t_e) = -\frac{E(\overline{T_e})}{1-\nu}\int_{t_{s0}}^{t_e}\overline{\frac{1}{3.v}\dot{v}}.dt - \frac{E(\overline{T_e})}{1-\nu^2}\frac{H}{2.R_m}Sh_r(t)\Big|_{t_r^*}^{t_e} \tag{3.37}$$

After integration

$$\overline{\sigma_{\theta\theta}}(x,t_e) = -\frac{E(\overline{T_e})}{1-\nu}\frac{1}{3}.\overline{\ln\left(\frac{v(x,r,t_e)}{v_s(x,r)}\right)} - \frac{E(\overline{T_e})}{1-\nu^2}\frac{H}{2.R_m}Sh_r(t)\Big|_{t_r^*}^{t_e} \tag{3.38}$$

The function $v_s(x,r)$ is the specific volume at the moment of solidification.

Substituting in equation 3.36 the equation 3.38 it follows that

$$F_e = \mu.\frac{2.\pi.H_{part}}{1-\nu}.E(\overline{T_e}).\int_o^L\left(-\frac{1}{3}.\overline{\ln\left(\frac{v(x,r,t_e)}{v_s(x,r)}\right)} - \frac{H}{(1+\nu).2.R_m}Sh_r(t)\Big|_{t_r^*}^{t_e}\right).dx \tag{3.39}$$

The expression 3.39 indicates that the ejection force is directly dependent on the elastic modulus at ejection temperature, the coefficient of friction (considered here as a constant), the thickness of the part and the variation of the (average) volume shrinkage between solidification and the ejection time.

The last term inside the integral is included if the tube shrinks in the thickness direction. This may happen for lower holding pressures or times leading to the reduction of the force required to eject the part.

3.2.3- Post ejection shrinkage

To calculate the as-moulded diametrical shrinkage, the shrinkage process will be split in four phases, figure 3.7:

1. From t=0 until the onset of thickness shrinkage $t=t_r^*$
2. From $t=t_r^*$ until the beginning of ejection $t=t_e$
3. From $t=t_e$ until the moment just after ejection $t=t_e'$
4. From $t=t_e'$ until the $t>t_e'$

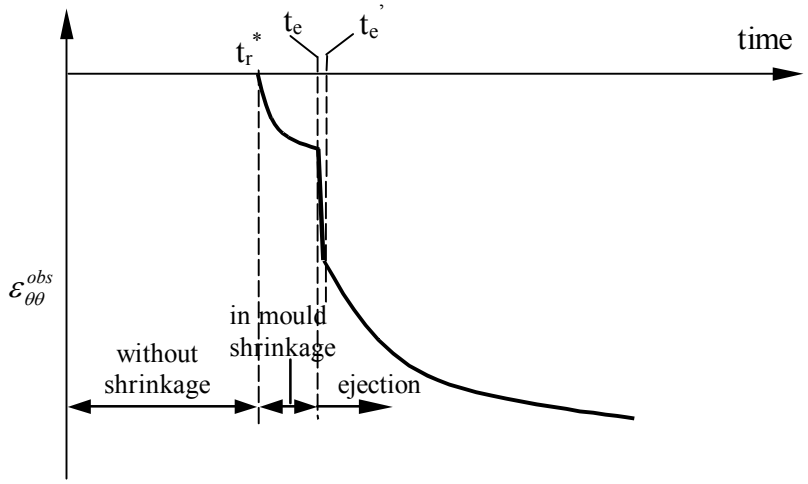

Figure 3.7- Schematic representation of the diametrical strain (shrinkage) evolution

1st phase ($0<t<t_r^*$)

In this phase there is no shrinkage inside the mould, and the moulding dimensions coincide with the impression. Thus

$$\varepsilon_{xx}^{obs} = \varepsilon_{\theta\theta}^{obs} = \varepsilon_{rr}^{obs} = 0$$

2st phase ($t_r^*<t<t_e$)

Provided the pressure of the moulding in the cavity reaches zero, the tube will shrink in the thickness direction. The $\varepsilon_{\theta\theta}^{obs}$ is calculated using the equation 3.31.

$$\varepsilon_{\theta\theta}^{obs}(x,t)\Big|_{t_r^*}^{t_e} = -Sh_r(x,t)\Big|_{t_r^*}^{t_e}\frac{H}{2.R_m}$$

During this process the external wall of the moulding moves away from the cavity wall.

3st phase ($t_e<t<t_e^{'}$)

This phase describes which happens during the short period of time after the beginning of ejection. In this analysis only the variation in the strain of the solid polymer is considered since it is supposed that the moulding is completely solidified at the moment of ejection At the end of ejection is considered that there are no external forces acting on the tube and thus $\overline{S}_{ii}(t_e^{'}) = 0$. If the ejection starts at the instant t = t_e, and the stresses just before ejection are given by $S_{ii}(r,t_e)$, the average stress change during the ejection process is $\Delta\overline{S}_{ii} = -\overline{S}_{ii}(t_e)$. Neglecting the transient effects of the thermal shrinkage during ejection (ΔT=0 during ejection) and substituting in equation 3.22 the equations 3.23 and 3.25, the following general expression for the variation of strain during ejection can be obtained:

$$\varepsilon_{\theta\theta}^{obs}(x,t)\Big|_{t_e}^{t_e^{'}} = \frac{1}{3}\int_{t_e}^{t_e^{'}} \overline{\frac{1}{\mathrm{v}}\dot{\mathrm{v}}}dt - \frac{1}{\mathrm{E}}\left[\overline{S}_{\theta\theta}(t_e) - \nu.\overline{S}_{xx}(t_e)\right] \tag{3.40a}$$

$$\varepsilon_{xx}^{obs}(x,t)\Big|_{t_e}^{t_e^{'}} = \frac{1}{3}\int_{t_e}^{t_e^{'}} \overline{\frac{1}{\mathrm{v}}\dot{\mathrm{v}}}dt - \frac{1}{\mathrm{E}}\left[\overline{S}_{xx}(t_e) - \nu.\overline{S}_{\theta\theta}(t_e)\right] \tag{3.40b}$$

$$\varepsilon_{rr}^{obs}(x,t)\Big|_{t_e}^{t_e^{'}} = \frac{1+\nu}{1-\nu}\frac{1}{3}\int_{t_e}^{t_e^{'}} \overline{\frac{1}{\mathrm{v}}\dot{\mathrm{v}}}dt - \frac{\nu}{1-\nu}\left(\varepsilon_{\theta\theta}^{obs} + \varepsilon_{xx}^{obs}\right)\Big|_{t_e}^{t_e^{'}} \tag{3.40c}$$

Averaging the stress distribution of equations 3.32a and 3.32b and substituting in equations 3.40, it results for the variation of the strain during ejection:

$$\varepsilon_{\theta\theta}^{obs}(x,t)\Big|_{t_e}^{t_e^{'}} = \frac{1}{3}\overline{\ln\left(\frac{\mathrm{v}(x,t_e^{'})}{\mathrm{v}_s(x)}\right)} + \frac{\mathrm{H}}{2.R_m}Sh_r(t)\Big|_{t_r^*}^{t_e} \tag{3.41a}$$

$$\varepsilon_{xx}^{obs}(x,t)\Big|_{t_e}^{t_e^{'}} = \frac{1}{3}\overline{\ln\left(\frac{\mathrm{v}(x,t_e^{'})}{\mathrm{v}_s(x)}\right)} \tag{3.41b}$$

$$\varepsilon_{rr}^{obs}(x,t)\Big|_{t_e}^{t_e^{'}} = \frac{1+\nu}{1-\nu}\frac{1}{3}\overline{\ln\left(\frac{\mathrm{v}(x,t_e^{'})}{\mathrm{v}(x,t_e)}\right)} - \frac{2\nu}{1-\nu}\frac{1}{3}\ln\left(\frac{\mathrm{v}(x,t_e^{'})}{\mathrm{v}_s(x)}\right) - \frac{\nu}{1-\nu}\frac{\mathrm{H}}{2.R_m}Sh_r(t)\Big|_{t_r^*}^{t_e} \tag{3.41c}$$

4th phase – from t=t'e until t>te'

The unconstrained shrinkage of the part in the tangential direction, t>te', after ejection from the mould can be calculated considering that:

- the material is free to shrink
- there are no pressure effects
- the average internal stress in the tangential direction is equal to zero, $\overline{S}_{\theta\theta}(t) = 0$.

The average internal stress, $\overline{S}_{\theta\theta}(t)$, is obtained averaging the equation 3.26 through thickness. The strain variation after ejection results from $\overline{S}_{\theta\theta}(t)$ becoming zero. Therefore

$$\varepsilon_{\theta\theta}^{obs}(x,t)\Big|_{t_e'}^{t} = \frac{1}{3}\int_{t_e'}^{t}\overline{\frac{1}{\mathrm{v}}\dot{\mathrm{v}}}.dt = \frac{1}{3}\overline{\ln\left(\frac{\mathrm{v}(x,t)}{\mathrm{v}(x,t_e')}\right)} \tag{3.42}$$

The total shrinkage of the average diameter is the sum of the following contributions:

i) the shrinkage from time 0 to t_r^* (which is zero in the case considered here),

ii) the thickness shrinkage, if exits, given by equations 3.28 and 3.31,

iii) the expansion (or shrinkage) during the ejection (equations 3.41),

iv) the shrinkage after ejection, which is unconstrained shrinkage.

Thus the final expressions for the diametrical and the thickness shrinkage are

(diametrical) $$Sh_{Dm}(x,t)\Big|_0^t = -\varepsilon_{\theta\theta}^{obs}(x,t)\Big|_{t_r^*}^{t_e} - \varepsilon_{\theta\theta}^{obs}(x,t)\Big|_{t_e}^{t_e'} - \varepsilon_{\theta\theta}^{obs}(x,t)\Big|_{t_e'}^{t} \tag{3.43}$$

(thickness) $$Sh_{r}(x,t)\Big|_0^t = -\varepsilon_{rr}^{obs}(x,t)\Big|_{t_r^*}^{t_e} - \varepsilon_{rr}^{obs}(x,t)\Big|_{t_e}^{t_e'} - \varepsilon_{rr}^{obs}(x,t)\Big|_{t_e'}^{t} \tag{3.44}$$

If the corresponding functions are replaced, the following final expressions result:

a) for the diametrical shrinkage

$$Sh_{Dm}(x,t)\Big|_0^t = -\frac{1}{3}\overline{\ln\left(\frac{\mathrm{v}(x,t)}{\mathrm{v}_s(x)}\right)} \tag{3.45}$$

b) for the thickness shrinkage

$$Sh_r(x,t)\Big|_0^t = -\frac{1+\nu}{1-\nu}\frac{1}{3}\overline{\ln\left(\frac{v(x,t)}{v(x,t_e)}\right)} + \frac{2\nu}{1-\nu}\frac{1}{3}\overline{\ln\left(\frac{v(x,t)}{v_s(x)}\right)} - \left(\frac{R_m - r_{0s}(t)}{R_m - R_0}\right)\frac{1}{3}\overline{\ln\left(\frac{v(x,t}{v(x,t_r^*)}\right)}\Bigg|_{t_r^*}^{t_e} - C_M.p_{gf}$$

(3.46)

The term $C_M.p_{gf}$, has been included here (as it was done in the case of the plate case) to account for the relative thickness variation of the as-moulded product due to the mould deformation. The term p_{gf} is the pressure distribution inside the impression at the instant the gate solidifies. The mould compliance C_M can be obtained by a simplified analysis of the core and cavity deformations, as will be shown following the figure 3.8.

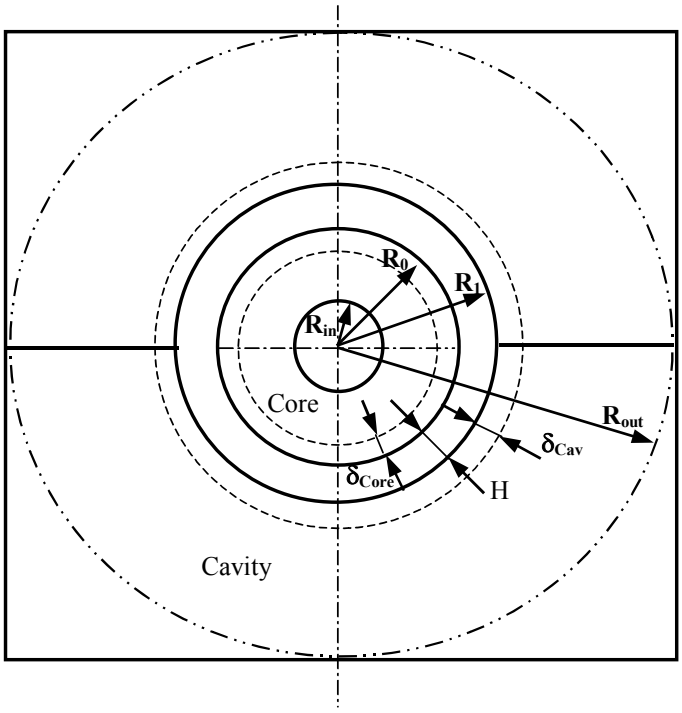

Figure 3.8- Schematic view of the cross section of the mould and the deformation caused by the moulding pressure

In the mould used in this work the dimensions shown in the figure 3.8 are

R_{in} = 7 mm (approximate dimension of the internal hole of the core)

R_0 = 30 mm (average diameter of the core)

R_1 = 32 mm (average diameter of the cavity)

R_{out} = 70 m (approximate dimension of the cavity insert)

The thickness shrinkage due to the mould deformation is given by

$$Sh_{r,mould} = \frac{\delta_{core} + \delta_{cav}}{H} \tag{3.47}$$

The core deformation can be calculated using the following expression [98]

$$\delta_{core} = R_0\left(\frac{{R_0}^2 + {R_{in}}^2}{{R_0}^2 - {R_{in}}^2} - \nu\right)\frac{p_{gf}}{\mathrm{E}} = \frac{k_{M,core}}{E}.p_{gf} \tag{3.48}$$

where

$$k_{M,core} = R_0\left(\frac{{R_0}^2 + {R_{in}}^2}{{R_0}^2 - {R_{in}}^2} - \nu\right)$$

For the cavity it can be written

$$\delta_{cav} = R_1\left(\frac{{R_{out}}^2 + {R_1}^2}{{R_{out}}^2 - {R_1}^2} + \nu\right)\frac{p_{gf}}{\mathrm{E}} = \frac{k_{M,cav}}{E}.p_{gf} \tag{3.49}$$

where

$$k_{M,cav} = R_1\left(\frac{{R_{out}}^2 + {R_1}^2}{{R_{out}}^2 - {R_1}^2} + \nu\right)$$

Substituting the equations 3.48 and 3.49 in equation 3.47, it is obtained

$$Sh_{r,mould} = \frac{k_{M,core} + k_{M,cav}}{E.H}\,p_{gf} = C_M.p_{gf}$$

where

$k_{M,core}$ = 24 mm for the core of the mould that produces the spider gated tube;

$k_{M,cav}$ = 60 mm for the cavity of the mould that produces the spider gated tube;

E - elastic modulus of the mould material (E=210 GPa, for steel);

H - thickness of the impression (2 mm).

The value estimated for the C_M to be added in the thickness shrinkage predictions of the tube is

$$C_M = \frac{k_{M,core} + k_{M,cav}}{E.H} = \frac{24 + 60}{210 \times 2} = 0.2\ \mathrm{GPa}^{-1}.$$

3.2.3.1- Calculation of the shrinkage of the internal and external diameter

The expression 3.41a gives the shrinkage in relation to the average diameter (or radius) of the tube (figure 3.9). In order to enable comparisons with the experimental diametrical shrinkage expressions that give the shrinkage of the internal, Sh_{Di}, and external, Sh_{De}, diameter are useful.

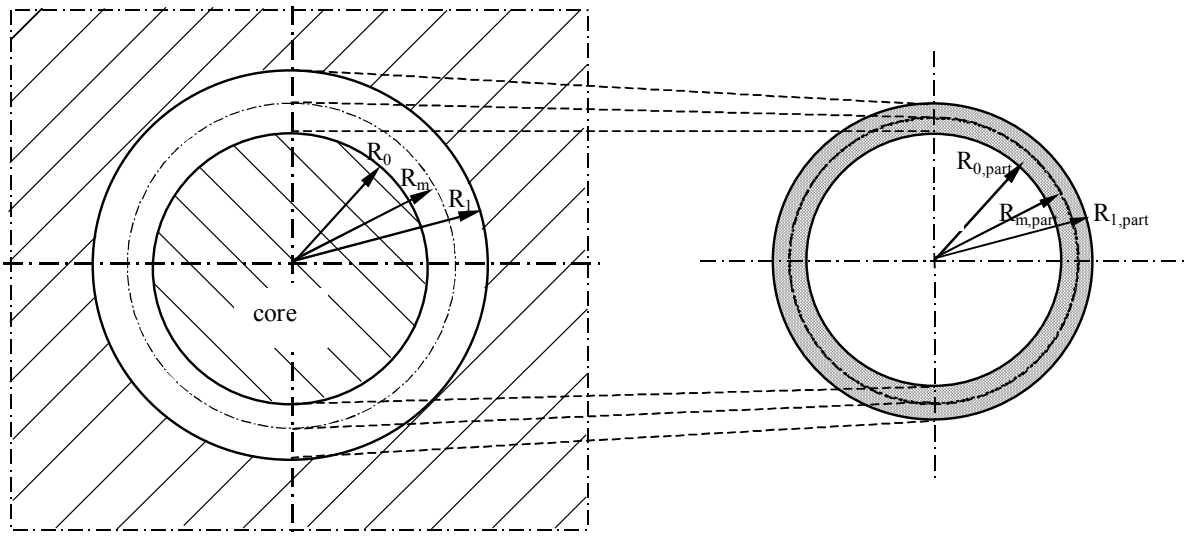

Figure 3.9- Schematic cross-section of the core and cavity of the mould, and part after ejection.

The diametrical shrinkage in relation to the average diameter is given by

$$Sh_{Dm} = \frac{R_m - R_{m,part}}{R_m} = \frac{R_1 + R_0 - R_{1,part} - R_{0,part}}{R_1 + R_0} \tag{3.50}$$

and the thickness shrinkage

$$Sh_r = \frac{H - H_{part}}{H} = \frac{R_1 - R_0 - R_{1,part} + R_{0,part}}{H} \tag{3.51}$$

The Sh_{Di} and Sh_{De}, are obtained using the equation 3.50, the equation 3.51, the average radius of the impression and the thickness, as follows:

Shrinkage of the internal diameter is given by

$$Sh_{Di} = \frac{R_0 - R_{0,part}}{R_0} = \frac{Sh_{Dm}.R_m - \frac{H}{2}.Sh_r}{R_m - \frac{H}{2}} \tag{3.52}$$

and the shrinkage of the internal diameter is given by

$$Sh_{De} = \frac{R_1 - R_{1,part}}{R_1} = \frac{Sh_{Dm}.R_m + \frac{H}{2}.Sh_r}{R_m + \frac{H}{2}} \tag{3.53}$$

4- INSTRUMENTED INJECTION MOULD

The ejection force required in injection moulding is influenced by factors that can be organised in two groups: factors independent from the mould (type of material and processing conditions) and factors related to the mould (part geometry, draft angle and core roughness). The experimental assessment of the ejection force required the development of a specific instrumented tool. This chapter describes the design of the instrumented mould for assessment of the force upon the ejection process of tubular mouldings.

4.1– The mouldings

For the convenience of modelling and analysis of the processing effect, the part should be filled with parallel flow. This is achieved in two configurations for the part: a cup and a tube. In both cases this implies that the gate must be at one of the extremes of the part. For the cup, a central pine gating system is used (figure 4.1.a), whereas for the tube a spider system with four injection points is applied (figure 4.1b). The nominal volume of the cup is 62 cm^3,and the tube is 56 cm^3. The runner systems have volumes of 3 cm^3 and 5 cm^3 respectively for these two mouldings.

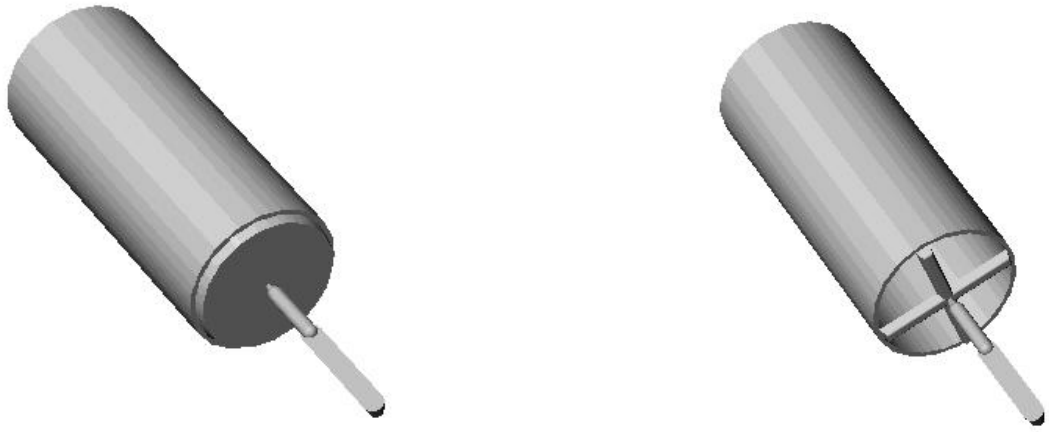

a) cup b) tube

Figure 4.1- Mouldings to be produced by the mould

4.2- The mould

The mould was designed for the production of the tubular parts with uniaxial flow. It is versatile enough to investigate geometry changes, the draft angle and core roughness, and to monitor the ejection force, the pressure and the mouldings surface temperature (figure 4.2). The versatility of the mould is achieved principally by the solution of interchangeable cores that can be machined in order to obtain the desired features.

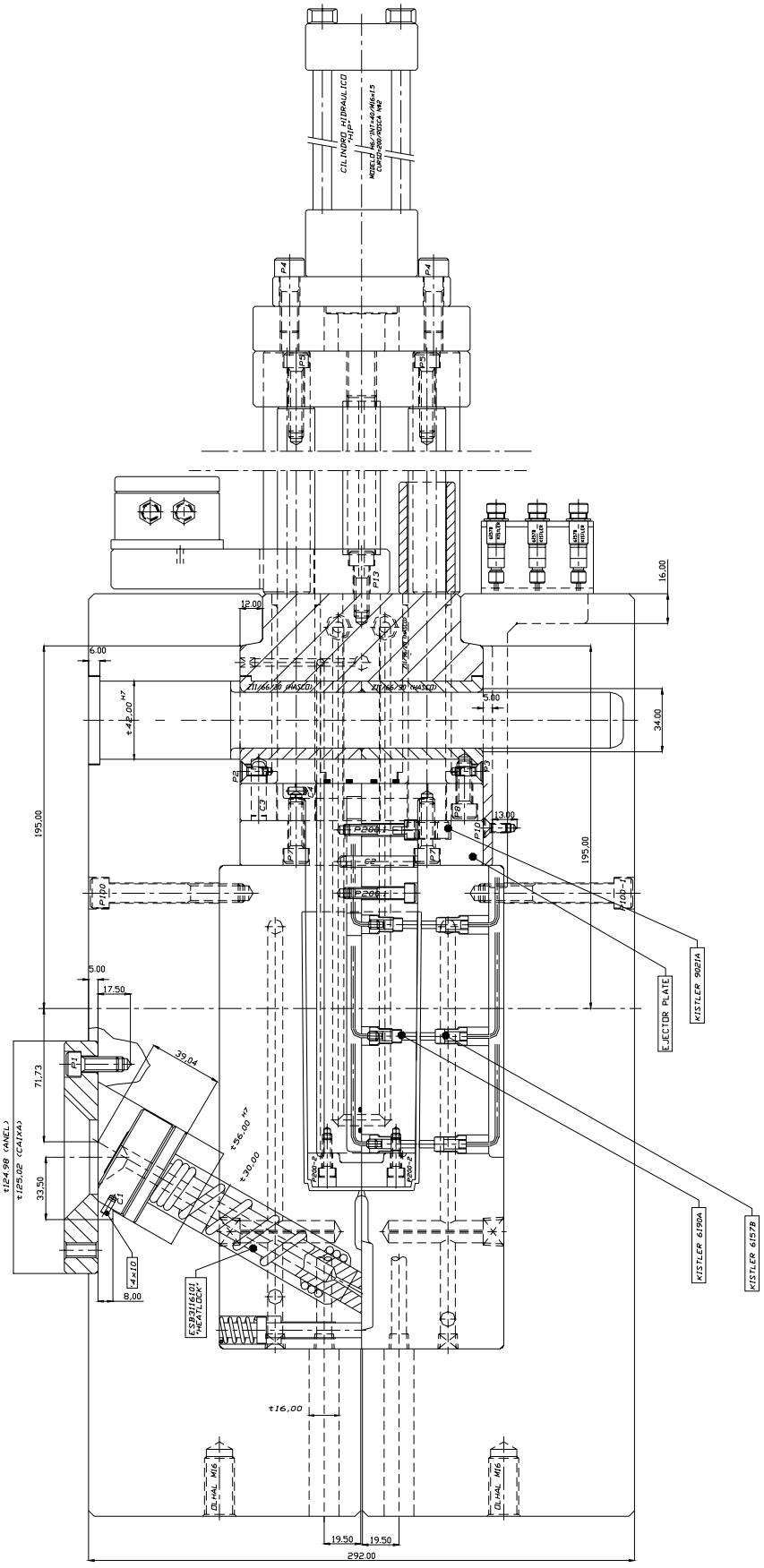

Figure 4.2- Cross-section view of the mould (simplified)

4.2.1- The interchangeable cores

To meet the objectives mentioned before, the mould was designed with interchangeable cavities and cores. The initial core geometry is conical with 60 mm in root diameter and 0.5º of draft angle. To make possible the assembly of the sensors in the core, this was manufactured into two halves coupled by circular fittings allowing the production of tubular mouldings with and without bottom (figure 4.3).

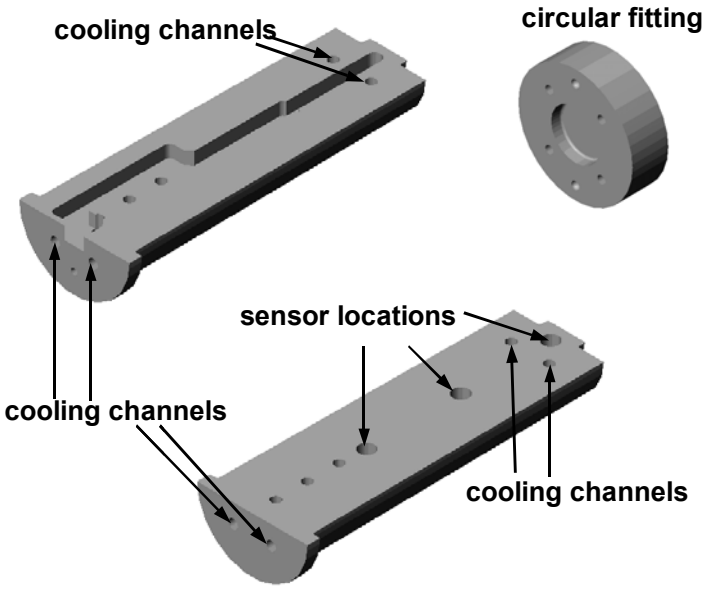

Figure 4.3- Components of the core

The core was also designed for the possibility of using compressed air for gas assisted ejection. The outlet of the air is in the parting line defined by the circular fitting and the two halves. This will make possible the study of the influence of the injected air in the ejection force, especially in the case of parts with bottom, where vacuum may result during ejection.

4.2.2- Runner system

Due to the length of the part (146 mm) and to allow for a balanced location in the mould, an inclined sprue with respect to the principal axis of the part is used. This inclination makes the ejection impossible if a cool sprue is used. This difficulty was overcome using a hot runner (figure 4.2). The hot runner selected (ESB3116101 from Heatlock) is used for shot weights, up to 2 kg for PP, and 0.7 kg for PC.

4.2.3– Temperature control system

The mould temperature control system is done by water lines in the two halves of the core and in the cavity plates, as shown in figure 4.4.

The system is constituted by four independent circuits, one in the fixed, the other in the moving part of the mould and the remaining two in the core. In the circuits of the moving and fixed part, the channels have 8 mm in diameter, with the *in* and *out* connections at the mould bottom. The core has the *in* and *out* connections at the top of the mould.

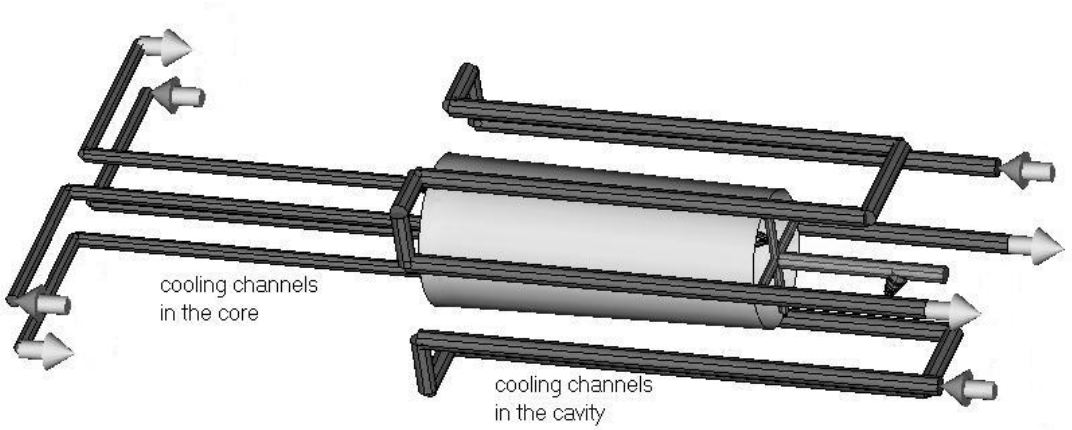

Figure 4.4 Layout of the cooling channels

4.2.4- The ejection system and mould operation

To avoid the measurement of forces parasite to the ejection, the ejection system is operated by a hydraulic cylinder that actuates the ejector plate. This system is mounted on the top of the mould. During ejection, the opening of the mould is done in two steps to prevent the contact between the part and the cavity. Firstly, the core and the whole ejection system follows the moving part of the mould until the daylight is enough for the ejection plate to actuate. Then the core and the ejection system stop, the movement of the moving part continuing. As a result, the core stays hanging in the mould daylight, causing that the ejection force will result only from the extraction of the part from the core (figure 4.5).

Mould Closed

- Injection, pressurisation and cooling

Opening of the Mould

- Movement of moving plate with the ejection system
- Locking of the ejection system and further movement of the moving plate

Ejection

- The hydraulic cylinder actuates the ejector plate

Resetting and Mould Closing

- The hydraulic cylinder moves back and the ejector plate resets
- Return of the moving plate and the ejection system to the initial position

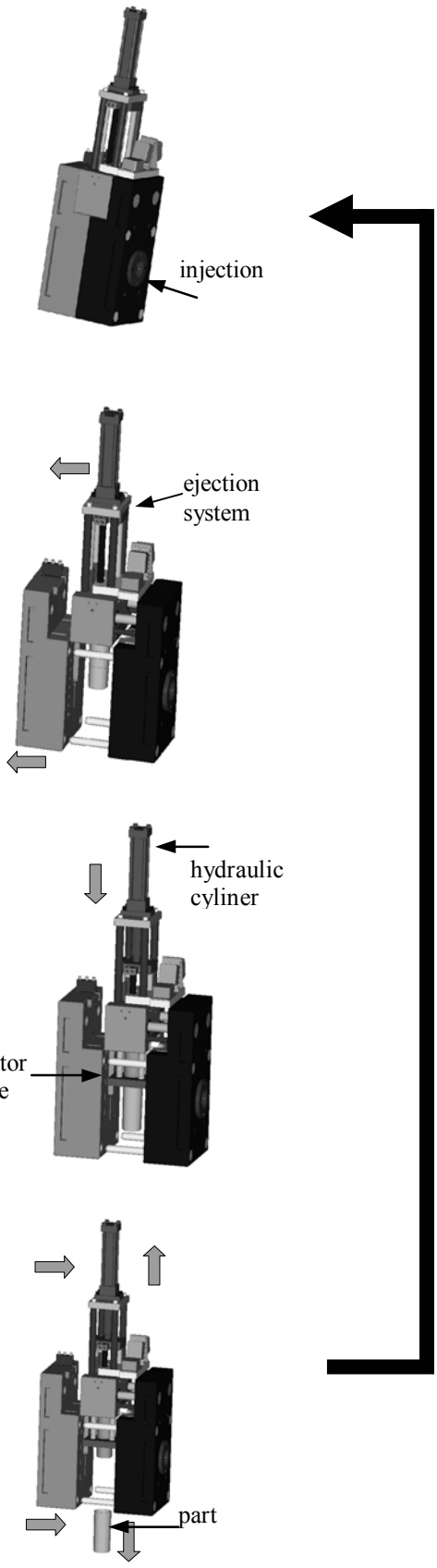

Figure 4.5- The mould in the moulding cycle

4.2.5- Instrumentation

The monitoring of pressure and temperature is done through a instrumentation system using three pressure sensors in the cavity (Kistler 6157 BA 0.4) C1, C2, and C3, and three pressure and temperature sensors in the core (Kistler 6190 A 0.4) B1/T1, B2/T2 e B3/T3. These core and cavity sensors are located along the flow path and face each other (figure 4.6).

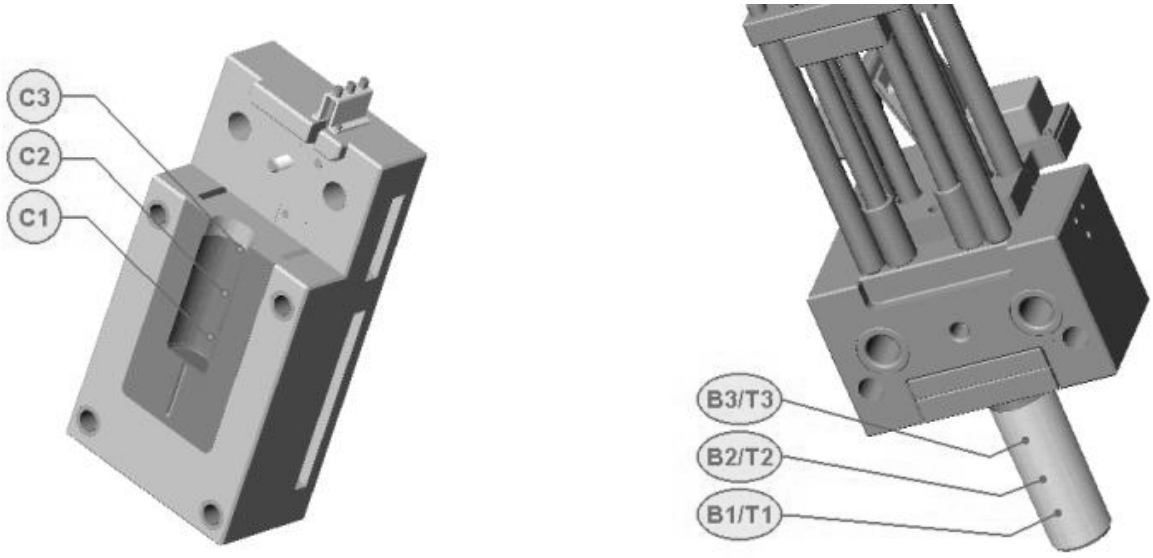

Figure 4.6- Location of the pressure and temperature sensors

The ejection force is measured by two piezoelectric load cells (Kistler 9021 A) located on the actuating bars of the ejector plate (figure 4.7), to avoid the measurement of forces parasite to the ejection.

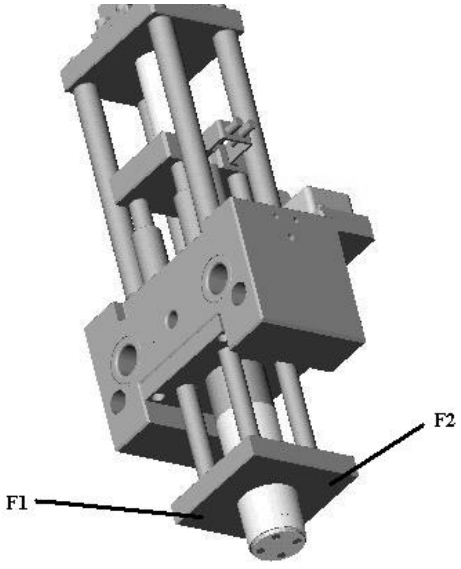

Figure 4.7- Load cell location

The acquisition and monitoring of the signal measured by the sensors is based on a data acquisition board, PCMCIA 2855 A1, and the software DATAFLOW, from Kistler, for data handling and visualization of the signal and signal condition, and amplifiers (figure 4.8). In each cycle the monitoring process is triggered by a switch that is actuated when the mould close.

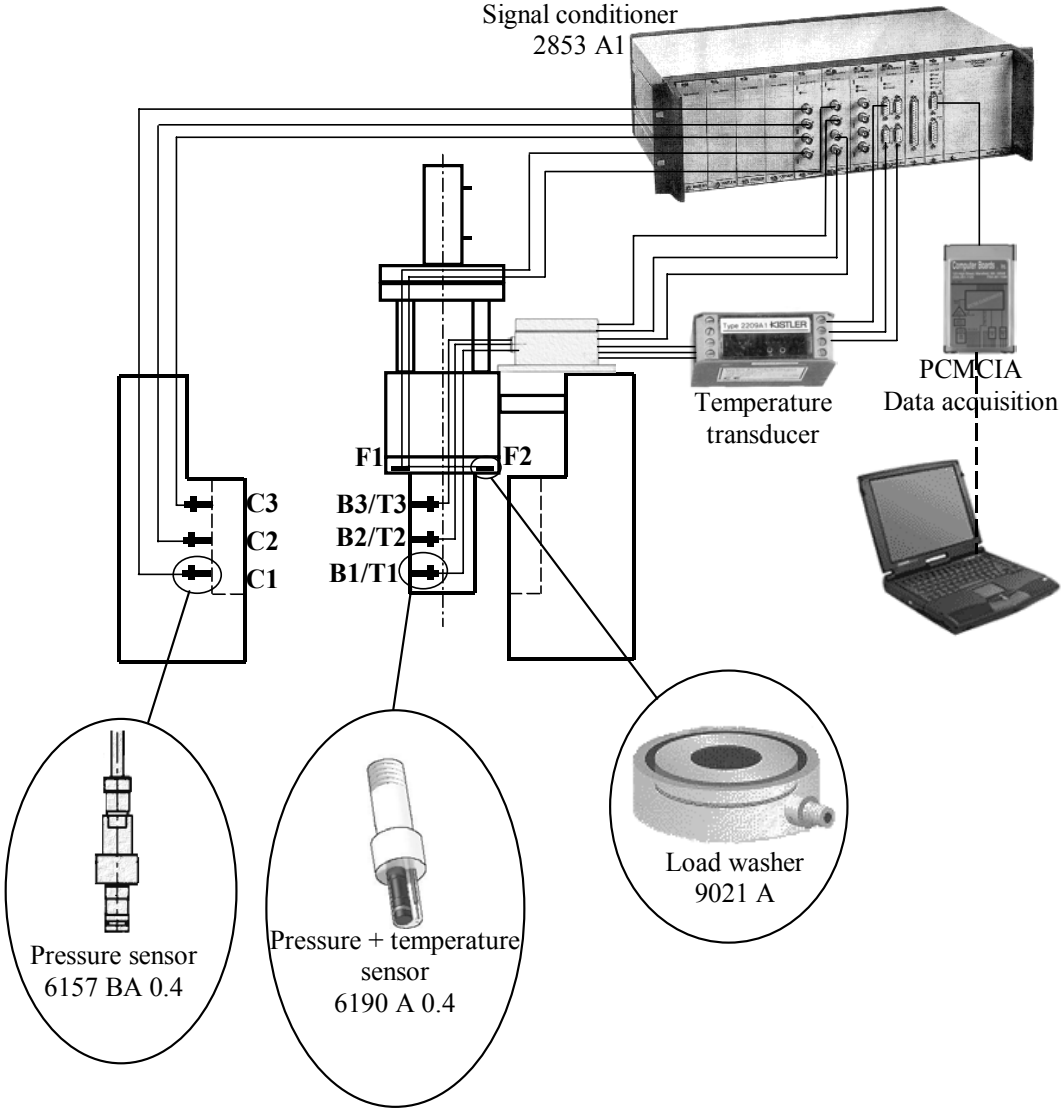

Figure 4.8- Acquisition data system

4.3- Instrumentation performance

4.3.1- Pressure data

Typical results of the pressure evolution measured in the mould walls alongside with the indication of the filling (I) and holding (II) phases are shown in figure 4.9.

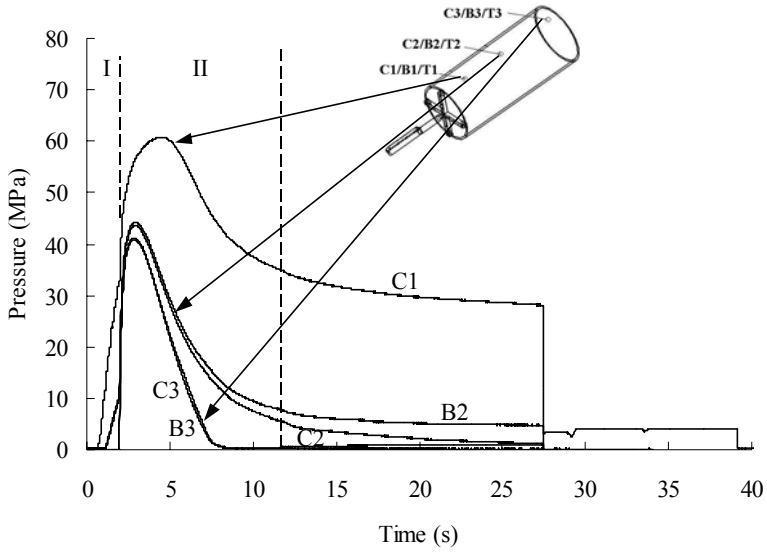

Figure 4.9- Typical pressure evolution along the moulding cycle

It is observable that the pressure measured by the first sensor is much higher than that of the sensors more distant from the gate. This pressure difference can be explained upon analysing the temperature data (figure 4.10) that shows a similar difference.

These results are characteristic of the process and can be used directly as input data in the prediction models, as well as to validate the injection moulding simulations and to assess the performance of simulation softwares used in this work.

4.3.2- Temperature data

The temperature evolution along the time in the three positions indicated in the figure 4.6. is shown in figure 4.10.

The first sensor measures a temperature at the core surface higher than that monitored by the sensors farther from the gate. The higher temperature of the material implies its lower viscosity, a lower thickness of the solidified layer and, consequently, better pressure transmission during the holding phase. The temperature data is used to validate the cooling simulations and to assess the performance of simulation softwares used in this work.

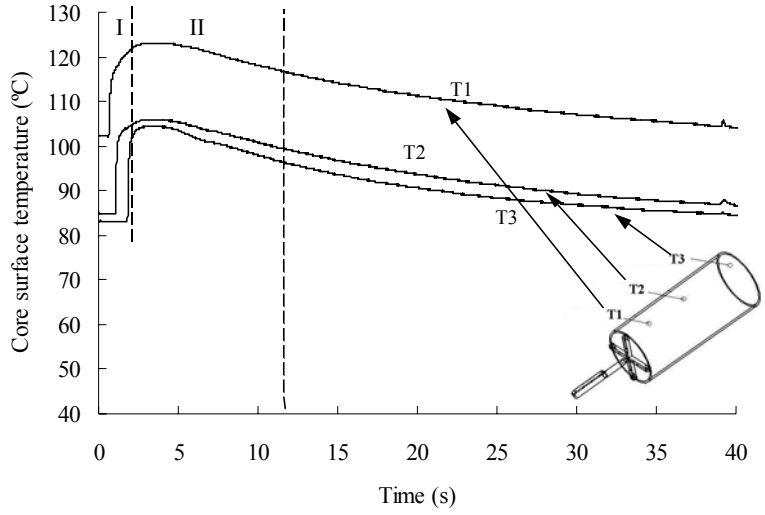

Figure 4.10- Typical temperature evolution along the moulding cycle

4.3.3- Force data

In the figure 4.11 the force evolution measured by the load cells during the ejection is shown. The ejection takes typically 200 ms. The shape of the curves shows that, during ejection it exists a sharp increase of the force, followed by a slow decrease until the base value. The sharp increase corresponds to the force required to overcome the static friction between part and core before the movement of the part. The slow decreasing of the force on one side is due, to the change from static to kinetic friction and, on the other side, to the reducing contact pressure during the ejection, resulting from the draft angle of the core.

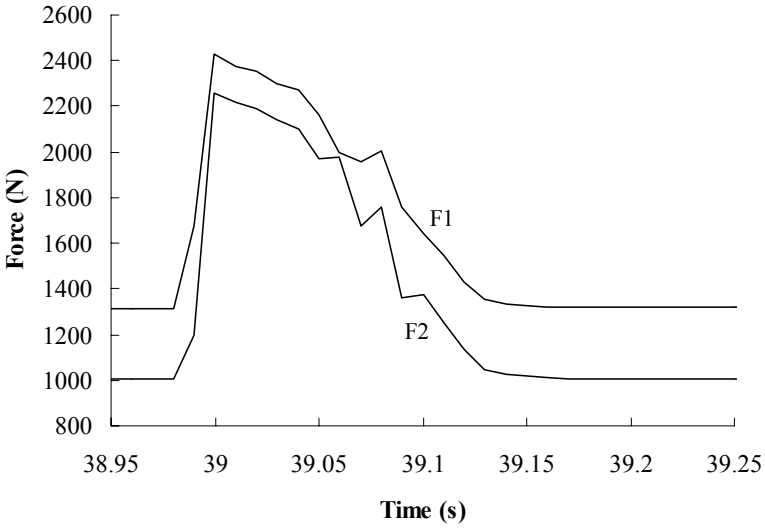

Figure 4.11- Typical force evolution during ejection

4.3.4- Reproducibility

To assess the reproducibility of the system 20 mouldings where produced in automatic cycle, after the stabilisation of the process. The study was based in tubular mouldings with the nominal dimensions of 2 mm in thickness, 60 mm of internal diameter and 146 mm in length. The injection moulding cell consists of a injection moulding machine Demag D100 NCIII of 1 MN of clamp force, one thermo-regulator and a drier with circulating air. The mouldings were produced in polycarbonate (Lexan 141R from General Electric Plastics).

The force at the moment of ejection is the measurement more relevant to the objective of the work. Its variation along 20 cycles is shown in figure 4.12. In the same figure the average and the limits of variation associated to the standard deviation are shown. The average variation with respect to the average of the measurements is 3.5%.

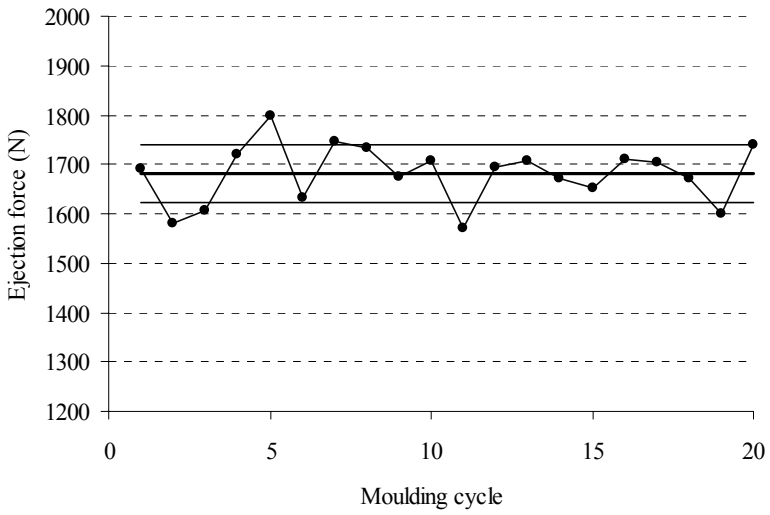

Figure 4.12- Ejection force variation during moulding

5- EXPERIMENTAL METHODS AND SIMULATION TECHNIQUES

This chapter describes the experimental methods and simulation techniques used in this work, namely:

- production of two types of mouldings with different processing conditions by injection moulding: a edge gated plate and a spider gated tube;
- measurement of the shrinkage evolution and the onset of shrinkage during the moulding of the plates using the strain gauge technique;
- measurement of the pressure and temperature evolution during processing;
- measurement of the force evolution during the ejection of the tubular mouldings;
- dimensional characterisation of the as-moulded parts using: a digital calliper, a LVDT, and a 3D measuring machine;
- simulation of the moulding production process with the commercial software, C-Mold v99.7 of Moldflow, and a software developed at the Università di Salerno, the UNISA program.

5.1- Raw materials

Two materials were used for the production of the mouldings: a polycarbonate and a isotatic polypropylene.

polycarbonate

The synthesis of polycarbonate is based on the reaction of bisphenol-A with carbonic acid derivatives. Polycarbonate is an amorphous polymer characterised by very good mechanical resistance and high tensile and impact properties. Its dimensional stability, even at high temperatures (~135ºC), and transparency makes it very suitable for technical applications. The commercially available materials include reinforced (usually, with glass fibres) and coloured grades, in a range from transparent to opaque varieties. The grade used here is a non-reinforced polymer from General Electric Plastics, Lexan 141R. This material is compounded with a release agent to improve demouldability.

Some relevant physical, mechanical, thermal and processing characteristics of Lexan 141R, as quoted by the manufacturer [119,120] are presented in the Table 5.1.

Table 5.1 - Typical properties of PC Lexan 141R

	ASTM Method	Value	Unit
Physical property			
Specific gravity	D 792	1.2	$Mg.m^{-3}$
Mechanical property			
Flexural modulus	D 790	2343	MPa
Tensile strength	D 638	69	MPa
Elongation at break	D 638	130	%
Charpy impact strength at 23ºC	D 256	31.8	$kJ.m^{-2}$
Thermal property			
Vicat softening point (50ºC/h 50N)	D 1525	154	ºC
H.D.T (1.82 MPa)	D 648	132	ºC
Processing characteristics			
Melt flow rate (300ºC,1.20 kg)	D 1238	10.5	g/600 s
Injection temperature range		270-310	ºC
Mould temperature range		70-100	ºC
Maximum shear stress		0.5	MPa
Maximum shear rate		40000	s^{-1}

The Lexan 141R was also characterised by dynamic mechanical analysis using a DMA7e Perkin-Elmer apparatus with a controlled cooling accessory, in the temperature range from +40ºC to +140ºC. The test was performed in the three-point bending mode at a heating rate of 4ºC/min and a frequency of 1 Hz. The storage modulus, E', and loss modulus, E'', obtained from the test performed by DMA are shown in figure 5.1.

These data were obtained to be used as input for the thermo-mechanical model for ejection force predictions.

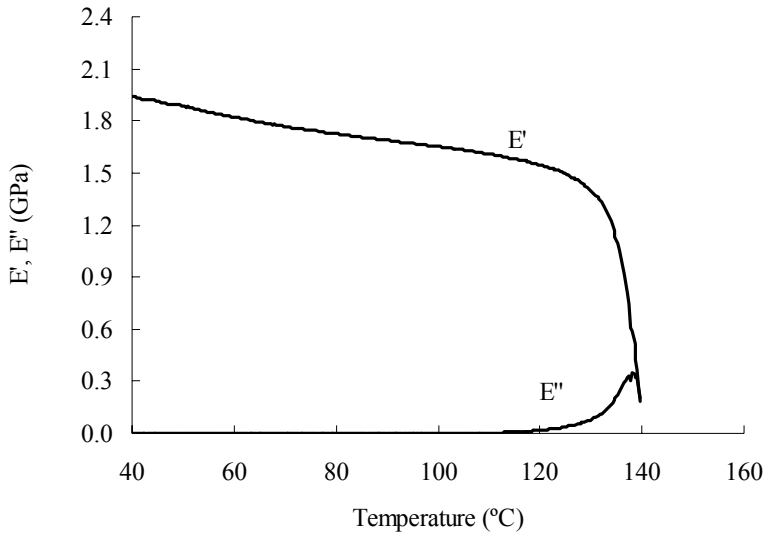

Figure 5.1- Storage modulus, E', and loss modulus, E'', of PC Lexan 141R

polypropylene

The isotatic polypropylene Hifax BA238G3 is a heterophasic polypropylene with increased isotatic index, supplied by Montell. This grade of polypropylene is compounded with about 26% in weight of ethylene-propylene rubber (about 50% of ethylene and propylene) and 1.5% talc.

It combines a excellent stiffness/impact strength balance, and a superior flowability with good aesthetics. It is mainly used in injection moulding of large and thin wall bumpers for the automotive industry.

Some relevant physical, mechanical, thermal and processing characteristics of Hifax BA238G3 as quoted by the manufacturer [121] are summarised in the Table 5.2.

Table 5.2 - Typical properties of iPP Hifax BA238G3

Properties	ASTM Method	Value	Unit
Physical			
Specific gravity	D 792	0.9	$Mg.m^{-3}$
Mechanical			
Flexural modulus	D 790	1000	MPa
Tensile strength	D 638	20	MPa
Elongation at break	D 638	400	%
Notched Izod impact strength at 23ºC	D 256	>600	$J.m^{-1}$
at 0ºC	D 256	140	$J.m^{-1}$
at -30ºC	D 256	80	$J.m^{-1}$
Thermal			
Vicat softening point (50ºC/h 50N)	D 1525	55	ºC
H.D.T (1.82 MPa)	D 648	50	ºC
Processing characteristics			
Melt flow rate (230ºC,2.16 kg)	D 1238L	13	g/600 s
Injection temperature range	-	180-290	ºC
Mould temperature range	-	20-60	ºC
Maximum shear stress	-	0.26	MPa
Maximum shear rate	-	24000	s^{-1}

The Hifax BA238G3 was also characterised in terms of their dynamic mechanical properties using a DMA7e Perkin-Elmer apparatus in the temperature range from +20ºC to +150ºC. The test was performed in the the bending mode at a heating rate of 4ºC/min and frequency of 1 Hz. In the figure 5.2 the moduli E' and E'', obtained from the test are represented. These data were obtained to be used as input for the thermo-mechanical model for ejection force predictions.

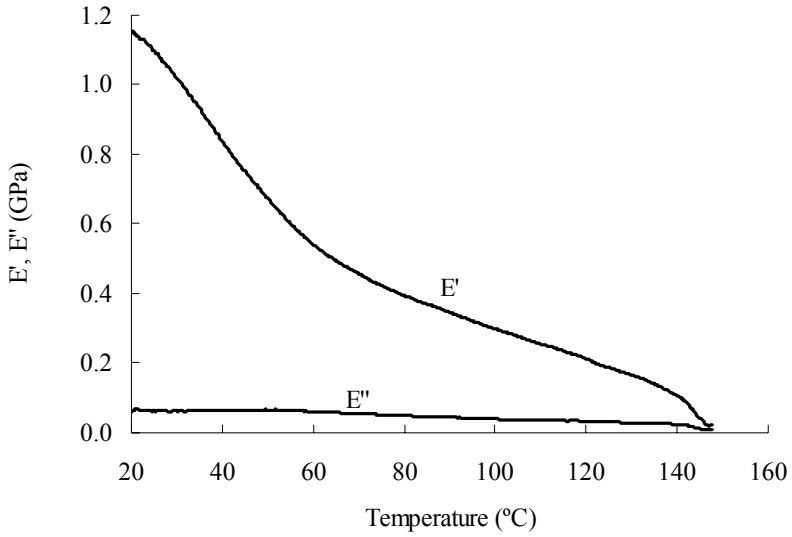

Figure 5.2- PP Hifax BA238G3 storage modulus, E', and loss modulus, E'', as measured by DMA

5.2- Processing

5.2.1- Mouldings and equipment

The materials were moulded into two geometries: a rectangular plate and a 2 mm thick tube.

5.2.1.1- Rectangular plate

The rectangular plates with nominal dimensions L=120mm, W=30mm, were produced in a injection moulding cell at the Università di Salerno, Italy. This cell consists of a injection moulding machine Penta P65 of 650 kN clamp force, a thermo regulator Piovan TH 9/OCNOT (using circulating oil as regulating medium) and a instrumented mould. The mould has the possibility of interchanging the cavity plate to produce parts with different configurations in terms of impression and gate thickness, namely (figure 5.3):

- 2 mm thick plate and 1.5 mm thick gate
- 4 mm thick plate and 2 mm thick gate

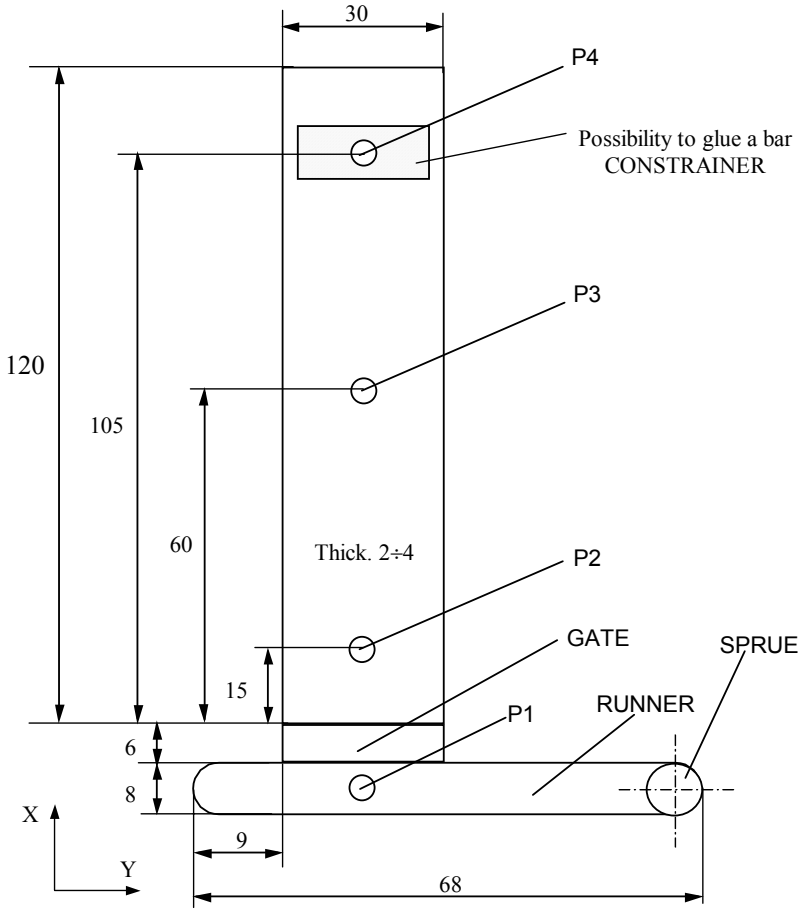

Figure 5.3- Top view of the instrumented cavity used to produce the edge gated plates

The moulding machine and the mould were equipped with five Kistler pressure transducers: one in the injection nozzle, one just before the gate, and three in the cavity, located in the fixed part of the mould, at 15, 60 and 105mm downstream from the gate. These positions will be referred to as P0, P1, P2, P3 and P4, respectively.

The injection nozzle used to produced the edge gated plates and the respective dimensions are shown in the figure 5.4. The nozzle geometry was considered in the mould filling simulations.

The pressure data in the five positions were recorded at 10 samples/second for all tests with a Lab View data acquisition system (National Instruments).

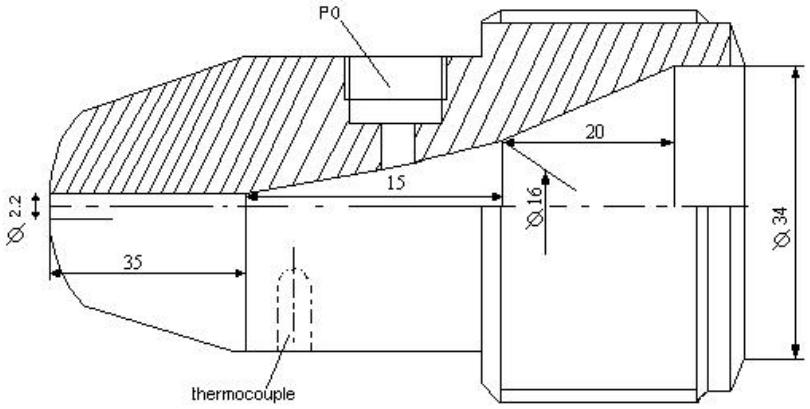

Figure 5.4- Nozzle used to produce the edge gated plates

In order to investigate the shrinkage differences between free shrinking samples and constrained during solidification samples, a series of experiments for iPP was performed with a modified impression. This was achieved by gluing with a cyanoacrylate glue, an aluminium bar of 26 mm × 6 mm × 0.5 mm onto the mould surface at 105 mm from the gate (figure 5.3).

5.2.1.2- Tube

The tubes with nominal dimensions of $\varnothing_{int}$=60mm, L=146mm,were produced in a injection-moulding cell at Centimfe (Marinha Grande), consisting of a injection moulding machine Demag D100 NCIII of 1 MN clamp force, two thermo regulators GWK TECO 80 (using circulating water as regulating medium), a drying system Motan, and the instrumented mould developed in this work (as described in chapter 4).

The mould was equipped with three pressure sensors in the cavity and three pressure/temperature in the core, along the flow path and facing each other, at 21, 79 and 139mm downstream from the gate (figure 5.5). These positions in the cavity will be referred to as C1, C2 and C3, and in the core as B1, B2 and B3, and T1, T2 and T3, for pressure and temperature sensors, respectively.

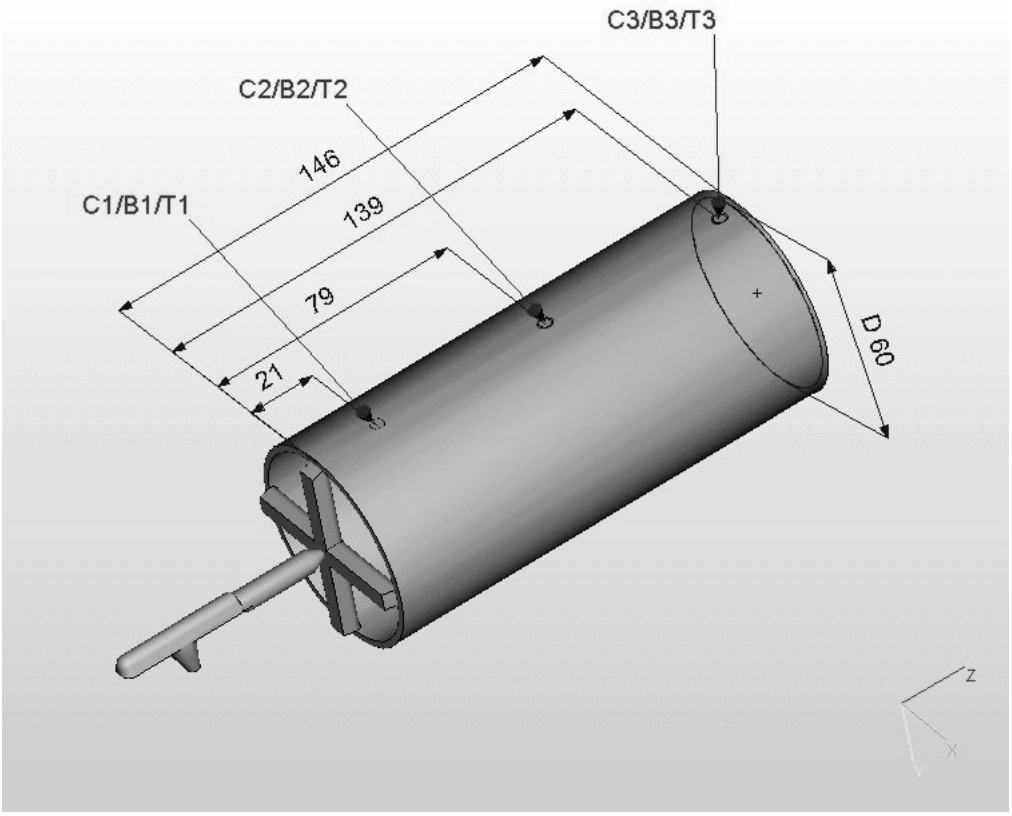

Figure 5.5- View of the spider gated tube and positions of the pressure/temperature sensors

The dimensions of the injection nozzle used to produced the tubes are shown in figure 5.6.

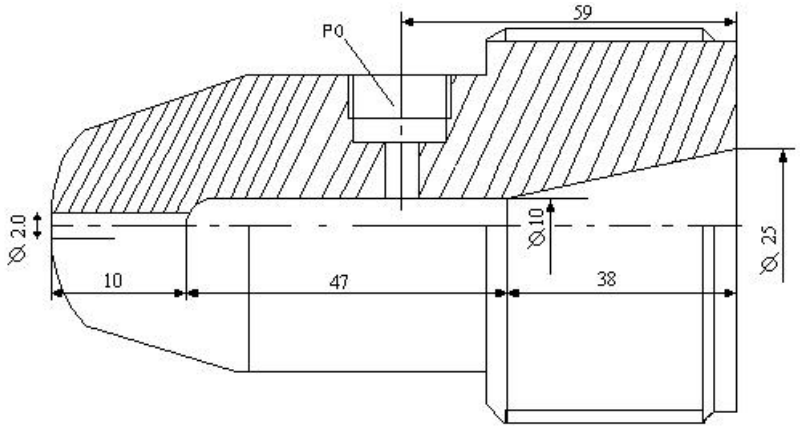

Figure 5.6- Drawing of the nozzle used to produce the spider gated tube

The force evolution during the ejection is monitored with two Kistler load cells with range capacity from 0.01 N to 35 kN. The location of the load cells in the ejector plate is indicated in figure 5.7.

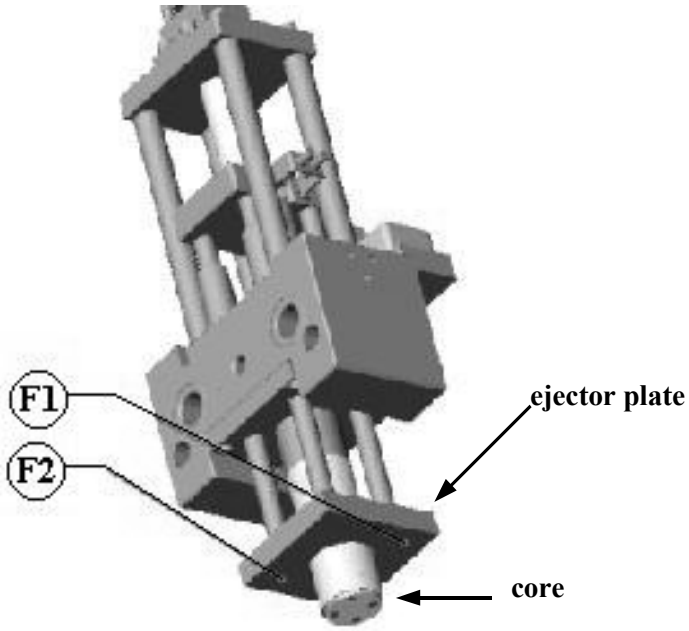

Figure 5.7- The ejection system and the location of the load cells

The pressure, temperature and force data were recorded at 100 samples/second for all tests with a Kistler data acquisition system. The fast acquisition rate was chosen to improve the accuracy of the monitoring of the ejection force evolution, which takes about 50 ms.

5.2.2- Moulding programme

The moulding conditions were selected considering the processing window recommended by the raw material manufacturers (section 5.1) and suggested from preliminary simulations.

The quoted mould temperatures refer to readings made at the moulding surface of the mould. The holding pressure was determined from the pressure measured in the nozzle at the position P0. In the absence of actual measurement, which happened in some cases of the tubular mouldings, the pressure in the nozzle was derived from the calibration curve indicated in the figure 5.8. The values shown in the figure were determined in preliminary experiences with the spider gated tubes. The mouldings were produced in polycarbonate, the mould temperature with 85ºC and the injection temperature at 310ºC.

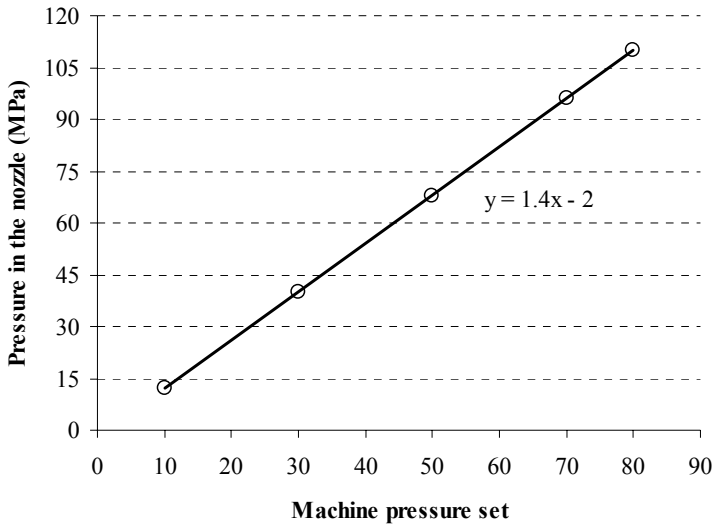

Figure 5.8- Relationship between machine pressure set and pressure measured in the nozzle

5.2.2.1- Moulding identification

The mouldings were identified by the follow code, corresponding to the processing variables used:

230.20.10.15

- The first number refers to the injection temperature given by the thermocouple in the nozzle (ºC);
- The second number indicates the pressure applied during the holding phase measured by the pressure transducer in the nozzle (MPa);
- The third number indicates for how long the holding pressure is applied (s);
- The fourth number gives the time from the end of holding stage until the mould opening (s).

5.2.2.2- Moulding conditions for polypropylene plates

All the mouldings were produced at a flow rate of 27 cm^3/s and mould wall temperature of 27 °C. The holding pressure, Ph, and the holding time, th, were varied as shown in the Table 5.3. The time after holding was kept to 15 s.

Table 5.3 - Processing conditions for iPP plates

Injection temp., Tinj (ºC)	Holding pressure, Ph (MPa)	Holding time, th (s)	Time after holding, ta (s)
230	20 70	10	15
	40	2 6	

In order to allow for the stabilisation of the process, 7 mouldings were rejected prior to the collection of the representative parts.

During some of the tests, the shrinkage evolution was monitored from the start of the injection to before the mould opening by means of a resistance strain gauge located at 60 mm from the gate (P3). The technique to measure the shrinkage evolution inside the mould using strain gauge is described in the next section 5.3.2.2.

The moulding programme shown in Table 5.3 was repeated in conditions where the mouldings were restrained from in-mould free shrinkage by means of a mechanical constraint as it was described in section 5.2.1.1. For all tests the as-moulded shrinkage was measured 10 minutes after ejection at a room temperature of 27 °C, and the results of these measurements were averaged over 3 consecutive mouldings for each combination of holding conditions.

5.2.2.3- Moulding conditions for polycarbonate plates

The material was dried in a oven with vacuum during 3 hours at 120ºC, before the production of the mouldings. All mouldings were produced with a nominal mould wall temperature of 80 °C. The holding pressure, Ph, and the holding time, th, were varied. The time after holding was kept

to 20 s. In order to allow for stabilisation of the process, 7 mouldings were rejected between each set up. The moulding programme is summarised in the Table 5.4.

Table 5.4 - Processing conditions of PC plates

Injection temp., Tinj (ºC)	Holding pressure, Ph (MPa)	Holding time, th (s)	Time after holding, ta (s)
310	36 66 80	15	20
	49	0 5 10	

For all tests the as-moulded shrinkage was measured 30 minutes after ejection at a room temperature of 20 °C, and the results of these measurements were averaged over 3 consecutive mouldings for each combination of moulding conditions.

5.2.2.4- Moulding conditions for polypropylene tubes

The following processing conditions were varied: injection temperature, Tinj, holding pressure, Ph, mould wall temperature, Tw, and the time after holding (cooling), ta.

The pressure during the holding stage was kept constant for 13 s (holding time, th). The ejection was done at a velocity of 45 $mm.s^{-1}$. The processing conditions are shown in the Tables 5.5 and 5.6, for two mould wall temperatures of 50ºC and 32ºC, respectively.

In order to allow for stabilisation of the process, 7 mouldings were rejected between each processing set up. The ejection force was measured in 5 consecutive cycles for each processing condition.

Table 5.5 - Processing conditions for iPP tubes with mould temperature of 50ºC

Injection temp., Tinj (ºC)	Holding pressure, Ph (MPa)	Holding time, th (s)	Time after holding, ta (s)
190	5 19 40 54	13	10
210	5 19 33 47		
	40		5 20 30 40
230			5 20 30
	5 19		10

Table 5.6 - Processing conditions for iPP tubes with mould temperature of 32ºC

Injection temp., Tinj (ºC)	Holding pressure, Ph (MPa)	Holding time, th (s)	Time after holding, ta (s)
230	12 19 33 47	13	10
	40		5 8 15 20 25

For all tests the as-moulded shrinkage was measured 24 hours after the ejection at a room temperature of 20 °C, and the results of these measurements were averaged over 3 consecutive mouldings for each combination of moulding conditions.

5.2.2.5- Moulding conditions for polycarbonate tubes

Before the production of the mouldings the material was dried during 3 hours at 120ºC. The mouldings were produced with a mould wall temperature of 85ºC. Several values were given to the holding pressure, Ph, and the holding time, th.

The time after holding was kept at 15 s. The ejection was made at 45 $mm.s^{-1}$.

The ejection force was measured in 5 consecutive cycles for each processing condition (Table 5.7). In order to allow for the stabilisation of the process, 7 mouldings were rejected between each processing set up.

Table 5.7 - Processing conditions for PC tubes

Injection temp., Tinj (ºC)	Holding pressure, Ph (MPa)	Holding time, th (s)	Time after holding, ta (s)
310	12 40 89 110	10	15
	68	2 5 8	

For all tests the as-moulded shrinkage was measured 24 hours after the ejection at a room temperature of 20 °C, and the results of these measurements were averaged over 3 consecutive cycles.

5.3- Recorded data

5.3.1- Ejection force

The ejection force of a moulding was determined from the two curves of the force evolution during ejection given by the load cells (figure 5.7). A typical variation of the force recorded by

the load cells is shown in the figure 5.9. The value of the ejection force for each moulding is calculated as

$$Fe = \mathrm{F1} + \mathrm{F2} \tag{5.1}$$

F1 and F2 are the force recorded by the load cells, and calculated from the corresponding baseline in the graphs.

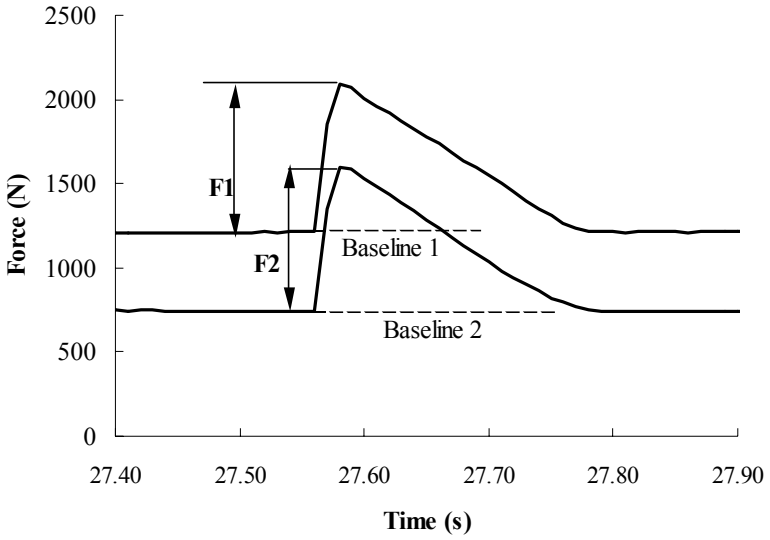

Figure 5.9- Typical curves of the forces measured by the load cells during the ejection

The ejection force corresponding to each processing condition was characterised by the average of 5 consecutive moulding cycles and the standard deviation.

5.3.2- Shrinkage

5.3.2.1- As-moulded shrinkage

The shrinkage is calculated in percentage as

$$Sh_i = \frac{D_{imp} - D_{part}}{D_{imp}} \tag{2.1}$$

where D_{imp} is the dimension in the impression in the i direction at the reference temperature of 20ºC and D_{part} is the corresponding part dimension. According to this definition, the shrinkage will be negative if the moulding dimension becomes larger than the impression.

The mouldings dimensions (length and width, for plates, or internal diameter, external diameter and length, for tubes) were measured at a temperature of 20ºC, except the iPP plates that were measured at 27ºC. Results of these measurements were corrected using the coefficient of thermal expansion of $9.4 \times 10^{-5}\ C^{-1}$, in order to obtain mouldings dimensions at the chosen measuring temperature (20ºC).

The shrinkage for each processing condition was characterised by the average of 3 consecutive mouldings and the standard deviation.

Rectangular plates

For the plates, the width dimensions at P2, P3 and P4, and the total length (figure 5.3) were measured with a digital calliper (accuracy 0.01mm). The associated error in shrinkage is ±0.01% in the length direction and ±0.03% in the width direction. The associated error in percentage is calculated dividing the accuracy of the measuring equipment by the nominal dimension being considered.

The thickness dimensions were measured at the positions P2, P3 and P4 using an LVDT (Sangamo, Schlumberger) of accuracy 0.001 mm. The associated error in shrinkage is ±0.05% for the 2 mm thick plate and ±0.025% for the 4 mm thick plate.

The dimensions of the impressions in the mould (length, width and thickness) at 20 °C, were determined after averaging 6 measurements at each location used for shrinkage measurements, as given in the Tables 5.8 and 5.9.

Table 5.8- Impression dimensions of the 2 mm thick plate at 20 ºC

Position	Width (mm)	Thickness (mm)	Length (mm)
P2	30.07	2.01	
P3	30.06	1.98	120.01
P4	30.05	3.00	

Table 5.9 - Impression dimensions of the 4 mm thick plate at 20 ºC

Position	Width (mm)	Thickness (mm)	Length (mm)
P2	29.94	3.90	
P3	29.96	3.91	120.05
P4	29.95	3.92	

Tubes

For the tubes, the diametrical dimensions at C1/B1, C2/B2 and C3/B3, and the total length (figure 5.6) of 3 consecutive mouldings were measured with a 3D measuring machine DEA-Beta (accuracy 0.02 mm). The associated error in shrinkage is ±0.03% and ±0.015% for diametrical and length direction, respectively.

The dimensions of the impression of the mould (length, diametrical cavity (C) and diametrical core (B)) at 20 °C, were determined at each location used for shrinkage measurements, and are given in the Table 5.10.

Table 5.10 - Impression dimensions for 2 mm thick tube at 20ºC

Position	Cavity (mm)	Core (mm)	Length (mm)
3	63.87	59.88	
2	62.81	58.83	145.93
1	61.82	57.82	

5.3.2.2- Shrinkage inside the mould using the strain gauge technique

The shrinkage measurements inside the mould for rectangular plates were done using a strain gauge placed on the cavity at the position P3 with the grid aligned in the flow direction. The cavity has a thin lateral channel and a terminal that allow the strain gauge wires to come out from the mould and assure no leakage of the polymer during the moulding (figure 5.10).

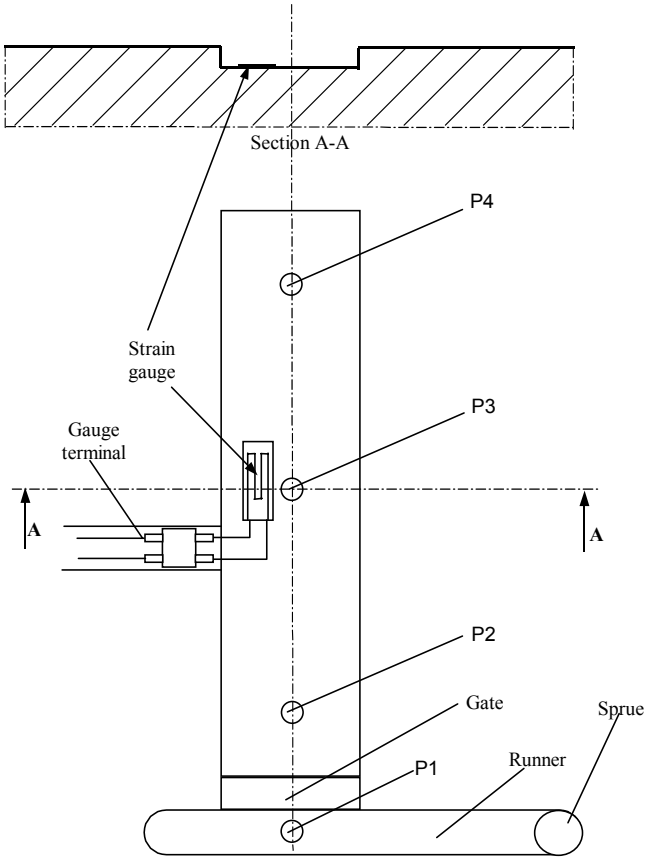

Figure 5.10- Top and cross-section view of the instrumented cavity with strain gauge and its connection.

During injection, the polymer solidifies onto the strain gauge and, through a thin adhesive layer, sticks to it (figure 5.11).

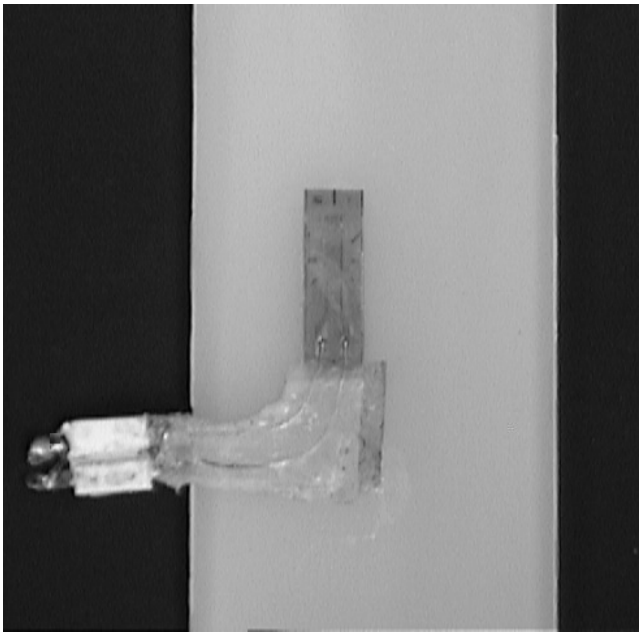

Figure 5.11- Rectangular plate with the strain gauge and terminal

The improvement of the strain gauge bonding to the polymer was done by means of a cyanoacrylate glue, that is applied on the strain gauge just before its placement on the cavity.

The strain gauge resistance variation, ΔR, evaluated by means of a Philips Strain Converter PR9872/20, was recorded and used to measure the strain of the sample using the following relationship [122]:

$$k_x.\varepsilon_x = \frac{\Delta R}{R} \tag{5.2}$$

where

ε_x - is the strain in x direction (parallel to the gauge axis)

k_x - is the gauge factor which depends on the particular gauge chosen and, in general, on the temperature, pressure, bonding type and substrate stiffness [123,124].

The strain gauges used were of the Kyowa KFRP-5-350-C1-1 type with:

- matrix dimensions: 15 mm×5 mm×0.06 mm
- matrix material: polyimide
- resistance: R=350 Ω
- gauge factor: k_x=2.01.

The resistance strain gauge used shows a very small dependence on the pressure and temperature variations, therefore being appropriate to measure the shrinkage inside the mould, as already reported by Pantani *et al.* [60,90].

5.4- Simulations

The moulding experiments were simulated with the commercial software, C-Mold v99.7 of Moldflow, and a software developed at the Università di Salerno, UNISA code. The later is an "open" software that allows modifications to account for aspects usually neglected by the commercial softwares, *e.g.* crystallisation kinetics and mould deformation.

In the first place, the purpose of the simulations was to help on the decision for the processing conditions of the moulding programme. The simulations were also used to:

- help on the analysis of the effect of the processing conditions on the experimental as-moulded shrinkage;
- compare the predicted pressure and temperature profiles, with experimental data, and to analyse the reason for discrepancies, if any;
- derive the crystallinity degree (only with the UNISA code), pressure, temperature and density histories in the mouldings. These data are required as input for the thermo-mechanical models for shrinkage and ejection force.

5.4.1- C-Mold

The models for the simulations, implemented in the C-Mold simulation package are based on a hybrid finite-element/finite-difference/control-volume numerical solution of the generalized Hele-Shaw flow of a compressible viscous fluid under non-isothermal conditions.

The rheological and pvT description therein implied is obtained by the Cross-WLF and the Tait modified equation, respectively. The material parameters used in both equations are described in the following sections. More details about the software are described in the company technical and related literature [23,37,38,125].

5.4.1.1- Mesh

Finite element meshes of the complete mouldings were constructed, including the runners, the nozzle of the injection moulding machines, and the cooling channels. The ideal number of 3-node elements was assessed by increasing the number of elements until no significant changes were observed in the results.

Rectangular plate

The geometric model of the plate for the simulations consisted of 536 elements for runners, gate and impression. The effect of the cooling system was analysed using a model of 144 elements. The runner and impression mesh used in the simulations is shown in figure 5.12.

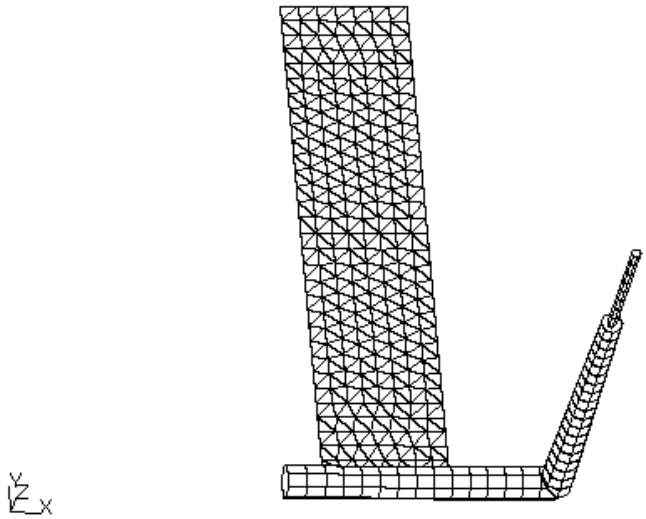

Figure 5.12- Mesh of the C-Mold model for the edge gated plate (536 elements)

Tube

The model of the tube with the spider gating system for the simulations consisted of 1004 elements for runners and impression. The effect of the cooling system was analysed using a model of 172 elements. The runner and impression mesh used in the simulation program is shown in figure 5.13.

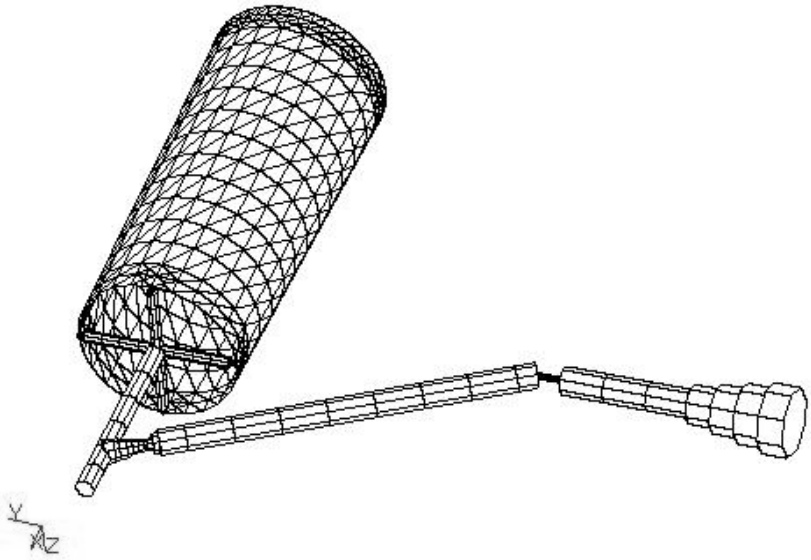

Figure 5.13- Mesh of the C-Mold model for the spider gated tube (1004 elements)

5.4.1.2- Rheology description

The viscosity of the materials is described by the Cross model

$$\eta(\gamma, T, p) = \frac{\eta_0}{1 + \left(\frac{\eta_0 \times \gamma}{\tau}\right)^{1-n}} \tag{5.3}$$

where the zero shear rate viscosity is given by the modified WLF equation

$$\eta_0(T, p) = D_1 \times \exp\left(\frac{-A_1 \times (T - D_2 - D_3 \times p)}{A_2 + T - D_2}\right) \tag{5.4}$$

Table 5.13 - Constants of Cross-WLF model (C-Mold v 99.7)

Parameters	PP Hifax BA238 G3	PC Lexan 141R	Unit
n	0.2992	0.17	
τ	25.23	716.502	kPa
D1	168×10^3	2.68×10^3	GPa.s
D2	263	417.15	K
D3*	0.5	0.2	$K.MPa^{-1}$
A1	31.67	30.2166	
A2	51.6	51.6	K

* these values are not included in the C-Mold database and were estimated from simulations and from values published in the literature [126, 127]

5.4.1.3- pvT description

The procedure for the pvT material characterisation used by the C-Mold laboratories was based on measurements of isothermal compression volume changes starting at each temperature from atmospheric pressure. For the materials used, the pvT behaviour is described by the modified form of the Tait equation

$$\mathrm{v}(T, p) = \mathrm{v}_0(T)\left[1 - C \times \ln\left(1 + \frac{p}{B(T)}\right)\right] + \mathrm{v}_t(T, p) \tag{5.5}$$

where

$$\mathrm{v}_0 = b1_m + b2_m \times \overline{T}$$

$$B(T) = b3_m \times \exp(-b4_m \times \overline{T}) \qquad \text{if } T > T_t(p) \qquad (5.6)$$

$$\mathrm{v}_t(T, p) = 0$$

and

$$\mathrm{v}_0 = b1_s + b2_s \times \overline{T}$$

$$B(T) = b3_s \times \exp(-b4_s \times \overline{T}) \qquad \text{if } T < T_t(p) \qquad (5.7)$$

$$\mathrm{v}_t(T, p) = b7 \times \exp(b8 \times T - b9 \times p)$$

C is the universal constant of 0.0894, and $\bar{T} \equiv T - b5$

The subscript *m* refers to the material when molten and the subscript *s* to the solid material. In addition, the transition temperature is assumed to be a linear function of the pressure:

$$T_t(p) = b5 + b6 \times p \qquad (5.8)$$

Table 5.14 - Constants of the modified form of the Tait equation.

Parameters	PP Hifax BA238 G3	PC Lexan 141R	Units
b5	428.15	417.15	K
b6	0.0715	0.348	$K.MPa^{-1}$
b1m	1.275	0.854	$m^3.Mg^{-1}$
b2m	$1.0x10^{-3}$	$0.566x10^{-3}$	$m^3.Mg^{-1}.K^{-1}$
b3m	86.6	182	MPa
b4m	$5.181x10^{-3}$	$4.0411x10^{-3}$	K^{-1}
b1s	1.184	0.854	$m^3.Mg^{-1}$
b2s	$0.6x10^{-3}$	$0.16x10^{-3}$	$m^3.Mg^{-1}.K^{-1}$
b3s	147	299	MPa
b4s	$4.589x10^{-3}$	$1.711x10^{-3}$	K^{-1}
b7	0.907	0	$m^3.Mg^{-1}$
b8	0.1256	0	K^{-1}
b9	$12.1x10^{-3}$	0	MPa^{-1}

5.4.2- UNISA program

The simulations (filling, holding and cooling) using the UNISA program are performed on the basis of the Lord and Williams [17,18] model and its extensions [33,34]. A laminar flow of the Hele-Shaw type of a viscous polymeric melt under non-isothermal conditions is considered. Complex geometries are obtained combining (in series or in parallel) simple cylindrical and rectangular elements.

A more complete description of the UNISA code is made in the references [128-130].

Some balance and constitutive equations, and boundary conditions are briefly described in the following sections, for the relevant phases of the moulding cycle.

5.4.2.1- Filling phase

The Lord and Williams model is applied to the filling stage of moulds with the cross section normal to the main flow direction gradually changing along the flow path (figure 5.14).

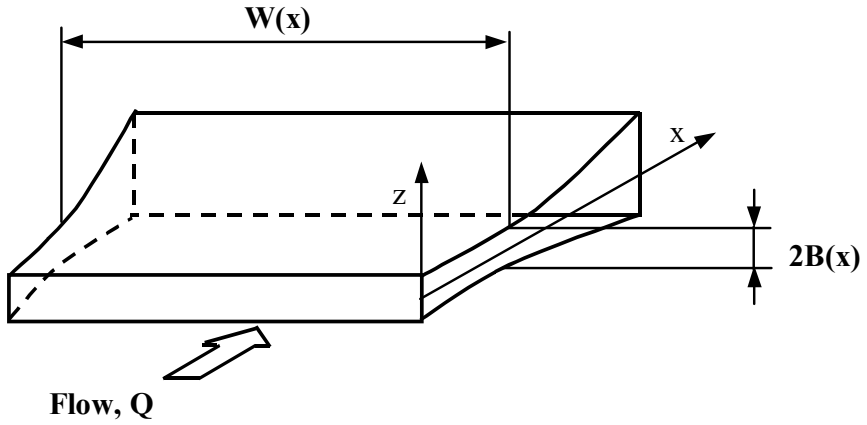

Figure 5.14- Scheme of rectangular cavity with cross section gradually changing in the flow direction

The axial convection, transverse conduction and heat generation, both viscous and due to the heat of crystallisation (if present), were kept in the energy balance together with the accumulation term. The balance equations for the parallel flow in the rectangular geometry are:

mass balance: $$Q = 2W(x)\int_0^{B(x)} u\,dz \tag{5.9}$$

momentum balance: $$u = -\frac{dp}{dx}\int_z^{B(x)} \frac{z}{\eta}dz \tag{5.10}$$

energy balance: $$\rho C_p\left(\frac{\partial T}{\partial t} + u\frac{\partial T}{\partial x}\right) = \frac{\partial}{\partial z}\left(k\frac{\partial T}{\partial z}\right) + z\frac{\partial p}{\partial x}\frac{\partial u}{\partial z} + \lambda.r_c \tag{5.11}$$

with

$$r_c = \frac{\partial \chi}{\partial t} + u.\frac{\partial \chi}{\partial x}$$

The last term in the equation 5.11 is zero for amorphous materials.

The thermal boundary and the starting conditions are:

inlet melt temperature $$T(x = 0, z, t) = T_{inj} \tag{5.12}$$

zero heat flux at the plan of symmetry $$\frac{\partial \mathrm{T}}{\partial \mathrm{z}}(\mathrm{x}, \mathrm{z} = 0, \mathrm{t}) = 0 \tag{5.13}$$

heat transfer at the mould wall $$-k\left|\frac{\partial T}{\partial z}\right|_{wall} = h\left(T_{wall} - T_{mold}\right) \tag{5.14}$$

Similar equations can be written for a cylindrical geometry with a radius smoothly varying along the flow direction, x.

The heat transfer coefficient of the mould, h, takes into account the thermal resistance between the polymer and the mould, and changes with the contact time, t_c. It decreases from a value at first contact, h_0 (20 W.m^{-2} K^{-1}), to a stationary value, h_1 (2.2 kW.m^{-2} K^{-1}), as a function of the square root of the reciprocal time, as described by the penetration theory [131].

$$h = h_0\sqrt{\frac{t^*}{t^* + t_c}} \tag{5.15}$$

where t^* is a very short time (0.1 s), which ensures that the heat transfer inside the mould soon becomes the controlling mechanism [130,132].

The crystallisation kinetics adopted in the simulation program is the non-isothermal formulation of the Avrami-Evans model due to Nakamura *et al* [133,134]

$$r_c = (\chi_e - \chi)\, n \times \ln 2 \times K(T) \left(\int_0^t K(T)dt \right)^{n-1} \tag{5.16}$$

where

χ_e is the equilibrium crystallinity fraction (considered as independent from temperature in this work);

n is the Avrami index;

K(T) is the kinetics constant which is described as:

$$K(T) = Ko \times \exp\left(\frac{-4 \times \ln 2 (T - T_{max})^2}{D^2} \right) \tag{5.17}$$

The analysis is simplified by considering that only one type of crystalline phase exists. The values of T_{max}, D, Ko and n were obtained for the polypropylene in this work, as listed in Table 5.15, by Pantani *et al.* [135].

Table 5.15 – Constants of polypropylene Hifax BA238G3 for crystallisation kinetics

Constant	Description	Value	Unit
χ_e	Equilibrium crystallinity degree	58%	-
n	Avrami index	0.3	-
K_0	Crystallisation kinetic constant	148.4	s^{-1}
T_{max}	Tamp. Maximum crystallisation rate	331	K
D	Constant in crystallisation kinetic curve	6.5 if $T<T_{max}$ 41 if $T>T_{max}$	K

5.4.2.2- Holding phase

The main difference between filling and holding is in the role played by the density changes in the polymer as a result from temperature, pressure and crystallinity variations. The density

changes have a reduced effect on the filling flow rate, but they are the true driving force for the extra flow taking place during the holding stages.

In each cross section perpendicular to the main flow direction at a distance *x* from the injection point, the mass flow rate during holding is determined by the density increase in the portion of the part delimited by each cross section to be analysed and upstream to the first completely solidified section, x_s, where the flow rate is zero (figure 5.15).

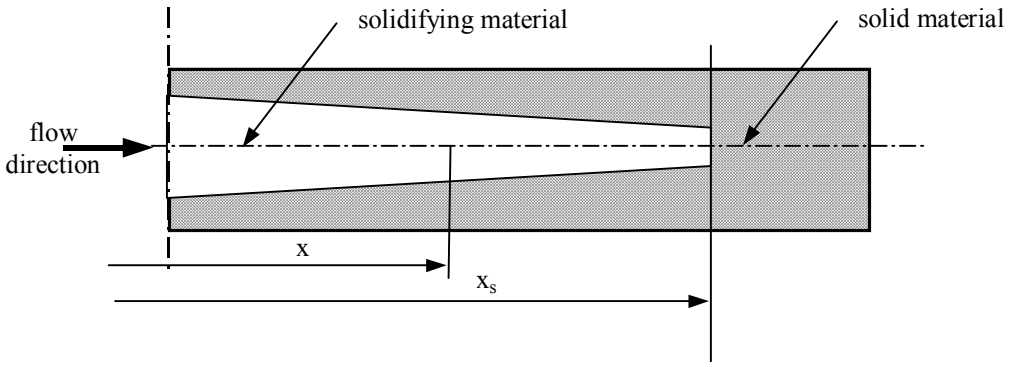

Figure 5.15- Schematic view of the solidification process

Thus the mass flow rate

$$\dot{M}(x,t) = 2\frac{\partial}{\partial t}\int_{x}^{x_s(t)} W(x) \int_{0}^{B(x,t)} \rho(x,z,t)\,dz\,dx \qquad (5.18)$$

From the end of the filling phase until the moment that a cross section undergoes complete solidification, the distance from the injection point to that point, x_s, is the current path length.

After complete solidification of the cross section that control the mass flow into the impression, which is usually the gate, the equation 5.18 describes the mass flow rate upstream to the solidified section whereas, as described next, the cooling model only applies further on.

The enlargement of the impression thickness, B, (figure 5.14) can be related to total pressure distribution acting against the mould walls. An injection mould, which is a mechanically complex system, makes the exact description of the mould deformation a rather difficult task. This results from the pressure distribution inside the impression that determines the mould deformation that, in turn, influences the pressure distribution. A simplified estimation of the actual dimension can be obtained with the relationship

$$B(x,t)=B_0(x)\,(1+ C_M.p(x,t)) \qquad (5.19)$$

where C_M is the mould compliance. If the equation 5.19 is used, at each time the local thickness is only dependent on the local pressure value.

The value of C_M used for the simulations of the edge gated plate according to Pantani [90], is 1 GPa^{-1} for the impression with 2 mm thick and 0.5 GPa^{-1} for the impression with 4 mm thick, as it was described in the chapter 3. For the spider gated tube the value of 0.2 GPa^{-1} was used as described in chapter 3.

Density description

The density was described as a simple weighed average of all phases composing the material.

For the iPP Hifax BA238 G3, a multiphase material, the density is described as:

$$\rho = z_R \ \rho_R + z_T \ \rho_T + (1 - z_R - z_T) \ \rho_P \tag{5.20}$$

where

ρ_R - density of the elastomeric phase (whose mass fraction is z_R)

ρ_T - density of the talc (whose mass fraction is z_T)

ρ_P - density of the iPP

The density of iPP was evaluated as the weighted average of the amorphous and crystalline densities according to:

$$\rho_P = \rho_C \chi + \rho_A (1 - \chi) \tag{5.21}$$

The χ refers to the single α-form equivalent crystallinity degree within the iPP phase only.

The density of the generic phase i is considered as a linear function of temperature and pressure:

$$\rho_i = \rho_i^o \left[1 - \alpha_i (T - T_o) + \beta_i (p - p_0)\right] \tag{5.22}$$

The constants used in equations 5.20 to 5.22 were previously determined, as in [135], for the iPP Hifax BA238G3 case and are listed in table 5.16.

Table 5.16 – Constants of polypropylene BA238G3 for density description

Constant	Description	Value	Unit
p_0	Reference pressure	0.1	MPa
T_0	Reference temperature	298	K
z_R	Mass fraction of EPR	0.27	kg/kg
z_T	Mass fraction of talc	0.015	kg/kg
α_A	Coeff. of thermal expansion for iPP amorphous phase	$6.3x10^{-4}$	K^{-1}
α_C	Coeff. of thermal expansion for iPP crystal phase	$2x10^{-4}$	K^{-1}
α_R	Coeff. of thermal expansion for EPR	$6.7x10^{-4}$	K^{-1}
α_T	Coeff. of thermal expansion for talc	0	K^{-1}
β_A	Compressibility of iPP amorphous phase	$9.1x10^{-4}$	MPa^{-1}
β_C	Compressibility of iPP crystal phase	$1x10^{-5}$	MPa^{-1}
β_R	Compressibility of EPR	$3.8x10^{-4}$	MPa^{-1}
β_T	Compressibility of talc	0	MPa^{-1}
$\rho_a°$	Density of iPP amorphous phase at To and p_o	0.8417	$Mg.m^{-3}$
$\rho_c°$	Density of iPP crystal phase at To and p_o	0.93	$Mg.m^{-3}$
$\rho_R°$	Density of EPR at To and p_o	0.86	$Mg.m^{-3}$
$\rho_T°$	Density of talc at To and p_o	2.7	$Mg.m^{-3}$

For the amorphous materials, only the equation 5.22 applies, where $T_0=T_g$ (glass transition temperature) at $p_0=0$. α and β are the thermal expansion coefficient and the compressibility, respectively, and refer to the melt if $T>T_g$ and to a solid if $T<T_g$. The constants for the polycarbonate Lexan 141R were determined from the pvT data in the C-Mold database, and are listed in Table 5.17.

Table 5.17 – Constants of polycarbonate Lexan 141R for density description

Constant	Description	Value	Unit
p_0	Reference pressure	0.1	MPa
T_0	Reference temperature	417	K
α_m	Melt coeff. of thermal expansion	$4.78x10^{-4}$	K^{-1}
α_s	Solid coeff. of thermal expansion	$1.84x10^{-4}$	K^{-1}
β_m	Melt compressibility	$3.99x10^{-4}$	MPa^{-1}
β_s	Solid compressibility	$2.65x10^{-4}$	MPa^{-1}
$\rho°$	Density at To and p_o	1.171	$Mg.m^{-3}$

The momentum balance equation, as described by equation 5.10, holds identically for the packing stage. The flow rate being much smaller during packing than during filling, the viscous dissipation term is not taken into account in the energy balance. All the other terms of equation 5.11 are kept in the energy balance. The initial temperature and pressure fields are those determined at the end of the filling stage; the equations 5.13 to 5.15 describe the other boundary conditions.

Cooling process

The cooling process starts downstream from the first solidified section, usually the gate. While the cooling takes place in the impression, the holding flow still continues to take place upstream to the gate (runner system).

During cooling, although of the impression volume decreases due to the mould deformation recovery, the mass per unit cavity length remains essentially constant with time. Thus

$$\int_0^{B(x,t)} \rho(P(x,t),T(x,z,t),\chi(x,z,t))dz = const \tag{5.23}$$

Thus, the local thickness, B(x,t), decreases with time only due to the mould deformation recovery. A more complete discussion of this model was made by Speranza [130].

6- RESULTS AND DISCUSSION

The results of this work are presented and discussed in the following main sections: Moulding pressure, Temperature evolution, Shrinkage and Ejection forces.

As it was pointed out in the literature that was reviewed in section 2.2, the pressure in the impression is directly correlated with the shrinkage. The recorded pressure and temperature profiles during processing are analysed and compared with simulations using the C-Mold v. 99.7 and the "open" program UNISA. The effects of the pressure on the viscosity, and the mould deformation on the predicted pressure evolution are examined.

The shrinkage evolution was measured using a recent technique making use of resistance strain gauges, and the shrinkage after ejection was calculated at room temperature. The results are analysed and compared with simulations using the C-Mold v. 99.7 and a thermo-mechanical model originally developed at the Università di Salerno and modified to suit specific aspects of this research, as shown in chapter 3.

The force evolution during the ejection and its maximum value for the case of tubular mouldings were monitored with the instrumented mould developed in this work. The ejection force is analysed and compared with predictions using a thermo-mechanical model developed in this work as already described in chapter 3.

6.1- Moulding pressure

The pressure evolution during the production of the samples is presented in this section. The experimental pressure evolution is used to obtain objective information about the flow rate, the extent of the filling, the holding and the cooling progress, and to validate some simulations. In some cases the difference between experimental and predicted pressures is analysed, examining the effect of the pressure on the viscosity and the mould deformation.

The complete pressure evolution data of the rectangular plate mouldings are included in Appendix A1.2 and of the tube mouldings in Appendix A2.2.

6.1.1- Experimental pressure evolution

During the production of the samples, the pressure inside the impression was measured using miniature piezoelectric sensors from Kistler. These sensors are suitable for direct pressure measurement in the impression, thus enabling to follow the actual moulding process.

6.1.1.1- Instrumentation reproducibility and performance

The pressure evolution inside the impression during five consecutive cycles for the moulding condition code 310.110.10.15., are shown in figure 6.1. in this figure the filling (I) and holding (II) phases are delimited.

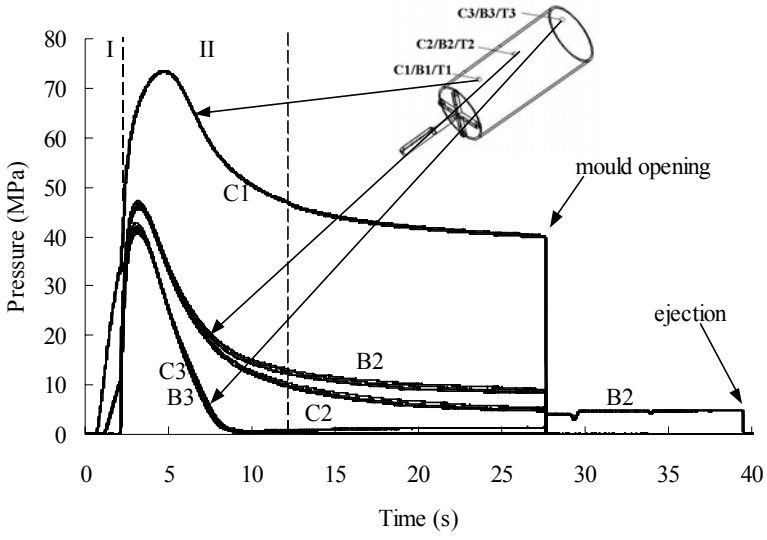

Figure 6.1- Pressure evolution inside the impression during five consecutive cycles in PC tubes, for the moulding condition code 310.110.10.15

The data were obtained from three pressure sensors in the cavity (C1, C2 and C3) and two in the core (B2 and B3), along the flow path. The sensors C2 and C3, and B2 and B3 face each other at 79 and 139 mm from the gate. The pressure evolution for this moulding condition was not measured by the sensor located in the core (C1) at 21 mm from the gate.

As it can be seen in the figure 6.1, the pressure evolution measured by each sensor during the five consecutive cycles, is very similar. The maximum difference between the values at a specific time of the pressure measurement of each sensor is about 2 MPa.

The pressure measured by the sensors located at position 2 (in the core and in the cavity) are very close up to 8 s and then diverge. In the figure 6.1, it can be also observed, that the sensor B2 measures a residual pressure (of about 5 MPa for this condition) during the interval from the mould opening to the ejection. The residual pressure that the sensors located in the core measure after the mould opening is not yet completely understood. However, the local elastic deformation of the sensors when subject to a high pressure during the holding phase seems to be possible explanation for this behaviour.

6.1.1.2- Rectangular plate

Pressure evolution for PC

The recorded pressure curves for some of the moulding settings are shown in figures 6.2 and 6.3. The upper line corresponds to the pressure measured by the transducer in the nozzle (position P0). The packing pressure is kept constant during the holding phase and then falls off. The small pressure peak at the nozzle at 22 s, in figure 6.2, corresponds to the back pressure during plasticisation. In the next figures the small pressure peak will be noted by the word “plasticisation”.

For a low holding pressure of 36 MPa (figure 6.2a) the pressure in the mould cavity becomes zero between 17 and 20 s. At this time, the thickness shrinkage starts and the moulding detach from the impression wall.

For a higher holding pressure of 80 MPa (figure 6.2b), the overpacking of the polymer in the impression at the moment at which the gate freezes-off is so high that the thermal contraction

due to cooling is not capable of overcoming the pressure effect, and the moulding remains in contact with the wall impression.

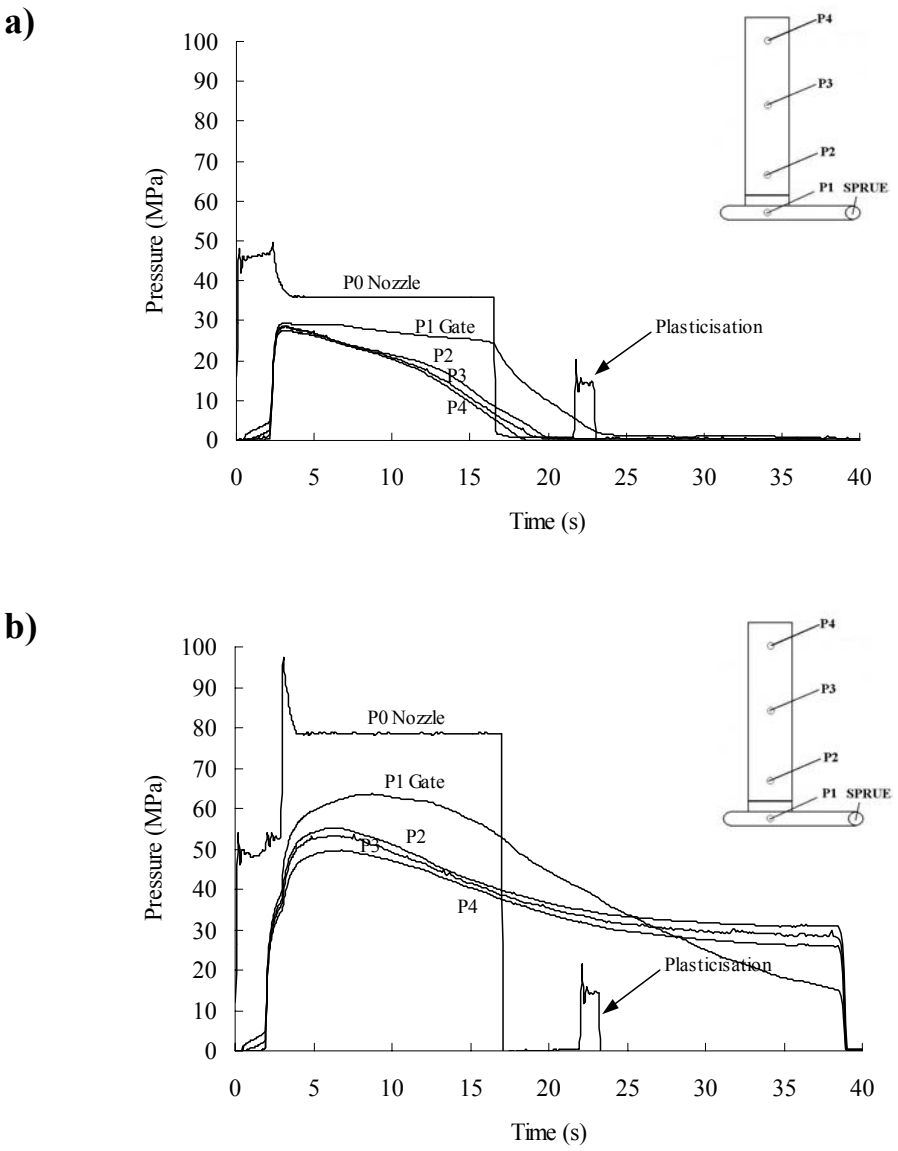

Figure 6.2- Influence of the holding pressure on the pressure curves in PC plates. Mouldings at Tinj=310ºC and holding pressure (Ph) of: a) 36 MPa and b) 80 MPa, with holding time of 15 s.

The gate sealing time, for the injection temperature of 310ºC, was estimated to be 10 s by observation of the onset of the pressure drop in the impression sensors as shown by P2 in figure 6.2a, and comparing the evolution of the pressure curves in figures 6.3, for holding times of 5 s and 15 s. During the holding phase, the mass flow through the gate counteracts the effect of the material volumetric decrease due to cooling, on the impression pressure evolution. If the holding pressure is released before the gate sealing time, the pressure decreases suddenly as it can be

observed in figure 6.3a. Increasing the holding time to 15 s (figure 6.3b), the pressure remains after the end of the holding phase and no back flow is apparent.

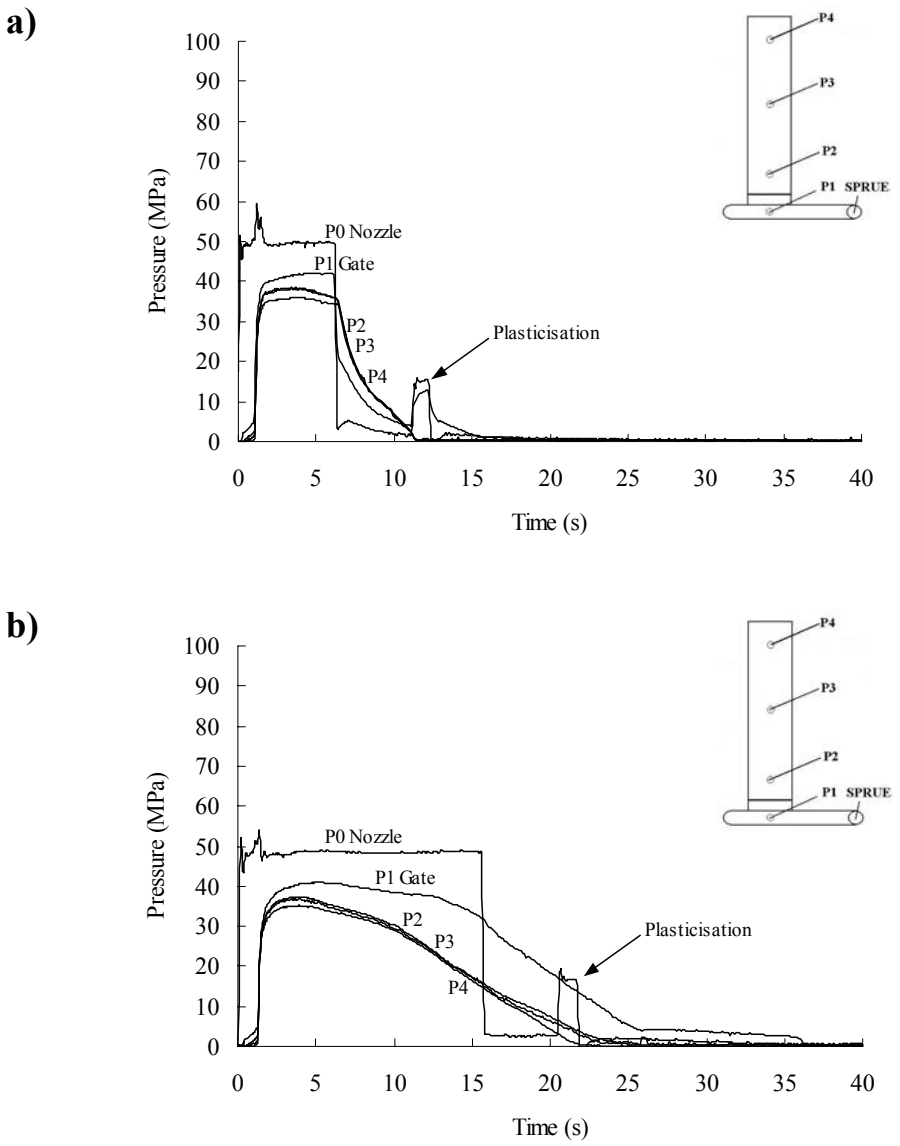

Figure 6.3- Influence of the holding time on the pressure curves in PC plates. Mouldings at Tinj=310ºC and holding time (th) of: a) 5 s and b) 15 s, with holding pressure of 49 MPa.

Pressure evolution for iPP

The recorded pressure curves for some of moulding conditions used for polypropylene are depicted in the figures 6.4 and 6.5. As it was indicated for polycarbonate, in the case of polypropylene it is also possible to observe that the pressure measured by the sensor in the

nozzle (position P0) during the filling and holding phases, and the pressure generated at the tip of the nozzle during plasticisation.

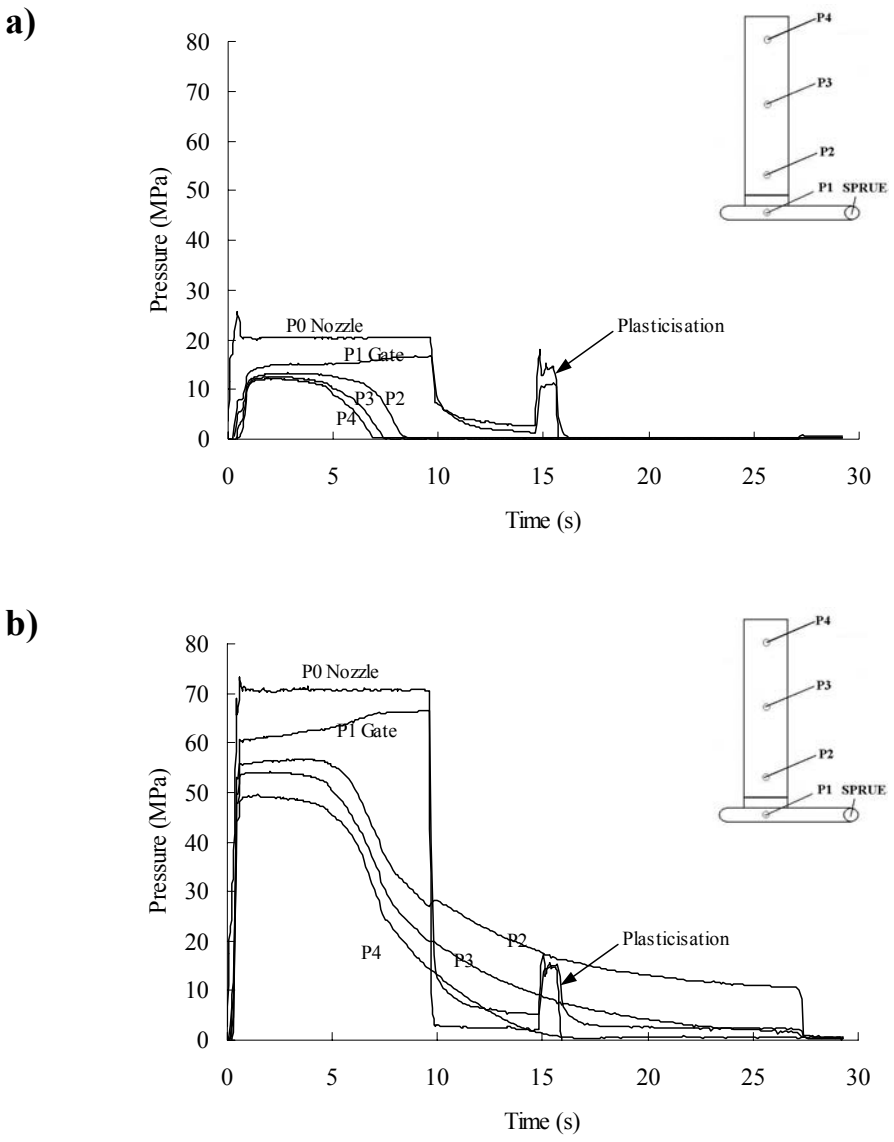

Figure 6.4- Influence of the holding pressure on the pressure curves in iPP plates. Mouldings at Tinj=230ºC and holding pressure (Ph) of: a) 20 MPa and b) 70 MPa, with holding time of 10 s.

For a low holding pressure of 20 MPa (figure 6.4a) the pressure in the mould cavity becomes zero at about 8 s (onset of thickness shrinkage). If the material is highly packed inside the impression at the instant of the gate solidification, the thermal shrinkage can not be sufficient (even for a material that shows a higher shrinkage) to compensate for the extra volume of polymer packed inside the impression, and a residual pressure remains as shown by the sensor P2 (figure 6.4b).

The gate sealing time was estimated to be 7 s by observation of the onset of the pressure drop indicated by P2 in figure 6.4a and comparing the pressure curves evolution in figures 6.5 (for holding times of 6 s and 10 s), or analysing the pressure evolution in the sensor P1 (just before the gate) in figures 6.4 and 6.5b. When the gate freezes off, the pressure in the position P1 increases, and the onset of that increase gives the gate sealing time.

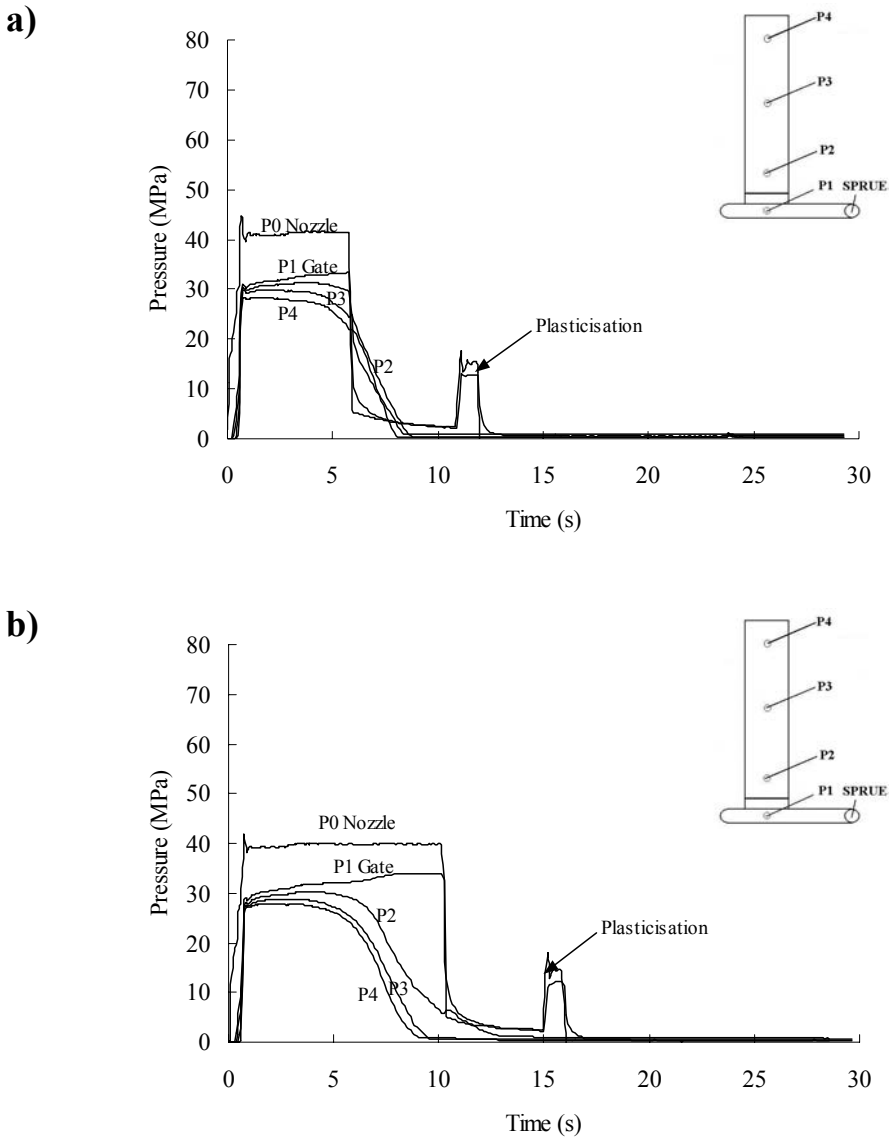

Figure 6.5- Influence of the holding time on the pressure curves in iPP plates. Mouldings at Tinj=230ºC and holding time (Ph) of: a) 6 s and b) 10 s, with holding pressure of 40 MPa.

6.1.1.3- Spider gated tube

The pressure inside the impression during the production of the tubular mouldings measured by the sensors located in the cavity side will be presented next alongside with the indication of the filling (I) and holding (II) phases.

Pressure evolution for PC

The pressure curves for cases of low and high holding pressures at different positions of sensors are shown in figures 6.6, as measured by the sensors located in the cavity.

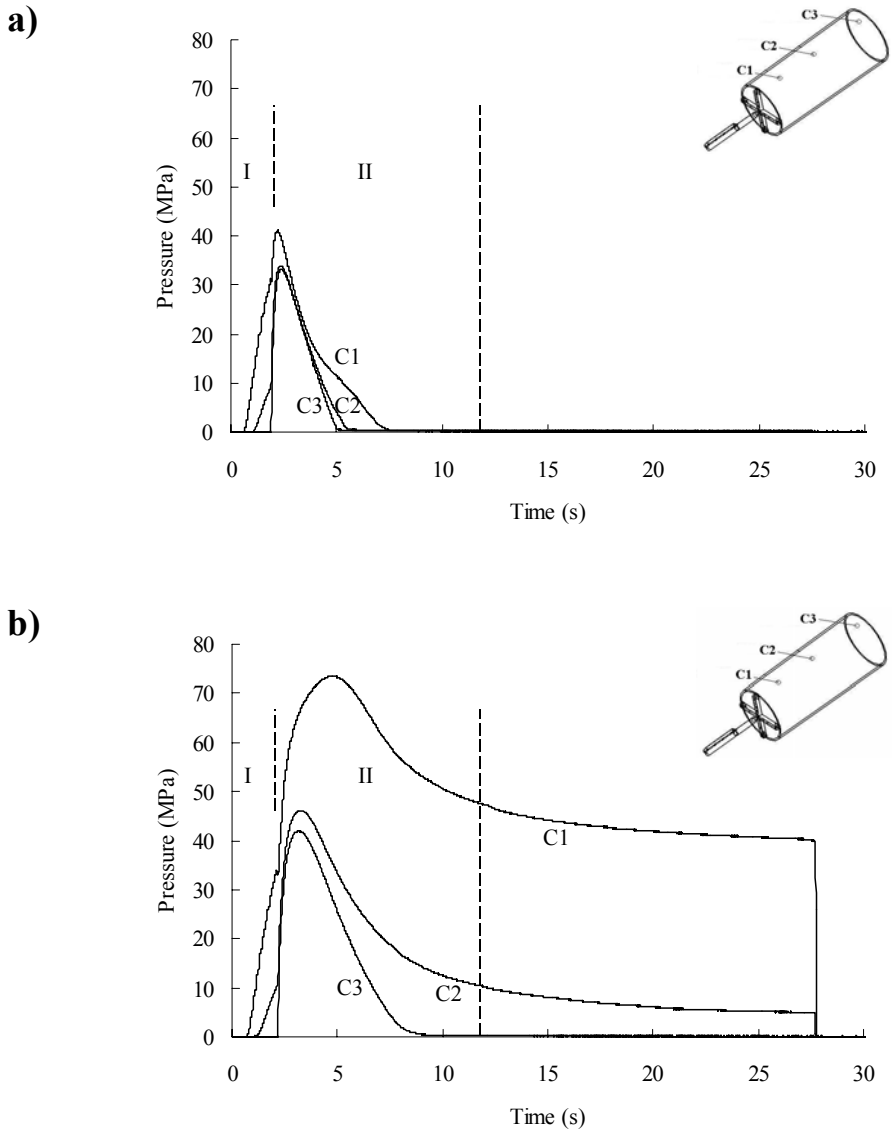

Figure 6.6- Influence of the holding pressure on the pressure curves in PC tubes. Mouldings at Tinj=310ºC and holding pressure (Ph) of: a) 12 MPa and b) 110 MPa, with holding time of 10 s.

The pressure data in the position C1 (just after the gate) gives important information about the solidification evolution in the gate and downstream from this position. The solidification evolution can be tracked considering the slope of the pressure curve in that position.

When no more material goes inside the impression, the pressure reduction is due only to the shrinkage caused by cooling, and takes place simultaneously with the elastic recovery of the mould deformation, which counteracts the pressure reduction. If the pressure inside the impression is not very high it becomes zero within the cycle time and after the gate freezing time, as it happens for the tests corresponding to figure 6.6a, with a holding pressure of 12 MPa.

Since the thermal profiles change along the flow path (figure 6.20), it can happen that the pressure curves in different positions of the impression diverge with time. This is the case of pressure curves in the positions C2 and C3, that being close up to 4 s then separate markedly.

For the experiment with th=5 s (figure 6.7a), the pressure near to the gate (position 1) decreases abruptly as soon as the holding pressure is released indicating that the gate is not yet completely blocked. Increasing the holding time to 10 s (figure 6.7b), the pressure remains after the end of the holding phase.

a)

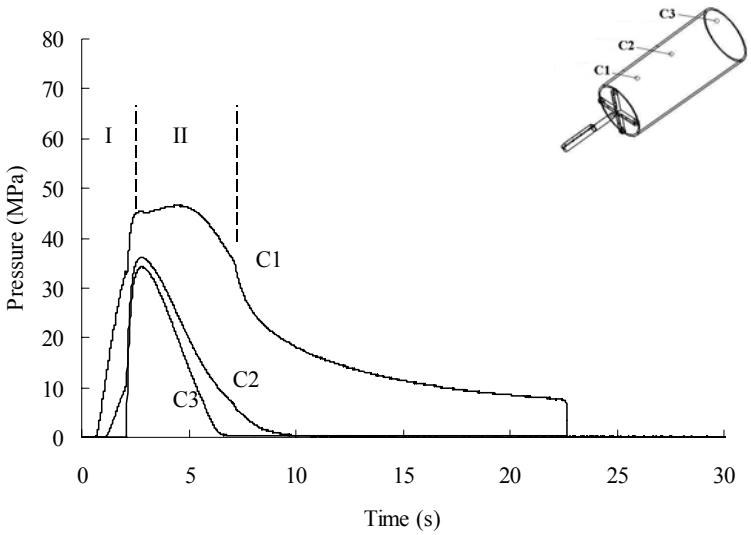

b)

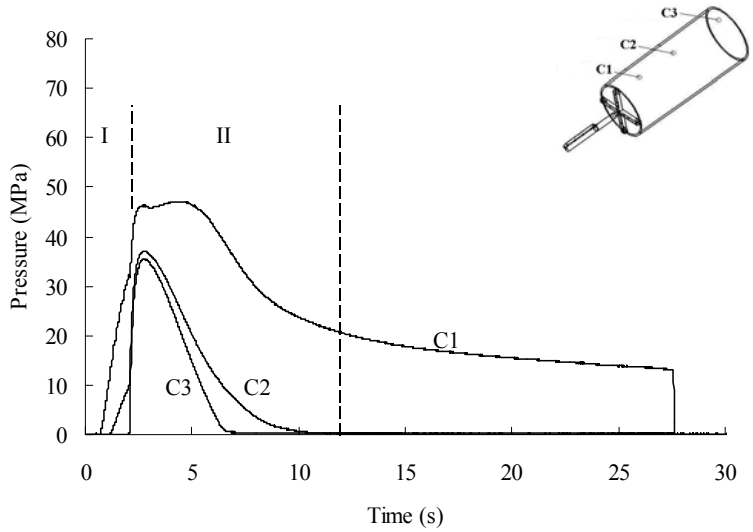

Figure 6.7- Influence of the holding time on the pressure curves in PC tubes. Mouldings at Tinj=310ºC and holding time (Ph) of: a) 5 s and b) 10 s, with holding pressure of 68 MPa.

Pressure evolution for iPP

The evolution of lower and higher holding pressures at different positions of the sensors are shown in figures 6.8 for the moulding conditions of: injection temperature (Tinj) of 210 ºC, mould wall temperature (Tw) of 50 ºC, holding time (th) of 13 s, time after holding stage (ta) of 10 s

As it can be observed, at about 8 s, an increase of pressure is recorded by the sensor C1 followed by a sharp decrease of pressure profiles measured by the sensors C2 and C3. The pressure peak, in the pressure evolution measured by the sensor just after the gate, indicates that the polymer solidifies in the impression between the positions C1 and C2.

The gate sealing time was estimated as 11 s, corresponding to the pressure peak measured by the sensors C1 as shown in the figures 6.8 for the two holding pressures of 19 MPa and 47 MPa.

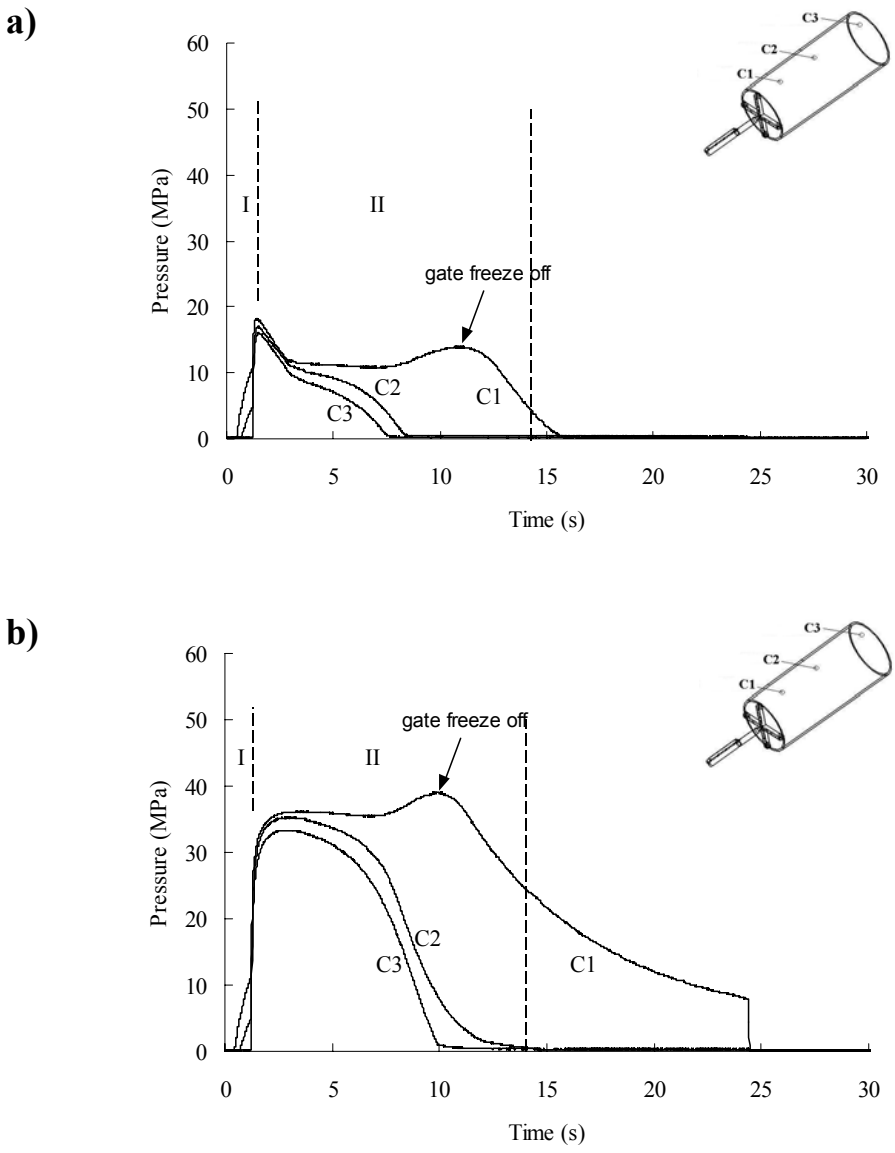

Figure 6.8- Influence of the holding pressure on the pressure curves in iPP tubes. Mouldings at Tinj=210ºC, Tw=50ºC and holding pressure (Ph) of: a) 19 MPa and b) 47 MPa, with holding time of 13 s.

In the figure 6.9 the pressure curves are shown for other mouldings conditions corresponding to: injection temperature (Tinj) of 190 ºC and 230 C, mould wall temperature (Tw) of 50 ºC, holding pressure (Ph) of 40 MPa, holding time (th) of 13 s, time after holding stage (ta) of 10 s.

The increase of the injection temperature delays the pressure drop in the impression for about 2 s and leads to a higher pressure inside the impression of about 5 MPa. The increase of temperature reduces the material viscosity, and more material can be introduced into the impression during the holding phase due to the lower pressure drop. The increase of the pressure inside the

impression resulting from the higher of injection temperature in fact is the reason already pointed out by some authors [51,52] to explain the decrease of the shrinkage when the injection temperature increases.

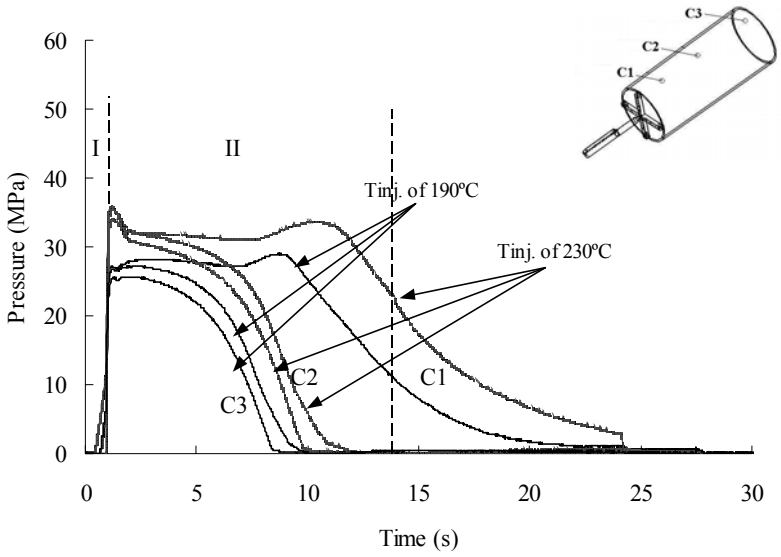

Figure 6.9- Pressure curves in iPP tubes with Tw=50ºC. Effect of injection temperature; moulding conditions codes 190.40.13.10 and 230.40.13.10.

6.1.1.4- Concluding remarks

The results reviewed in this *Experimental pressure evolution* section suggest that:

- The pressure evolution measurements, during consecutive cycles, show that the sensors used allow for a reliable and reproducible measurement in the mould cavity;
- Mouldings with PC requires a relatively higher pressure to fill the mouldings than when iPP is used. This is an expected result, since the PC has a higher melt viscosity;
- Polycarbonate leads to a higher residual pressure than polypropylene for both geometries, due to its lower thermal contraction;
- In the spider gated tube, the pressure profiles at different positions diverge with the time. This behaviour means that the thermal profiles change along the impression;
- The pressure evolution in iPP tubes shows that the cavity pressure increases with the injection temperature and that the gate sealing-off time also increases. The increase of the injection temperature causing a reduction of the viscosity, makes the flow easier and leads to a higher pressure in the impression due to the smaller pressure drop in the flow length during the holding phase.

6.1.2- Simulations

The pressure curve evolution in the mouldings was simulated imposing a pressure identical to that experimentally measured in the nozzle. The flow rate used in the simulations was determined from the volume between the two first pressure transducer locations in the impression, divided by the time that the melt took to flow between them.

The pressure evolution obtained in the simulations will be compared with the experimental data in some moulding conditions. For the geometries and materials used the pressure profile comparison will be done for one position only in the impression.

The effect of considering or neglecting the effect of pressure on the viscosity and mould deformation will be also analysed.

In order to quantify the analysis, the average absolute deviation between the predicted and the experimental pressure evolution in the impression was calculated, using the expression:

$$\text{Deviation} = \frac{\sum_{i=1}^{m}\sum_{j=1}^{n}\left|p_{\exp}(i,j) - p_{pred}(i,j)\right|}{n\text{x}m} \qquad (6.2)$$

The indices *i* and *j* refer to location along the flow path and time, respectively.

For the calculations of the deviation for each condition, 3 positions along the flow path and 10 points per second during the time that the mould is closed (corresponding to the time that the sensors acquired the pressure signal) were used.

6.1.2.1- Analysis with C-Mold

The simulations were done using the standard parameters given in the material database. In some cases some parameters were changed as it will be mentioned whenever appropriate.

6.1.2.1.1- Effect of pressure on viscosity

In the C-Mold database the parameter accounting for pressure in the viscosity (variable D3 of equation 5.4) is set to zero. If the effect of pressure on the viscosity is considered it results in an

increment of the viscosity, thus increasing the pressure drop from the nozzle to the mould impression as it was already pointed out by Lord [19].

Pressure evolution for iPP

The simulated pressure evolution at the middle position in the cavity (position P3 for the plate and position C2 for the tube), is shown in the figure 6.10 for the plate and in the figure 6.11 for tube geometry.

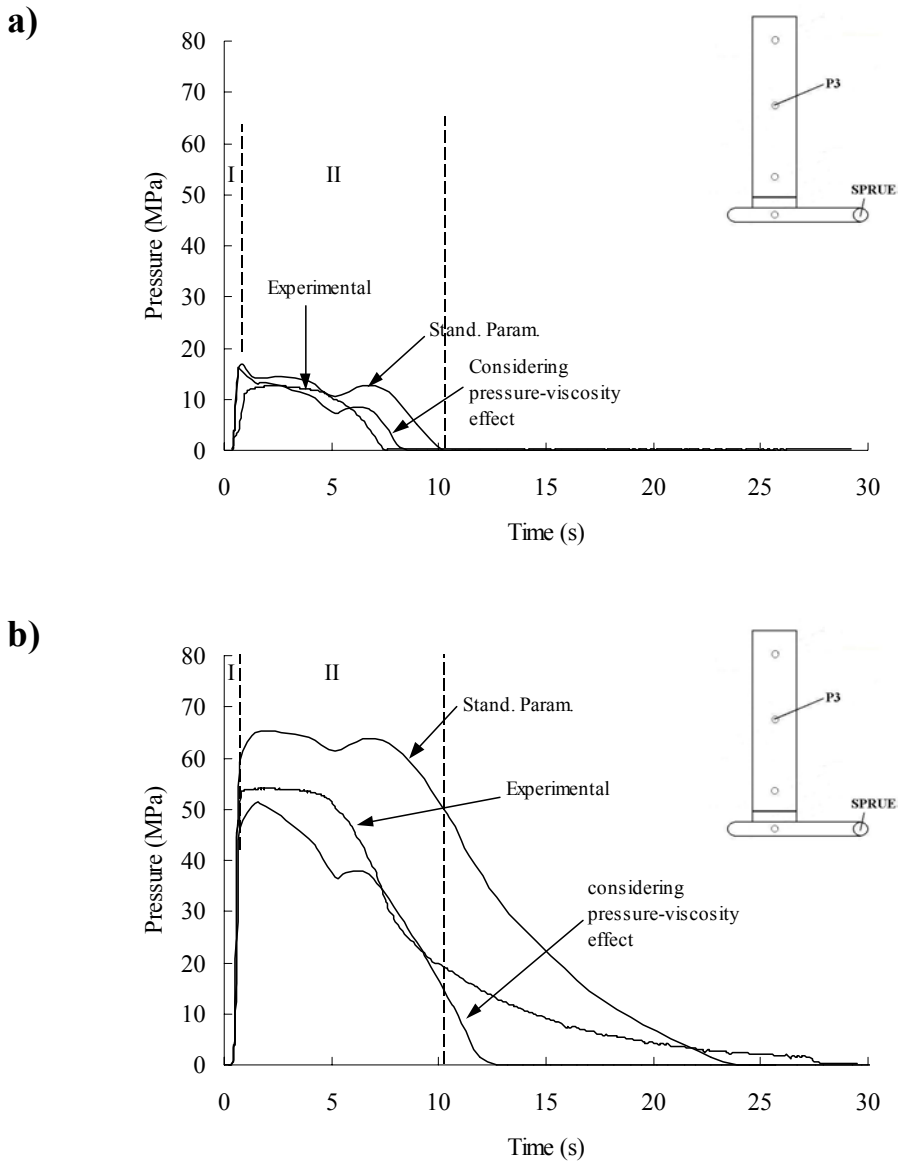

Figure 6.10- Comparison between experimental pressure evolution, simulation performed with standard C-Mold parameters and considering the effect of pressure on viscosity, at position P3 in iPP plates. Moulding conditions codes: a) 230.20.10.15 and b) 230.70.10.15

In the figures 6.10 and 6.11, the pressure predictions, after setting the parameter accounting for pressure on viscosity in the WLF equation to 0.5 K.MPa^{-1} (all the other parameters were left unchanged) are also included. As it was mentioned in section 5.4.1.2, the parameter accounting for pressure on viscosity in the WLF equation was estimated from previous simulations and from data published in the literature [126,127].

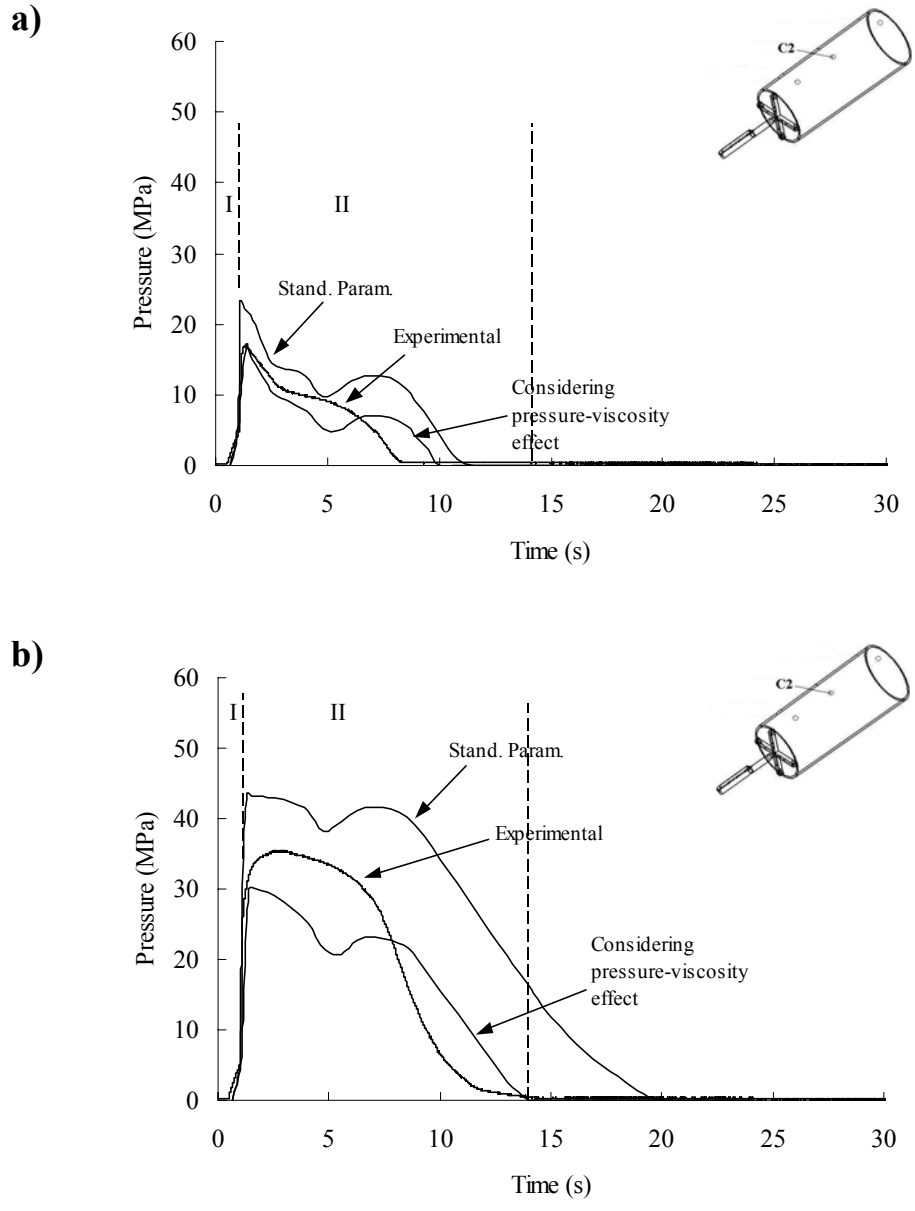

Figure 6.11- Comparison between experimental pressure evolution, simulation performed with standard C-Mold parameters, and considering the effect of pressure on viscosity, at position C2 in iPP tubes, with Tw=50ºC. Moulding conditions codes: a) 210.19.13.10 and b) 210.47.13.10.

The results of the pressure predictions are qualitatively in good agreement with measurements for all moulding conditions used in both geometries. However, the C-Mold pressure predictions, using their own database parameters, were always higher than the experimental values in the holding stage when the material experiences lower shear rates.

The higher values of the pressure during the holding phase, as predicted by default by the C-Mold program, indicate that the pressure drop from the nozzle to the impression is lower than the actual pressure drop. This discrepancy is mainly due to the effect of pressure on viscosity being not described in the C-Mold database for Hifax BA238G3. In this database the parameter accounting for pressure in the WLF equation is set to zero.

The deviation between the predicted pressure evolution and the experimental pressure evolution in the impression, are presented in the Tables 6.1 and 6.2 for the rectangular plate and tube.

Table 6.1 – Deviation between the predicted from C-Mold and experimental pressure evolution in iPP plates.

Condition	Deviation		Precision improvement (%)
	Using standard parameter (MPa)	Considering p-v effect (MPa)	
230.20.10.15	4.8	2.8	41.7
230.40.10.15	9.9	3.6	63.6
230.70.10.15	14.2	6.6	53.5

Table 6.2 – Deviation between the predicted from C-Mold and experimental pressure evolution in iPP tubes with Tw=50ºC.

Condition	Deviation		Precision improvement (%)
	Using standard parameter (MPa)	Considering p-v effect (MPa)	
210.19.13.10	3.6	1.5	58.3
210.33.13.10	5.8	2	65.5
210.40.13.10	3.8	2.7	28.9
210.47.13.10	8.9	3.5	60.7

The predictions considering the pressure effect on the viscosity imply a higher material viscosity in the simulation of the holding phase. This results in a larger pressure drop in the flow path, and the prediction of a lower pressure in the impression, therefore improving the precision of the pressure predictions in about 55% for both geometries.

6.1.2.1.2- Effect of mould deformation

The effect of the mould deformation on the pressure evolution was studied recently by Delaunay *et al* [137]. Comparing the pressure evolution in moulds with different designs for stiffness it was shown that the pressure evolution depends on the mould deformability.

The effect of the mould deformability was taken into account in the simulations, by assigning the corrected material compressibility to the mould compliance. In this work the *corrected* material compressibility (β_{new}) was obtained changing the parameter *b3* in the Tait equation (since β is inversely proportional to *b3*) in order to obtain:

$$\beta_{new} = \beta_{C\text{-}Mold} + C_M \quad (6.1)$$

where the subscripts *new* and *C-Mold* refer to the values in the simulations and in the C-Mold database, respectively.

The mould compliance C_M is related to the local rigidity of the mould. For the mould that produces the edge gated plates, as defined and estimated in section 3.1.1, the value of C_M takes the value of 1 GPa^{-1} and 0.5 GPa^{-1}, for the 2 mm and 4 mm thick mouldings, respectively. It is worth mentioning that the thickness of the impression used to produce the plate mouldings in PC is of 4 mm.

For the mould that produces the spider gated tubes the value of C_M=0.2 GPa^{-1}, was defined and estimated in section 3.2.3.

Pressure evolution for PC

The simulated pressure curves near the gate (position P2 for the plate and position C1 for the tube) for some tests are shown in figures 6.12 and 6.13, for the plate and tube geometries, respectively.

The results of pressure predictions, setting the parameter accounting for pressure on viscosity to 0.2 $K.MPa^{-1}$, in the WLF equation are qualitatively in good agreement with measurements for all moulding conditions used in both geometries. The value of the parameter accounting for pressure on viscosity was estimated from previous simulations and from values published in the literature [126,127], as it was mentioned in section 5.4.1.2.

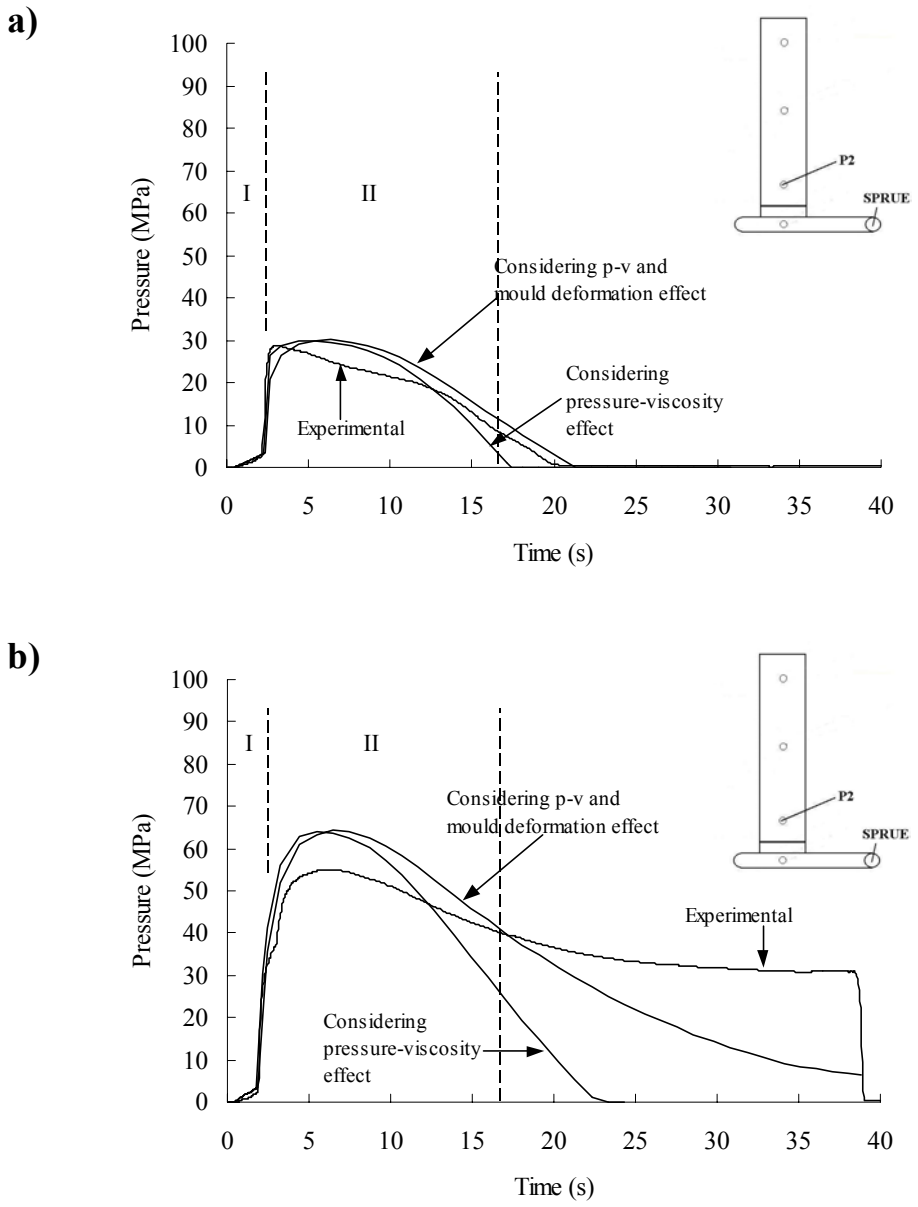

Figure 6.12- Comparison between experimental pressure evolution and simulation considering the effect of pressure on viscosity and the mould deformation, at position P2 in PC plates. Moulding conditions codes: a) 310.36.15.20 and b) 310.80.15.20

During the holding and the cooling stages, the simulated pressure decay is faster than the experimental decay. This effect is much more evident for the mouldings produced with higher pressures.

The lower decay rate of experimental pressure in relation to the simulated pressure is explained considering that after the gate sealing, the mould gradually recovers the deformation keeping the material under compression [55,82,89,136]. This effect is not described by the C-Mold software.

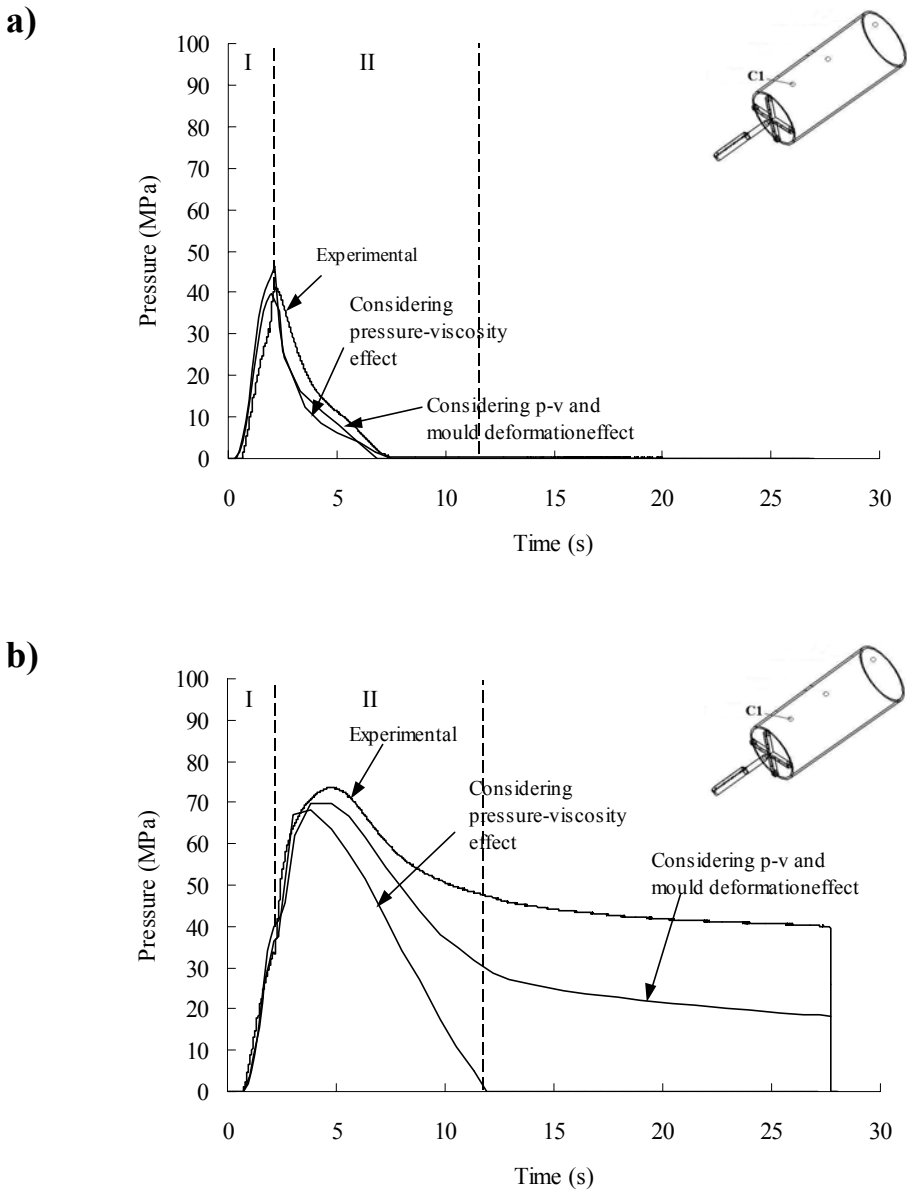

Figure 6.13- Comparison between experimental pressure evolution and simulation considering the effect of pressure on viscosity and the mould deformation, at position C1 in PC tubes. Moulding conditions codes: a) 310.12.10.15 and b) 310.110.10.15

In the figures 6.12 and 6.13, the pressure predictions, using the *new* value of material compressibility, are also included.

The deviation between the predicted pressure and the experimental pressure evolutions in the impression, are presented in the Tables 6.3 and 6.4 for the rectangular plate and the tube.

It is observable that if the mould deformation is considered the precision of the pressure prediction improves in about 32 %, especially at higher holding pressures.

Table 6.3 – Deviation between the predicted from C-Mold and experimental pressure evolution in PC plates.

Condition	Deviation		Precision improvement (%)
	Considering p-v effect (MPa)	Considering p-v + mould def. effect (MPa)	
310.36.15.20	3	2.9	3.3
310.49.15.20	4	4	0
310.66.15.20	13.6	8.2	39.7
310.80.15.20	19.1	10.6	44.5

Table 6.4 – Deviation between the predicted from C-Mold and experimental pressure evolution in PC tubes.

Condition	Deviation		Precision. improvement (%)
	Considering p-v effect (MPa)	Consid. p-v + mould def. effect (MPa)	
310.12.10.15	4.9	4.5	8.2
310.40.10.15	4.1	4	2.5
310.68.10.15	7.6	6.8	10.5
310.89.10.15	10.5	6.5	38.1
310.110.10.15	15	8.1	46

6.1.2.2- Analysis with UNISA

The experimental pressure data were also compared with predictions of the UNISA "open" code developed at the University of Salerno. This program takes into account the material crystallisation and the mould deformation. The material rheological data were taken from the C-Mold database. The effect of pressure on viscosity was considered as it was done for the C-Mold simulations.

6.1.2.2.1- Simulated pressure evolution for iPP

The simulated pressure curves at the middle position in the cavity (position C2 for the tube and position P3 for the plate) for some tests are shown in figures 6.14 and 6.15, for the tube and the plate geometries, respectively. In the simulations, the effect of pressure on the viscosity was considered using the parameter D3 in the WLF equation equal to 0.5 $K.MPa^{-1}$ (same value as used in the C-Mold simulations) and the mould deformation was also considered. As it was

mentioned in the section 5.4.2, the UNISA program allows for the introduction of the mould deformation effect in the main equations that describe the holding and the cooling phases.

For the simulations, values of C_M equal to 0.2 GPa^{-1} and 1 GPa^{-1}, for the spider gated tube and for the edge gated plate, respectively, were used. The values for C_M, as defined and calculated in sections 3.1.1 and 3.2.3, give the relative thickness variation of the impression due to the mould deformation. For the case of the tube, the pressure predictions considering the effect of pressure on the viscosity are also compared with the predictions disregarding the effect of pressure on the viscosity.

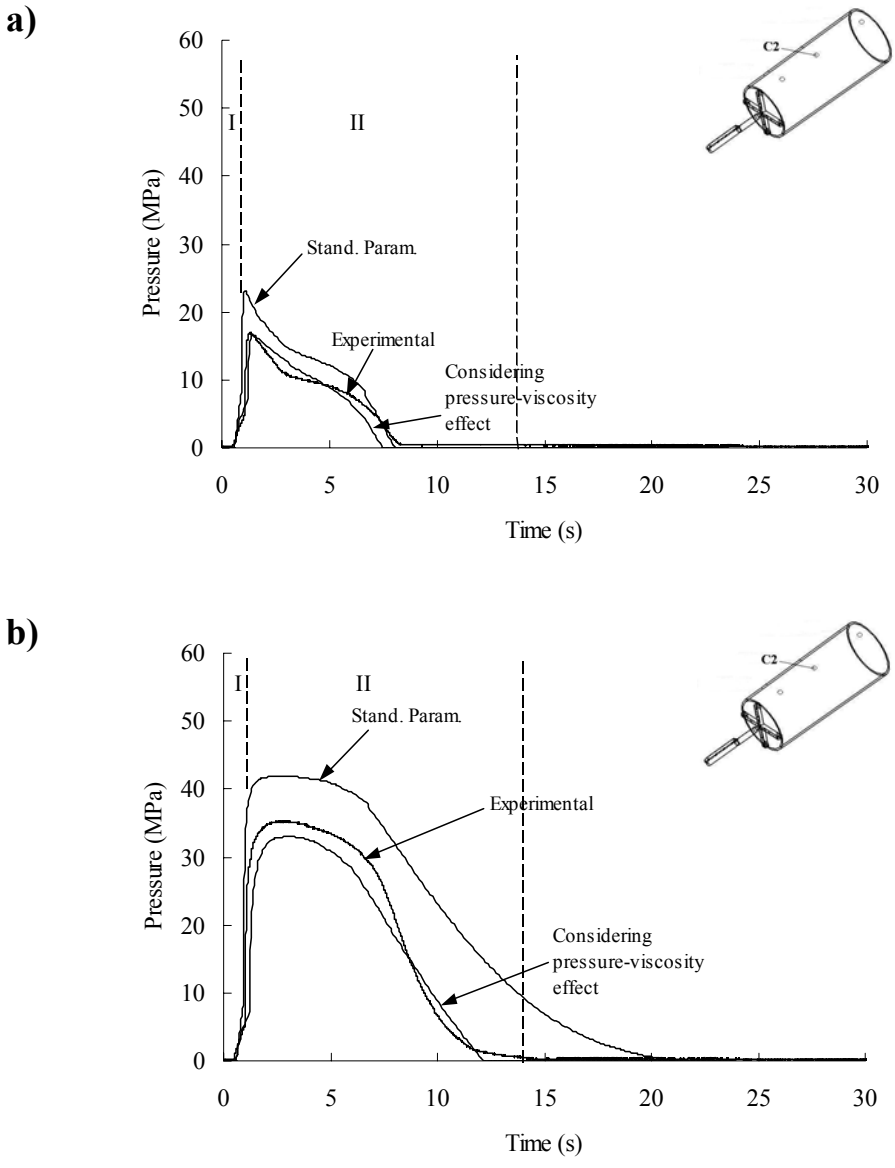

Figure 6.14- Comparison between experimental pressure evolution and UNISA code simulation considering the pressure viscosity effect, at position C2 in iPP tubes, with Tw=50ºC. Moulding conditions codes: a) 210.19.13.10 and b) 210.47.13.10

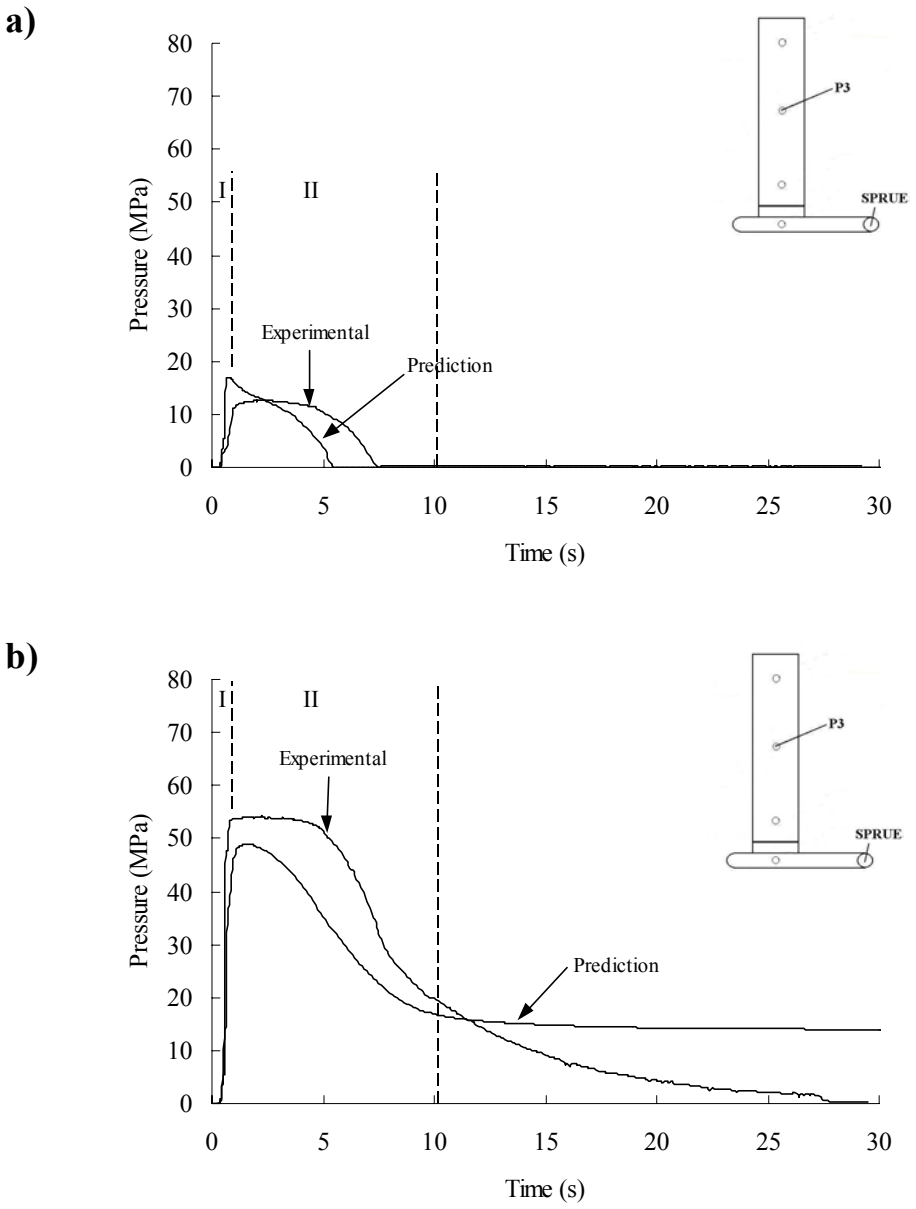

Figure 6.15- Comparison between experimental pressure evolution and UNISA code simulation, at position P3 in iPP plates. Moulding conditions codes: a) 230.20.10.15 and b) 230.70.10.15

The results of the pressure evolution are qualitatively in good agreement with the experimental data for all moulding conditions used. The agreement between experimental and predicted pressure evolutions is improved when the effect of pressure on viscosity is considered, even recalling that the gate freeze-off time is underpredicted in the edge gated plate case. This causes the prediction of a slightly faster pressure drop inside the cavity with respect to measurements (figure 6.15a).

The deviation between the predicted pressure evolution and the experimental pressure evolution in the cavity, are presented in the Tables 6.5 and 6.6 for the rectangular plate and the tube.

Table 6.5 – Deviation between the predicted from UNISA and experimental pressure evolution in iPP plates.

Condition	Deviation
	Considering p-v effect (MPa)
230.20.10.15	3.9
230.40.10.15	4.8
230.70.10.15	8.1

Table 6.6 – Deviation between the predicted from UNISA and experimental pressure evolution in iPP tubes with Tw=50ºC.

Condition	Deviation		Precision Improvement (%)
	Using standard parameter (MPa)	Considering p-v effect (MPa)	
210.19.13.10	3.1	2.1	58.3
210.33.13.10	2.9	1.9	65.5
210.40.13.10	6.9	2.6	28.9
210.47.13.10	6	2.4	60.7

6.1.2.2.2- Simulated pressure evolution for PC

The simulated pressure curves near the gate (position C1 for the tube and position P3 for the plate) for some tests are shown in figures 6.16 and 6.17, for the tube and the plate geometries, respectively. As it was done with the C-Mold simulations, the effect of pressure on viscosity (parameter D3=0.2 $K.MPa^{-1}$) was considered.

In all simulations the effect of mould deformation was considered. For the simulations a value of C_M equal to 0.5 GPa^{-1} was used for the mould that produces the 4 mm-thick plates, and of 0.2 GPa^{-1} for the mould that produces the 2 mm-thick tubes. It must be pointed out that C_M, as defined and calculated in sections 3.1.1 and 3.2.3, is dependent on the impression thickness.

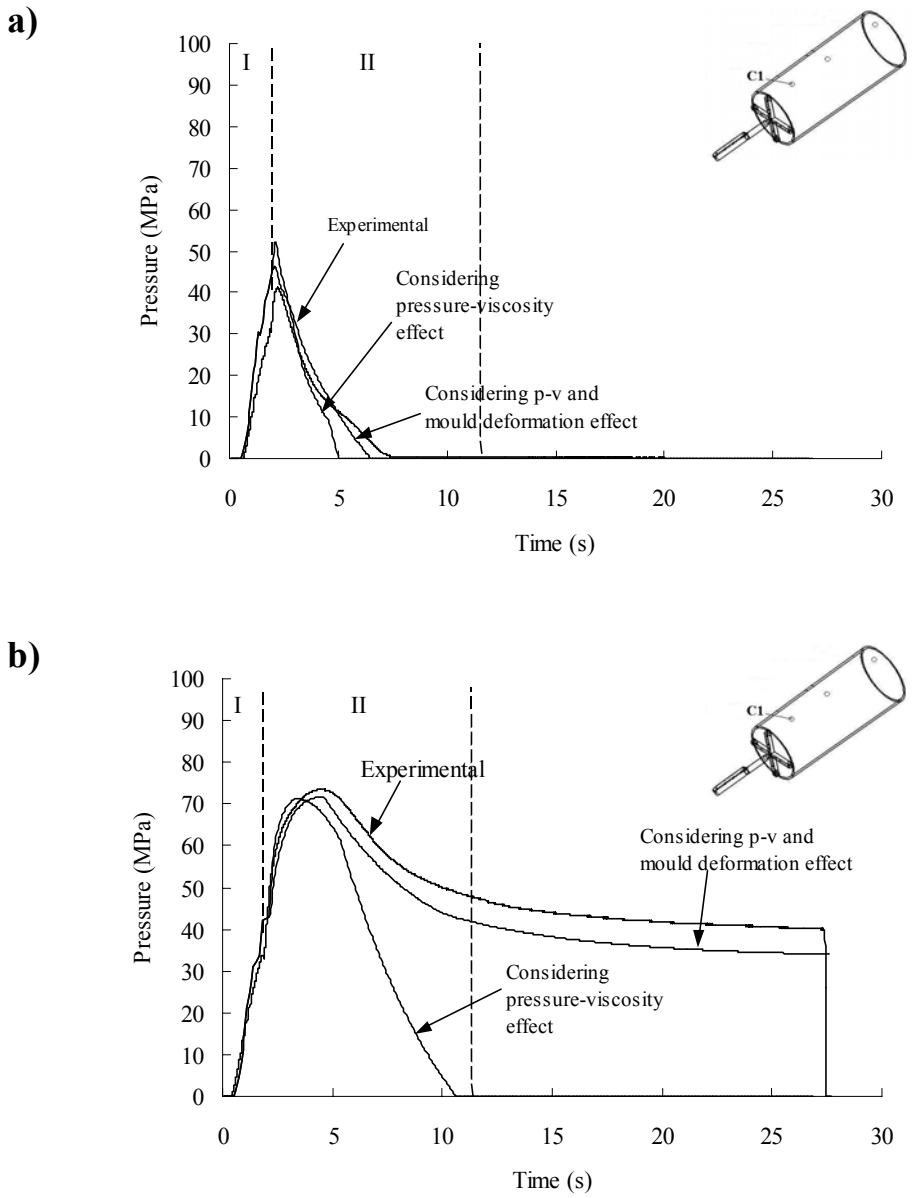

Figure 6.16- Comparison between experimental pressure evolution and UNISA code simulation considering the effect of pressure on viscosity and mould deformation, at position C1 in PC tubes. Moulding conditions codes: a) 310.12.10.15 and b) 310.110.10.15

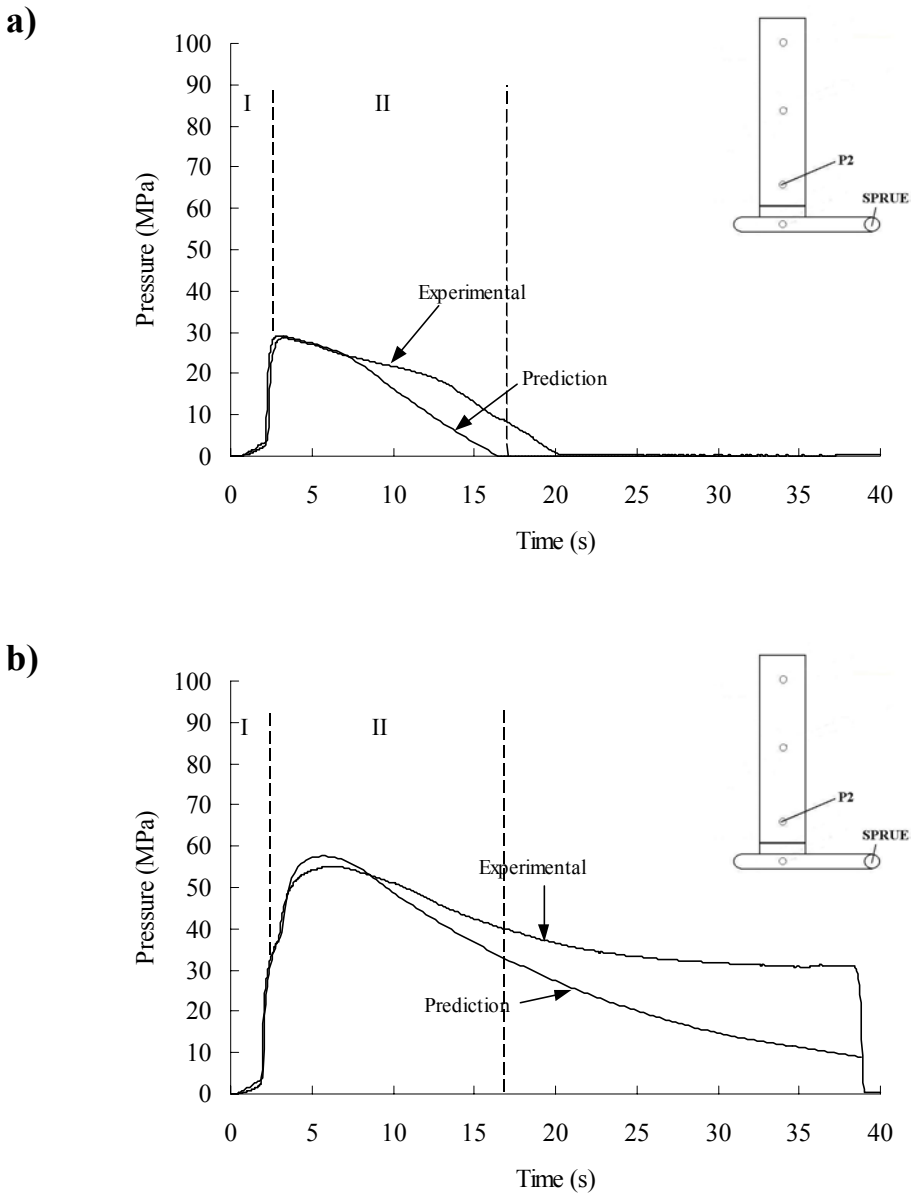

Figure 6.17- Comparison between experimental pressure evolution and UNISA code simulation, at position P2 in PC plates. Moulding conditions codes: a) 310.36.15.20 and b) 310.80.15.20.

The results of the pressure evolution compare satisfactorily with the experimental data for all moulding conditions used, especially when the mould deformation effect is considered.

The deviations between the predicted pressure evolution and the experimental pressure evolution in the impression, are presented in the Tables 6.7 and 6.8 for the rectangular plate and the tube.

Table 6.7 – Deviation between the predicted from UNISA and experimental pressure evolution in PC plates.

Condition	Deviation
	Considering p-v + mould def. effect (MPa)
310.36.15.20	3.6
310.49.15.20	2.9
310.66.15.20	10.8
310.80.15.20	9.9

The results of the deviation indicate that when using the UNISA code and considering the effect of mould deformation reduce the deviation between the predicted and the experimental pressure evolution in about 64%.

Table 6.8 – Deviation between the predicted from UNISA and experimental pressure evolution in PC tubes.

Condition	Deviation		Precision improvement (%)
	Considering p-v effect (MPa)	Consid. p-v + mould def. (MPa)	
310.12.10.15	4.6	4.4	20
310.40.10.15	6.7	2.5	62.7
310.68.10.15	8.5	5	41.2
310.89.10.15	12.6	2.5	80.2
310.110.10.15	16.9	3.4	79.9

6.1.2.3- Concluding remarks

The simulations performed using the C-Mold and the UNISA program suggests that:

- The pressure predictions are qualitatively in good agreement with the measurements for all moulding conditions used in both geometries and materials. However some appreciable quantitative discrepancies can be observed when the effect pressure on viscosity and the mould deformation are not considered.

- The results of deviation for the polypropylene case, indicate that considering the effect of pressure on viscosity reduces the deviation between the predicted and the experimental pressure evolution in about 55%.
- In the case of iPP plates the deviation of the UNISA program is greater than the deviation of C-Mold: This is due to the under predicted gate freeze-off time.
- The results of the deviation for the polycarbonate case indicate that considering the effect of mould deformation reduces the deviation between the predicted and the experimental pressure evolution in about 32% using the C-Mold and in about 64% using the UNISA program.
- The methodology used to take into account the effect of the mould deformation on the pressure evolution prediction seems to be the reason for the differences when using the C-Mold and UNISA programs.

6.2- Temperature evolution

6.2.1- Experimental data

6.2.1.1- Temperature evolution in iPP tubes

A plot of the core surface temperature evolution at the position T2, obtained during the processing of iPP tubes is shown in the figure 6.18. The effect of the injection temperature is also shown.

As it can be seen in the figure, as soon as the polymer reaches the sensor, the temperature increases for about 11ºC in the case of Tinj=190ºC and 13ºC in the cases of higher Tinj. The differences observed in the core surface temperature, for different injection temperatures decrease with the time.

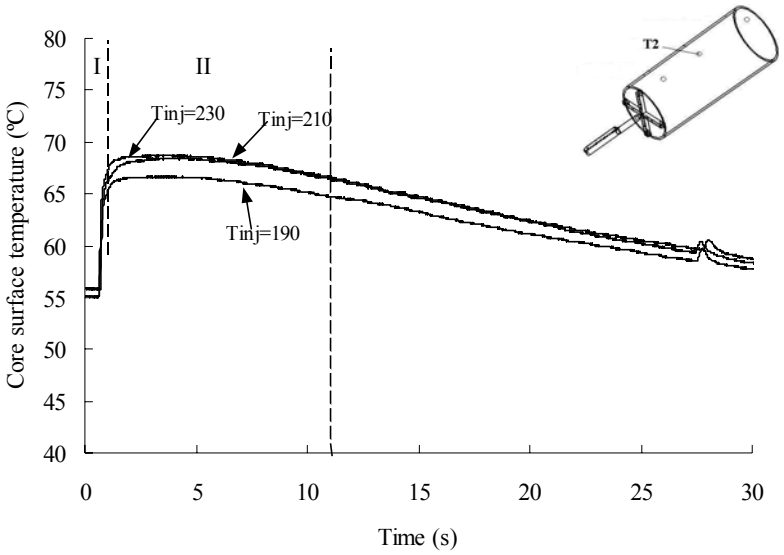

Figure 6.18- Core surface temperature evolution in position 2 in iPP tubes. Effect of injection temperature with holding pressure of 40 MPa and holding time of 13 s

In the figures 6.19a and 6.19b the core surface temperature evolution is shown at the positions T2 and T3, respectively. These data correspond to the condition Tinj=210ºC and holding pressures of 5 MPa and 40 MPa. In the same figure it is also shown the pressure evolution at those positions, as measured by the sensors in the core, for the condition with holding pressure of 5 MPa.

The results of the core surface temperature evolution seem to be affected by the holding pressure condition. As the figure 6.19 shows, the surface temperature of the core for holding pressures of 5 MPa and 40 MPa, are close up to 4 s and then diverge.

Comparing the curves of pressure and surface temperature of the core it is possible to attribute the temperature difference to the detachment of the moulding from the core (which happens at the time indicated by the dashed line). This separation results from the larger thickness shrinkage due to the low holding pressure. The observation that the moulding can detach from the mould wall and its effect on the cooling progress were also studied by other authors using the ultrasonic and infrared techniques [138], and thermal sensors [139].

The evolution of surface temperature at the core for the Ph=5 MPa stops declining at about 7 s. The temperature rises again to a value similar to the corresponding to the condition for Ph=40 MPa. This is attributed to the material contacting again the core (as a result from the diametrical shrinkage) resulting in a better heat transfer and increase of the surface temperature at the core.

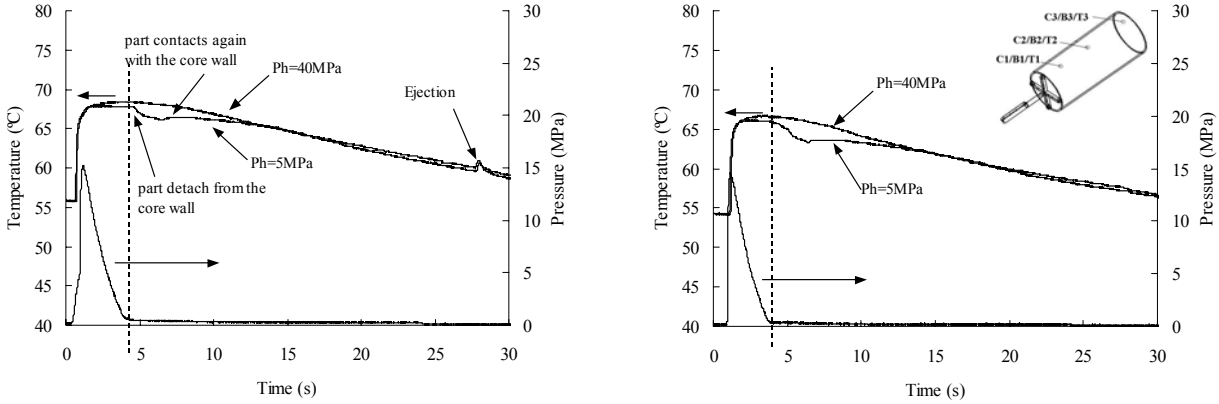

a) position 2 b) position 3

Figure 6.19- Core surface temperature and pressure evolution in different positions for iPP tubes. Effect of holding pressure with Tinj=210ºC

6.2.1.2- Temperature evolution in PC tubes

A plot of the evolution of the surface temperature at the core along the flow path is shown in figure 6.21. This temperature evolution is independent from the moulding conditions for the case of PC. As it can be seen in the figure, the temperature at the position 1 is about 20ºC higher that at the other positions. This observation explains the divergence of the pressure curves in different positions of the impression that was observed in figure 6.6.

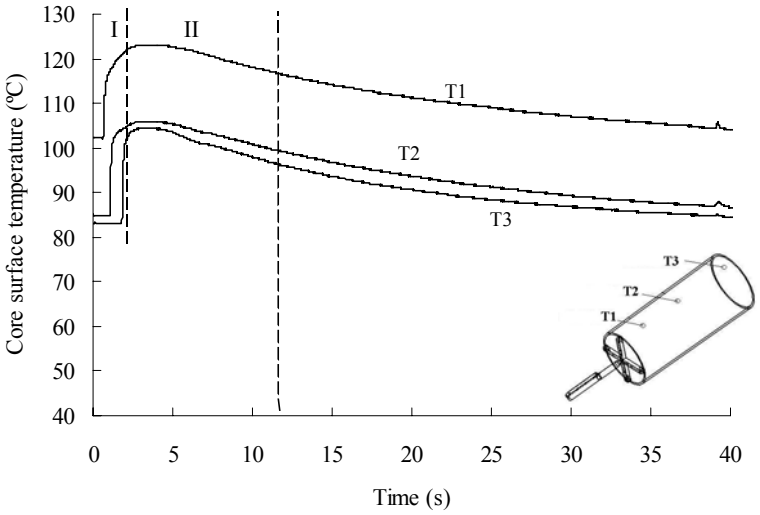

Figure 6.20- Surface temperature evolution at the core along the flow path in PC tubes. Moulding condition code 310.68.10.15

6.2.2- Analysis with C-Mold

In all the simulations using the program C-Mold the effect of the cooling system was taken into account. The heat transfer coefficient between the mould wall and the polymer was set to the standard C-Mold value of 25 $kW.m^{-2}.K^{-1}$.

6.2.2.1- Temperature evolution in PC tubes

The effect of the cooling system on the mouldings was analysed considering the cooling channels architecture shown in the figure 6.21. In this figure the cooling channels of the core and the cavity are shown together with the runner system.

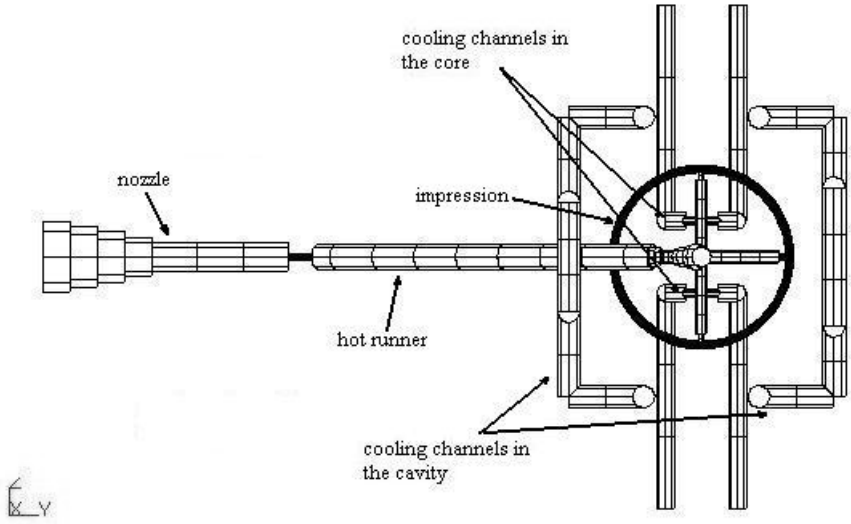

Figure 6.21- Top view of the tube moulding and cooling channels

The evolution of the temperature at the core surface in the positions T1 and T3, alongside the C-Mold predictions are shown in figure 6.22. The comparison of these temperature curves indicates that the prediction of the surface temperature at the core agrees well with the experimental data.

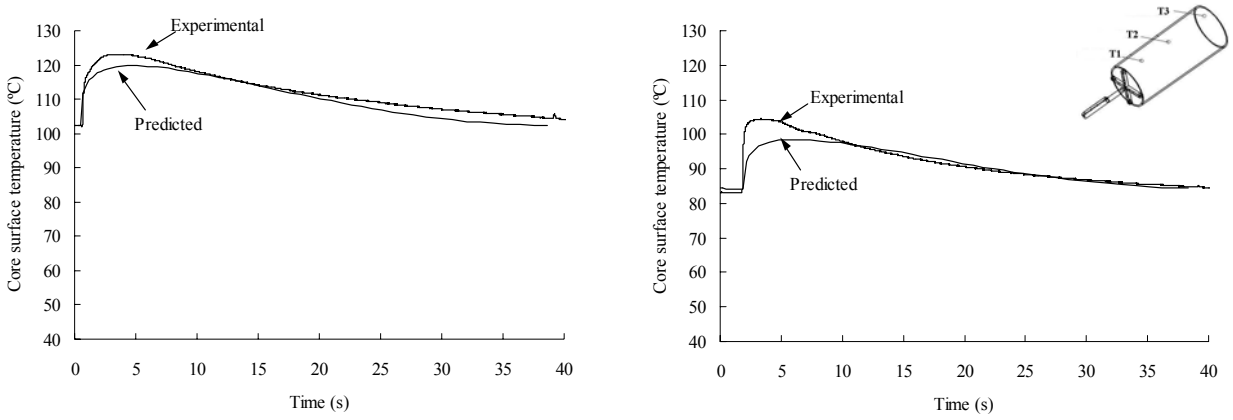

a) Position T1 b) Position T3

Figure 6.22- Experimental core surface temperature evolution and C-Mold prediction in PC tubes. Moulding condition code 310.68.10.15.

The temperature evolution through the thickness of the part, as predicted by the C-Mold, for a moulding with a holding pressure of 68 MPa, is shown in the figure 6.23. It is observable that the distribution is symmetric with respect to the impression midplane.

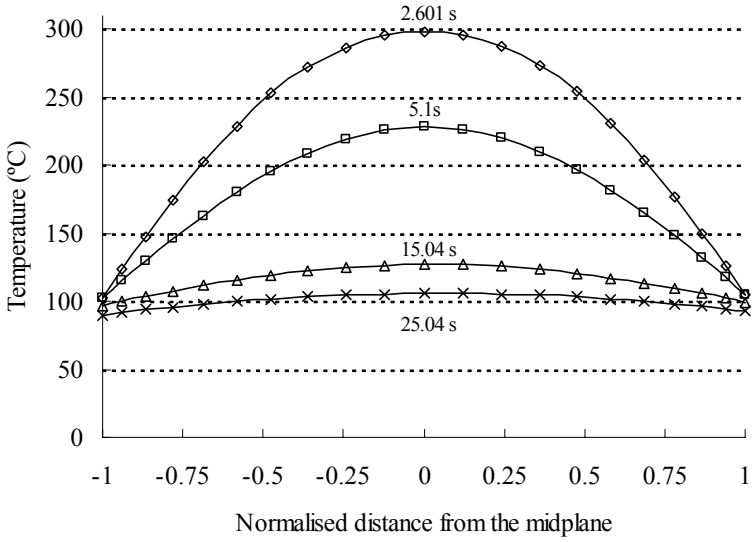

Figure 6.23- C-Mold predicted through thickness temperature profile at different times at the position T2, in PC tubes. Moulding condition code 310.68.10.15.

6.2.2.2- Temperature evolution for iPP

In the figure 6.24 it is shown the evolution of the experimental surface temperature at the core in the position T2, and the C-Mold predictions for the test with the injection temperature of 210ºC and the holding pressure of 5 MPa.

The predicted core surface temperature evolution is qualitatively in agreement with the experimental data. However, the software does not predict the slight deviation of the core surface temperature at *ca*. 4 s that can be seen in the experimental curve. This is probably due to the fact that the C-Mold software assumes that the material is in perfect contact with the mould wall until ejection.

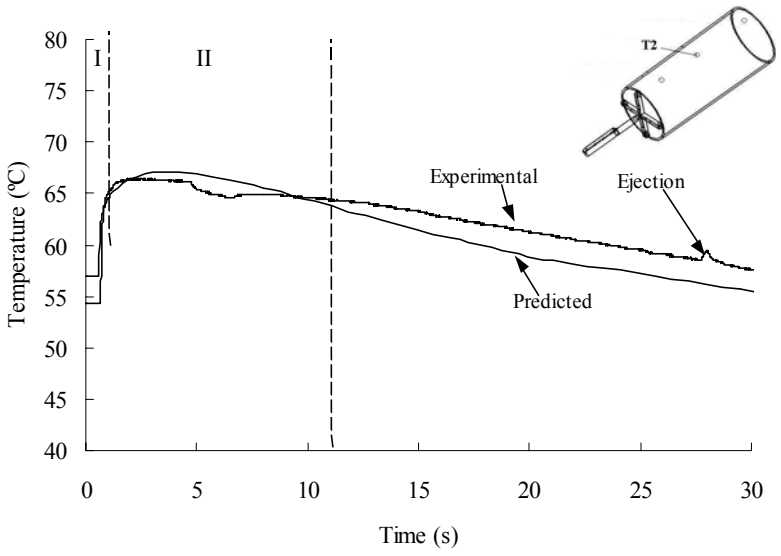

Figure 6.24- Comparison between experimental core surface temperature evolution and C-Mold software in iPP tubes. Moulding condition 210.5.13.10. and mould temperature of 50ºC.

The predicted evolution of the temperature through the moulding thickness for mouldings with the test code 210.40.13.10 and mould temperature of 50ºC is shown in figure 6.25. Again the simulation shows a symmetric distribution with respect to the impression midplane.

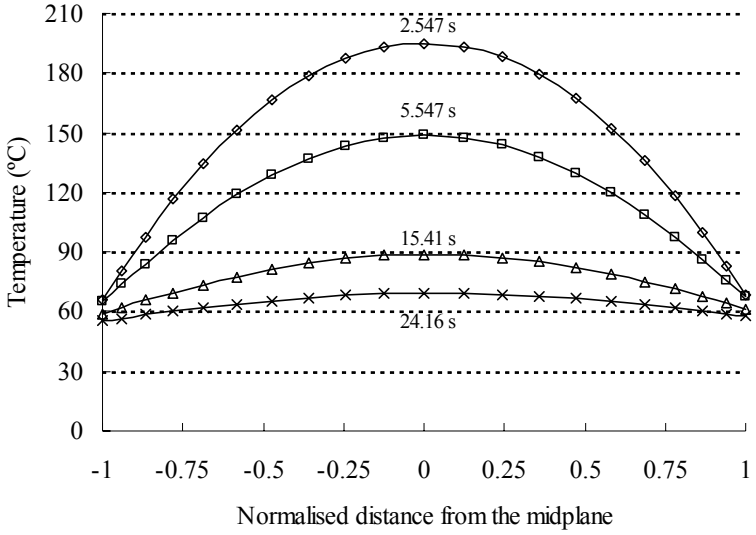

Figure 6.25- C-Mold predicted temperature profile through thickness at different times at the position T2, in iPP tubes. Moulding condition 210.40.13.10 and mould temperature of Tw=50ºC.

The influence of the layout of the cooling system, as it was done for the tubular mouldings, was analysed for the case of the plate mouldings. In this case the cooling channel architecture is shown in figure 6.26. In this figure the control temperature system that includes the cooling channels placed in the core and in the cavity can be seen together with the runner system and the impression.

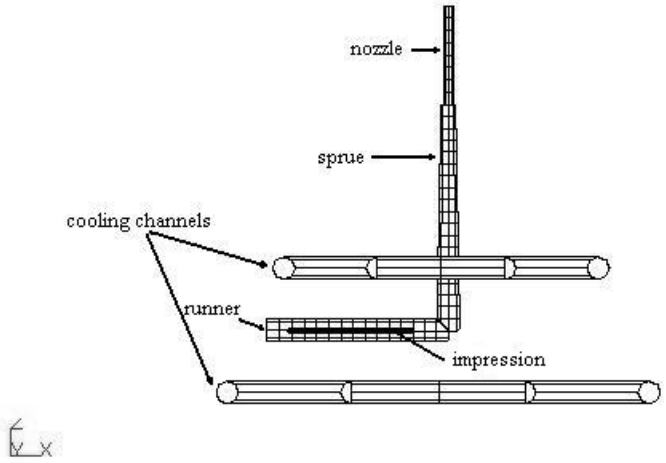

Figure 6.26- Side view of the plate moulding and cooling channels

The cooling rate at solidification (the temperature of solidification assumed in the C-Mold database is 122ºC), for different positions through the thickness, are shown in figure 6.27 for both geometries used in this work.

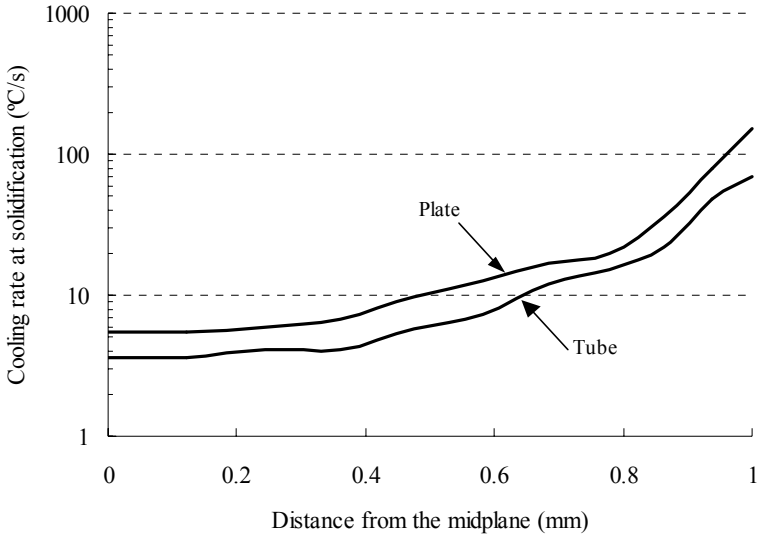

Figure 6.27- Cooling rate at solidification in the middle position in the impression, in the plate and tube geometry

The comparison is made at the middle position in the impression, for the moulding condition with the code 230.40.10.15 and mould temperature of 27ºC for the plates, and with the 230.40.13.10 and mould temperature of 50ºC, for the tubes.

The cooling rate reaches several tens of degrees per second at the moulding wall. The high cooling rate experienced by the material in relation to the cooling rate used to evaluate the temperature of solidification (4ºC/min) will decrease the actual temperature of solidification.

6.2.3- Concluding remarks

The results shown in this *Temperature evolution* section indicate that:

- In opposition to the PC tube, the results of the core surface temperature evolution measured in the iPP tube are affected by the holding pressure. The difference between the temperature evolution for lower and higher holding pressures results from the larger thickness shrinkage. For low holding pressure the moulding detachs from the mould wall affecting the cooling progress.

- The prediction of the surface temperature at the core by C-Mold agrees well with the experimental data in the case of PC tube. When iPP is used some deviation is observed probably due to the software considering that the material is in perfect contact with the mould wall until ejection.

6.3- Shrinkage

The major shrinkage results in the rectangular plate and tube mouldings are presented in this section. The effect of the processing variables on shrinkage variation are analyse.

The complete shrinkage data of the rectangular plate mouldings are included in Appendix A1.3.1 and of the tube mouldings in Appendix A2.3.1.

6.3.1- Free-shrinking plates

6.3.1.1- Effect of the holding pressure

The results of the as-moulded shrinkage in the flow and the across flow directions, as a function of the holding pressure, for iPP and PC are shown in the figures 6.28 and 6.29, respectively.

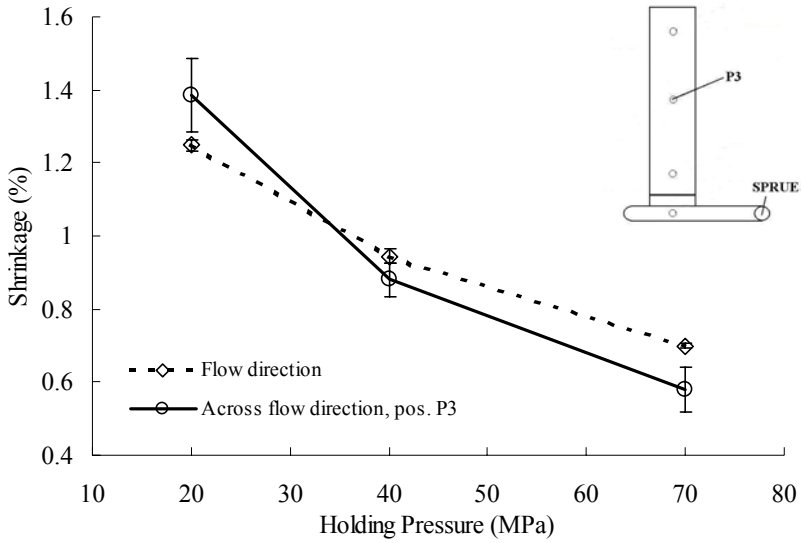

Figure 6.28- Effect of the holding pressure on the as-moulded shrinkage in flow and across flow directions, for free-shrinking iPP plates moulded with holding time of 10 s.

For the materials analysed, the in-plane shrinkage decreases inversely to the pressure applied during the holding phase, at an average rate of *ca.* 0.14 %/10 MPa for iPP and 0.07 %/10 MPa for PC. Moreover, the results show that the shrinkage in the flow and the across flow directions are similar, this suggesting the presence of an equibiaxial strain field during cooling.

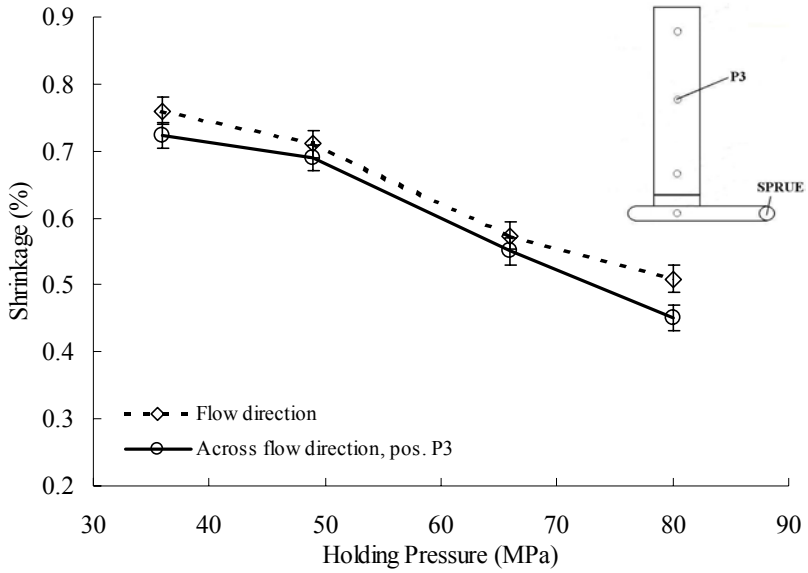

Figure 6.29- Effect of the holding pressure on the as-moulded shrinkage in flow and across flow directions, for free-shrinking PC plates moulded with holding time of 15 s.

In the figure 6.30 for iPP and in the figure 6.31 for PC the results of the thickness shrinkage as a function of the holding pressure are shown.

In contrast with the in-plane shrinkage, the thickness shrinkage is negative (which means an expansion of the moulding). Furthermore, the absolute thickness shrinkage is larger than the in-plane shrinkage, decreasing inversely to the holding pressure at an average rate of *ca.* 1%/10 MPa for iPP and 1.1%/10 MPa for PC.

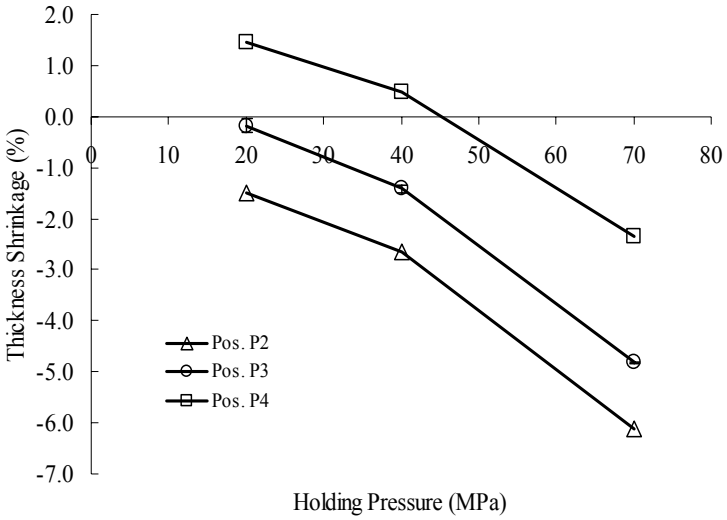

Figure 6.30- Effect of the holding pressure on the as-moulded thickness shrinkage, for free shrinkage iPP plates moulded with holding time of 10 s.

As it can be seen in the figures 6.30 and 6.31, the difference is maximum at the positions near the gate, where the pressure is higher. As it was observed in this work and already reported in the literature [*e.g.* 52,55,63,90] this large difference between the in-plane and the thickness shrinkage is probably due to the mould deformation and a slight opening during the filling and packing stages, or due to the elastic expansion upon mould opening of the compressed material.

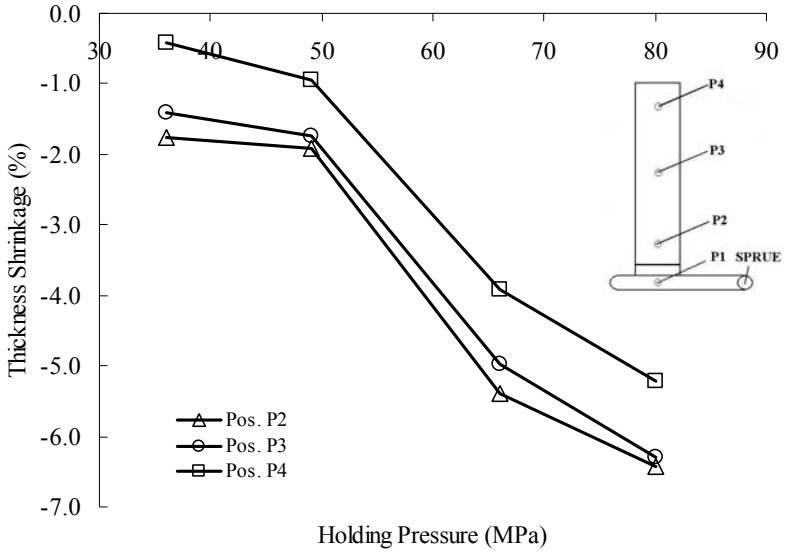

Figure 6.31- Effect of the holding pressure on the as-moulded thickness shrinkage, for free shrinkage PC plates moulded with holding time of 15 s

6.3.1.2- Effect of the holding time

Results of the as-moulded shrinkage in the flow and the across flow directions, as a function of the holding time, for iPP are shown in figure 6.32. It can be seen that holding times larger than

6 s do not cause a significant reduction in shrinkage. In fact, as the pressure evolution experiments confirmed, for a Ph= 40 MPa the gate freezes at about 6 s after injection.

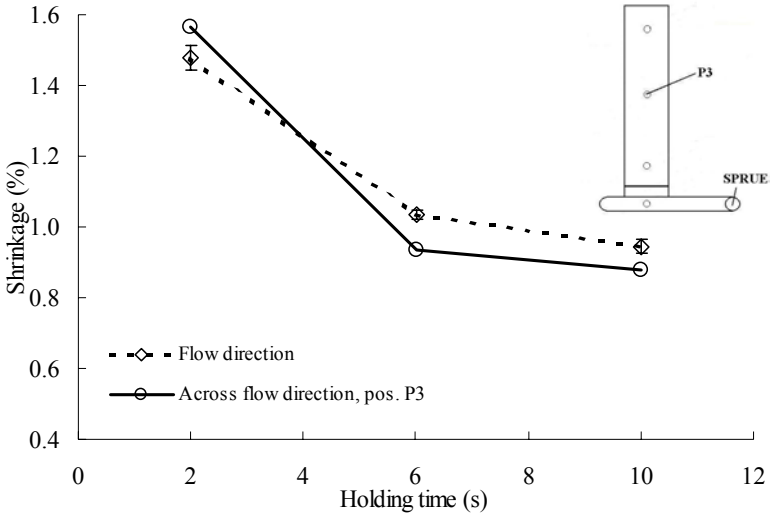

Figure 6.32- Effect of the holding time on the as-moulded shrinkage in the flow and the across flow directions, for the free shrinkage iPP plates moulded with holding pressure of 40 MPa

For the PC plate case, the results of the as-moulded shrinkage in the flow and the across flow directions as shown in figure 6.33, reveal that a holding time higher than 10 s does not cause a significant shrinkage reduction. As already mentioned on discussing the pressure evolution experiments, for a holding pressure of 49 MPa the gate freezes off at about 8 s after injection.

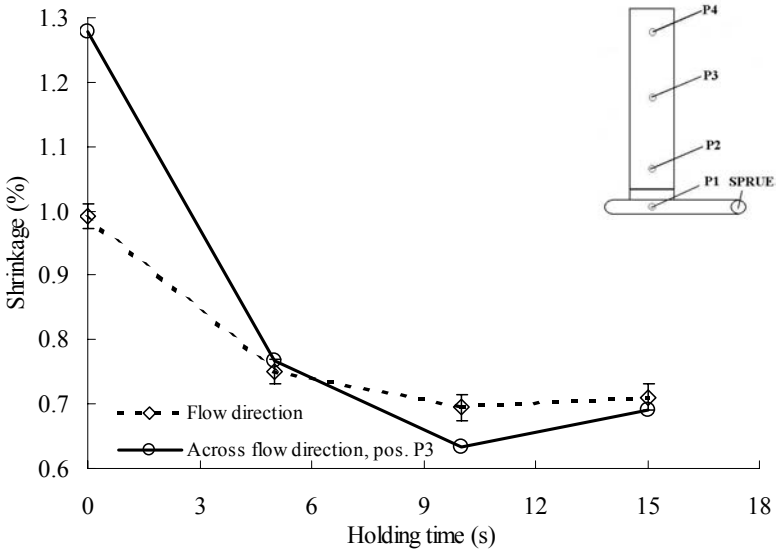

Figure 6.33- Effect of the holding time on the as-moulded shrinkage in the flow and the across flow directions, for free shrinkage PC plates moulded with holding pressure of 49 MPa.

It can be observed that when no pressure is applied during the holding phase, i.e. th=0 s, the across flow shrinkage is larger than the shrinkage in the flow direction. This result confirms that the shrinkage in the across flow direction starts before the shrinkage in the flow direction and before complete solidification as already reported by Pantani *et al.* [86,90].

Results of the thickness shrinkage as a function of the holding time, for iPP and PC, are shown in the figures 6.34 and 6.35, respectively. The data were collected at the positions P2, P3 and P4.

The thickness shrinkage is negative (expansion) and larger than the in-plane shrinkage. As it was mentioned in the previous section, this is probably due to the elastic expansion of the compressed material or to the mould deformation caused by the injection pressure.

As observed for the in-plane shrinkage for holding times higher than 6 s in the cases of iPP and 10 s for PC, significant thickness shrinkage changes are not observed. This observation confirmed that the gate freezes off at about 6 s after injection in the iPP case and at about 8 s in the PC case.

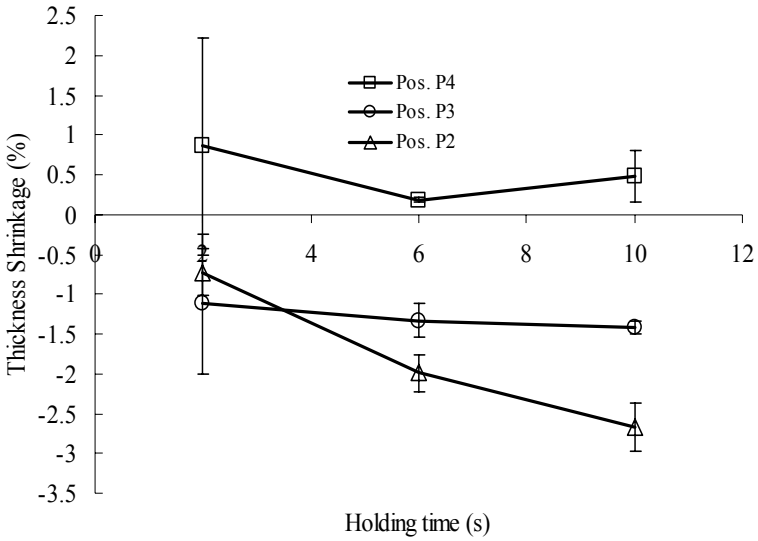

Figure 6.34- Effect of the holding time on the as-moulded thickness shrinkage, for free shrinkage iPP plates moulded with holding pressure of 40 MPa.

The larger scatter of the shrinkage data at shorter holding times in the iPP case, has been attributed to surface undulations [86]. For shorter holding times or lower pressures, the mouldings may detach from the mould wall. In this case the temperature of the solidified layer near the mould surface increases due to the heat conduction from the middle layers of the

moulding, and an expansion results. After a while, the temperature lowers again and the moulding re-starts to shrink.

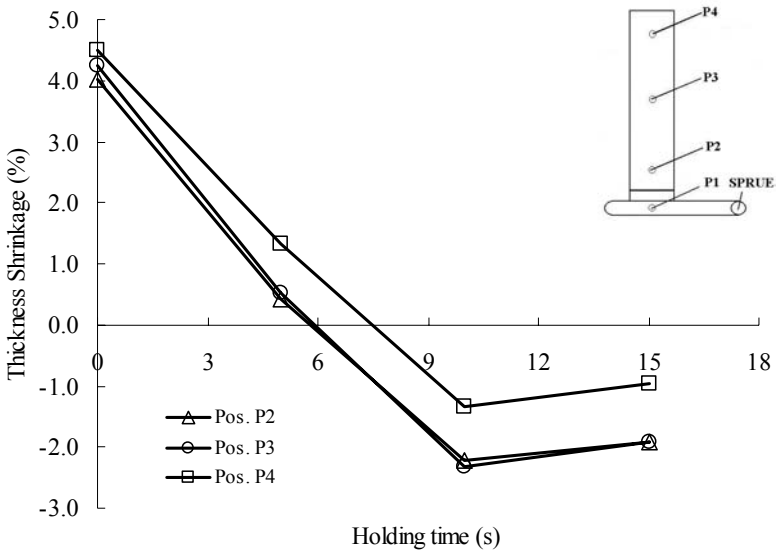

Figure 6.35- Effect of the holding time on the as-moulded thickness shrinkage, for free shrinkage PC plates with holding pressure of 49 MPa.

6.3.1.3- Shrinkage evolution inside the mould using the strain gauge technique

A typical strain gauge recording is given in the figure 6.36 for the case of holding pressure of 20 MPa being applied to a iPP plate moulding. As it can be seen, the strain (as it was defined previously is negative with respect to the shrinkage) does not show before 6.5 s. At this moment (the shrinkage onset) it starts quickly.

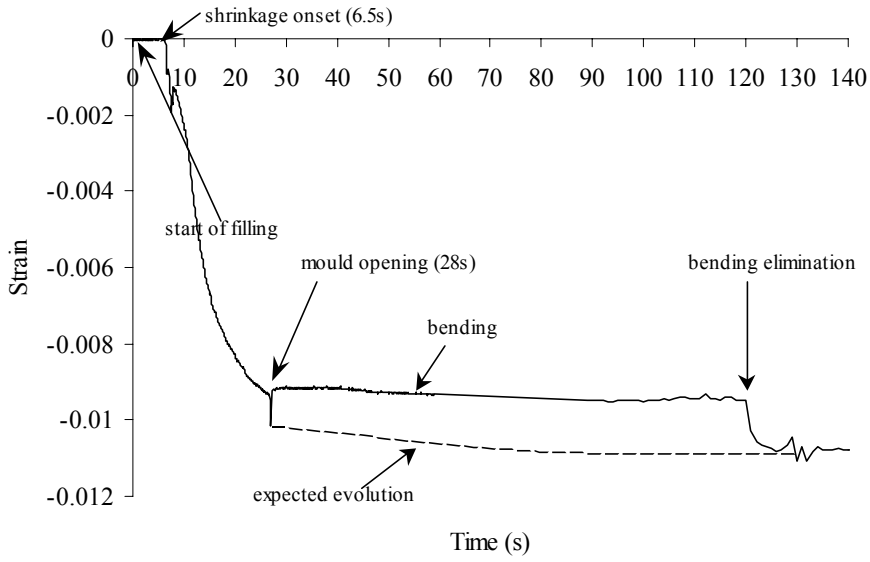

Figure 6.36- Strain curves recording by strain gauge in iPP plates moulded with holding pressure of 20 MPa.

At 28 s the mould opens, and a step in the strain variation is observable. This behaviour can be related to adhesion or geometrical constraints (like corners). After that the deformation comes back to the previous value. The explanation for this behaviour is associated to a bending effect: the samples bend (stretching the strain gauge) when the mould opens. In this experiment and at about 120 s the bending effect was eliminated by gluing a strip in the mould and forcing the plate to stay flat. Thus the signal came back to a value that could be expected if bending had not occurred.

Using the strain gauge technique makes possible to obtain the actual shrinkage data and determine the shrinkage onset inside the mould. The results of the shrinkage onset as a function of the holding pressure are summarised in figure 6.37. The shrinkage onset is noticeably delayed by increasing the holding pressure.

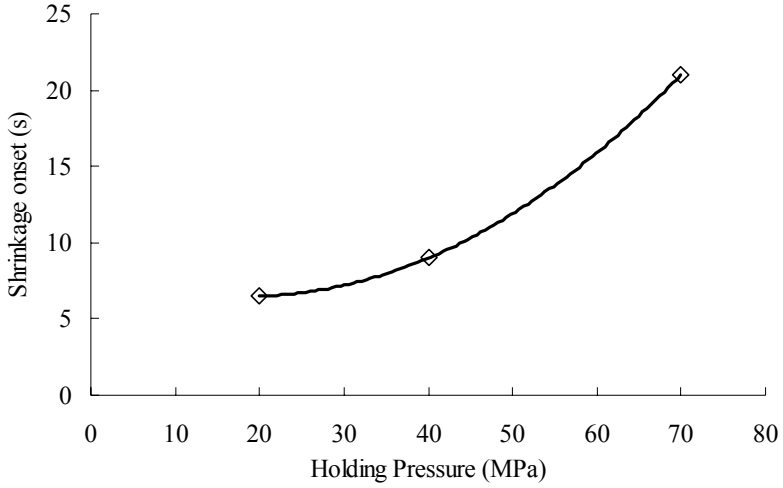

Figure 6.37- Experimental shrinkage onset as a function of the holding pressure in iPP plates.

The shrinkage history is therefore dependent on the holding pressure. The strain gauge data for holding pressures of 20 MPa and 40 MPa are given in the figure 6.38. For the Ph=20 MPa case, the strain decreases very quickly in the mould and, as expected, it is higher than when a pressure of Ph=40 MPa is applied instead.

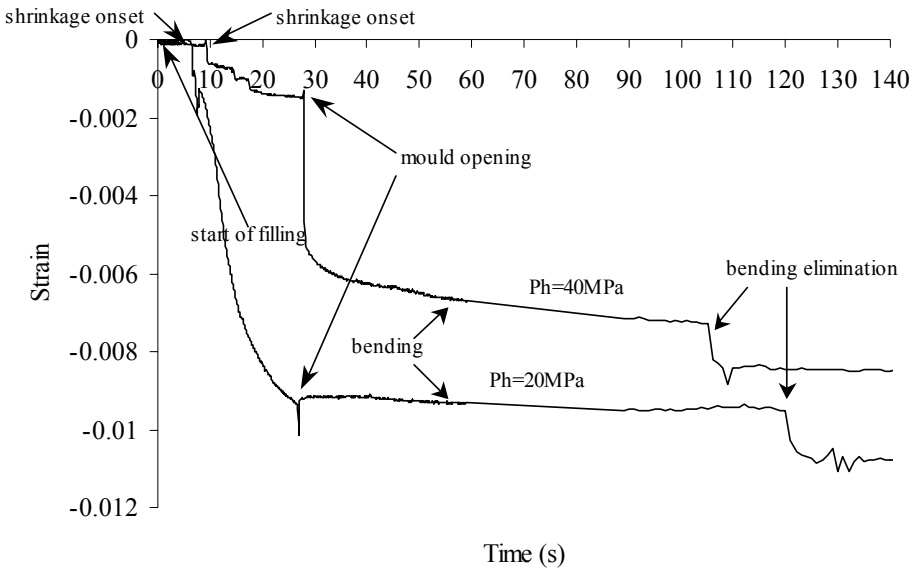

Figure 6.38- Strain curves measured by strain gauge in iPP plates, for holding pressures of 20 MPa and 40 MPa.

The results obtained when a holding pressure of 20 MPa is applied in the free shrinking and in the constrained shrinking situations are presented in the figure 6.39. It is possible to observe that the shrinkage in the constrained case takes place inside the mould in spite of the presence of the constraint. There are two explanations for it, as proposed by Pantani *et al.* [60]: one is the local character of the measured shrinkage irrespectively from the constraint; the other derives from the constrainer being not completely rigid and thus being able to slide inside the mould.

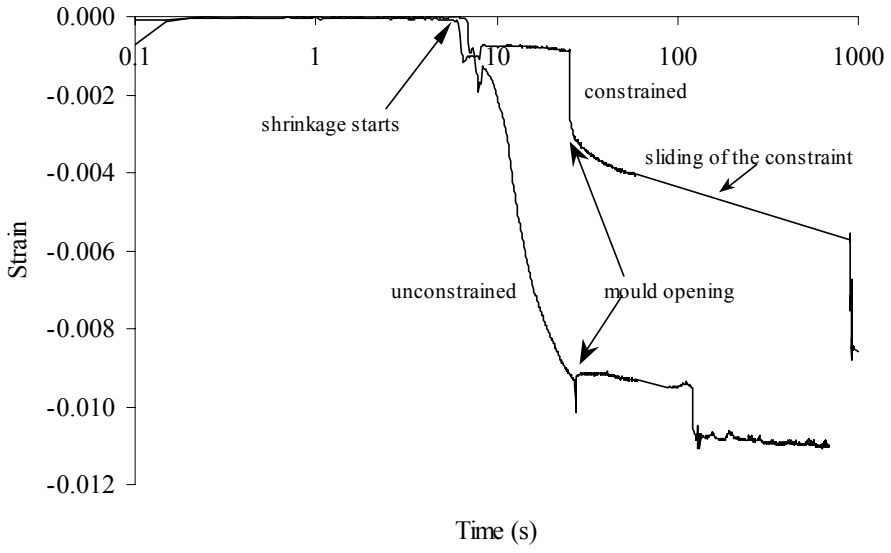

Figure 6.39- Strain curves measured by strain gauge in iPP plates, for holding pressure of 20 MPa, constrained and unconstrained case.

In the figure 6.39 it is also possible to observe that the presence of the constrainer affects the evolution of the shrinkage. The shrinkage in the constrained case is smaller than in the unconstrained case and the difference between both cases increases with the time.

Comparison between strain gauge and calliper data of the final shrinkage is shown in Table 6.9. The callipers give a measurement of the integral across and in-flow direction shrinkage, whereas the strain gauges give a local reading. This consideration may explain the small differences between strain gauge and calliper results.

Table 6.9 – As-moulded shrinkage measured with callipers and strain gauges

Ph (MPa)	th (s)	constraint	Strain Gauge (%)		Callipers (%)
			ε_x	ε_y	
20	10	yes	0.9	-	1.04±0.05
20	10	no	1.1	-	1.25±0.02
40	10	no	-	0.95	0.88±0.04
40	10	no	0.9	-	0.94±0.02
70	10	no	.65		0.70±0.01

6.3.2- Shrinkage in the constrained situation

6.3.2.1- Constrained plates

The results of the as-moulded shrinkage obtained from constrained and unconstrained mouldings, as a function of the holding pressure and the holding time are shown in figures 6.40 and 6.41, respectively.

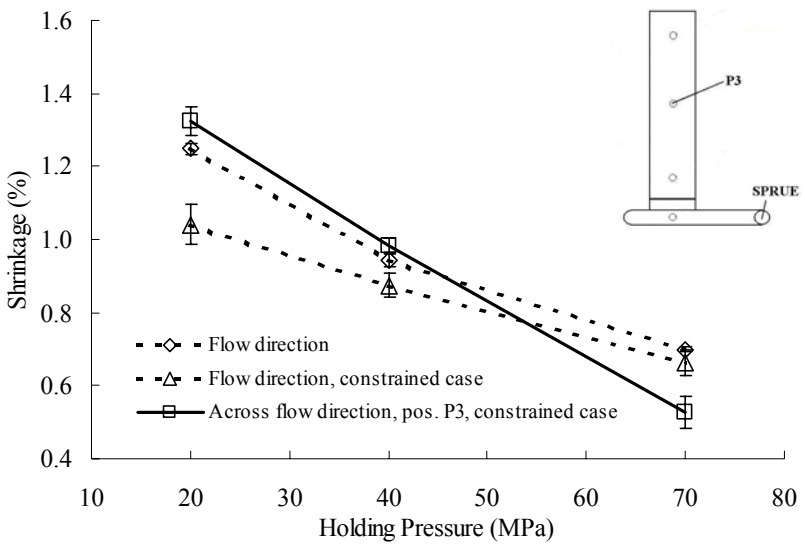

Figure 6.40- Comparison of the free and constrained as-moulded shrinkage, in the flow and across flow directions, in iPP plate case, as a function of holding pressure with holding time of 10 s.

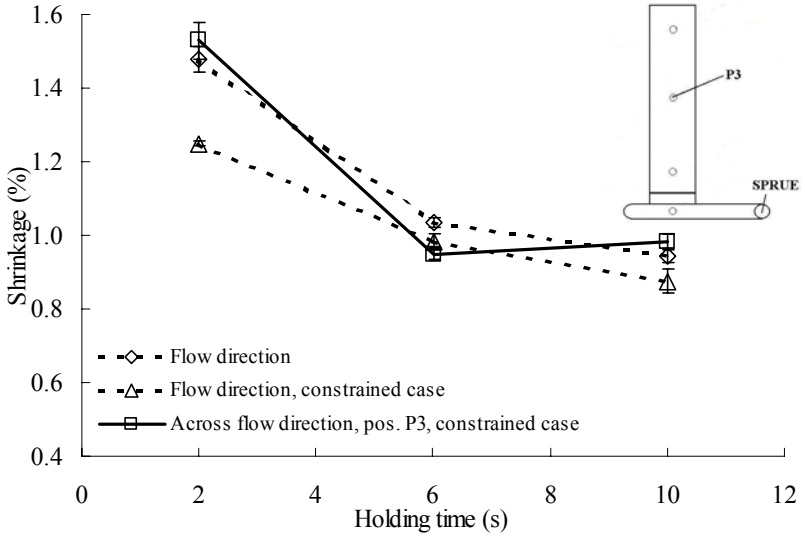

Figure 6.41- Comparison of the free and constrained as-moulded shrinkage, in the flow and the across flow directions, in iPP plate case, as a function of holding time with holding pressure of 40 MPa.

The effect of constraints on the as-moulded shrinkage is significant when the holding pressure is low or the holding time is short, and it vanishes at high holding pressures and long holding times. This is a clear indication that in these conditions shrinkage starts in the mould before complete solidification. In fact, the only effect of the constraint in the mould may be of preventing the sample from undergoing shrinkage inside the mould: if the shrinkage would start after complete solidification, its effect would be zero on the dimensions of elastic solid. Moreover, the results

show that the shrinkage in the flow and the across flow directions have similar values when the constraint is not present, and that the across flow shrinkage is very little affected by the constraint in the flow direction.

6.3.2.2- Tubular parts

6.3.2.2.1- Variation along the flow path

Diametrical shrinkage

In the figures 6.42 and 6.43, the data show a slight increase of the diametrical shrinkage as one moves along the flow path, for both materials in study. The increase of the shrinkage is more significant in the external perimeter (that is free to shrink). The higher shrinkage that the external diameter shows in relation to the internal diameter at a position far away from the gate indicates that the shrinkage starts inside the mould. The external diameter can shrink inside the mould and the internal diameter is restrained from it due to the core.

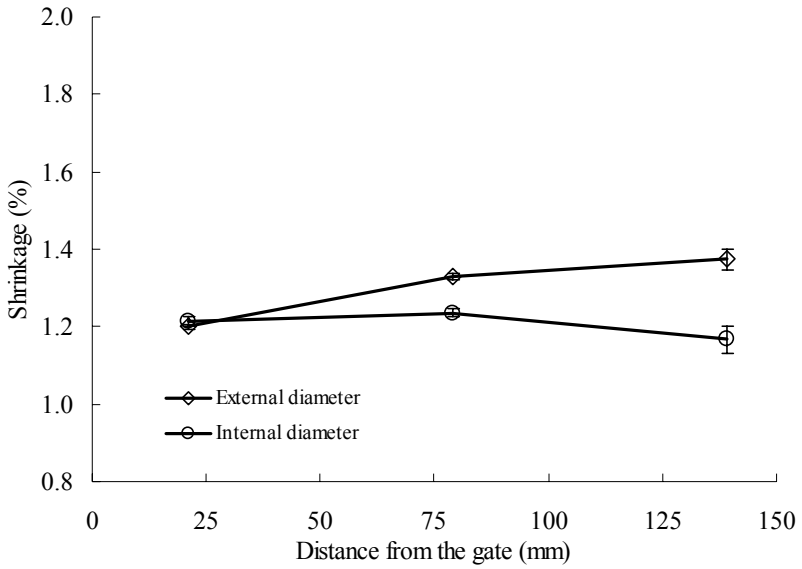

Figure 6.42- As-moulded diametrical shrinkage for different positions along the flow path in the impression, in iPP tubes. Moulding condition code 210.40.13.10 and mould temperature of 50ºC.

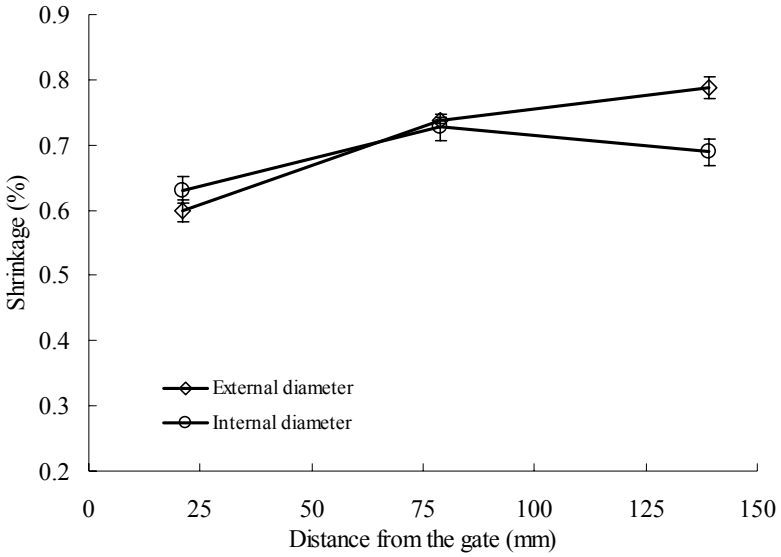

Figure 6.43- As-moulded diametrical shrinkage for different positions along the flow path in the impression, in PC tubes. Moulding condition code 310.68.10.15.

Thickness shrinkage

The results of the thickness shrinkage at different positions along the flow path are shown in the figure 6.44 for iPP tube and in figure 6.45 for PC. As it was observed with the diametrical shrinkage results, the thickness shrinkage increases with the flow path. This behaviour is related with the pressure inside the impression decreasing with the distance from the gate.

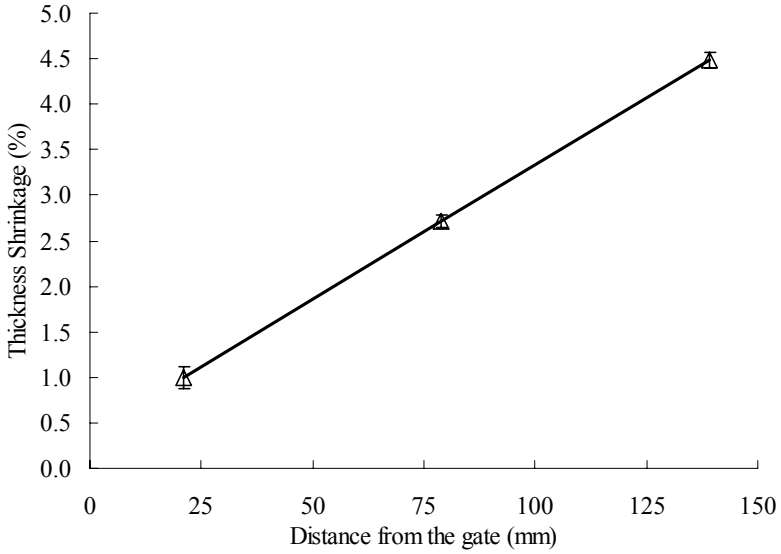

Figure 6.44- As-moulded thickness shrinkage for different positions along the flow path in the impression in iPP tubes. Moulding condition code 210.40.13.10 and mould temperature of 50ºC.

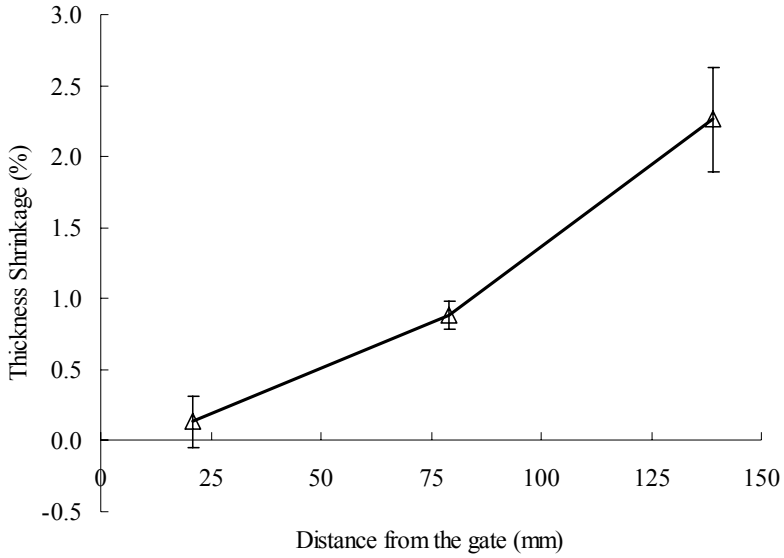

Figure 6.45- As-moulded thickness shrinkage for different positions along the flow path in the impression in PC tubes. Moulding condition code 310.68.10.15.

6.3.2.2.2- Effect of the holding pressure

Diametrical shrinkage

The results of the as-moulded diametrical shrinkage at a midway position in the impression (position 2), for iPP and PC, are summarised in figures 6.46 and 6.47, respectively.

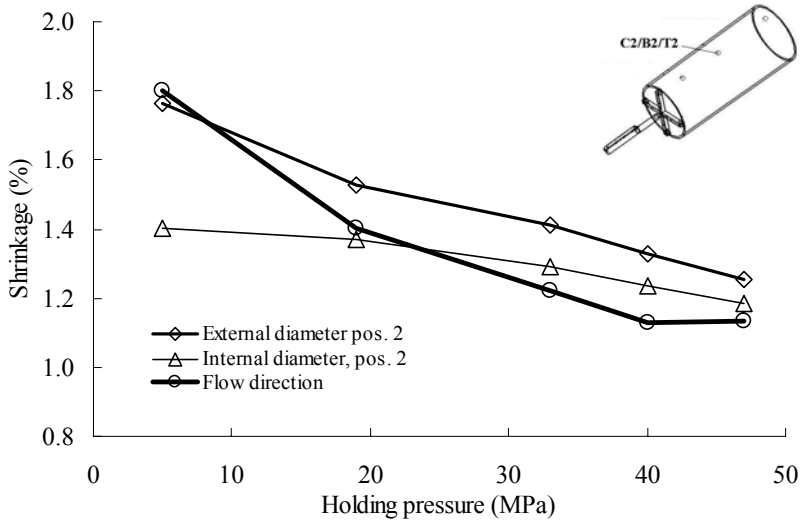

Figure 6.46- Influence of holding pressure on the as-moulded diametrical shrinkage at position 2 and shrinkage in flow direction, for iPP. Mouldings at Tinj=210ºC, Tw= 50ºC and ta=10 s.

for both materials the shrinkage is dependent on the pressure applied during the holding phase. The diametrical shrinkage decreases with this variable and the reduction is more pronounced in the external diameter.

In the as-moulded diametrical shrinkage for PC (figure 6.47) it can be noticed a slight difference in the external and internal shrinkage behaviour in the case of the iPP. At Ph=68 MPa an inversion on the behaviour exists between the external and internal diametrical shrinkage. This inversion is probably related to the thickness shrinkage variation.

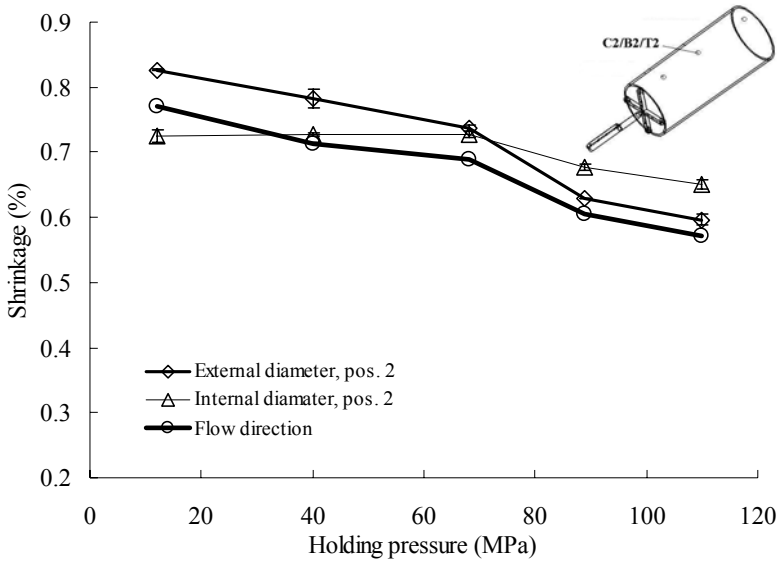

Figure 6.47- Influence of holding pressure on the as-moulded diametrical shrinkage at position 2 and shrinkage in flow direction, for PC. Mouldings with a constant holding time of 10 s.

The results of the as-moulded shrinkage in the flow direction for both materials is also shown in the figures 6.46 and 6.47. As observed for the diametrical shrinkage the result shows that the same dependency on the holding pressure exists. It can also be seen that for low holding pressures the shrinkage in the flow direction and the shrinkage of the external diameter are more significant than when higher pressures are applied during the holding stage. For this case, this indicates that the shrinkage probably starts before complete solidification.

Thickness shrinkage

Results of the thickness shrinkage at different positions as a function of the holding pressure for the iPP and PC are depicted in the figures 6.48 and 6.49, respectively.

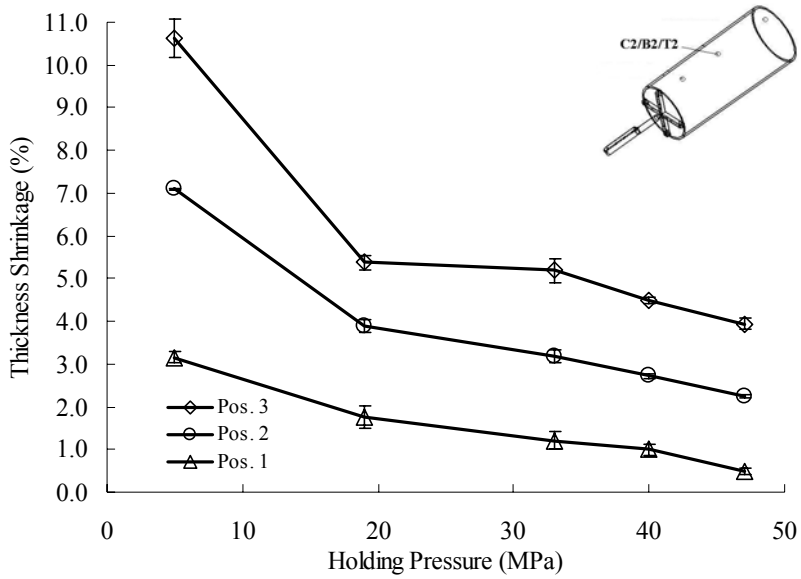

Figure 6.48- Influence of holding pressure on the as-moulded thickness shrinkage, in iPP tubes. Mouldings at Tinj=210ºC, Tw= 50ºC and ta=10 s.

The thickness shrinkage also decreases with the holding pressure and shows larger values than the diametrical shrinkage and the shrinkage in the flow direction. The thickness shrinkage increases with the distance from the gate, as observed for the diametrical shrinkage and the in-flow direction shrinkage. As expected, the shrinkage is larger for iPP than for PC. For higher holding pressures and near the gate, an expansion on the thickness direction (negative shrinkage) can also be observed.

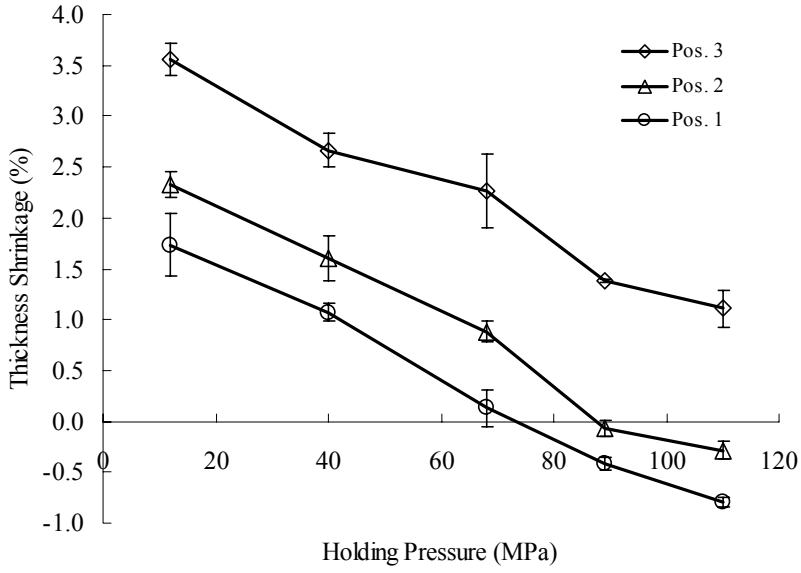

Figure 6.49- Influence of holding pressure on the as-moulded thickness shrinkage, in iPP tubes. Mouldings with a constant holding time of 10 s.

6.3.2.2.3- Effect of the holding time

The effect of the holding time in the shrinkage was analysed for the case of tubes moulded in polycarbonate. The as-moulded diametrical shrinkage at a midway position in the impression and the shrinkage in the flow direction, as a function of the holding time, are shown in figure 6.50. A holding time larger than 5 s, does not cause the shrinkage to decrease. In fact, as the pressure evolution experiments confirmed, for a holding pressure of 68 MPa the gate freezes at about 5 s after the injection.

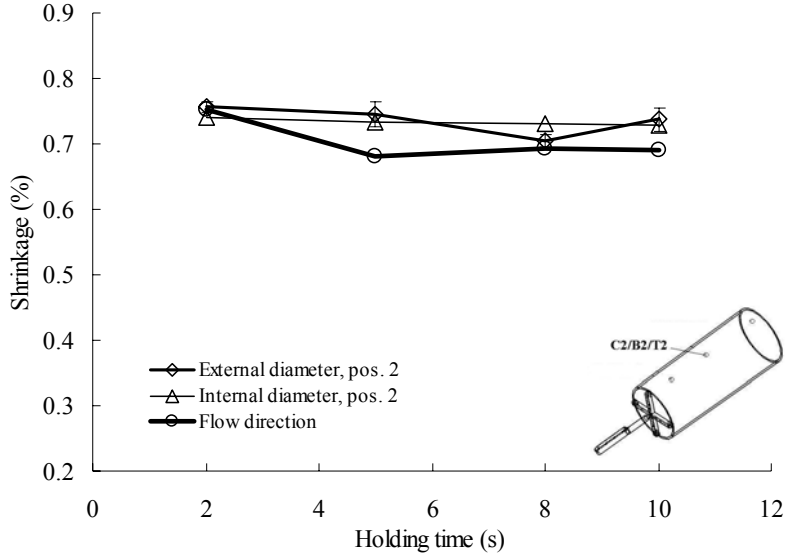

Figure 6.50- As-moulded diametrical shrinkage at position 2 and shrinkage in the flow direction, as a function of holding time, for PC with holding pressure of 68 MPa.

6.3.2.2.4- Effect of the injection temperature

The effect of injection temperature in the shrinkage was analysed for the case of tubes moulded in polypropylene.

The results of the as-moulded shrinkage, for iPP with Ph=40 MPa, Tw=50ºC, th=13 s, ta=10 and different injection temperatures, are condensed in the figure 6.51.

The results indicate a slight decline of the shrinkage when the injection temperature increases. The increase of the injection temperature results in a higher pressure inside the impression during the holding stage, as it was observed in the pressure evolution experiments (figure 6.9). The higher pressure during the holding stage improves the compensation of the volumetric shrinkage during the cooling and the compression of the melt.

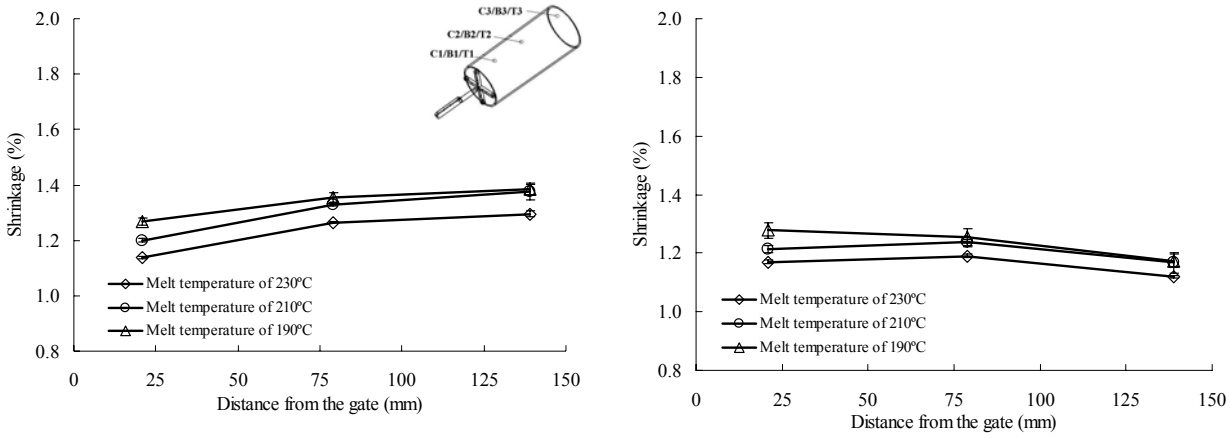

a) external diametrical shrinkage b) internal diametrical shrinkage

Figure 6.51- Influence of injection temperature on the as-moulded diametrical shrinkage for different positions along the flow path in the impression. Tubes moulded in iPP with Ph=40 MPa and th=13 s.

In the figure 6.52, the results of the as-moulded shrinkage in the flow direction as a function of the holding pressure at different injection temperatures are presented.

The results show that when lower holding pressures are applied the shrinkage decreases with the injection temperature and this effect attenuates when higher pressures are applied during the holding stage. This behaviour suggests that for controlling the shrinkage acting on the injection temperature is more effective at lower holding pressures.

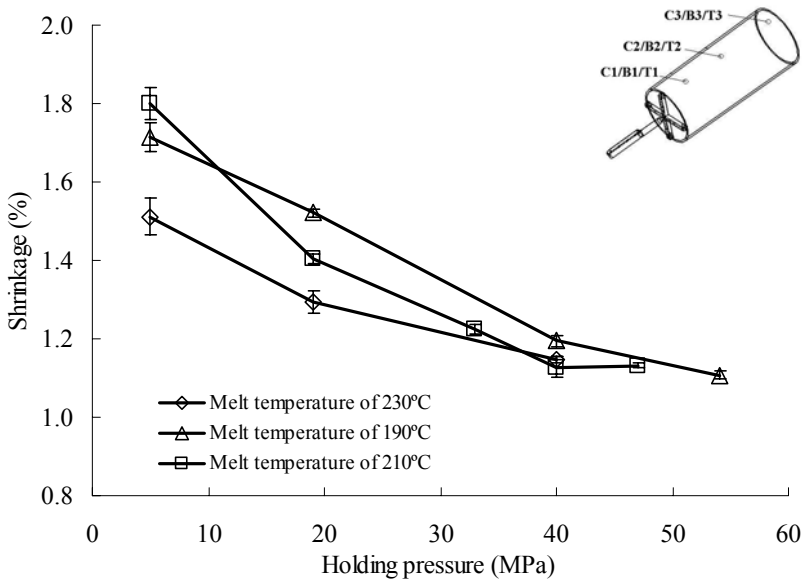

Figure 6.52- Influence of injection temperature on the as-moulded shrinkage in the flow direction as a function of the holding pressure, in iPP tubes with th=13 s.

6.3.2.2.5- Effect of the wall temperature at ejection

The effect of the wall temperature at ejection in the shrinkage was analysed for the iPP tubes.

The as-moulded shrinkage data, for the mouldings produced at Tinj=210ºC, Ph=40 MPa, Tw=50 ºC, th=13 s and different surface temperatures at ejection, are reported in the figures 6.53 and 6.54.

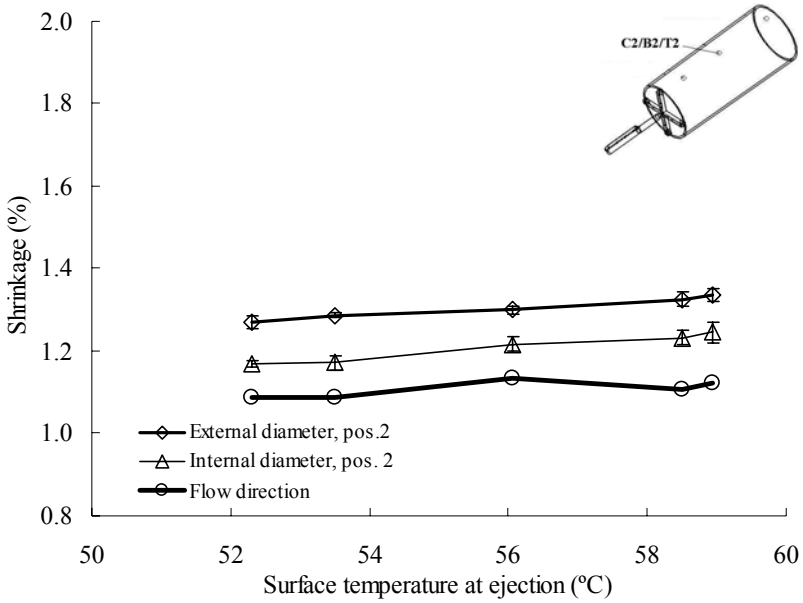

Figure 6.53- As-moulded diametrical shrinkage at position 2 and shrinkage in the flow direction as a function of surface temperature at ejection, for iPP with Tinj=210ºC, Ph= 40 MPa, Tw= 52ºC, th=13 s.

The results of the as-moulded diametrical shrinkage seem to be not affected by the time after holding, ta, and consequently by the surface temperature at ejection. This can indicate that the part is completely solidified before ejection. For this holding condition the shrinkage, starts after complete solidification, and no effect of ejection occurs on the as-moulded shrinkage. However, the shrinkage at the moment of ejection is different, as indicated by the ejection force measurements (section 6.4).

Results of the thickness shrinkage at different positions as a function of the surface temperature at ejection are shown in the figure 6.54. The results confirms that the time after holding, ta, and thus the surface temperature at ejection, do not affect the as-moulded shrinkage. However the thickness shrinkage increases with the position along the flow path.

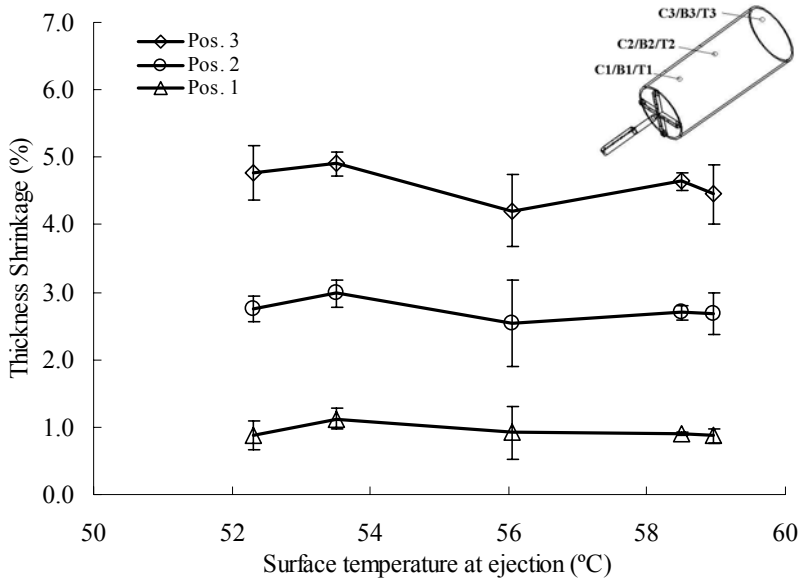

Figure 6.54- As-moulded thickness shrinkage as a function of surface temperatures at ejection, in iPP tubes with Tinj=210ºC, Ph= 40 MPa, Tw= 52ºC, th=13 s.

6.3.2.3- Concluding remarks

From analysing the as-moulded shrinkage in the plates and in the tubes, and the shrinkage evolution measured by the strain gauge technique, it is possible to summarise the following statements:

- The effect of constraints on the as-moulded shrinkage is significant when the holding pressure is small or the holding time is short, and it vanishes with high holding pressures and long holding times;
- The holding history is the main factor that affects the shrinkage. For low holding pressures the part may shrink inside the mould before complete solidification. In this case the shrinkage is larger than in the constrained situation. This can be shown by comparing the case of the external and the internal diametrical shrinkage of iPP tubes, and comparing the shrinkage in the flow direction in the free shrinking and constrained conditions;
- The increase of the injection temperature is more effective in the reduction on shrinkage for low holding pressures. The increase of the injection temperature results in a higher pressure inside the impression during the holding stage and consequently in a smaller shrinkage;
- The shrinkage seems to be not affected by the wall temperature at ejection. This indicates that the shrinkage starts after complete solidification;

- The strain gauge technique is a powerful technique to obtain the complete shrinkage evolution as from its onset.

6.3.3- Shrinkage prediction with C-Mold

The experimental results of the shrinkage are compared with simulations using the C-Mold version 99.7 considering the effect of pressure on the viscosity. Some shrinkage results with iPP are also compared with predictions neglecting the effect of pressure on viscosity (standard data). In order to increase the accuracy of the numerical solution, the default number of layers across the thickness was increased from the standard number of 12 up to 20. This caused an average decrease of 0.03% in the shrinkage predictions.

As specified in the C-Mold user's manual [85], the model implemented for shrinkage simulation is limited to the constrained shrinkage situation. Since the geometry is described by the mid-surface, the shrinkage predictions are limited to the mid-plane surface of the tubes.

The complete shrinkage predictions of the rectangular plate mouldings are included in Appendix A1.3.2 and of the tube mouldings in Appendix A2.3.2.

6.3.3.1- Effect of the solidification temperature

Shrinkage in iPP plates

The experimental and the C-Mold predictions data of the shrinkage in the flow direction are presented in figures 6.55 and 6.56.

The trend shown in the experimental results for the shrinkage are described by the C-Mold program using standard database parameters, but the predictions tend to overestimate the shrinkage especially when low holding pressures or short times are used (dotted line in the figures). This effect is certainly not related to the discrepancy between experimental and calculated pressure curves. Indeed, as mentioned in section 6.1.2 (see figure 6.10), C-Mold pressure simulations keep always above the experimental values.

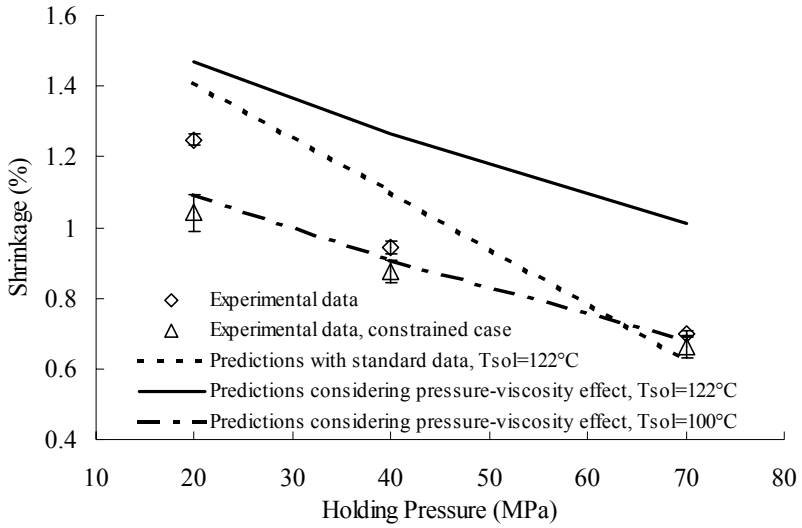

Figure 6.55- Comparison between as-moulded shrinkage (symbols) in the flow direction, for free and constrained shrinkage cases in iPP plates, and C-Mold predictions (lines). Different holding pressures with th=10 s.

If the pressure effect on the viscosity is considered a better trend of the shrinkage evolution is obtained, as shown by the full line in the figures 6.55 and 6.56, but the effect of reducing the solidification pressure increases substantially the shrinkage prediction.

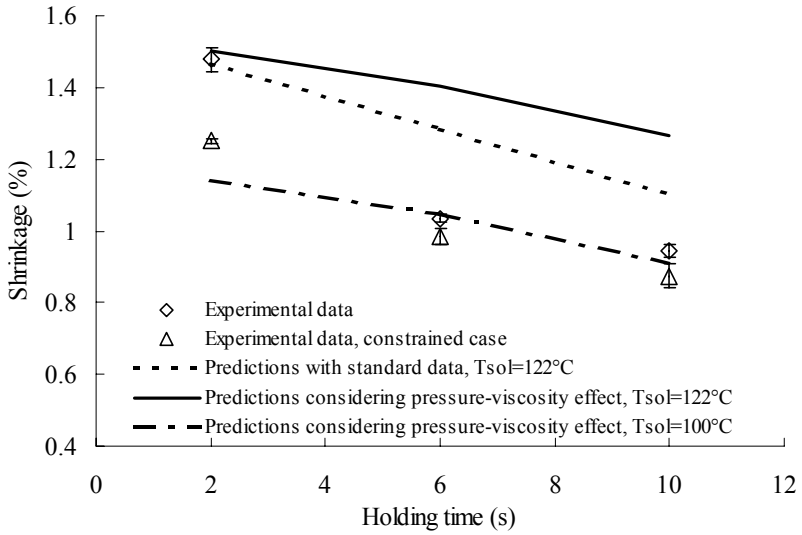

Figure 6.56- Comparison between as-moulded shrinkage (symbols) in the flow direction, for free and constrained shrinkage cases in iPP plates, and C-Mold predictions (lines). Different holding times with Ph=40 MPa

A possible reason for the discrepancy between measured and predicted shrinkage is the use of a unique temperature for the “flow” switch for the viscosity model (infinite below Tsol) as well as a “start stress build up” switch from purely viscous fluid (zero elastic modulus) to a purely

elastic solid (constant modulus below Tsol). It is well known that a semi-crystalline polymer, under high cooling rates has the melt-solid transition at a lower temperature. Due to the extremely high cooling rates, especially at the skin, the melt-solid transition temperature must be much lower than that measured during tests performed at low cooling rates. As stated in the C-Mold database the melt-solid transition temperature is of 122°C, and was determined by differential scanning calorimetry at a cooling rate of 20ºC/min [125].

In the figures 6.55 and 6.56 it can be noticed that the slope of shrinkage data versus holding parameters (in the constrained shrinkage case) is correctly described if the pressure effect on viscosity is accounted for in the simulations. The use of a lower transition temperature causes minor changes in the pressure evolution and shifts the shrinkage predictions towards the experimental values, due to the smaller contraction after solidification.

C-Mold simulations accounting for the effect of pressure on viscosity were therefore repeated adopting a value of 100°C (better estimation of the shrinkage prediction for the iPP plates with the moulding condition code 230.40.10.15) instead of 122°C (as in the C-Mold database) as solidification temperature. The results are also reported in figures 6.55 and 6.56 (mixed lines), and, as expected, become much closer to the experimental data. Indeed, as it was recently pointed out in the C-Mold literature [85], to achieve better predictions for semi-crystalline materials, it is necessary to describe the material pvT behaviour in terms of the process conditions, namely using the effective high cooling rate.

In the Table 6.10 the absolute value of the difference between the experimental shrinkage are compared with the predictions in the flow direction considering the C-Mold standard parameters of the material database, the effect of pressure on the viscosity and the solidification temperature of 100ºC.

Table 6.10 – Comparison of the difference between the experimental shrinkage and the predictions with C-Mold in iPP plates

Condition	Using standard parameters	Considering p-v effect	Considering Tsol=100ºC
	Diff. Sh_x (%)	Diff. Sh_x (%)	Diff. Sh_x (%)
230.20.10.15	0.37	0.43	0.05
230.40.10.15	0.23	0.39	0.03
230.70.10.15	0.04	0.35	0.02
230.40.2.15	0.17	0.20	0.16
230.40.6.15	0.25	0.42	0.06
Average	0.21	0.36	0.06
Stand. Deviation	0.11	0.08	0.05

It can be seen in figures 6.55 and 6.56, and comparing the difference between the experimental and C-Mold predictions presented in the table 6.10, the solidification temperature affects significantly the shrinkage predictions. This was already reported elsewhere [72] and it is referred to by other authors [90,140].

Shrinkage in iPP tubes

The as-moulded diametrical and the in-flow direction shrinkages, and the corresponding C-Mold predictions are shown in figures 6.57 and 6.58. It must be pointed out that the diametrical shrinkage predictions of C-Mold correspond to the mid-plane surface of the mouldings.

The C-Mold predictions using standard database parameters, as observed for the plate case, tend to overestimate the shrinkage (dotted line in the figures). This behaviour seems to be not related to the discrepancy between experimental and predicted pressure results. As it can be seen in the figure 6.11, the C-Mold pressure simulation keeps always above the experimental data.

In the figures 6.57 and 6.58, the effect of pressure on viscosity is also considered and the slope of shrinkage evolution is correctly described, as shown by the full line. Nevertheless the reduction of the solidification pressure increases the shrinkage estimation.

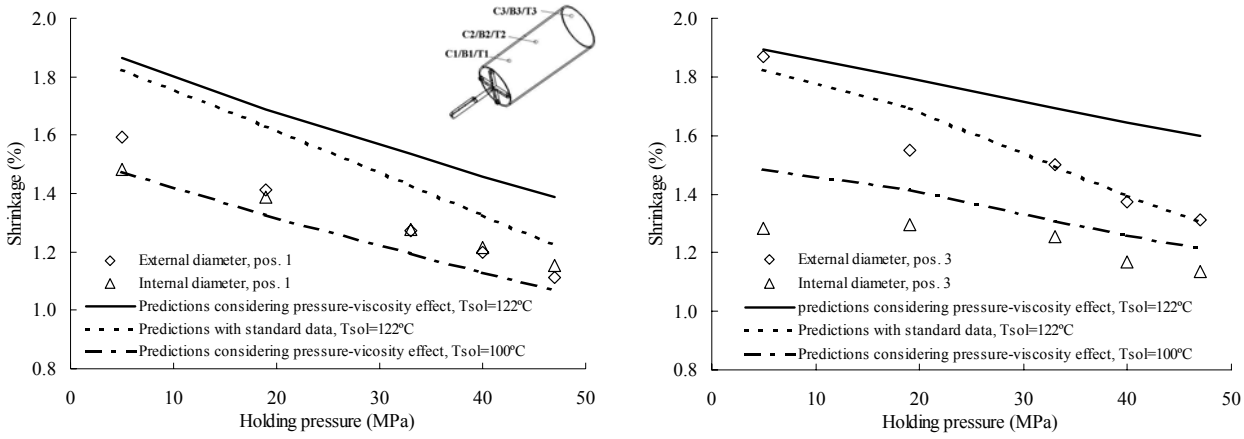

a) position 1 b) position 3

Figure 6.57- Comparison between as-moulded diametrical shrinkage (symbols) as function of holding pressure for iPP with Tinj=210, Tw=52ºC, th=13 s, ta=10s, and C-Mold predictions (lines).

The effect of using different solidification temperatures in C-Mold simulations is also shown in the figures, where shrinkage predictions (full and mixed lines) are compared with experimental data (symbols).

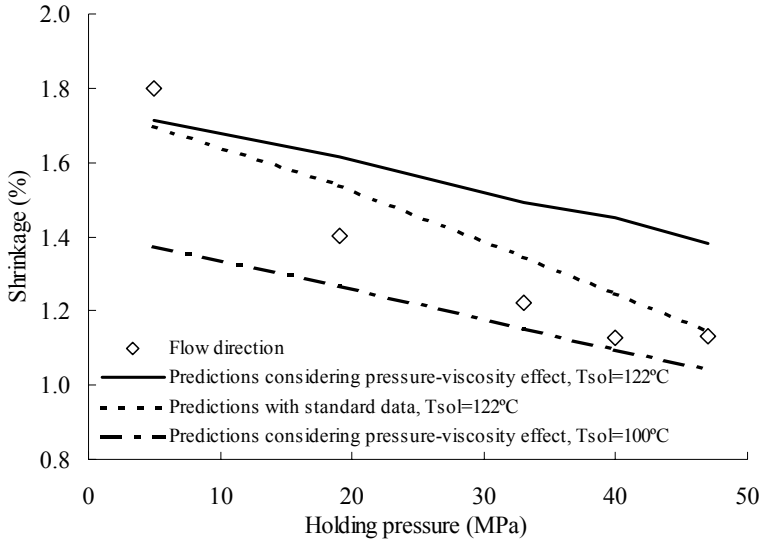

Figure 6.58- Comparison between as-moulded shrinkage in flow direction (symbols) as a function of holding pressure for iPP tube with Tinj=210, Tw=52ºC, th=13 s, ta=10s, and C-Mold predictions (lines).

In the Table 6.11 the absolute value of the difference between the experimental shrinkage and the predictions considering the C-Mold standard parameters of the material database, the effect of pressure on the viscosity and the solidification temperature of 100ºC are listed. As expected, adopting a value of the solidification temperature lower than that quoted in the C-Mold database (100ºC instead of 122ºC), causes the predictions to become much closer to the experimental data.

Table 6.11 – Comparison of the difference between the experimental shrinkage and the predictions with C-Mold in iPP tubes

Condition	Using standard parameters				Considering p-v effect				Considering Tsol=100ºC			
	Diff. Sh_x (%)	Diff. Sh_θ (%)			Diff. Sh_x (%)	Diff. Sh_θ (%)			Diff. Sh_x (%)	Diff. Sh_θ (%)		
		P1	P2	P3		P1	P2	P3		P1	P2	P3
210.5.13.10	0.11	0.28	0.28	0.24	0.09	0.33	0.29	0.31	0.43	0.06	0.06	0.10
210.19.13.10	0.13	0.23	0.27	0.26	0.21	0.29	0.39	0.37	0.13	0.07	0.01	0.01
210.33.13.10	0.12	0.16	0.17	0.12	0.27	0.26	0.37	0.31	0.07	0.08	0.03	0.07
210.40.13.10	0.12	0.12	0.15	0.12	0.33	0.25	0.39	0.37	0.03	0.08	0.01	0.01
210.47.13.10	0.01	0.09	0.10	0.07	0.25	0.25	0.40	0.37	0.09	0.06	0.00	0.01
Average	0.10	0.18	0.19	0.16	0.23	0.28	0.37	0.35	0.15	0.07	0.02	0.04
Stand. Deviation	0.04	0.07	0.07	0.08	0.08	0.03	0.04	0.03	0.14	0.01	0.02	0.04

The predicted shrinkage in the flow direction, as it is shown in the table 6.11 and in the figure 6.58, is underestimated for tests considering a lower holding pressure (moulding condition code

of 210.5.13.10). Under these conditions the shrinkage in the flow direction should start in the mould before complete solidification, and this effect is not taken into account by C-Mold.

6.3.3.2- Effect of mould deformation

Shrinkage in PC plates

Experimental results of the as-moulded shrinkage in the flow direction, as a function of the holding pressure and time, and the predictions from C-Mold, either considering or neglecting the mould deformation are shown in the figures 6.59 and 6.60 respectively.

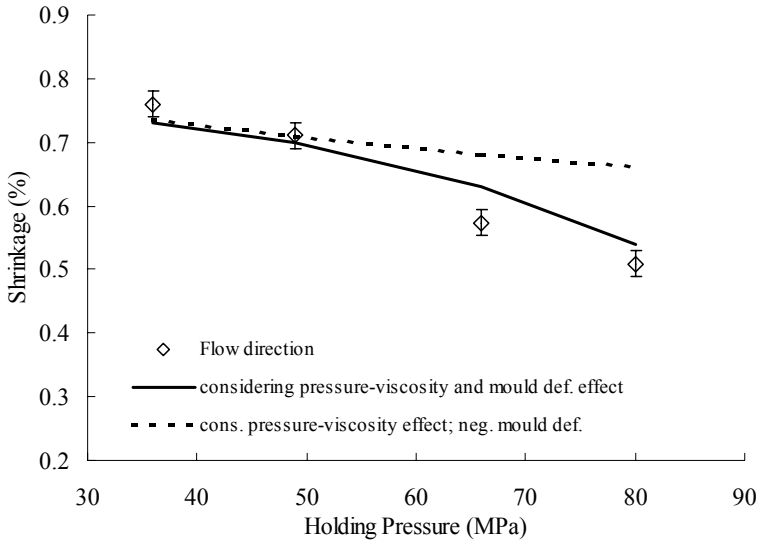

Figure 6.59- Comparison between as-moulded shrinkage (symbols) in flow direction, and C-Mold predictions (lines) in PC plates. Different holding pressures with th=15 s

As it was explained already in the section 6.1.2.1, the mould deformation is considered by changing the parameter b3 in the Tait equation, in order to obtain an equivalent material compressibility that includes the mould compliance.

The trend shown by the experimental shrinkage data is suggested by the C-Mold software predictions. However, the as-moulded shrinkage is overestimated for the highest applied holding pressures in the case of considering the pressure viscosity effect but neglecting the mould deformation (figure 6.59).

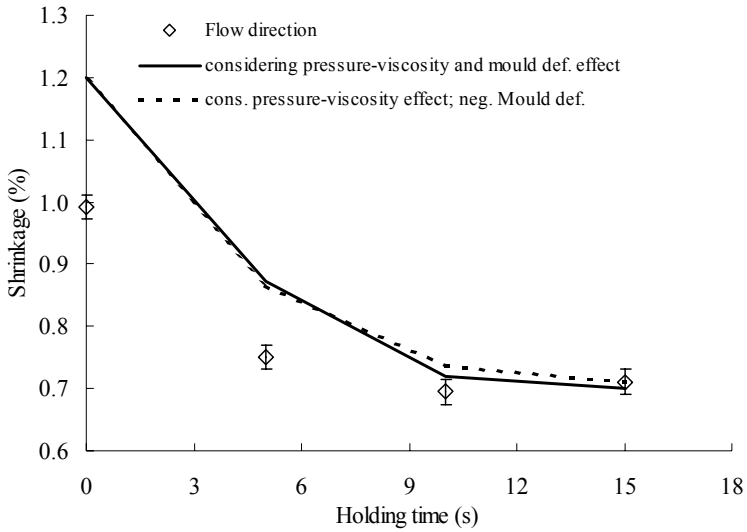

Figure 6.60- Comparison between as-moulded shrinkage (symbols) in flow direction, and C-Mold predictions (lines) in PC plates. Different holding times with Ph=49 MPa.

The Table 6.12 compares the absolute values of the difference between the experimental shrinkage and the predictions considering the C-Mold standard parameters of the material database, the effect of pressure on the viscosity and taking into account the mould deformation.

Table 6.12 – Comparison of the difference between the experimental shrinkage and the predictions with C-Mold in PC plates

Condition	Using standard Parameters				Considering p-v effect				Considering p-v + mould def. effect			
	Diff. Sh_x (%)	Diff. Sh_y (%)			Diff. Sh_x (%)	Diff. Sh_y (%)			Diff. Sh_x (%)	Diff. Sh_y (%)		
		P2	P3	P4		P2	P3	P4		P2	P3	P4
310.36.15.20	0.05	0.01	0.00	0.03	0.02	0.02	0.02	0.00	0.03	0.01	0.01	0.01
310.49.15.20	0.04	0.01	0.01	0.01	0.00	0.03	0.03	0.04	0.01	0.02	0.01	0.02
310.66.15.20	0.03	0.08	0.06	0.07	0.11	0.16	0.14	0.16	0.06	0.11	0.09	0.11
310.80.15.20	0.01	0.05	0.09	0.05	0.15	0.19	0.22	0.18	0.03	0.06	0.10	0.08
310.49.0.20	0.23	0.03	0.04	0.19	0.20	0.00	0.08	0.20	0.21	0.01	0.08	0.19
310.49.5.20	0.11	0.10	0.11	0.07	0.12	0.11	0.10	0.08	0.12	0.12	0.11	0.08
310.49.10.20	0.02	0.04	0.09	0.07	0.04	0.07	0.10	0.09	0.03	0.05	0.09	0.08
Average	0.07	0.05	0.06	0.07	0.09	0.09	0.10	0.10	0.07	0.05	0.07	0.08
Standard Deviation	0.07	0.03	0.04	0.05	0.07	0.07	0.06	0.07	0.07	0.04	0.04	0.06

The C-Mold shrinkage predictions taking into account the mould deformation agree better with experimental data. This better result, is certainly related to the close agreement between the experimental pressure evolution and the C-Mold predictions, as it can be seen in the figures 6.12, and not to the increase of the material compressibility. In fact, a complementary simulation confirms that at C-Mold the elastic modulus and the Poisson's ratio of the material are used to calculate the material compressibility.

Shrinkage in PC tubes

Experimental results of shrinkage as a function of the holding pressure alongside with the predictions from C-Mold considering the effect of pressure on viscosity, and considering or neglecting the mould deformation are shown in the figures 6.61 and 6.62. The trend shown by the experimental shrinkage data is also shown by the C-Mold software predictions.

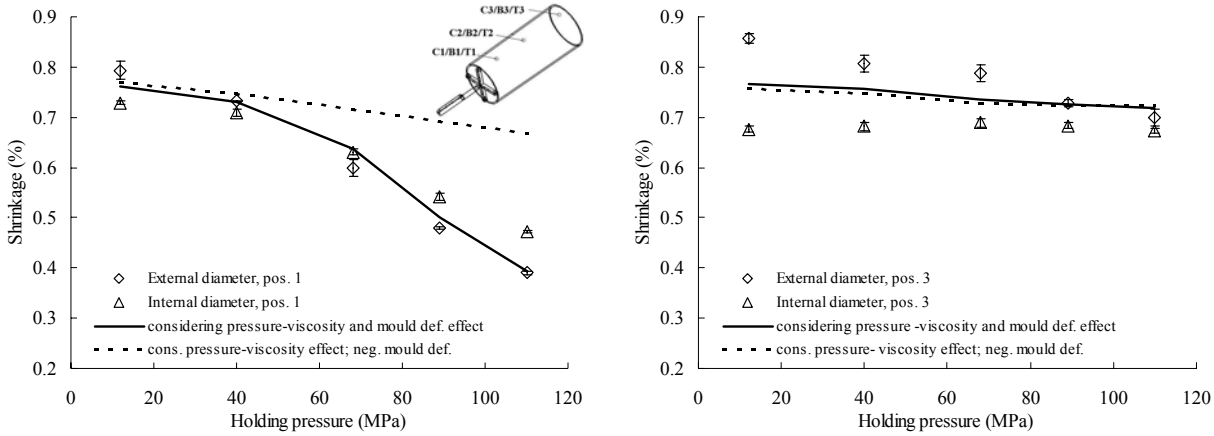

a) position 1 b) position 3

Figure 6.61- Comparison between the as-moulded diametrical shrinkage (symbols) as a function of the holding pressure for PC with th=10 s, and C-Mold predictions (lines).

The as-moulded shrinkage in the flow direction (figure 6.62) and the diametrical shrinkage (figure 6.61) at the position 1, 21 mm from the gate and, in a less evident way, at the position 3, 139 mm from the gate, are overestimated when mould deformation is neglected and higher pressures are applied during the holding stage. In these cases, the experimental pressures are substantially higher than predicted, probably due to the mould deformation (see figure 6.13).

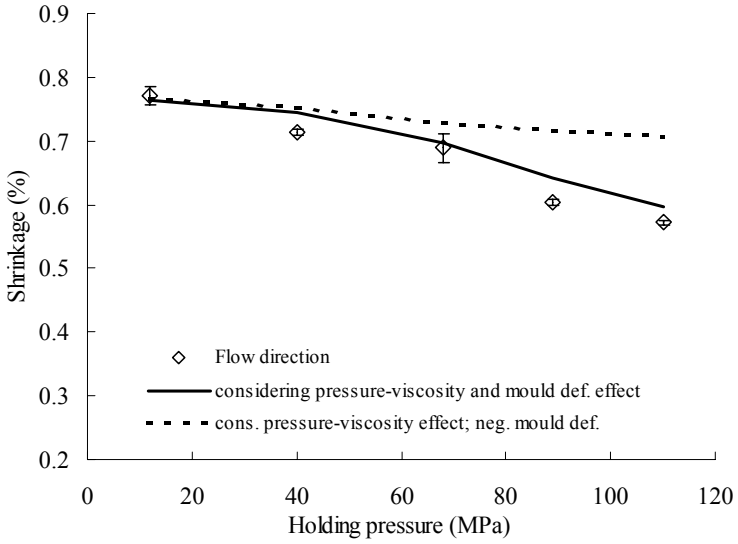

Figure 6.62- Comparison between as-moulded shrinkage in the flow direction (symbols) as a function of the holding pressure in PC tubes with th=10 s, and C-Mold predictions (lines).

In the Table 6.13 the difference between the experimental shrinkage is compared with the predictions considering the C-Mold standard parameters of the material database, the effect of pressure on the viscosity and taking into account the mould deformation. As expected, and also observed in the plate case, the C-Mold shrinkage predictions considering the mould deformation agree better with the experimental shrinkage in both cases.

Table 6.13 – Comparison of the difference between the experimental shrinkage and the predictions with C-Mold in PC tubes

Condition	Using standard Parameters				Considering p-v effect				Considering p-v + mould def. effect			
	Diff. Sh_x (%)	Diff. Sh_θ (%)			Diff. Sh_x (%)	Diff. Sh_θ (%)			Diff. Sh_x (%)	Diff. Sh_θ (%)		
		P1	P2	P3		P1	P2	P3		P1	P2	P3
310.12.10.15	0.03	0.01	0.02	0.02	0.00	0.01	0.00	0.02	0.01	0.00	0.01	0.01
310.40.10.15	0.00	0.01	0.03	0.02	0.04	0.03	0.00	0.00	0.03	0.01	0.01	0.01
310.68.10.15	0.06	0.02	0.07	0.07	0.04	0.10	0.01	0.01	0.01	0.02	0.01	0.01
310.89.10.15	0.11	0.14	0.08	0.14	0.11	0.18	0.08	0.01	0.04	0.01	0.04	0.02
310.110.10.15	0.28	0.31	0.26	0.32	0.13	0.24	0.10	0.03	0.02	0.04	0.05	0.03
Average	0.10	0.10	0.09	0.11	0.07	0.11	0.04	0.02	0.02	0.02	0.03	0.01
Standard Deviation	0.10	0.12	0.09	0.11	0.05	0.09	0.04	0.01	0.01	0.01	0.02	0.01

6.3.3.3- Concluding remarks

The results of shrinkage predictions performed by the C-Mold suggest that:

- The trend of C-Mold shrinkage predictions, for iPP, are qualitatively in good agreement with the measurements, specially when the effect of pressure on viscosity is considered.
- As expected for iPP, adopting a value of the solidification temperature lower than the quoted in the C-Mold database, that is obtained by a cooling rate of 20ºC/min (much lower that the effective cooling rate), causes the predictions to become much closer to the experimental data.
- The C-Mold shrinkage predictions, for PC, taking into account the mould deformation agree better with experimental data. This better result is certainly related to the close agreement between the experimental pressure evolution and the C-Mold predictions.

6.3.4- Shrinkage prediction with the thermo-mechanical model

The shrinkage can be more precisely predicted using the thermo-mechanical model already described in section 3.1. The flow chart describing the main steps involved in the computation of the shrinkage predictions is presented in the figure 6.63.

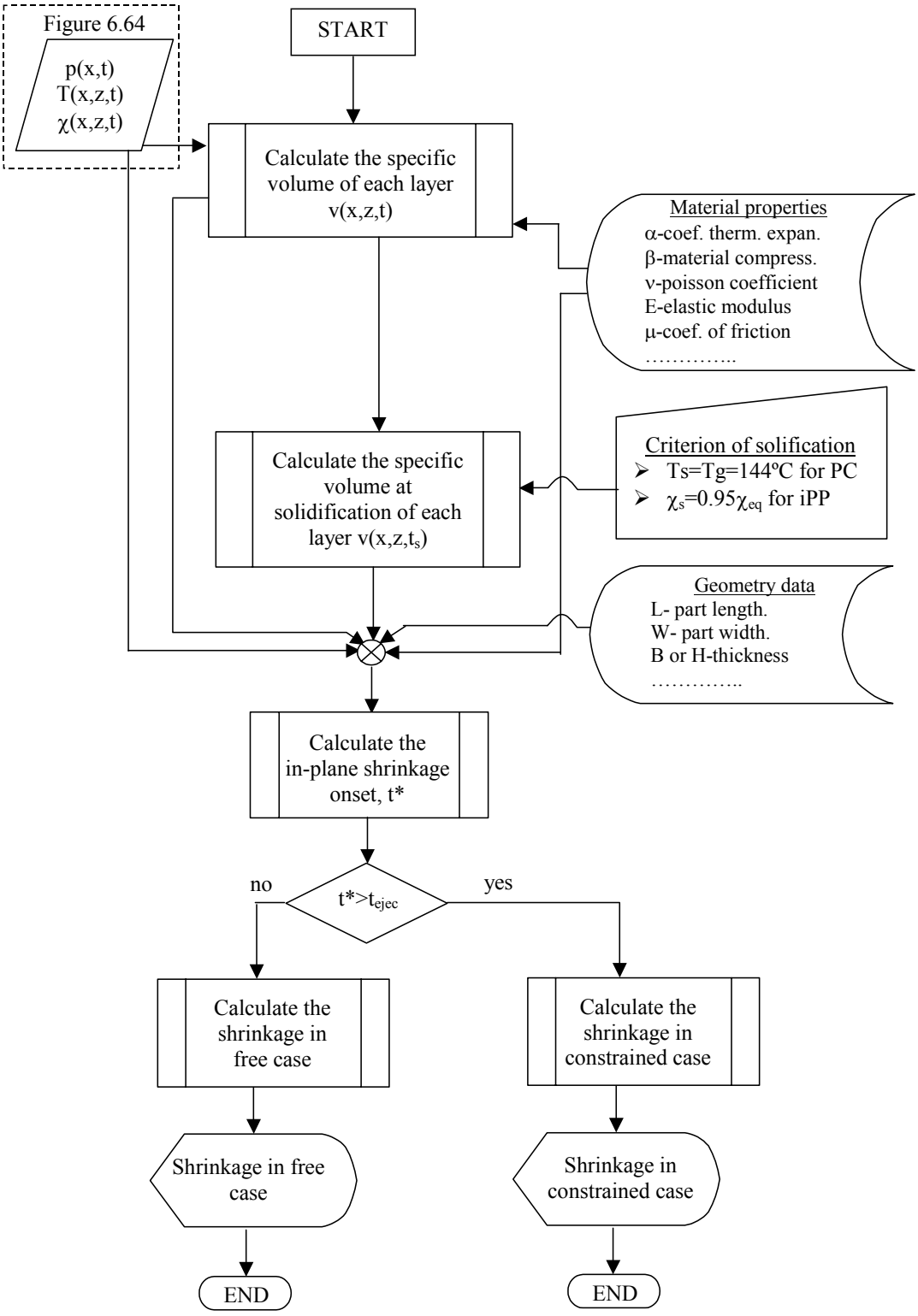

Figure 6.63- Sequence of the solution process of the thermo-mechanical model to predict the shrinkage.

The input data for the constrained and free shrinkage models, namely the temperature, degree of crystallinity and respective density curves were obtained from the UNISA (as described in section 5.4.2) in the case of polypropylene Hifax Ba238G3 and from C-Mold in the case of polycarbonate Lexan 141R, as shown in the figure 6.64.

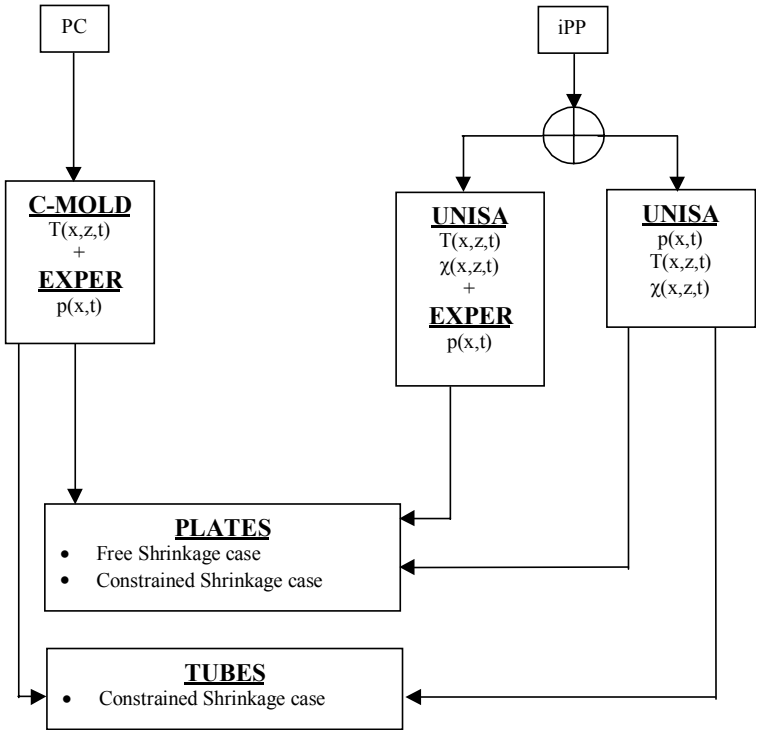

Figure 6.64- Description of the input data, derived from the injection moulding simulation softwares used in this work, to predict the shrinkage using the thermo-mechanical model.

Using the input data derived from the injection moulding simulation softwares and the material properties, the specific volume of each layer, v(x,z,t), is calculated. The specific volume at solidification of each layer, $v(x,z,t_s)$ is then calculated using the degree of crystallinity as the criterion of solidification for the case of iPP. The degree of crystallinity as criterion of solidification from the mechanical point of view seems to be more precise for a semi-crystalline polymer than the solidification temperature, as already reported elsewhere [72].

The degree of crystallinity above which the iPP was assumed to be a elastic solid is 95% of the crystallinity equilibrium value of the polypropylene phase, $\chi_{eq.}$. This value was obtained by De Santis [141] upon comparison of the storage modulus obtained by DMA and the crystallinity curve obtained by DSC at the same heating rate (4ºC/min).

Finally, depending on the condition that the shrinkage begins before or after the ejection of the part, the free (equations 3.17 and 3.19) or the constrained (equations 3.20 and 3.21 for the plates, and 3.45 and 3.46 for the tubes) shrinkage models are applied to calculate the shrinkage.

Shrinkage in iPP plates

In figures 6.65 and 6.66, results of the in-flow direction shrinkage as function of the holding pressure and time are compared with the predictions of the free and constrained shrinkage cases, which are modelled with the equations 3.19 and 3.20, respectively. It is possible to see in these figures that the predictions satisfactorily agree with experimental as-moulded shrinkage results, and that the effect of constraints on the as-moulded shrinkage is correctly described.

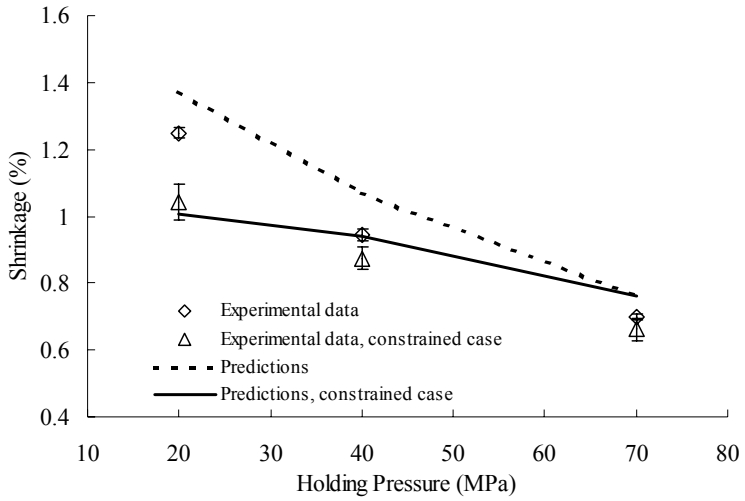

Figure 6.65- Comparison between the as-moulded shrinkage (symbols) in flow direction, for free and constrained shrinkage in iPP plate case, and the thermo-mechanical model with simulated pressure from UNISA program (lines). Mouldings with a different holding pressures and a constant th=10 s.

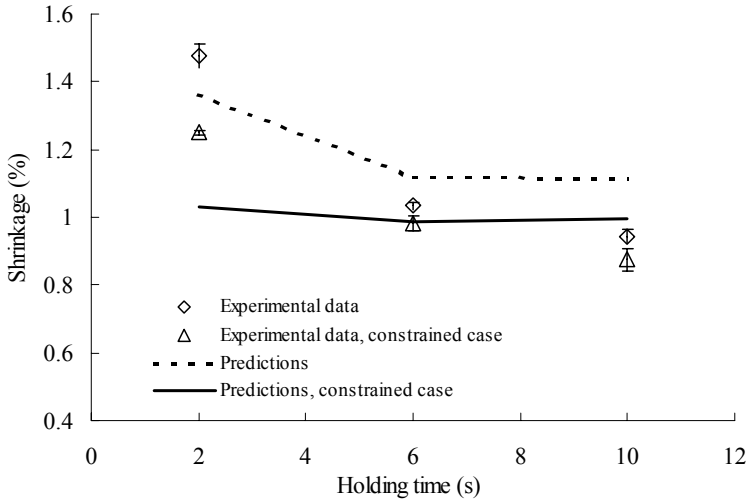

Figure 6.66- Comparison between as-moulded shrinkage (symbols) in the flow direction, for free and constrained shrinkage in iPP plate case, and the thermo-mechanical model with simulated pressure from UNISA program (lines). Mouldings with a different holding times and a constant Ph=40 MPa.

In order to check the relevance of the pressure curve description on the shrinkage calculations, these were repeated inputting experimental values of pressure instead of the simulated ones. Results are shown in figures 6.67 and 6.68, and reveal that if a correct description for pressure evolution is used a good prediction of shrinkage is reached by the thermo-mechanical model proposed in section 3.1.

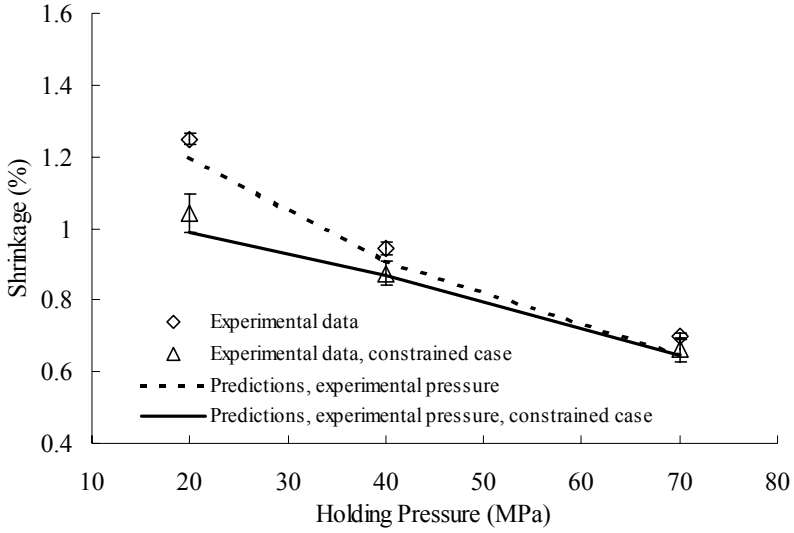

Figure 6.67- Comparison between the as-moulded shrinkage (symbols) in the flow direction, for free and constrained shrinkage in iPP plate case, and the thermo-mechanical model with experimental pressure (lines). Mouldings with a different holding pressures and a constant th=10 s.

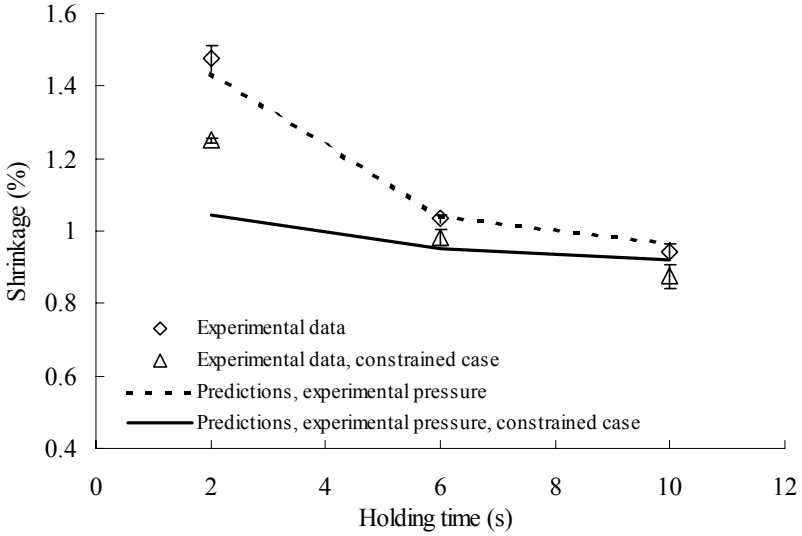

Figure 6.68- Comparison between as-moulded shrinkage (symbols) in flow direction, for free and constrained shrinkage in iPP plate case, and the thermo-mechanical model with experimental pressure (lines). Mouldings with different holding times and a constant Ph=40 MPa.

In the Table 6.14 the absolute values of the difference between the experimental shrinkage and the predictions with the thermo-mechanical model inputting experimental values of pressure and the predicted by UNISA software are presented.

Table 6.14 – Comparison of the difference between the experimental shrinkage and the predictions in iPP plates with the thermo-mechanical model

Condition	**UNISA** p(x,t) T(x,z,t) χ(x,z,t)		**UNISA** T(x,z,t) χ(x,z,t) **EXPER** p(x,t)	
	Free	Constrained	Free	Constrained
230.20.10.15	0.12	0.03	0.05	0.05
230.40.10.15	0.13	0.07	0.03	0.01
230.70.10.15	0.06	0.10	0.06	0.02
230.40.2.15	0.11	0.27	0.04	0.25
230.40.6.15	0.09	0.00	0.01	0.03
Average	0.10	0.09	0.04	0.07
Standard Deviation	0.02	0.09	0.02	0.09

It is possible to see in the Table 6.14 that the predictions satisfactorily agree with experimental shrinkage results in free and constrained situation. Slight differences are observed, and they can be ascribed to a non-perfect description of the pressure curves used in the calculations. The absolute values of the difference between the experimental and predicted values reveal that, if a correct description for pressure evolution is used, a good prediction of shrinkage is obtained by the thermo-mechanical model.

The model under predict the shrinkage in the constrained case for the low holding time. This can be attributed to the constrainer being not completely rigid (due to the great tendency of the moulding to shrinkage) and thus to permit the shrinkage occurs inside the mould.

The results for the shrinkage onset inside the mould as a function of the holding pressure are shown in figure 6.69 (lines). In this case calculations were also performed with both experimental and predicted pressure curves obtained with the UNISA program. It results clear from the figure that the predictions agree well with the experimental data, especially when considering experimental pressure data.

A correct estimation of the time at which shrinkage starts, the shrinkage onset, confirms that the force balance inside the mould (equation 3.6) is correctly described and allows for a correct shrinkage prediction in the case of the shrinkage starting before complete solidification.

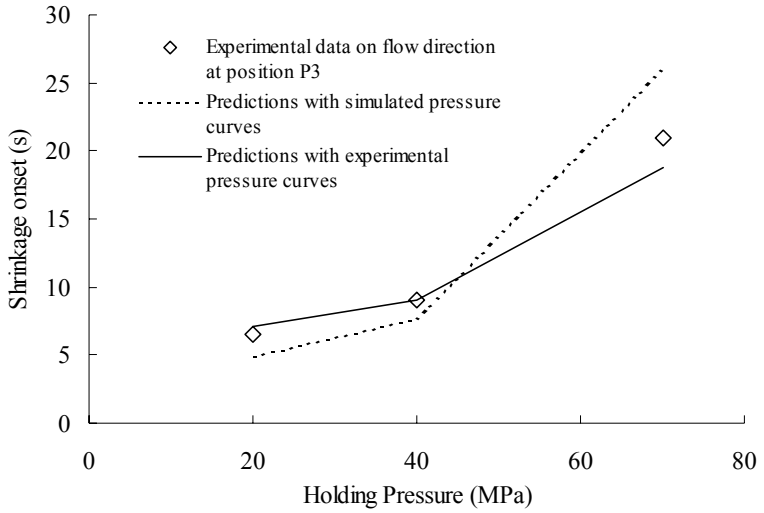

Figure 6.69- Comparison between the shrinkage onset inside the mould and the predictions using the experimental and simulated pressure curves from UNISA program.

Shrinkage in PC plates

Results of the as-moulded shrinkage in the flow direction as a function of the holding pressure are shown in figure 6.70 and compared with the predictions of the constrained and free shrinkage cases. The predicted temperature profile obtained by the C-Mold software was used for the shrinkage calculations. The pressure curves were obtained experimentally.

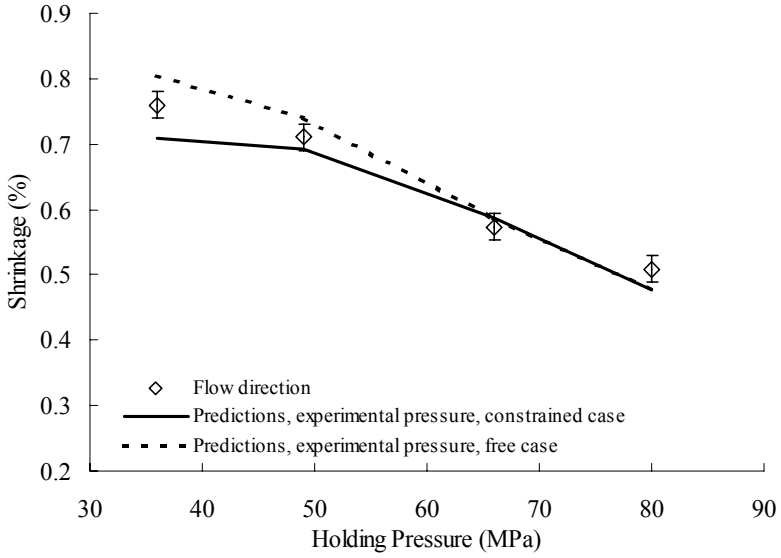

Figure 6.70- Comparison between the as-moulded shrinkage (symbols) in the flow direction, and the thermo-mechanical model with experimental pressure (lines) for free and constrained shrinkage in PC plates.

In the Table 6.15 the absolute value of the difference between the experimental shrinkage and the predictions with the thermo-mechanical model are compared.

Table 6.15 – Comparison of the difference between the experimental shrinkage and the predictions in PC plates with the thermo-mechanical model

Condition	**C-Mold** T(x,z,t) **EXPER** p(x,t)							
	Free				Constrained			
	Diff. Sh_x (%)	Diff. Sh_y (%)			Diff. Sh_x (%)	Diff. Sh_y (%)		
		P2	P3	P4		P2	P3	P4
310.36.15.20	0.04	0.06	0.08	0.09	0.05	0.09	0.11	0.13
310.49.15.20	0.03	0.06	0.05	0.06	0.02	0.08	0.07	0.09
310.66.15.20	0.01	0.05	0.04	0.07	0.01	0.05	0.04	0.07
310.80.15.20	0.03	0.04	0.09	0.02	0.03	0.04	0.09	0.02
Average	0.03	0.05	0.06	0.06	0.03	0.07	0.08	0.08
Standard Deviation	0.01	0.01	0.02	0.02	0.01	0.02	0.03	0.04

From the figure 6.70 and the table 6.15 it can be seen that the quality of the agreement between the predictions and experimental as-moulded shrinkage data is good. However, the predictions using the model for the free shrinkage case agree better for lower holding pressure (Ph=36 MPa), than using the model for the constrained case. This suggests that for holding pressure of 36 MPa the shrinkage starts before complete solidification.

Shrinkage in iPP tubes

In the figure 6.71 the experimental results of the diametrical shrinkage in the positions 1 and 3 as function of the holding pressure are compared with the predictions of the thermo-mechanical model derived in section 3.2.3 (equations 3.52 and 3.53). The input data for the model, namely the pressure, temperature and crystallinity were obtained using the UNISA program.

It can be observed in figure 6.71a (position1) that the inversion of the trend between the internal and external diametrical shrinkage is predicted.

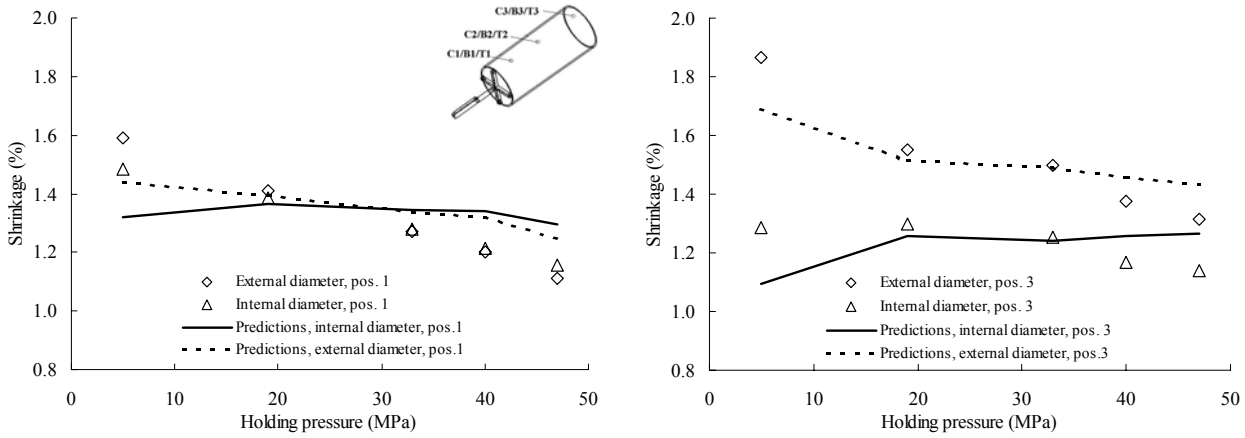

a) Position 1 b) Position 3

Figure 6.71- Comparison between the as-moulded diametrical shrinkage for iPP (symbols) and the thermo-mechanical model with input data from UNISA program (lines). Mouldings with Tinj=210ºC, Tw=50ºC, th=13s, ta=10s.

In the Table 6.16 the absolute values of the difference between the experimental shrinkage and the predictions with the thermo-mechanical model are compared.

Table 6.16 – Comparison of the difference between the experimental shrinkage and the predictions in iPP tubes with the thermo-mechanical model.

Condition	**UNISA** p(x,t) T(x,z,t) χ(x,z,t)						
	Diff. Sh_x (%)	Diff. $Sh_{\theta\ ext.}$ (%)			Diff. $Sh_{\theta\ int.}$ (%)		
		P1	P2	P3	P1	P2	P3
210.5.13.10.	0.42	0.15	0.21	0.18	0.16	0.23	0.19
210.19.13.10.	0.02	0.02	0.08	0.04	0.02	0.08	0.04
210.33.13.10.	0.13	0.06	0.00	0.01	0.07	0.01	0.01
210.40.13.10.	0.21	0.12	0.04	0.08	0.13	0.05	0.09
210.47.13.10.	0.18	0.13	0.09	0.12	0.14	0.09	0.13
Average	0.19	0.10	0.09	0.09	0.10	0.09	0.09
Standard Deviation	0.13	0.05	0.07	0.06	0.05	0.07	0.06

It is noticeable, in the figure 6.71 and in the Table 6.16, the differences of the diametrical shrinkage predictions for both extremes values of the holding pressure. The slight differences observed can be attributed to a non-perfect description of the predicted temperature and pressure curves. At lower holding pressures the moulding may detach from the mould wall surface

resulting in poor heat transfer by conduction. This may lead to a deviation between the cooling rate experienced by the material in relation to the predicted, and consequently to a different degree of crystallinity.

The experimental results of shrinkage in the flow direction as a function of the holding pressure and the predictions of the model, that assumes no shrinkage inside the mould, are compared in figure 6.72.

As it can be observed at low holding pressures in the figure 6.72 and in the Table 6.16, there is a significant difference between the experimental and the predicted shrinkage in the flow direction. This indicates that the shrinkage starts inside the mould before complete solidification, and that the boundary condition of constraint is no more valid.

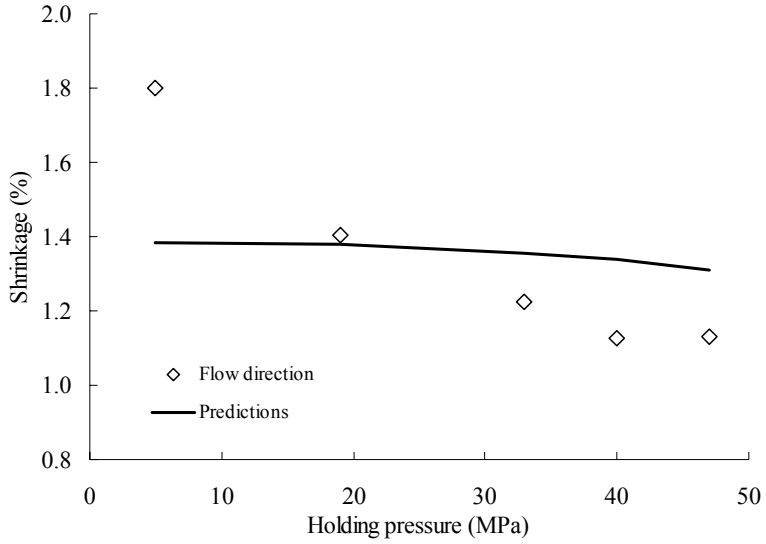

Figure 6.72- Comparison between the as-moulded shrinkage in flow direction in iPP tube case (symbols) and the thermo-mechanical model with input data from UNISA program (line). Mouldings with Tinj=210ºC, Tw=50ºC, th=13s, ta=10s.

Shrinkage in PC tubes

In figures 6.73 the results of the diametrical shrinkage in position 2 as a function of the holding pressure are compared with the predictions of the thermo-mechanical model (equations 3.52 and 3.53), using a pressure profile simulated with C-Mold. The predictions agree well with the experimental as-moulded diametrical shrinkage. The inversion of the trend between the internal and external diametrical shrinkage is also predicted.

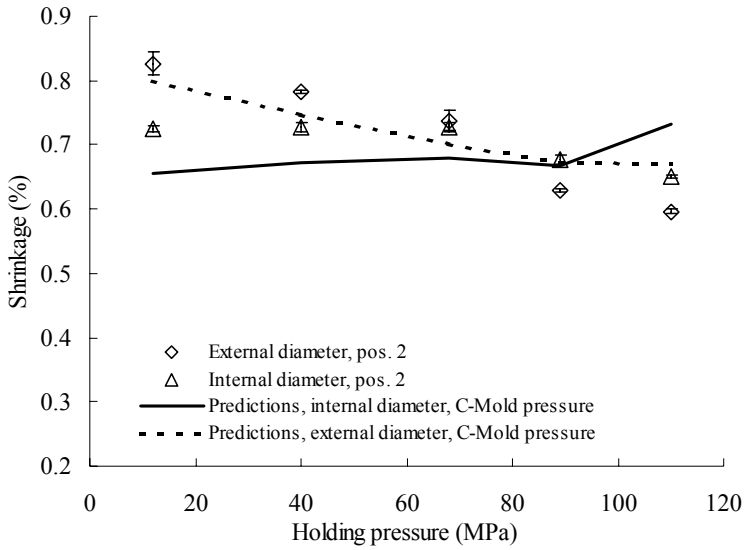

Figure 6.73- Comparison between as-moulded diametrical shrinkage for PC (symbols) vs holding pressure at a constant holding time of 10 s, and the thermo-mechanical model (lines) with simulated pressure from C-Mold.

In figures 6.74 the thickness shrinkage results in positions 1, 2 and 3 as a function of holding pressure are compared with the predictions of the model presented in section 3.2.3. It can be observed that the predictions that include the mould compliance C_M=0.2 GPa^{-1} satisfactorily agree with experimental thickness shrinkage.

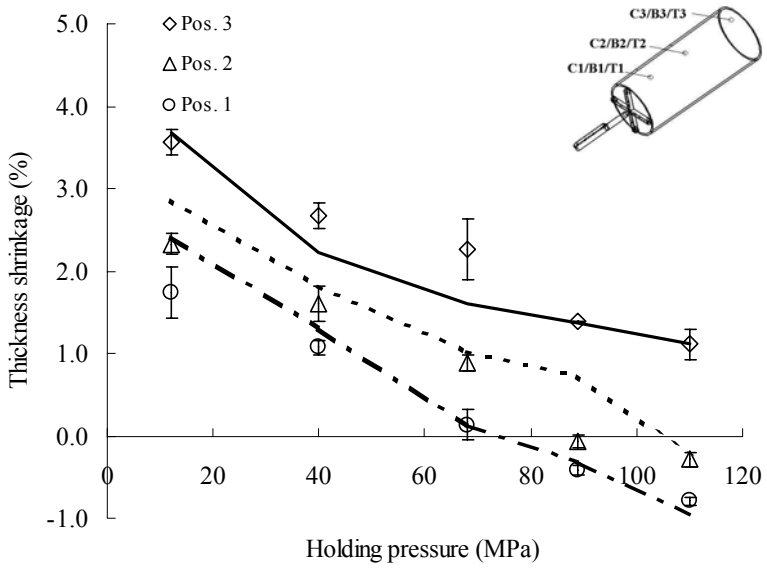

Figure 6.74- Comparison between the thickness shrinkage in PC tubes (symbols) vs holding pressure at a constant holding time of 10 s, and the thermo-mechanical model (lines) with simulated pressure from C-Mold.

In the Table 6.17 the absolute value of the difference between the experimental shrinkage are compared with the predictions with the thermo-mechanical model inputting the simulated pressure from C-Mold. Slight differences are observed, and can be the result of to a non-perfect description of the predicted pressure curves.

Table 6.17 – Comparison of the difference between the experimental shrinkage and the predictions in PC tubes with the thermo-mechanical model inputting the simulated pressure from C-Mold.

Condition	**C-Mold** T(x,z,t) p(x,t)									
	Diff. Sh_x (%)	Diff. $Sh_{\theta\ ext.}$ (%)			Diff. $Sh_{\theta\ int.}$ (%)			Diff. Sh_z (%)		
		P1	P2	P3	P1	P2	P3	P1	P2	P3
310.12.10.15	0.03	0.00	0.03	0.02	0.05	0.07	0.04	0.67	0.54	0.11
310.40.10.15	0.00	0.01	0.04	0.05	0.01	0.06	0.02	0.24	0.21	0.44
310.68.10.15	0.00	0.05	0.04	0.06	0.06	0.05	0.02	0.00	0.13	0.65
310.89.10.15	0.04	0.07	0.04	0.02	0.07	0.01	0.02	0.10	0.80	0.01
310.110.10.15	0.06	0.06	0.07	0.01	0.08	0.08	0.01	0.17	0.05	0.00
Average	0.03	0.04	0.04	0.03	0.05	0.05	0.02	0.24	0.35	0.24
Standard Deviation	0.02	0.03	0.02	0.02	0.02	0.02	0.01	0.23	0.28	0.26

In order to check the relevance of the pressure curve description on the shrinkage calculations, these were repeated inputting experimental values of pressure instead of simulated ones. Results are also shown in figures 6.75 and 6.76.

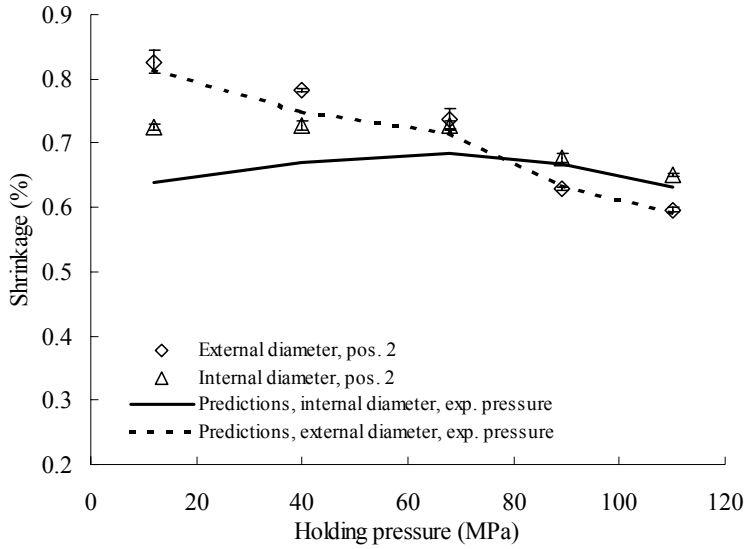

Figure 6.75- Comparison between as-moulded diametrical shrinkage for PC (symbols) vs holding pressure at a constant holding time of 10 s, and the thermo-mechanical model (lines) with experimental pressure.

It can be observed in figure 6.76 that the predictions satisfactorily agree with experimental thickness shrinkage. These results confirms that the inclusion of the mould compliance of C_M=0.2 GPa^{-1} allows for a correct thickness shrinkage prediction, confirming the importance of including the mould deformation in the model.

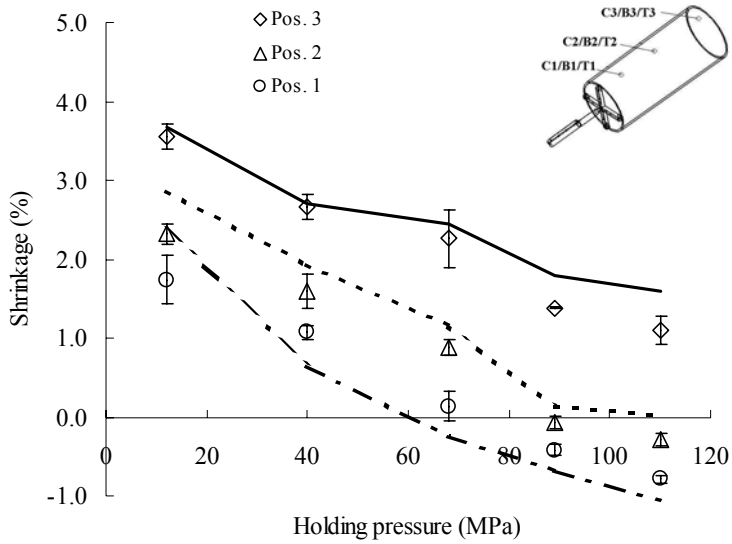

Figure 6.76- Comparison between the thickness shrinkage in PC tubes (symbols) vs holding pressure at a constant holding time of 10 s, and the thermo-mechanical model (lines) with experimental pressure.

In the Table 6.18 the absolute value of the difference between the experimental shrinkage are compared with the predictions with the thermo-mechanical model inputting the experimental pressure. The results reveal that, if a correct description for pressure evolution is used, a good prediction of shrinkage is reached by the model.

Table 6.18 – Comparison of the difference between the experimental shrinkage and the predictions in PC tubes with the thermo-mechanical model inputting the experimental pressure.

Condition	**C-Mold** T(x,z,t) **EXPER** p(x,t)									
	Diff. Sh_x (%)	Diff. $Sh_{\theta\ ext.}$ (%)			Diff. $Sh_{\theta\ int.}$ (%)			Diff. Sh_z (%)		
		P1	P2	P3	P1	P2	P3	P1	P2	P3
310.12.10.15	0.03	0.01	0.01	0.00	0.06	0.09	0.06	0.71	0.54	0.11
310.40.10.15	0.00	0.01	0.03	0.02	0.01	0.06	0.03	0.43	0.33	0.03
310.68.10.15	0.04	0.07	0.02	0.02	0.05	0.04	0.04	0.39	0.27	0.18
310.89.10.15	0.02	0.11	0.00	0.01	0.10	0.01	0.02	0.27	0.19	0.42
310.110.10.15	0.04	0.15	0.01	0.03	0.15	0.02	0.00	0.27	0.29	0.49
Average	0.03	0.07	0.02	0.02	0.07	0.04	0.03	0.42	0.32	0.25
Standard Deviation	0.01	0.06	0.01	0.01	0.05	0.03	0.02	0.16	0.12	0.18

The results of the as-moulded shrinkage in the flow direction are compared with the predictions of the thermo-mechanical model, in figure 6.77. As it is shown in the figure and the Table 6.18, the comparison of experimental and predicted results (using experimental profiles of pressure as input), suggest that the model assuming no shrinkage inside the mould predicts the shrinkage accurately.

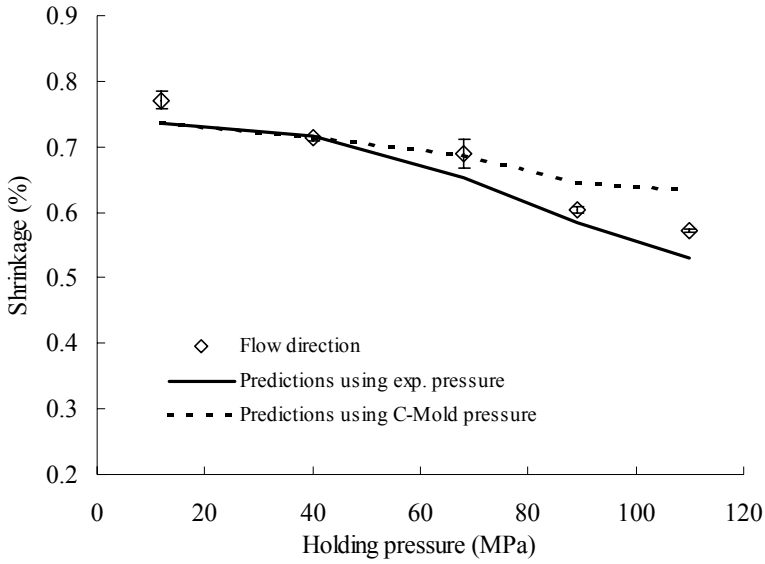

Figure 6.77- Comparison between as-moulded shrinkage in flow direction in PC tubes (symbols) vs holding pressure at a constant holding time of 10 s, and the thermo-mechanical model (line).

6.3.4.1- Concluding remarks

The results of shrinkage predictions using the thermo-mechanical model derived in this research suggest that:

- The model using the experimental profiles of pressure as input predicts the shrinkage accurately.
- The inversion of the trend between the internal and external diametrical shrinkage, observed in the PC and iPP tubes, are predicted by the model developed in this work.
- In opposition to the case of iPP tubes, the results reveal that no shrinkage in the flow direction occurs inside the mould in the PC tube.
- The thickness shrinkage for the PC case considering the mould compliance value of C_M=0.2 GPa^{-1} is correctly predicted. This confirms the importance of including the mould deformation in the model.

6.4- Ejection Forces

6.4.1- Experimental ejection forces for iPP

The force required to eject the tubes, as measured by the instrumented mould developed in this work are presented in this section. The effect of the processing variables is discussed considering that the shrinkage is the main cause to the generation of frictional forces upon ejection.

The complete ejection force data are included in Appendix A2.4.

6.4.1.1- Effect of the surface temperature of the core at ejection

The surface temperature was calculated as the average of the temperature at ejection, measured by the thermocouples located in the core at 79 and 139 mm from the gate (T2 and T3). Different surface temperatures at ejection were achieved by varying the time after the holding phase, ta.

The experimental ejection forces measurements for iPP as a function of the surface temperature at ejection are shown in the figure 6.78. The results indicate that the temperature at the surface of the core influences substantially the ejection force. In particular, this force decreases when the surface temperature increases, at a rate of *ca.* 40 N/ºC. From the ejection force model derived in section 3.2, this is an expected result of the concurrent effect of the reduction of the modulus and of the shrinkage at ejection both having an influence in that sense.

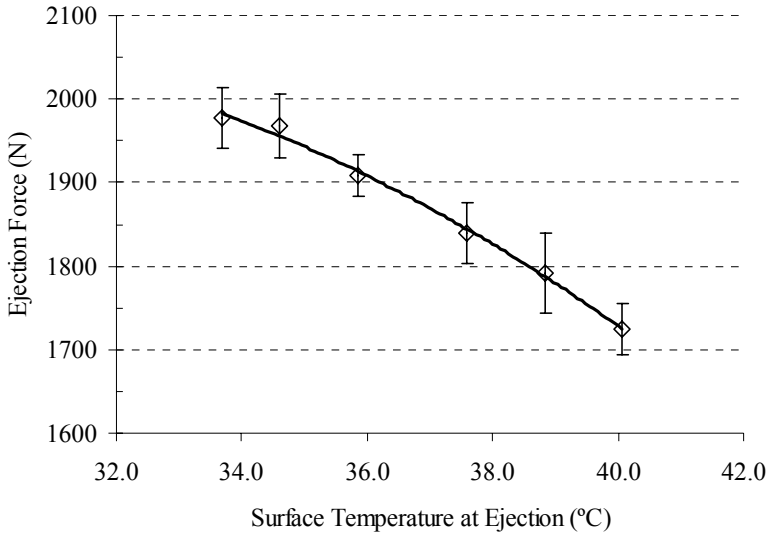

Figure 6.78- Influence of the surface temperature on the ejection force for iPP. Mouldings with Tinj=230ºC, Tw= 32ºC and Ph=40 MPa

6.4.1.2- Effect of the injection temperature

The dependence of the ejection force on the surface temperature at ejection for injection temperatures of 210ºC and 230ºC are plotted in figure 6.79. The data show that the ejection force decreases slightly with the injection temperature (at about 3.5 N/ºC). The increase of the injection temperature results in a smaller shrinkage (as was already shown in figures 6.51 and 6.52) due to the increased pressure transmission during the holding stage.

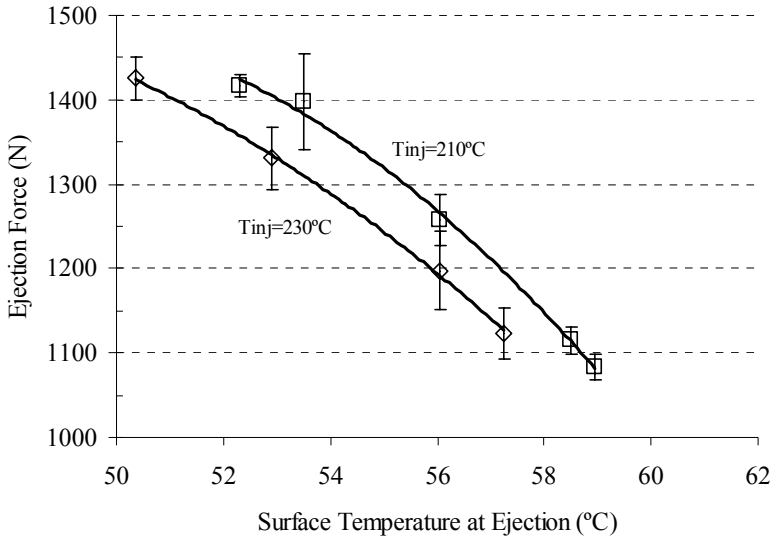

Figure 6.79- The ejection force for iPP as a function of the core surface temperature at ejection. Mouldings with Tw= 50ºC and Ph=40 MPa. Effect of injection temperature.

6.4.1.3- Effect of the mould temperature

The ejection force as a function of the core surface temperature at ejection for mould wall temperatures of 32ºC and 50ºC are shown in the figure 6.80. The results show the effect of the part temperature at ejection on the ejection force. Between parenthesis are given the time at ejection.

For a constant time after the holding phase, ta, (different surface temperature at ejection), the ejection force varies inversely to the mould temperature. This result is expected since the increase of the mould temperature corresponds to a higher part temperature at ejection. As it was mentioned in the case of the surface temperature, the increase of the mould temperature results in a reduction of the elastic modulus and of the shrinkage at ejection, both contributing to reduce the ejection force.

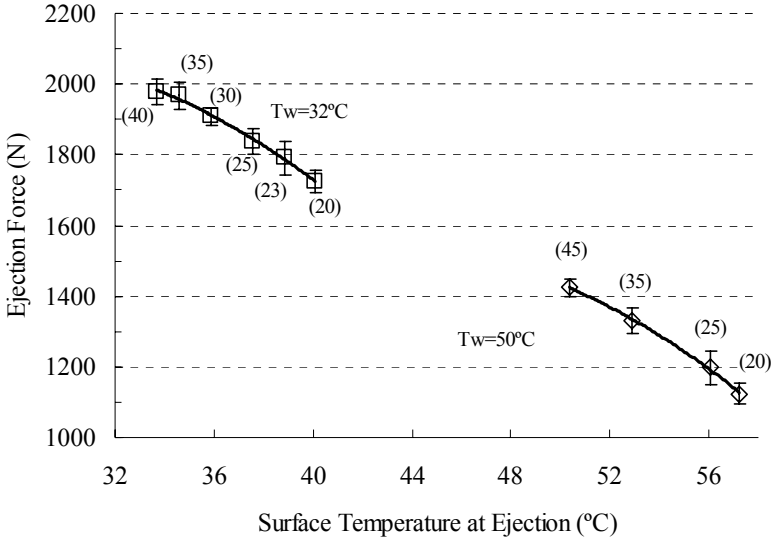

Figure 6.80- The ejection force for iPP as a function of the core surface temperature at ejection. Mouldings with Tinj=230ºC and Ph=40 MPa. The effect of the mould temperature is shown for 32ºC and 50ºC.

6.4.1.4- Effect of the holding pressure

The experimental ejection force data for iPP when the holding pressure is varied, for the mould temperatures (Tw) of 32ºC and 50ºC, are shown in figure 6.81 and 6.82 respectively.

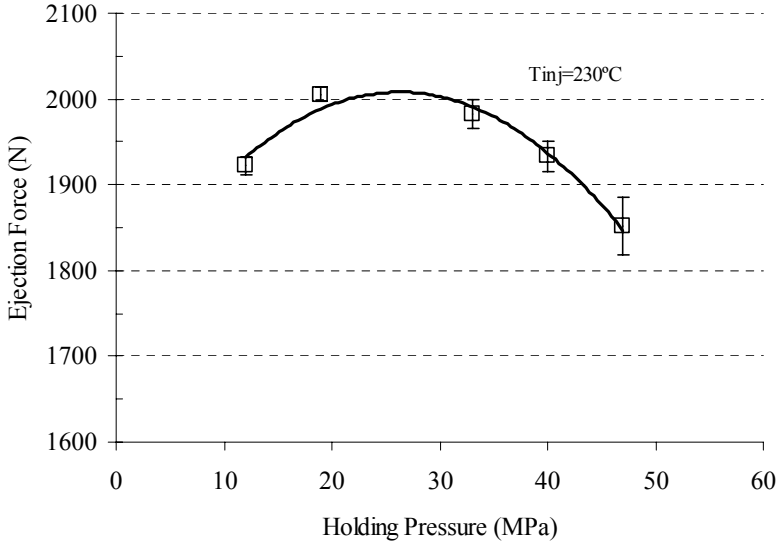

Figure 6.81- The influence of holding pressure on the ejection force for iPP. Mouldings with Tw=32ºC and Tinj=230ºC.

The effect of varying the holding pressure on the ejection force is generally in the sense of its reduction with rising pressure. However, when low holding pressure is used a much lower than expected value is observed. This arises from the larger through thickness shrinkage that causes the detachment of the material from the moulding cavity surface which causes the temperature to remain higher due to the poor heat conduction. Consequently a decrease in the ejection force occurs due to the higher temperature of the moulding, as observed in the figures 6.78 to 6.80.

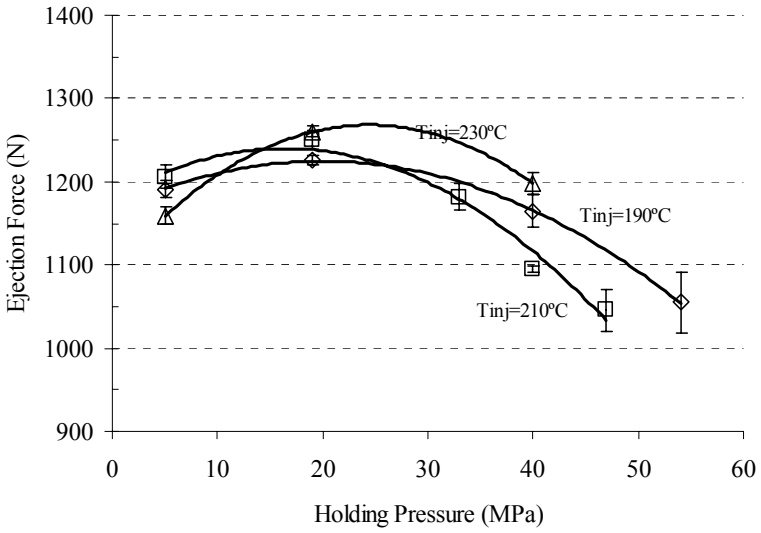

Figure 6.82- The ejection force for iPP as a function of the holding pressure. Mouldings with Tw=50ºC and different injection temperatures.

6.4.2- Experimental ejection forces for PC

6.4.2.1- Effect of the holding conditions

The ejection forces in function of the holding pressure and time, are shown in figures 6.83 and 6.84, respectively.

The ejection force changes inversely with respect to the holding pressure (figure 6.83). The reduced contact pressure is responsible for this behaviour and it results from the decreasing diametrical shrinkage associated to the holding pressure increase, that implies a smaller force being required to eject the moulding. It is worth noting that the ejection forces of the iPP mouldings are lower than when PC is used, regardless of the higher shrinkage that occurs with polypropylene. This results certainly from the lower modulus and coefficient of friction of iPP compared to PC.

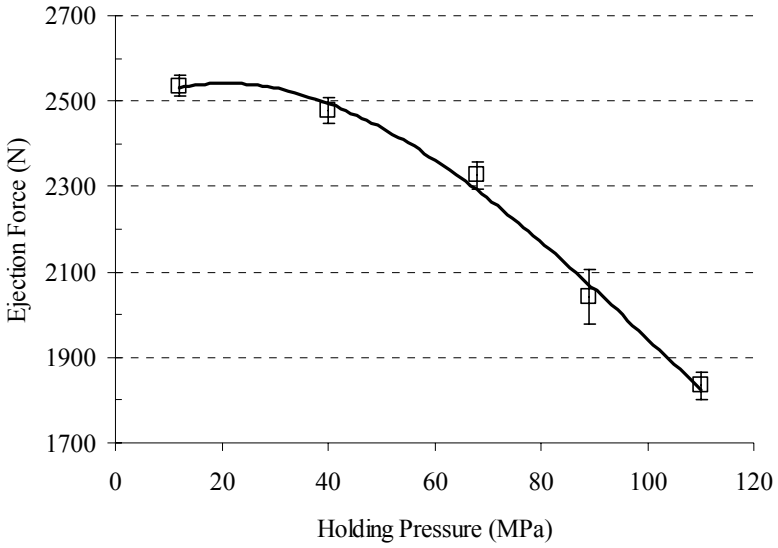

Figure 6.83- Influence of the holding pressure on the ejection force, for PC. Mouldings with Tinj=310ºC,Tw=85ºC and th=10s.

The holding time for a Ph=68 MPa does not affect the ejection force. As it was also observed for the diametrical shrinkage results, the increase of the holding time does not cause significant changes on the shrinkage. This is the result of the fast solidification of the material having less molten layers during the holding stage. This makes difficult the introduction of more material into the impression and consequently minimise the effect of holding time on the shrinkage and ejection force.

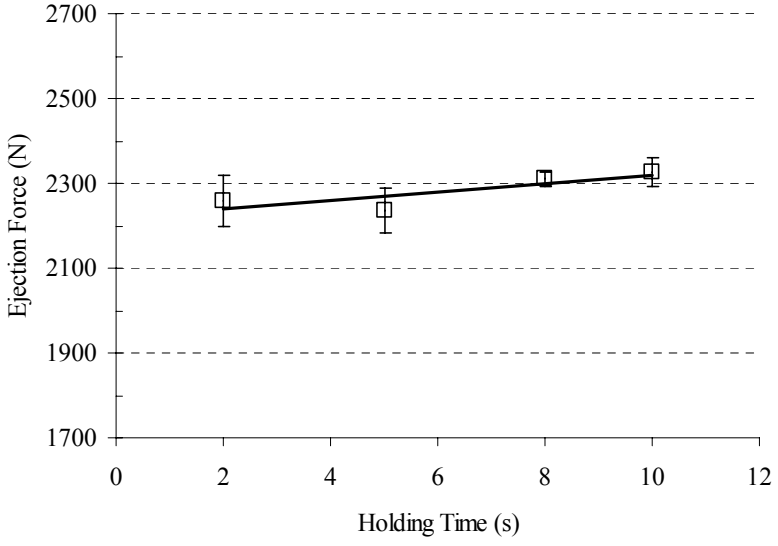

Figure 6.84- Influence of the holding time on the ejection force, for PC. Mouldings with Tinj=310ºC,Tw=85ºC and Ph=68MPa.

6.4.3- Analysis with the thermo-mechanical model

Ejection force predictions were obtained using the thermo-mechanical model already described in section 3.2. In the figure 6.85 the main steps involved in the computation of the ejection force predictions and the inputs are presented.

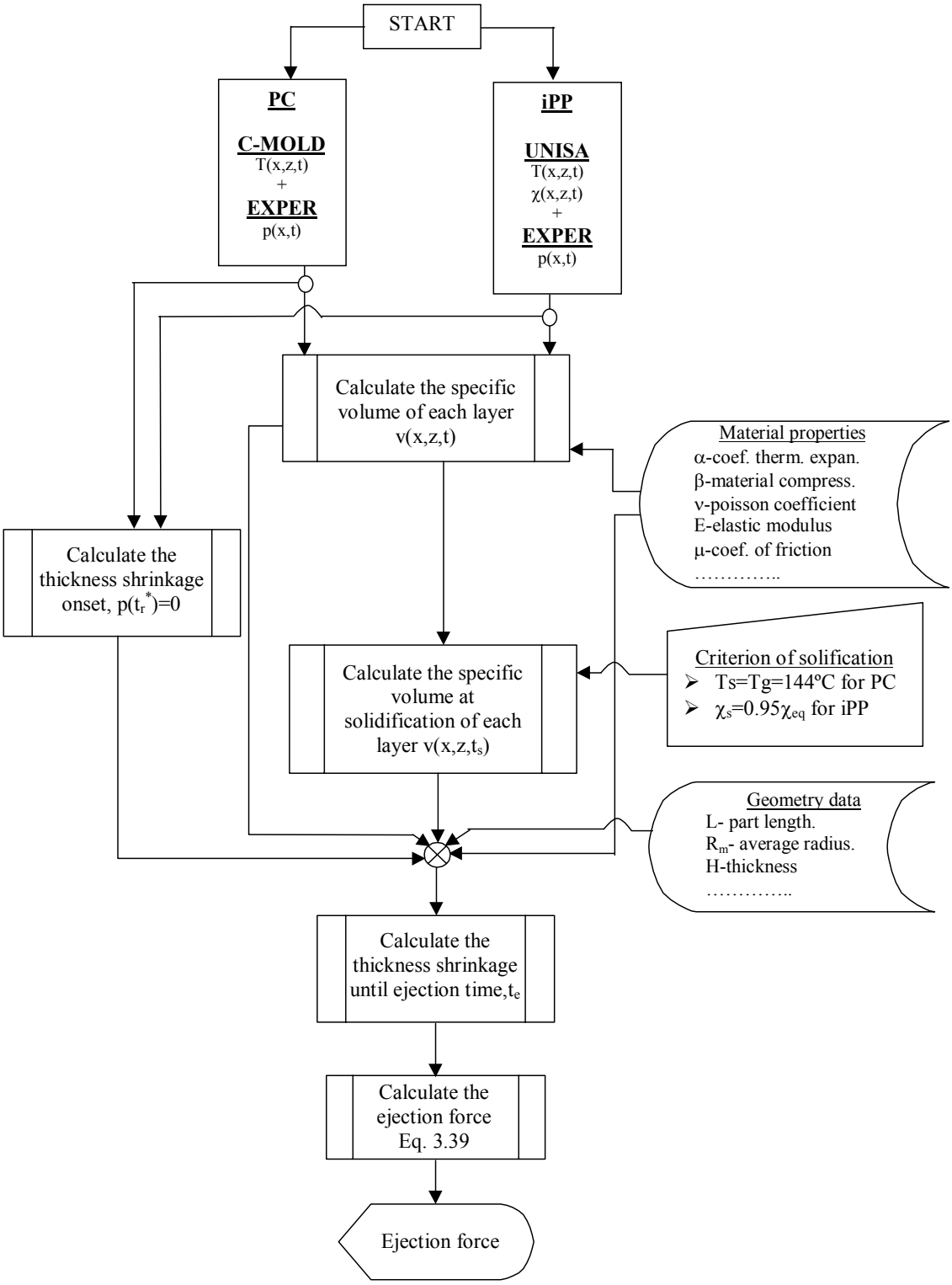

Figure 6.85- Sequence of the solution process of the thermo-mechanical model and the input data to predict the ejection force

The input data for the ejection force model, namely the temperature, degree of crystallinity and corresponding density curves were obtained (as it was done before in the shrinkage predictions) from the UNISA program in the case of polypropylene and from the C-Mold program in the case of polycarbonate.

From the input data and the material properties, the specific volume of each layer, v(x,z,t), is calculated. Then as it was done in the shrinkage prediction the specific volume at solidification of each layer, $v(x,z,t_s)$ is calculated using the degree of crystallinity as the criterion of solidification for the case of iPP, and the glass transition temperature for the case of PC.

Depending on the thickness shrinkage occurring inside the mould or after the mould opening, which is described by the condition $p(t_r^*)=0$, the ejection force is calculated including, or not including the thickness shrinkage using equation 3.39.

$$F_e = \mu.\frac{2.\pi.H_{part}}{1-\nu}.\mathrm{E}(\overline{\mathrm{T_e}}).\int_o^L\left(-\frac{1}{3}.\ln\left(\overline{\frac{\mathrm{v(x,r,t_e)}}{\mathrm{v_s(x,r)}}}\right)-\frac{\mathrm{H}}{(1+\nu).2.R_m}Sh_r(t)\Big|_{t_r^*}^{t_e}\right).dx \qquad (3.39)$$

This expression indicates that the ejection force is dependent on the elastic modulus at the ejection temperature, the thickness of the part, the variation of the (average) volume shrinkage between solidification and the ejection time, and the coefficient of friction (here is considered as a constant).

For the calculation of the ejection force the static coefficient of friction (μ) was estimated as 0.3 for PC and 0.18 for iPP [101]. Nevertheless the coefficient of friction is dependent on the surface temperature and the roughness of the surface, but the data are not yet readily available, in spite of some research being under way [142].

The inclusion of the last term inside the integral depends on the condition of the tube shrinking in the thickness direction. This may happen for lower holding pressures or shorter times leading to the reduction of the force required to eject the part.

6.4.3.1- Predicting ejection force for iPP

The comparison between the experimental (mouldings with Tinj=210ºC and Tw=50ºC) and predicted ejection force as a function of the holding pressure is shown in figure 6.86.

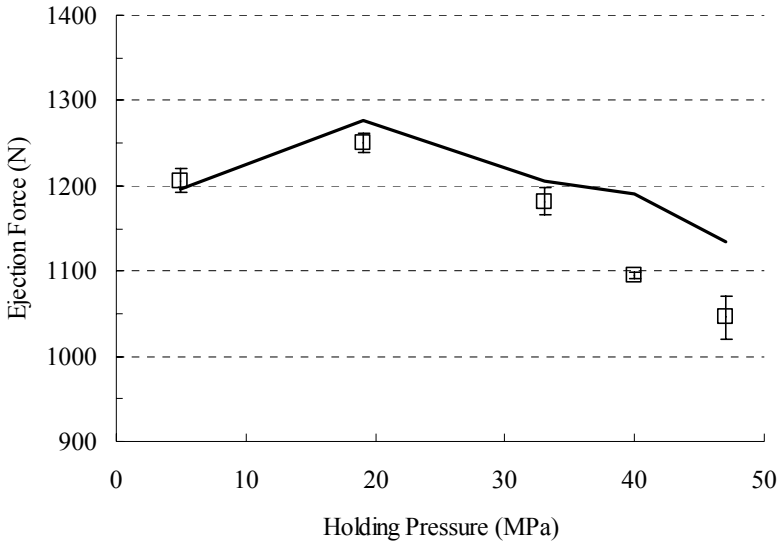

Figure 6.86- Comparison of the experimental (symbols) and predicted (line) ejection force for iPP. Effect of holding pressure. Mouldings with Tinj=210ºc and Tw=50ºC

As discussed previously in the section 6.4.1.4., the effect of the variation of the holding pressure on the ejection force is generally in the sense of its reduction with rising pressure. However an opposite trend at small holding pressures is observed. This behaviour is predicted by the model and is due to the following counteracting effects: the volumetric shrinkage increases when the holding pressure decreases, thus contributing to an increase of the ejection forces; however this effect is compensated by an increase of the thickness shrinkage. At higher holding pressures the reduction of the volumetric shrinkage overcomes the effect of the thickness expansion.

A prediction of the ejection force as a function of the surface temperature of the core was made for polypropylene using the previously referred to thermo-mechanical model (figure 6.87).

On the basis of the model the decrease of the ejection force with the rise of the surface temperature of the core is an expected result since a concurrent effect of reduction of the modulus and the volumetric shrinkage at ejection pointing together in that direction exists.

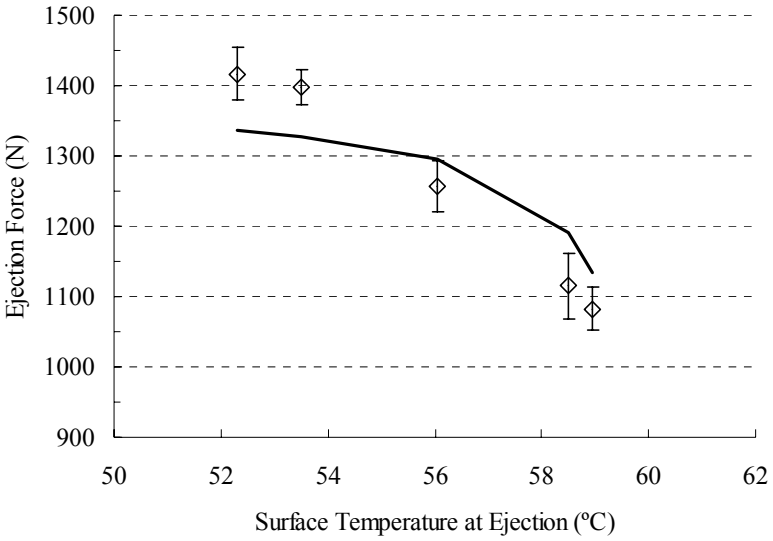

Figure 6.87- Comparison of the experimental (symbols) and predicted (line) ejection force for iPP. Effect of the surface temperature of the core at ejection. Mouldings with Tinj=210ºC.

As it can be seen in the Table 6.19 were the relative errors between the experimental ejection forces and the predictions are compared, the model in general is in close agreement with the experimental data (an average error in absolute value of 4.4% is observed).

Table 6.19 – Comparison of the error between the experimental ejection force and the predictions in iPP tubes with the thermo-mechanical model.

Condition	Error (%)
210.5.13.10	0.8
210.19.13.10	-2.1
210.33.13.10	-2.1
210.47.13.10	-8.6
210.40.13.5	-4.8
210.40.13.10	-7.9
210.40.13.20	-3.0
210.40.13.30	4.9
210.40.13.40	5.6
Absolute average	4.4

6.4.3.2- Predicting ejection force for PC

The comparison between the experimental and the prediction of the ejection force as function of the holding pressure is shown in figure 6.88.

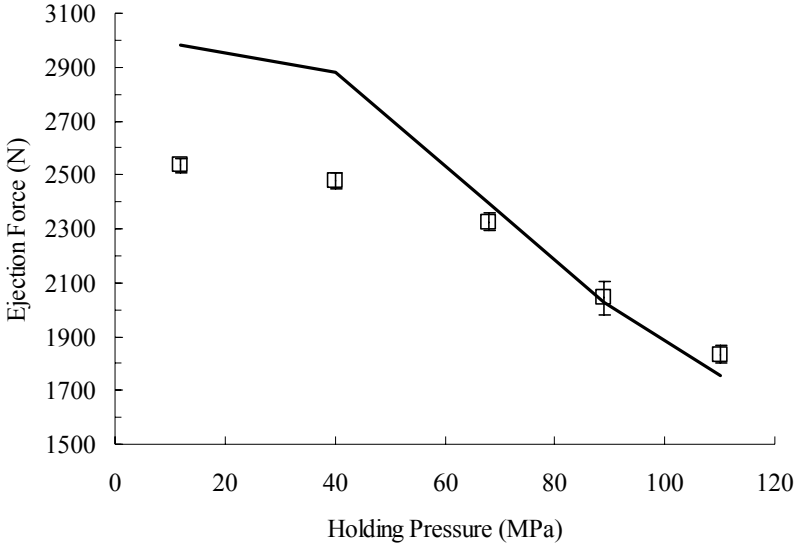

Figure 6.88- Comparison of the experimental (symbols) and predicted (line) ejection force for PC. Effect of holding pressure.

As it can be seen in the Table 6.20 and in the figure 6.88, in general the model agrees well with the experimental data. However, some divergence is observed at low and very high pressures. The divergence at low holding pressures is possibly due to some error on the simulated temperatures. This is caused by the detachment of the material from the moulding cavity surface, which is apparent from the interpretation of figure 6.19 which causes the temperature to remain higher due to the poor heat conduction. This effect is not considered by the simulation softwares. The divergence at high holding pressures is possibly caused by the variation of the coefficient of friction being not considered. In fact it is now known that the coefficient of friction on the ejection situation of a moulding is linked to a replication effect that is likely to be more pronounced at high moulding pressures [113]

Table 6.20 – Comparison of the error between the experimental ejection force and the predictions in PC tubes with the thermo-mechanical model.

Condition	Error (%)
310.12.10.15	-17.6
310.40.10.15	-16.3
310.68.10.15	-3.0
310.89.10.15	0.8
310.110.10.15	4.2
Absolute average	8.4

6.4.4- Concluding remarks

The effect of some processing variables on the ejection force of a tubular moulding was analysed. It was concluded that:

- The temperature at the surface of the core substantially influences the ejection force. This force decreases when the surface temperature increases, at a rate of *ca.* 40 N/ºC, due to the combined effect of the reduction of the modulus and of the shrinkage at ejection;
- The ejection force shows a slight tendency to drop with the injection temperature, at about 3.5 N/ºC, due to the shrinkage reduction. The increased pressure field during the holding stage is the responsible for that reduction;
- The ejection force varies inversely to the mould temperature. This result is expected since the increase of the mould temperature, for a constant ejection time, corresponds to a higher surface temperature at ejection;
- In a general the ejection force changes inversely with respect to the holding pressure. The reduction of the diametrical shrinkage associated to the holding pressure raise, that implies a smaller force to eject the moulding, is responsible for this behaviour;
- At low holding pressures a much lower than expected value of the ejection force is observed. This arises from the larger through-thickness shrinkage that causes the detachment of the material from the moulding cavity surface which causes the temperature to remain higher due to the poor heat conduction. Consequently a decrease in the ejection force results from the higher temperature of the moulding;
- The ejection forces of the iPP mouldings are lower than when PC is used, regardless of the higher shrinkage that occurs with polypropylene. This results certainly from the lower modulus and coefficient of friction of iPP compared to PC
- For iPP, the prediction of the ejection force as a function of the surface temperature of the core using the thermo-mechanical model is in close agreement with the experimental data. A maximum deviation of 5% between the predicted and experimental data is observed.
- For both materials, the thermo-mechanical model agrees well with the experimental data in function of the holding pressure.
- Some divergence for PC case, at low holding pressures is possibly due to some divergence on the simulated temperatures caused by the detachment of the material from the moulding cavity surface which causes the temperature to remain higher due to the poorer heat conduction. This effect is not considered in the simulations softwares.

7- CONCLUSIONS

This work must be seen as a part of a full engineering exercise involving a large design and development team covering aspects from material characteristics, tool design and manufacture, production and assessment of parts, and modelling of features of the process. This exercise aimed at a more precise description of the process and at helping the tool designers for injection moulding.

Specifically, in the strict context of this research work in this thesis a major contribution was given to the design of a tool, the extension of a thermo-mechanical model for the shrinkage to the case of restrained tubular mouldings, the development of a model for predicting ejection forces and, obviously, the assessment of the data from the experimental programme. Consequently, aspects such as detailed consideration of the crystallinity process in injection moulding, or the manufacturing of the tool are aside to the body of this research.

Thus, two major "visible" outcomes emerge from this work:

a) An innovative injection mould with which it is possible to monitor on line the ejection force of parts with a complex geometry that is representative of real life situations.

b) A set of models and programs that can enable a closer predictions of the shrinkage and of the ejection force required in the mouldings of components with deep cavities.

The work also includes a study of the shrinkage and ejection force of mouldings in two materials a amorphous (polycarbonate) and a semi-crystalline (polypropylene).

As a result of this experimental and theoretical study on the shrinkage and on the ejection force in injection moulding products, the following conclusions are established and grouped according to the main objectives of the work as indicated at the end of chapter 2.

7.1- The instrumented mould

Measuring ejection forces in actual operating conditions has been less reported in the literature due to the mechanical complexity associated to a suitable tool. The prototype mould developed in this work enable the monitoring of the ejection force on line.

- The system is quite reliable and reproducible, giving data with an amplitude of variation with respect to the average of the measurements of 3.5%, which is in line with the precision of the injection moulding process.
- The monitoring system includes load cells, pressure sensors, thermocouples, and if required, is compatible with the use of electric strain gauges for direct measurement of the moulding shrinkage.
- The use of pressure sensors in the core side appears to be non-effective, the recorded data after the filling stage being meaningless in the context of the injection moulding process.
- The use of a spider gating system is quiet efficient to guarantee a quasi-uniform parallel flow in the mouldings.
- The mould can be easily adapted to other thicknesses and surface roughness through quick exchange of the core block.

7.2- Shrinkage

The assessment of shrinkage was done using a recent technique of in-mould application of electric strain gauges on the moulding surface. The technique allows for a continuous monitoring of the shrinkage since the filling of the moulding.

Experimental data

- The holding history is the main factor that affects the shrinkage. For low holding pressures the part may shrink inside the mould before complete solidification. This is evident when comparing the external and the internal diametrical shrinkage of iPP tubes, or the shrinkage in the flow direction in the case of plates allowed to free shrinking or restrained from it.
- The effect of restraining the free shrinkage during the moulding process is significant on the as-moulded shrinkage when the holding pressure is small or the holding time is short, and it vanishes at high holding pressures and long holding times. The final shrinkage is smaller than in the case of free shrinkage.
- The shrinkage in tube case seems to be not affected by the wall temperature at ejection. This indicates that the shrinkage starts after complete solidification;
- The strain gauge technique is a useful method to obtain the complete shrinkage evolution as from its onset.
- The increase of the injection temperature results in a higher pressure inside the impression during the holding stage and consequently in a smaller shrinkage. The increase of the injection temperature is more effective in the reduction on shrinkage for low holding pressures.

Prediction of the shrinkage

The shrinkage in the two “simple” geometries analysed was estimated by resorting to a commercial software C-Mold version 99.7.

- Within this work a thermo-mechanical model was developed for a more precise description of the shrinkage mechanism.
- The trend shown by the experimental results for the shrinkage is shown by this software using their standard database parameters. However the predictions tend to overestimate the actual shrinkage.
- The predictions of the shrinkage using C-Mold overestimates the actual data by a sizeable difference. The difference is ascribed to a coarse description of the solidification temperature

point, which does not consider the effect of high cooling rates. A better description of shrinkage is achievable if a solidification temperature much smaller than that quoted in the database is used. This is justified by the temperature data having been determined at cooling rates much slower than those experienced by the polymer during solidification.

- The thermo-mechanical model developed in the work gives a satisfactory and a better description of the shrinkage and also of its onset inside the mould.
- For the case of semi-crystalline materials it is important to consider the degree of crystallinity (which depends on the cooling rate).
- It was concluded that the degree of crystallinity is suitable criterion of solidification for describing de shrinkage process.

Effect of mould deformation

- The mould deformation caused by the internal pressure during moulding is not considered by the available programs.
- The C-Mold shrinkage may account for the mould deformation material compressibility as an indirect correcting factor.
- The better predictions, considering the material compressibility, is certainly related to the close agreement between the experimental pressure evolution and the C-Mold predictions, and not to the increase of the material compressibility. A complementary C-Mold simulation confirms that the C-Mold used the elastic modulus and the Poisson ratio of the material to calculate the material compressibility.

7.3- Ejection force

One of the main objectives of the work was the precise assessment of the ejection forces required in critical cases of injection moulding.

The effect of processing variables on the ejection force of a tubular moulding was analysed. A thermo-mechanical model based on the computation of the actual shrinkage was developed to estimate those forces. The model developed in the work describes the case of semi-crystalline

materials. For the operation of the program, friction data between the core and the part is required.

Experimental data

- The research instrumented tool allows the direct measurement of the ejection force with a degree of repeatability close to that characteristic of injection moulding, i.e., smaller than 3.5%.

Effect of the surface temperature of the core at ejection

- The results indicate that the temperature at the surface of the core influences substantially the ejection force. In particular, this force decreases when surface temperature increases, at a rate of *ca.* 40 N/ºC. This is an expected result of the concurrent effect of the reduction of the modulus and of the shrinkage at ejection, both having an influence in that sense.

Effect of the injection temperature

- The ejection force decreases slightly with the injection temperature , at about 3.5 N/ºC. The increment of the injection temperature results in a smaller shrinkage due to the increased pressure transmission during the holding stage.

Effect of the mould temperature

- The ejection force varies inversely to the mould temperature. This result is expected since the increase of the mould temperature corresponds to a higher, surface temperature at ejection.
- The increase of mould temperature results in a reduction of the elastic modulus and of the shrinkage at ejection, both contributing to reduce the ejection force.

Effect of the holding pressure

- The ejection force changes inversely with respect to the holding pressure. The reduced contact pressure is responsible for this behaviour and it results from the decreasing diametrical shrinkage associated to the holding pressure increase, that implies a smaller force to eject the moulding.
- Conversely, at low holding pressures a much lower than expected value of the ejection force is observed. This arises from the larger through thickness shrinkage that causes the detachment of the material from the moulding cavity surface which causes the temperature to remain higher due to the poor heat conduction. Consequently a decrease in the ejection force occurs due to the higher temperature of the moulding.
- The ejection forces of the semi-crystalline iPP mouldings are lower than the amorphous PC ones, regardless of the higher shrinkage that occurs with polypropylene. This is attributable to the lower modulus and coefficient of friction of iPP in comparison to PC

Prediction of the ejection force

- The prediction of the ejection force as a function of the surface temperature of the core, for polypropylene mouldings, is in close agreement with the, experimental data (an maximum deviation of 5% between the predicted and experimental data is observed).
- The decrease of the ejection force with the rise of the surface temperature of the core is an expected result and it derives from the concurrent effect of the reduction of the modulus and the volumetric shrinkage at ejection, pointing together in that direction
- The thermo-mechanical model results agree well with the experimental data when the holding pressure is analysed as the variable.
- Some divergence for PC case at low holding pressures is observed. The divergence at low holding pressure is possibly due to some divergence on simulated temperatures caused by the detachment of the material from the moulding cavity surface which causes the temperature to remain higher due to the poor heat conduction.
- Divergence is also observed at high holding pressures, in this case being caused by the variation of the coefficient of friction.

8- FURTHER WORK

This work pointed out to new directions on the application of computer techniques, on the study and comprehension of the relationships between the processing and the mould design. Suitable points for further work include:

- The study of the shrinkage and ejection forces in the context of other materials: amorphous, semi-crystalline and short fibre reinforced.
- The study to more complex geometries. The forces resulting from the existence of ribs, resulting from pressure and mould deformation, is a topic of interest to be studied.
- The quantitatively study of the effect of the coatings used in mould cavities or cores.
- Integration of the algorithm of prediction with a injection moulding simulation program, and building up of a database with relevant information on materials and experimental data on ejection force.
- The extension of the termo-mechanical models to more complicate geometries, making use of the F.E.M technique.
- The integration of the prediction of ejection force with the detail design of the ejection system, namely on the ejector pin location. This will follow the trend and need to further develop an integrated tool methodology for injection mould design.

9- REFERENCES

[1] - **Moldes Portugal**. Lisboa: ICEP investimentos, comércio e turismo de Portugal, 1999. 326 p. ISBN 0874-3282

[2] Johannaber, F. - **Injection Molding Machines: a user's guide**. 2º ed., München: Hanser, 1985. 293 p. ISBN 3-446-13575-8.

[3] Viana, J.C. – **Mechanical Characterisation of Injection Moulded Plates.** Guimarães: Universidade do Minho, 1999. 250 p. PhD Thesis.

[4] White, J.L.- The injection Molding Process, in Bernhatdt E.C. (ed.) - **Computer Aided Engineering for Injection Molding**. Munich: Hanser, 1983. ISBN 3-446-13950-8. p. 86-113

[5] Osswald, T.A. – **Polymer Processing Fundamentals**, Munich: Hanser, 1998. 229 p. ISBN 1-56990-262-3

[6] Tadmor, Z. and Gogos, C.G. – **Principles of Polymer Processing**. New York: John Wiley & Sons, 1979. 736 p. ISBN 0-471-84320-2

[7] Avery, J. – **Injection Molding Alternatives: A guide for designers and product engineers**. Munich: Hanser, 1998. 331 p. ISBN 1-56990-251-8.

[8] - **Plastics Processing. Injection Molding, Extrusion, Die Casting**. Winterthur: Kistler Instrumente AG, 1998.

[9] Jansen, K.M.B – Residual Stresses in Quenched and Injection Moulded Products, **Intern. Polym. Process.**, Vol. 9: nº 1 (1994) p. 82-89.

[10] Viana, J.C., Cunha, A.M. and Billon, N. – The tensile behaviour of an injection moulding propylene-ethylene copolymer: effect of the local thermomechanical conditions, **Intern. Polym.**, nº 43 (1997), p. 159-166.

[11] Brito, A.M, Cunha, A.M. Pouzada, A.S. and Crawford, R.J. – Predicting the skin-core boundary lcation in injection mouldings, **Intern. Polym. Proc.**, vol. 6: nº 4 (1991), p. 370-377.

[12] Jensen, R. – The mould filling process: technical requirements and findings, in Rheinfeld, D. (ed.) – **Injection Moulding Technology**, Düsseldorf: VDI-Verlag, 1981. ISBN 3-18-404067-4. p. 173-195

[13] Tucker, C.L., - **Fundamentals of Computer Modeling for Polymer Processing**, Munich: Hanser, 1989. 623 p. ISBN 3-446-14704-7.

[14] Harry, D.H., Parrot, R.G. – Numerical simulation of injection mold filling, **Polym. Eng. Sci.**, vol. 10 (1970), p. 209-

[15] Kamal, M.R., Kenig, S. – The injection molding of thermoplastics, Part I: Theoretical Model, **Polym. Eng. Sci.**, vol. 12, (1972), p.294-301.

[16] Kamal, M.R., Kenig, S. – The injection molding of thermoplastics, Part II: Experimental Test of the Model, **Polym. Eng. Sci.**, vol. 12 (1972), p.302-308.

[17] Williams, G, Lord, H.A. - Mold-filling studies for the injection molding of thermoplastic materials Part I, **Polym. Eng. Sci.**, vol. 15: nº 8 (1975), p. 553- 568.

[18] Lord, H.A.,Williams, G. - Mold-filling studies for the injection molding of thermoplastic materials Part II, **Polym. Eng. Sci.**, vol. 15: nº 8 (1975), p. 569-582 .

[19] Lord, H.A. – Flow of polymers with pressure-dependent viscosity in injection molding dies, **Polym. Eng. Sci.**, Vol. 19: nº7 (1979), p.469-473.

[20] Broyer, E., Gutfinger, C. and Tadmor, Z. – Flow analysis network (FAN) – Method for solving flow problems in polymer processing, **Polym. Eng. Sci**., vol. 14 (1974), p. 660-

[21] Ryan, M.E., Chung, T.S. – Conformal mapping analysis of injection mold filling, **Polym. Eng. Sci**, vol. 20 (1980), p. 642-

[22] Kuo, Y., Kamal, M.R. – The fluid mechanics and heat transfer of injection mold filling of thermoplastics materials. **A.I.CH.E.J.**. vol. 22: nº 4 (1976), p. 661-669 .

[23] Hieber, C. A., Shen S. F. - A finite-element/finite-difference simulation of the injection-molding filling process. **J. of Non-Newtonian Fluid Mechanics**, vol. 7: (1980), p.1-32.

[24] Wang, V.W., Hieber, C.A., Wang, K.K – Dynamic simulation and graphics for the injection molding of three-dimensional thin parts. **J. of Polym. Eng.**. vol. 7: nº 1 (1986), p.21-45.

[25] Isayev, A.I., Hieber, C.A. – Toward a viscoelastic modelling of the injection molding of polymers. **Rheol. Acta**. nº 19 (1980), p. 168-182.

[26] Leonov, A.I., - Non-equilibrium thermodynamics and rheology of viscoelastic polymer media. **Rheol. Acta**. nº 15, (1976), p.85-98.

[27] Papathanasiou, T.D., Kamal, M.R. – Filling of a complex-shaped mold with a viscoelastic polymer. Part I: The mathematical model. **Polym. Eng. Sci.**. vol. 33: nº 7 (1993), p.400-409.

[28] Kamal, M.R., Papathanasiou, T.D. - Filling of a complex-shaped mold with a viscoelastic polymer. Part II: Comparison with experimental data. **Polym. Eng. Sci.**. vol. 33: nº 7 (1993), p.410-417.

[29] Kamal, M.R., Chiu, E., Lafleur, P.G., Ryan, M.E. – Computer simulation of injection mold filling for viscoelastic melts with fountain flow. **Polym. Eng. Sci.**. vol. 26: nº 3 (1986), p.190-196.

[30] Mavridis, H., Hrymak, A.N., Vlachopoulos, J. – Finite element simulation of fountain flow in injection molding. **Polym. Eng. Sci.**. vol. 26: nº 7 (1986), p.449-454.

[31] Mavridis, H., Hrymak, A.N., Vlachopoulos, J.- The effect of fountain flow on molecular orientation in injection molding. **J. of Rheology**. vol. 32: nº 6 (1988), p.639-663.

[32] Kuo, Y., Kamal, M.R. – **Flows of thermoplastics in the filling and packing stages of injection molding**. Proceedings of Int. Conf. Polym. Processing. Cambridge. Massachusetts. 1977, p.329-348.

[33] Titomanlio, G., Acierno, D., La Mantia, F.P. - Modelling of the packing step in the injection moulding of thermoplastic materials. **Ing. Chim. It**. nº 16 (1980), p.110- .

[34] Titomanlio, G., Piccarolo, S., Levati, G. - On the packing-holding flow in the injection moulding of thermoplastic polymers. **J. Appl. Polym. Sci.**. nº 35 (1988), p. 1483- .

[35] Nguyen, K.T., Kamal, M.R. – Analysis of the packing stage of a viscoelastic melt. **Polym. Eng. Sci.**. vol. 33: nº 11 (1993), p.665-674.

[36] Huilier, D.G.F. – Modelling of injection mold post-filling: A review and some critical problems to solve. **J. of Polym. Eng.**. vol. 9: nº 4 (1990), p. 237-302.

[37] Chiang, H.H., Hieber, C.A., Wang, K.K. – A unified simulation of the filling and post-filling stages in injection molding. Part I: Formulation. **Polym. Eng. Sci.**. vol. 31: nº 2 (1993), p.116-124.

[38] Chiang, H.H., Hieber, C.A., Wang, K.K. – A unified simulation of the filling and post-filling stages in injection molding. Part II: Experimental work. **Polym. Eng. Sci.**. vol. 31: nº 2 (1993), p.125-139.

[39] Hieber, C.A. - , in Isayev, A.I. (ed) – **Injection and compression molding fundamentals**, New York: Marcel Dekker, 1987. 703 p.

[40] Hetu, J.F., Gao, D.M., Garcia-Rejon, A., Salloum, G. – 3D finite element method for the simulation of the filling stage in injection molding. **Polym. Eng. Sci.**. vol. 38: nº 2 (1998), p. 223-236.

[41] Ilinca, F., Hétu, J.-F. – Three-dimensional filling and post-filling simulation of polymer injection molding. **Intern. Polym. Process.**. vol. 16: nº 3 (2001), p.291-301

[42] Pichelin, E., Coupez, T. – Finite element solution of the 3D mold filling problem for viscous incompressible fluid. **Comput. Methods Appl. Mech. Eng.**. nº 163 (1998), p. 359-371.

[43] Coupez, T., Daboussy, D., Bigot, E. – **Mesh adaptation for 3D injection numerical simulation**. Proceedings of 15th annual meeting of the Polymer Processing Society. Hertogenbosch, 1999.

[44] Brito, A.M., Cunha, A.M. – I**njection moulding visualisation with a siding frame mould**. Proceedings of 14th annual meeting of the Polymer Processing Society. Yokohama, 1998. p. 130-131

[45] Yokoi, H. – **Progress in Visualization Technologies for Analysing Injection Molding Phenomena**. Proceedings of 16th annual meeting of the Polymer Processing Society. Shanghai, 2000. p.136-137.

[46] Dias, G.R., Cunha, A.M., Brito, A.M., Vincent, M. – **Solidified layer growth visualization as a function of the progressing conditions.** Proceedings of 16th annual meeting of the Polymer Processing Society. Shanghai: June, 2000. p. 199-200.

[47] Dias, G.R., Brito, A.M., Cunha, A.M. – **Analysis of the flow front profile by in-line visualization of the filling stage.** Proceedings of 58th annual meeting of the Society of Plastics Engineers. Orlando: April, 2000.

[48] Williams, R.F., Pacoast, L.H. – Effect of process variables on mold shrinkage. **Modern Plastics Intern.**. (1967), p. 185-192

[49] Pierick, D., Noller, R.,- **The effect of processing conditions on shrinkage**. Proceedings of 49th annual meeting of the Society of Plastics Engineers. vol. 1., Montreal, 1991. p. 252-258.

[50] Bain, M.F., Janicki, S.L., Ulmer, A.S., Thomas, L.S. – **Mold shrinkage: Not a single data point**. Proceedings of 50th annual meeting of the Society of Plastics Engineers. Detroit, 1992.

[51] Mamat, A., Trochu, F., Sanschagrin, B. - Shrinkage analysis of injection polypropylene parts. **Polym. Eng. Science.**. vol. 35: nº 19 (1995), p. 1511-1520 .

[52] Jansen, K. M. B., van Dijk, D. J., Husselman, M. H.- Effect of processing conditions on shrinkage in injection molding. **Polym. Eng. Sci.**. vol. 38: nº 5 (1998), p. 838-846.

[53] Chang, T. C., Faison, E. III – Shrinkage behavior and optimization of injection molded parts studied by the Taguchi Method. **Polym. Eng. Sci.**. vol. 41: nº 5 (2001), p. 703-710.

[54] Han, S., Wang, K.K. – Shrinkage prediction for slowly-crystallizing thermoplastic polymers in injection molding. **Intern. Polym. Process.**. vol. 12: nº 3 (1997), p-228-237.

[55] Leo, V., Cuvelliez, C. - The effect of the packing parameters, gate geometry, and mold elasticity on the final dimensions of molded part. **Polym. Eng. Sci.**. vol. 36: nº 15 (1996), p. 1961-1971.

[56] Jansen, K.M.B. – Measurement and prediction of anisotropy in injection moulded PP products. **Intern. Polym. Process.**. vol. 13: nº 3 (1998), p. 309-317.

[57] Jansen, K.M.B., van Dijk, D. J., Freriksen, J.A. – Shrinkage anisotropy in fiber reinforced injection molded products. **Polym. Comp.**. vol. 19: nº 4 (1998). p. 325-334.

[58] Shay, R.M., Foss, P.H., Mentzer, C.C. – **Comparison of C-Mold predictions and experimental shrinkage: Fiber-filled materials**. Proceedings of 54th annual meeting of the Society of Plastics Engineers. Indianapolis, 1996.

[59] Pontes, A. J., Neves, N. M., Velosa, J. C., Faria, A. R., Pouzada, A. S. - **Glass fibre contents of PP plates and their properties: Part I: Shrinkage and changes in time.** Proceedings of 10th meeting of the Portuguese Society Materials. Coimbra: April, 2001.

[60] Pantani, R., Jansen, K. M. B., Titomanlio, G.,- In-mould shrinkage measurements of PS samples with strain gages. **Intern. Polym. Process.**. vol. 12: nº4 (1997), p. 396-402.

[61] Titomanlio, G., Jansen, K.M.B. – In-mold shrinkage and stress prediction in injection molding. **Polym. Eng. Sci.**, vol. 36: nº 15 (1996). p. 2041-2049.

[62] Bushko, W.C., Stokes, V.K. – Solidification of thermoviscoelastic melts. Part IV: Effects of boundary conditions on shrinkage and residual stresses. **Polym. Eng. Sci.**. vol. 36: nº 5 (1996), p. 658-675.

[63] Jansen, K. M. B., Pantani, R, Titomanlio, G. - As-moulded shrinkage measurements on polystyrene injection moulded products. **Polym. Eng. Sci.**. vol. 38: nº 2 (1998), p. 254-264.

[64] Bernhardt, E.C. – **Cavity dimensioning using computerized shrinkage evaluation software**. Proceedings of 47th annual meeting of the Society of Plastics Engineers. New York, 1989. p. 1262

[65] Austin, C. – **Predicting mechanical properties of injection molded parts from computer analyses**. Proceedings of 46th annual meeting of the Society of Plastics Engineers. Atlanta, 1988. p. 1560-1563

[66] - **Moldflow Help version 9.5.0, Theoretical basis for shrinkage calculations**, 1998.

[67] Stitz, S. – Is it really possible to predict shrinkage and warpage?. **Kunststoffe German Plastics**. vol. 81: nº 10 (1991), p. 27-29.

[68] Kennedy, P. – **Flow analysis of injection molds**. Munich: Carl Hanser Verlag, 1995. 237p. ISBN 3-446-18050-8.

[69] Isayev, A.I., Hariharan, T. – Volumetric effects in the injection molding polymers. **Polym. Eng. Sci.**. vol. 25: nº 5 (1985), p. 271-278

[70] Menges, G., Schmidt, T., Pötsch, G. – Shrinkage calculation programs improve molding quality. **Modern Plastics Intern.**. (1987), p. 68-71

[71] Yang, S.Y., Hon, M.Y. – **Simulation of cooling process during injection molding with a non-equilibrium state model**. Proceedings of 10th annual meeting of the Polymer Processing Society. Akron, Ohio, 1994.

[72] Pontes, A.J., Pantani, R., Titomanlio, G., Pouzada, A.S. – Solidification criterion on shrinkage predictions for semi-crystalline injection moulded samples. **Intern. Polym. Process.**. vol. 15: nº 3, (2000). p. 284-290.

[73] Menges, G., Dierkes, A., Schmidt, L., Winkel, E. – **Residual stresses in plastics due to cooling**. Proceedings of 38th annual meeting of the Society of Plastics Engineers. New York, 1980. p. 300-306.

[74] Fleishmann, E., Koppelman, J. – Effect of cooling rate and shear induced crystallisation on the pressure-specific volume-temperature diagram of isotatic polypropylene. **J. Appl. Polym. Sci.**. vol. 14, (1990). p. 1115-1121.

[75] Gedde, U.W. – **Polymer physics**, London: Chapman & Hall, 1995. 298 P. ISBN 0-412-59020-4

[76] Chang, R.Y. Chen, C.H., Su, K.S. – Modifying the tait equation with cooling-rate effects to predict the pressure-volume-temperature behaviors of amorphous polymers: Modeling and experiments. **Polym. Eng. Sci.**. vol. 36: nº 13 (1996), p. 1789-1795.

[77] Titomanlio, G., Brucato, V., Kamal, M.R. – Mechanism of cooling stress build-up in injection molding of thermoplatic polymers. **Intern. Polym. Process.**. vol. 1: nº 2 (1987), p. 55-59.

[78] Jansen, K.M.B., Titomanlio, G. – Effect of pressure history on shrinkage and residual stresses-injection molding with constrained shrinkage. **Polym. Eng. Sci.**. vol. 36: nº 15 (1996), p. 2029-2040.

[79] Bushko, W.C., Stokes, V.K. – Solidification of thermoviscoelastic melts. Part I: Formulation of model problem. **Polym. Eng. Sci.**. vol. 35: nº 4 (1995). p. 351-364.

[80] Bushko, W.C., Stokes, V.K. – Solidification of thermoviscoelastic melts. Part II: Effects of processing conditions on shrinkage and residual stresses. **Polym. Eng. Sci.** vol. 35: nº 4 (1995). p. 365-383.

[81] Bushko, W.C., Stokes, V.K. – Solidification of thermoviscoelastic melts. Part III: Effects of mold surface temperature differences on warpage and residual stresses. **Polym. Eng. Sci.**. vol. 36: nº 3 (1996). p. 322-335.

[82] Baaijens, F.T.P. - Calculation of residual stresses in injection molded products. **Rheol. Acta**. vol. 30: nº 3 (1991), p. 284-299.

[83] Douven, L.F.A., Baaijens, F.P.T., Meijer, H.E.H. – The computation of properties of injection-moulded products. **Prog. Polym. Sci.**. vol. 20 (1995). p. 403-457

[84] Chiang, H.H., Himasekhar, K., Lautenbach, S., Santhanam, Wang, K.K. – **Assessment of shrinkage and warpage using an integrated analysis of molding dynamics**. Proceedings of 49th annual meeting of the Society of Plastics Engineers. Montreal, 1991. p. 242-249.

[85] - **C-Mold 99.7 User's Guide, Shrinkage & Warpage**, 1999.

[86] Pantani, R., Titomanlio, G – Analysis of shrinkage development of injection moulded PS samples. **Intern. Polym. Process.**, vol. 14: nº 2 (1999), p. 183-190

[87] Burke, C., Kazmer, D. – **An experimental validation of shrinkage/warpage predictor**. Proceedings of 50th annual meeting of the Society of Plastics Engineers. Detroit, 1992. p. 1354-1363.

[88] Wu, S.S. – **CAE application: Shrinkage and warpage of an injection molded part**. Proceedings of 55th annual meeting of the Society of Plastics Engineers. Toronto, 1997.

[89] Jansen, K.M.B., van Dijk, D.J., Burgers, E.V. – Experimental validation of shrinkage predictions for injection molded products. **Intern. Polym. Process.**. vol. 13: nº 1 (1998). p. 99-104.

[90] Pantani, R. – **Analysis of shrinkage development in injection moulded samples**. Salerno: Università degli Studi di Salerno, 1999. 161 p. PhD Thesis.

[91] Choi, D.-S, Im, Y.-T – Prediction of shrinkage and warpage in consideration of residual stress in integrated simulation of injection molding. **Composite Structures.** vol. 47 (1999). p. 655-665.

[92] Neto, H. – Simultaneous engineering technology. Proceedings of 47th annual meeting of the Society of Plastics Engineers. New York, 1989.

[93] Oliveira, V., Pouzada, A.S. – Product development. **O Molde**, nº50 (2001), p.6-10.

[94] Yue, M. – **Tooling project management of injection molding**. Proceedings of 58th annual meeting of the Society of Plastics Engineers. Orlando: May, 2000.

[95] Saraiva, V.M., Lima, M., Pouzada, A.S. – **Concurrent engineering in the design of injection moulds for plastics**. Proceedings of 2nd Int. Conf. on Advanced Engineering Design. Glasgow, Scotland: June, 2001.

[96] Duff, A.L. – **Increased speed to market using CAE simulation for injection molded plastics parts**. Proceedings of 58th annual meeting of the Society of Plastics Engineers. Orlando: May, 2000.

[97] Wang, Z., Lee, K.S., Fuh, J.Y.H, Li, Z., Zhang, Y.F., Nee, A.Y.C., Yang, D.C.H – Optimum ejector system design for plastic injection mould. **Int. J. Mater. & Product Technol.**. vol. 11: nº 5/6 (1996), p. 371-385.

[98] Menges, G., Mohren, P.- **How to make injection molds**. New York: Hanser, 1986. 540 p. ISBN 3-446-16305-0.

[99] Pye, R.G.W. - **Injection mould design**. 4th ed. Harlow: Longman Scientific & Technical, 1989. 754 p. ISBN 0-582-01611-8

[100] Wang, H., Kabanemi, K.K., Salloum, G. – **Prediction of ejection force and ejection-induced stress in injection molding of plastics**. Proceedings of 55th annual meeting of the Society of Plastics Engineers. Toronto, 1997.

[101] Wang, H., Kabanemi, K.K., Salloum, G. - Numerical and experimental studies on the ejection of injection-molded plastic products. **Polym. Eng. Science**. Vol. 40: nº 3 (2000), p. 826-840.

[102] Struik, L.C.E – Orientation effects and cooling stresses in amorphous polymers. **Polym. Eng. Sci.**. vol. 18: nº 10 (1978), p. 799-811

[103] Isayev, A. I. - **Injection and compression molding fundamentals**., New York: Marcel Dekker, 1987. 703 p.

[104] Kaminski, A. - Messen un berechnen von entformungskäften an geometrisch einfachen formteilen. **Kunststoffe**. vol. 66: nº 4 (1976), p. 208-214

[105] Kaminski, A. – Demoulding. in Rheinfeld, D. (ed.) – **Injection Moulding Technology**. Düsseldorf: VDI-Verlag, 1981. . ISBN 3-18-404067-4. p. 233-261

[106] Wang, H., Connolly, R., Salloum, G. - **Mould-part interaction mechanisms and their effect on ejection of injection molded plastics parts**. Proceedings of Mechanics in Design, CSME Forum, Hamilton: May, 1996. p. 502-512.

[107] Burke, C., Malloy, R.- **An experimental study of the ejection forces encountered during injection molding**. Proceedings of 49th annual meeting of the Society of Plastics Engineers. Montreal, 1991. p. 1781-1787

[108] Balsamo, R., Hayward, D., Malloy, R.- **An experimental evaluation of ejection forces: frictional effects**. Proceedings of 51st annual meeting of the Society of Plastics Engineers. New Orleans, 1993.

[109] Shen, K., Chen, L., Jiang, L. – Calculation of ejection force of hollow, thin walled, and injection moulded cones. **Plastics, Rubber and Composites**. vol. 28: nº 7 (1999), p. 341-345.

[110] Sasaki, T., Koga, N., Shirai, K., Kobayashi, Y., Toyoshima, A. – An experimental study on ejection force of injection molding. **J. of Precision Engineering**. vol. 24: nº 3 (2000), p.270-273

[111] Pontes, A. J., Pinho, A. M., Miranda, A. S. e Pouzada, A. S., Influência das Condições de Processamento na Força de Extracção em Moldes de Injecção de Termoplásticos. **O Molde.** nº 34 (1997), p. 25-33.

[112] Pontes, A.J., Titomanlio, G., Pouzada, A.S. – **The influence of processing conditions in ejection forces of injection moulded parts**, Proceedings of 15th annual meeting of the Polymer Processing Society. S Hertogenbosch, 1999

[113] Menges, G., Bangert, H.- Measurement of coefficients of static friction as means of determining opening and demoulding forces in injection moulds. **Kunststoffe**. vol. 71: nº 9 (1981), p. 13-16.

[114] Kabanemi, K.K., Vaillancourt, H., Wang,H., Salloum, G. – Residual stresses, shrinkage, and warpage of complex injection molded products: Numerical simulation and experimental validation. **Polym. Eng. Sci.**. vol. 38: nº 1 (1998), p. 21-37.

[115] Buckley, C.P. – Prediction of stress in a linear viscoelastic solid strained while cooling. **Rheol. Acta**. vol. 27: nº 3 (1988), p. 224-229.

[116] Benham, P.P., Crawford, R.J. – **Mechanics of engineering materials**. Harlow: Longman Scientific & Technical, 1991. 626 p. ISBN 0-582-28640-9

[117] Timoshenko, S.P., Goodier, J.N. – **Theory of elasticity**. 3rd ed. New York: McGraw-Hill, 1970. 567 p. ISBN 07-064720-8.

[118] - **Engineering Materials Design Guide**. General Electric Plastics Europe.

[119] - **A guide to successful injection moulding.** General Electric Plastics Europe

[120] - **GE-Select, Engineering Thermoplastics Resin Database**, General Electric Plastics, 1996.

[121] - **Development data**, Montell polyolefins, 1998

[122] Hoffmann, K. – **An introduction to measurements using strain gages**. Darmstadt: Hottinger Baldwin Messtechnik GmbH, 1989. 291 p.

[123] Murray, W. M., Miller, W.R. – **The bonded electrical resistance strain gage**. New York: Oxford University Press, 1992.

[124] Jansen, K.M.B – Effect of pressure on electrical resistance strain gages. **Experimental Mechanics**.

[125] - **C-Mold 99.7 User's guide**, 1999.

[126] Brydson, J. – **Flow properties of polymer melts**. 2nd ed. London: George Goodwin Ltd, 1981. 226 p. ISBN 0-7114-5681-X

[127] Van Krevelen, D.W. – **Properties of Polymers: their correlation with chemical structure; their numerical estimation and prediction from additive group contributions**. 3rd ed. Amsterdam: Elsevier, 1997. 875 p. ISBN 0-444-82877-X

[128] Titomanlio, G, Speranza, V., Brucato, V. - On the simulation of thermoplastic injection moulding process. Part I. **Int. Polym. Process.**. vol. 10: nº 1 (1995), p. 55-61

[129] Titomanlio, G, Speranza, V., Brucato, V. - On the simulation of thermoplastic injection moulding process. Part II. **Int. Polym. Process.**. vol. 12: nº 1 (1997), p. 45-53

[130] Speranza, V. - **Analisi e simulazione del processo di stampaggio ad iniezione**. Salerno: Universita' degli Studi di Salerno, 1999. 139 p. Phd Thesis.

[131] Bird, R.B., Stewart, W.E. Lightfoot, E.N. – **Transport Phenomena**. New York: Wiley, 1960. 780 p. ISBN 0-471-07395-4

[132] Brucato, V., Titomanlio, G. - Modified thermal diffusivity in the simulation of injection moulding filling with crystalline polymers. **Acta Polimerica**. nº 40 (1989), p. 384-

[133] Nakamura, K., Watanabe, T., Katayama, K., Amano, T – Some aspects of nonisothermal crystallization of polymers: I Relation between crystallization temperarure, crystallinity, and coolig conditions. **J. Appl. Polym. Sci.**. vol. 16 (1972), p. 1077-1091.

[134] Nakamura, K., Katayama, K., Amano, T. – Some aspects of nonisothermal crystallization of polymers: II Consideration of the isokinetic condition. **J. Appl. Polym. Sci.**. vol. 17: nº 4 (1973), p. 1031-1041.

[135] Pantani, R, Titomanlio, G. - Description of PVT behaviour of an industrial polypropylene-EPR co-polymer in process conditions. **J. Appl. Polym. Sci**. vol. 81:n º 2 (2000), p. 267-278.

[136] Boitout, F. Agassant, J.F., Vincent, M. – Elastic calculation of residual stresses in injection molding – Influence of mold deformation and pressure in the liquid. **Intern. Polym. Process.**. vol. 10: nº 3 (1995), p.237-242.

[137] Delaunay, D., Le Bot, P., Fulchiron, R., Luye, J.F., Regnier, G. – Nature of contact between polymer and mold in injection molding. Part II: Influence of a mold deflection on pressure history and shrinkage. **Polym. Eng. Sci.**. vol. 40: nº 7 (2000), p. 1682-1691.

[138] Wang, H., Prystay, M., Caoa, B., Jen, C.K. – **Gap between mold and part and its effect on cooling of injection-molded plastics**. Proceedings of 55th annual meeting of the Society of Plastics Engineers. Toronto, 1997.

[139] Delaunay, D., Le Bot, P., Fulchiron, R., Luye, J.F., Regnier, G. – Nature of contact between polymer and mold in injection molding. Part I: Influence of a non-perfect thermal contact. **Polym. Eng. Sci.**. vol. 40: nº 7 (2000), p. 1682-1691.

[140] Shay, R.M., Foss, P.H., Mentzer, C.C. – **Comparison of C-Mold predictions and experimental shrinkages: Fiber-filled materilas**. Proceedings of 56th annual meeting of the Society of Plastics Engineers. Indianapolis, 1996.

[141] De Santis, F - **Analisi del ritiro di manufatti polimerici semicristallini ottenuti per stampaggio ad iniezione**. Salerno: Universita' degli Studi di Salerno, 1999. Master thesis.

[142] Ferreira, E.C., Neves, N.M., Muschalle, R., Pouzada, A.S. – **Friction properties of thermoplastics in injection molding**. Proceedings of 59th annual meeting of the Society of Plastics Engineers. Dallas, 2001.